Study of the role of AHP6 in the control of phyllotaxis in Arabidopsis thaliana : robustness and spatio-temporal coordination in the development of self-organized organisms

Fabrice Besnard

THÈSE DE DOCTORAT
DE L'ÉCOLE NORMALE SUPÉRIEURE DE LYON

Discipline: Biologie
Spécialités: Biologie du Développement, Biologie des Plantes

Présentée par
Fabrice Besnard

Pour obtenir le grade de Docteur en sciences de l'École Normale Supérieure de Lyon

Titre:
Étude du rôle de *AHP6* dans le contrôle de la phyllotaxie chez *Arabidopsis thaliana*
Robustesse et Coordination spatio-temporelle au cours du développement de structures auto-organisées

Soutenance le 21 octobre 2011

Jury:

Rapporteurs :	Professor Malcom BENNETT
	Docteur François PARCY
Examinateur :	Docteur Stéphane DOUADY
Directeur du Jury:	Professeur Arezki BOUDAOUD
Directeur de thèse :	Docteur Teva VERNOUX

THESIS
Ecole Normale Supérieure de Lyon

defended by
Fabrice Besnard

Title **:**

Study of the role of the *AHP6* gene in the control of Phyllotaxis in *Arabidopsis thaliana*
Robustness and coupling between space and time during pattern formation

Acknowledgments

I would like to thank François Parcy, Malcom Bennett, Stéphane Douady, Arezki Boudaoud for taking part to my thesis committee.

Remerciements

Pour les suivants, je pense qu'ils aimeront autant que je leur adresse mes remerciements en français. Je les remercie donc déjà de me permettre de coucher dans ma langue natale ces quelques lignes, qui resteront une des rares enclaves de la langue de Molière dans ce manuscrit anglophone !

Je remercie Teva Vernoux, pour m'avoir accueilli dans son équipe et pour m'avoir formé et accompagné avec attention, rigueur et enthousiasme depuis mon master2. Merci surtout de m'avoir fait toujours confiance, avoir su partager mes déceptions et mes excitations scientifiques, bref de m'avoir permis de m'amuser et m'épanouir avec ce sujet (ce qui est, on l'oublie souvent, le but premier de nos recherches !)

Je remercie Jan Traas de m'avoir en premier accueilli au RDP au sein de son équipe et d'avoir toujours suivi mes travaux avec intérêt. Merci pour ses conseils avisés, les nombreuses discussions scientifiques qui nous ont permis de mûrir nos idées et pour son implication dans la rédaction des papiers.

Je remercie évidemment l'ensemble des personnes qui ont collaboré à mon projet de thèse : au RDP, Benjamin Marteaux, Valérie Morin, Géraldine Brunoud, Coralie Cellier, Frédérique Rozier, Jonathan Legrand, Vincent Mirabet, Arezki Boudaoud, Pradeep Das, Sophie Chamot ; à Montpellier (INRIA Virtual Plant) Yann Guédon, Yassin Refahi, Étienne Farcot, Christophe Godin ; en Finlande, Ykä Helariutta, Anthony Bishopp. Le travail en équipe fut pour moi une des sources de motivation les plus importantes de ma thèse.

Merci aussi à Laurent Laplaze et Gaël Yvert d'avoir fait partie de mon comité de thèse.

Merci à Teva, Yann, Jan, Charlie, Vincent, Arezki, Olivier, Zachi-Zacho et Sarah d'avoir corrigé ce manuscrit.

Je remercie tout particulièrement ceux qui ont eu la dure tâche de me former ou qui ont été assez gentil(le)s pour passer du temps à m'apprendre les rudiments de la paillasse : Teva, Gégé, Valérie et

Pierrot pour le maniement de la pipette en bio mol, Teva, Gégé et Soazig pour la main verte avec les plantes ; Frédérique pour l'art de la cyto ; Sophie, Sandrine et Anne-Marie pour leur conseils en bioch ; Pradeep, le dieu (et parfois le fantôme) du confocal et aussi Christophe, Claire et Olga sans l'aide de qui j'aurais sans doute déjà détruit un onéreux microscope dans un regrettable accès de colère.

Un grand merci aux sécessionnistes de l'équipe biophysique, Pradeep, Arezki, Olivier et Vincent, toujours prêts à donner de leur temps pour discuter, relire un rapport ou coacher un oral.

Merci aussi à Alexis, Priscilla et Isabelle d'avoir veillé sur mes plantes (et de n'avoir jamais mis à exécution leur menace de jeter mes vieilles plantes contaminées qui grainent partout), et à Stéphanie et Laetitia de compenser avec patience mon incurie pour les tâches administratives et logistiques... Et donc merci au passage à Aurélie V. et Catherine d'avoir su me rappeler les « dead-lines » importantes et m'indiquer les démarches à suivre quand il le fallait ! Merci à Hervé et Claudia pour leur travail quotidien et leur constante bonne humeur.

Merci aux enseignants avec qui j'ai interagi pendant mon monitorat, notamment l'équipe de choc du TP de physio veg, Christine, Christophe et Nathalie ! Merci aux étudiants d'avoir essuyé les plâtres de mes premiers cours ou TD et mille fois merci à ceux qui ont su me faire passer ne serait-ce qu'un début de retour positif : un seul de ce genre de récompense redonne souvent de l'énergie pour au moins une année !

Mes remerciements s'adressent enfin à l'ensemble des membres du RDP : l'ambiance qui y règne est assez incroyable, aussi bien propice au travail qu'à l'amusement. Merci donc à tous les intermittents de la sciences pour les workshops-by-night de haute qualité, aux thésards, stagiaires, retraités, promus et auteurs de papiers acceptés pour leurs pots inoubliables, à Pierrot pour son « pilou-pilou », aux instigateurs(-trices surtout) des goûters d'après lab-meeting, aux compagnons de rando dans les montagnes, de skis sur les pistes et de pichet au Ninkasi ! Merci aussi aux footeux, pas tous RDP, de l'équipe des « débutantes ».

Merci à l'ensemble des thésards pour cette ambiance solidaire et amicale, en particulier les deux autres thésards de l'équipe -ou presque !, Marina et Jo.

Merci aussi aux batteurs de pavé avec qui j'ai pu partager mes convictions, mes indignations et mes espoirs : Aurélie V., Philippe, Christophe, Annie, Vanessa, Gigi, Patoche, Michiel et même Alexis ! Votre mobilisation m'a conforté dans l'idée que, dans une thèse comme ailleurs, qu'importe le résultat, l'échec vient toujours du renoncement. Et merci à Philippe d'avoir veillé à notre

éducation politique et citoyenne en apportant régulièrement « le palmipède » et Libé dans la salle conviviale !

Je n'oublie pas non plus le trio de choc de mon bureau : Sophie, Marina et Aurélie (et Merlin qui s'est invité sur la fin, mais est resté d'une discrétion exemplaire). Je peux bien avouer maintenant que leur débit intarissable est un bien faible dérangement en comparaison de la bonne humeur que elles apportent dans ce bureau. Enfin, si on exclut le tricot, les poules et les poneys, évidemment.

Enfin, je remercie tous ceux qui m'ont permis, en m'offrant la possibilité de m'extraire de ma thèse, d'éviter l'overdose et d'y revenir avec plus d'entrain !

Merci donc à mes colocs passés (TomTom, Camille), présents (Chloé, Alice, Zacho, Julien), et à ceux de passage (Steph, Ariel, Lopette,...). Merci à tous les athlètes du Lyon Athlé et à Yvan, le coach du groupe. Merci à la joyeuse bande la Science-ac, à Paris et à Lyon.

Merci aux potos de longue date, de Saint-Malo, de Rennes, de Paris, de Montpellier, de Lyon ou de Suisse ! Grâce à vous, je n'aurais pas non plus cessé de voyager en France et dans le monde pendant cette thèse et je compte bien continuer ainsi ! Enfin, aux membres de ma famille qui auront compris en lisant la phrase précédente que ma thèse et l'éloignement lyonnais n'étaient que deux mauvaises excuses pour justifier mon impardonnable manque de visites, j'adresse mes plus sincères remerciements pour le constant soutien qu'ils m'apportent et l'affection dont ils me témoignent.

Merci enfin à Sarah de n'avoir pas été jalouse de la petite mauvaise herbe avec qui je passe mes journées.

Je profite enfin de cet espace pour diffuser le poème de notre collègue Philippe Vergne (on reconnaîtra le style et le choix des références!), dont il a tiré l'inspiration de nos activités scientifiques et de l'ambiance exceptionnelle de notre labo, qui a été entre-aperçue dans ces remerciements.

En espérant avoir été à la hauteur des attentes de Philippe, je souhaite que les lecteurs de cette thèse y trouvent, au-delà de l'austère vernis scientifique, une possible source de « plaisir, de rêve et de frémissement » !

Labo

Des princesses et des loups en diamant, fiers d'exister, un peu enfants,
Et des gens fulgurants, et des gens rassurants,
De brillants commandants, durs au mal, et porteurs d'allant,
De vieux rampants veillant, s'battant, serrant les dents.
Faire plaisir, rêver et frémir,
Partager l'instant, pas mourir, pas faillir,
Et souffrir aussi dans l'néant, dans les soirs d'acharnement.
Fermer les blessures, provoquer l'futur,
En quête de la grâce ou du gros coup,
Et vivants et debout toujours, pour des quelqu'uns, des étoiles
Qu'on croise, et qui t'impriment pour longtemps, une émotion, une limite.

Table of contents

INTRODUCTORY PAGES

Acknowledgments....3
Remerciements....3
Table of contents....7
List of main Abbreviations....12
Nomenclature....12
Abstract of the thesis....13

INTRODUCTION ….....(15-124)

Phyllotaxis in Plants, a field for developmental biology and interdisciplinarity....17

I. PHYLLOTAXIS AT A MACROSCOPIC SCALE: INTERACTIONS BETWEEN ORGANS IN THE SAM....21

I.1. Describing phyllotaxis: the mathematical beauty of plants....21
I.2. Experiments in Phyllotaxis: the model of inhibitory fields in the shoot apical meristem....25
I.3. Modeling Phyllotaxis: a dynamic self-iterative process of pattern formation....29
I.3.1. Understanding the properties of phyllotaxis by theoretical models....29
I.3.2. The model of phyllotaxis proposed by Douady and Couder supports the Inhibitory fields theory of Snow and Snow....33
I.3.3. The lessons from the model: answers, predictions and limits....35

II. THE SAM AT A MICROSCOPIC SCALE: SIGNALING IN A MULTICELLULAR OBJECT. 43

II.1. Morphogenesis at the SAM: highly dynamic cells produce a stable structure....43
II.2. Patterning of the SAM is under genetic control....45
II.3. Signals behind cell-cell communication and growth coordination in the SAM 49
II.4. Specificity of signaling in plants and in the SAM....51

III. CONTROL OF ORGANOGENESIS AND PHYLLOTAXIS BY DYNAMIC POLAR AUXIN TRANSPORT....57

III.1. The chemical hypothesis for the nature of inhibitory fields....57
III.2. Auxin is polarly transported from cell to cell....57
III.3. Auxin transport controls organogenesis and phyllotaxis at the shoot apical meristem....61

III.4. A self-regulatory network of auxin carriers provides a plausible model for the control of phyllotaxis 63
III.5. How do cell perceive auxin and polarize in a multicellular context ?.....67
III.6. A possible role for PIN1 efflux carrier phosphorylation in phyllotaxis?.....71
IV. MULTIPLE FEEDBACK LOOPS INTEGRATING MECHANICAL SIGNALS AND HORMONAL CROSSTALK DURING PHYLLOTAXIS.....75
IV.1. Role of Mechanical signals in phyllotaxis.....75
IV.1.1. A biophysical mechanism is not likely at the origin of the phyllotactic pattern.....75
IV.1.2. A possible cooperation of mechanical signals with auxin?.....79
IV.2. Complex hormonal crosstalks during organogenesis.....83
V. OBJECTIVE OF MY THESIS: IDENTIFYING NEW REGULATORS OF ORGANOGENESIS AND PHYLLOTAXIS.....91
V.1. Actual questions in phyllotaxis and possible hypothesis for further research.....91
V.2. Objectives and Strategy developed during my phD.....93
References - Introduction.....97

CHAPTER 1: IDENTIFICATION OF PERTURBATION PATTERNS IN FIBONACCI SPIRALS SUGGEST A NEW ROLE FOR CYTOKININ SIGNALING IN COORDINATING SPACE AND TIME IN PHYLLOTAXIS.....(125-186)

ABSTRACT.....129
1 Introduction.....131
2 Results.....137
2.1 Measurements of divergence angle sequences between siliques and analysis of spiral orientation.....137
2.2 Exploratory analysis suggest that both wild-type and ahp6-1 mutants have structured perturbation motifs.....137
2.3 Identification of permutations patterns in the sequences of measured divergence angles using Hidden Markov Chains (HMC).....139
2.4 Characterization of permutation patterns using HMC and Combinatorial Mixture models. 143
2.5 Permutations patterns in ahp6 mutants are more numerous, longer and more complex..147
2.6 Classification of individuals belonging to different genetic backgrounds confirm the role of AHP6.....149
2.7 A Permutation between two organs is often associated with a non-elongated internode.153

2.8 Patterns of propagation of permutation in sequences suggest a role of direct neighbors 155
2.9 Within baseline segments, the canonical divergence angle is robustly set but can significantly differ from the theoretical golden angle (137.5º).....157
2.10 Exploring local dependencies in baseline segments by sample auto-correlation.....159
3 Discussion.....163
3.1 Possible origins of Permutations and putative role for AHP6 functions in Arabidopsis. 163
3.2 A body of facts sustaining the theory of local inhibitory interactions between primordia. 167
3.3 Concluding remarks.....171
References - Chapter 1.....173
4. Supplementary Information.....179
4.1. Materials and methods.....179
4.1.1. Plants, culture conditions and materials.....179
4.1.2. Measurement protocol.....179
4.1.3. Stationarity assumption of measured sequences.....180
4.1.4. Extraction of intervals of synchronized organs between permutation.....180
Supplementary References – Chapter 1.....181
4.2. Supplementary figures.....182
Appendices (detailed materials and methods for the mathematical analysis)

CHAPTER 2: STUDY OF THE ROLE OF *AHP6* AT THE SHOOT APICAL MERISTEM OF *ARABIDOPSIS THALIANA*.....(187-244)

INTRODUCTION.....189
I. CYTOKININ INHIBITORY FIELDS PROVIDE ROBUSTNESS TO THE TEMPORAL PATTERNS OF PHYLLOTAXIS.....191
ABSTRACT.....193
1. Results and discussion.....195
References – Chapter II, Part I.....205
2. Supporting Information 211
2.1. Material and Methods.....211
2.1.1. Plant material and growth conditions.....211
2.1.2. In situ hybridization, microscopy and live imaging.....211
2.1.3. Real-Time quantitative RT-PCR experiments.....213

2.1.4. Microarray data analysis....213
2.1.5. Measures of phyllotactic sequences and models used for characterization of permutation patterns....215
Supplementary references – ChapII, Part I....215
2.2. Supplementary Figures....219
II. GENETIC INTERACTIONS OF AHP6 WITH THE PROTEIN KINASE PINOID, A REGULATOR OF POLAR AUXIN TRANSPORT....233
1. Results and discussion....235
1. Genetic interactions between AHP6 and PINOID in the control of phyllotaxis....235
2. Synergistic interaction of PINOID and AHP6 in flower and carpel development....237
2. Materials and Methods....237
references – Chapter II, part II....241

CHAPTER 3: MODELING NOISE AND ROBUSTNESS IN PHYLLOTAXIS..... (245-284)

I. INTRODUCTION....247
II. NOISE AND ROBUSTNESS IN PHYLLOTAXIS....251
ABSTRACT....253
1. Introduction....255
2. Results....257
2.1. The role of noise....257
a) Threshold noise....259
b) Size noise....261
2.2. Correcting noise....263
a) Possible scenarios....263
b) Post-initiation noise correction....265
3. Discussion....267
4. Supplementary Information....273
4.1. Supplementary figures....273
4.2. Materials and Methods....273
a) Deterministic model....273
b) Model with noise....275
c) Secondary field....275
References – Chap III....277

CONCLUSION AND PERSPECTIVES.....(285-331)

I.DISCUSSION OF OUR RESULTS.....289

I.1.AHP6 inhibitory fields: a new mechanism controlling the robustness of temporal patterns in Arabidopsis phyllotaxis.....289

1.1.Plastochron instabilities supports the « Snow and Sow » hypothesis and are likely the cause of post-meristematic permutations in phyllotaxis.....289

1.2.co-initiations can be explained by stochasticity and other factors in the frame of theoretical models of phyllotaxis.....291

1.3.AHP6 controls specifically the rhythmicity of the plastochron by a mechanism involving cytokinin inhibitory fields.....295

1.4.Importance of plastochron regularity in the control of the segmented architecture of shoots.....301

I.2.Auxin inhibitory fields: new insights on the spacing mechanism controlling phyllotaxis....303

2.1.New arguments supporting the existence of local inhibitory fields.....303

2.2.New predictions concerning the auxin fields in the SAM.....305

I.3.Other inhibitory fields ? Proposition of a model with multiple hierarchical fields.....309

I.4.A new role for cytokinin in organogenesis reveals the complexity of hormonal crosstalk controlling development.....311

I.5.Why has a mechanism evolved that limits co-initiations in phyllotaxis?.....313

II.PERSPECTIVES.....319

II.1.Phenotyping phyllotaxis in different plants.....319

II.2.Exploring the molecular network behind the effect of AHP6 fields and the auxin-cytokinin crosstalk.....321

II.3.EXPLORING THE AUXIN FIELDS BY NEW EXPERIMENTAL AND MODELING APPROACHES.....323

APPENDICES

General list of figures.....331
General list of tables.....333
Origins of pictures and photographs re-used in the figures of this manuscript.....334

List of main Abbreviations

35S : promotor of the 35S RNA from the cauliflower mosaic virus
ADN : desoxyribonucleic acid
ARN : ribonucleic acid
ARNm : messenger RNA
BAP : N^6-Benzyl Aminopurine
bp : baise pair
CK : cytokinin
CMM : combinatorial mixture model
Col-0 : Columbia-0 ecotype
CZ : central zone
GFP : green fluorescent protein
HA : hemmaglutinin
HMC : hidden Markov chain
HPt : histidine-containing phosphotransfer protein
IAA : indole-3-acetic acid
NPA : 1-N-naphthylphthalamic acid
PCR : polymerase chain reaction
PZ : peripheral zone
qRT-PCR : quantitative reverse-transcription- polymerase chain reaction
S&S Snow and Snow
SAM : shoot apical meristem
WS : Wassilewskija ecotype

Nomenclature

AHP6 : wild-type *AHP6* gene
AHP6 : protein encoded by the *AHP6* gene
ahp6-1 : mutated allele number 1 of the *AHP6* gene
ahp6 : mutant plant for *AHP6*

Abstract of the thesis

During development, plant aerial organs are produced along the stems following stereotyped patterns. This so-called phyllotaxis is initiated at the shoot meristem, which contains the stem cell niche: organs are produced iteratively and their precise position is thought to depend on dynamic interactions with preexisting organs. These interactions would notably result from inhibitory fields generated by the polar transport of the plant hormone auxin. To investigate whether other factors than auxin regulate phyllotaxis, we studied the potential role of cytokinin signaling. We developed a new pipeline of methods based on statistics to analyze phyllotactic patterns. This approach allowed us to identify phyllotactic perturbations in mutants of the *AHP6* (*ARABIDOPSIS HISTIDINE PHOSPHOTRANSFER protein 6*), an inhibitor of cytokinin signaling that suggested perturbations in the plastochron, the time between two organ initiations. This was further confirmed using confocal live-imaging. We demonstrated that AHP6 controls the regularity of the plastochron, and our results suggest that the defective phyllotaxis in *ahp6* is caused by concomitant initiations of two or three organs in the meristem. Interestingly, *AHP6* is expressed in organs and the protein can move beyond these domains, generating cytokinin signaling inhibitory fields. To explore further the putative role of these secondary fields, we generated a mathematical model of phyllotaxis. This suggested that plastochron instabilities could be caused by noise affecting the threshold at which meristematic cells are recruited into organs. Inhibitory fields generated by AHP6 could filter out the effect of noise by modifying the kinetics of early organ emergence. Consistently, the properties of AHP6 fields fit the model predictions and our experimental data show that AHP6 and cytokinin modulate auxin signaling during organ emergence. We thus propose a model in which auxin transport and signaling robustly control organ positioning but generates plastochron instablities in noisy backgrounds. In this scenario cytokinin inhibitory fields would stabilize the rhythmicity of organ initiation, ensuring a robust coupling of space and time during pattern formation.

Keywords: phyllotaxis, shoot apical meristem, auxin-cytokinin crosstalk, *Arabidopsis*, inhibitory fields, noise and robustness, developmental pattern, dynamical system model, pattern analysis.

Phyllotaxis: from old considerations to current questions

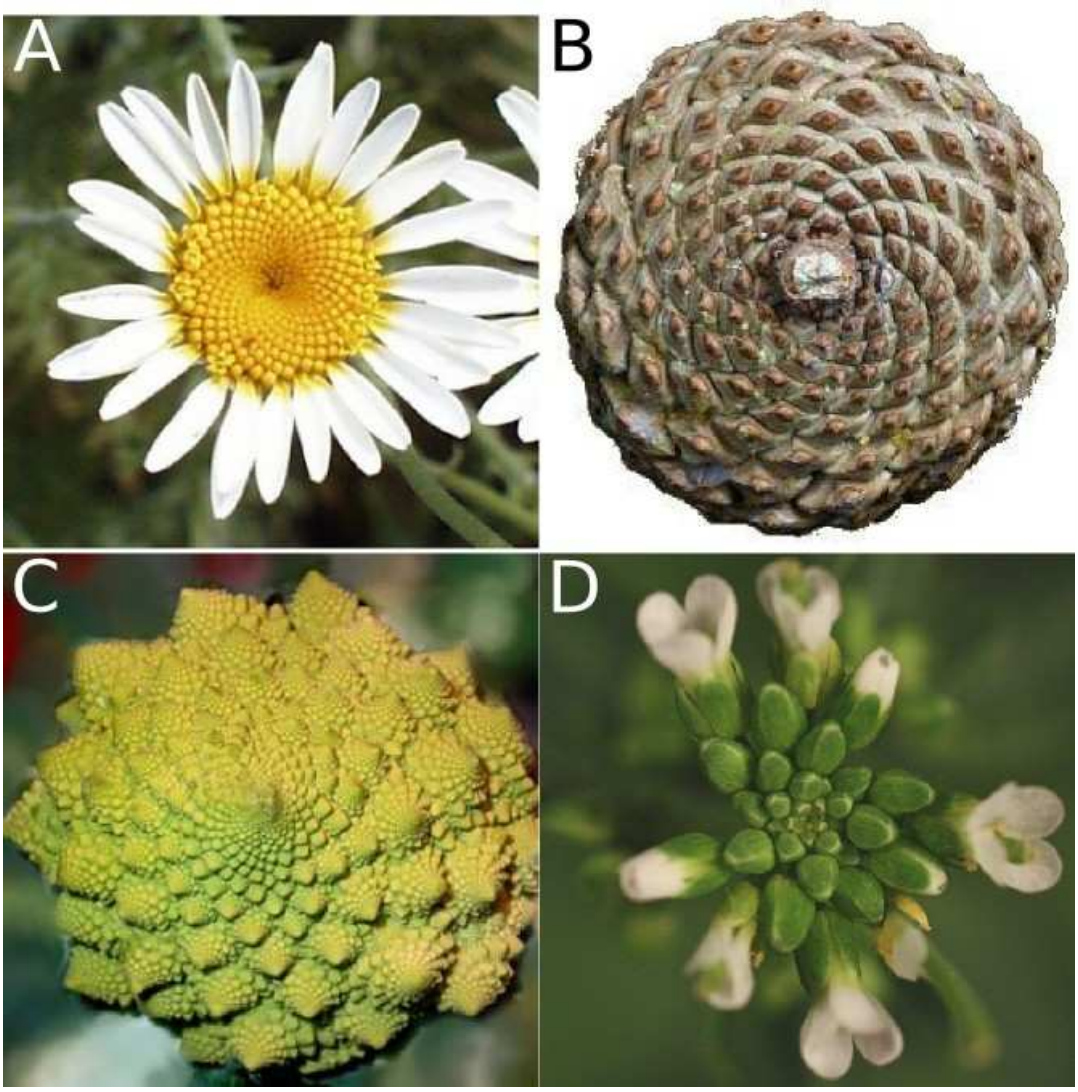

Figure 1: **Phyllotaxis is the geometrical pattern made by plant organs around axes.** Regular patterns of different types are generally present in the shoots of vascular plants. They are particularly conspicuous in compact botanical structures like the following: **(A)** a compound flower of a Daisy (*Leucanthemum sp.*), **(B)** a Pine cone, **(C)** an inflorescence of *Brassica oleracea* var. *Botrytis*, **(D)** an inflorescence of the model plant *Arabidopsis thaliana*. In all these examples, plants exhibit a spiral phyllotaxis, the most common arrangement found in nature.

Phyllotaxis in Plants, a field for developmental biology and interdisciplinarity

Phyllotaxis (from the greek taxis= arrangement and Phyllo=leaf) refers to regular patterns made by the particular arrangement of similar elements of a plants around the main axes, like leaves, buds, flowers or floral organs (e.g. petals or stamens)(Cris Kuhlemeier 2007). Indeed, from grasses to trees, plants with very different architecture and growth habit share a same feature: the disposition of organs around stems is never random and display obvious regularities. Phyllotaxis is conspicuous in many plants, notably in compact parts where organs stay in close contact, like leaves in a rosette or flowers in inflorescences. The scales of pine cones or the seeds of sunflowers are famous examples of complex and highly organized phyllotaxis (figure 1). More generally, spikemosses, horsetails, ferns and even some mosses also produce organs with a spatial regularity, indicating that phyllotaxis is a very common feature of apical shoot growth in a large majority of embryophyta (figure 2). Importantly, a stem-cell containing tissue at the tip of axis is responsible for the permanent production of organs and their special arrangement. In seed plants where it is well conserved, this tissue is composed of thousands of undifferentiated cells and is called the shoot apical meristem (SAM)(figure 3)(Barton 2010; Ha et al. 2010).

Considering phyllotaxis, two major types of questions can be asked by a biologist, asking either for a causal or a functional explanation of the phenomenon. First, what mechanisms can generate such patterns in a living organism? To answer this question, research is devoted to decipher the mechanistic principles, to identify the cellular behaviors and to reconstruct molecular networks involved in the process. The second question is: why such a mode of development has evolved? This requires to trace the history of aerial plant patterns and to identify the particular events and the selection pressures that have participated to the evolution and spread of phyllotaxis among land plants.

As a developmental biologist, I worked during my phD more on the “How” than the “Why”. However, these two questions are linked: some results concerning the developmental mechanisms may shed light on the evolution of such patterns.

Complex and organized patterns generated by living organisms are not specific to plants. They are very common in nature, especially in multi-cellular organisms. In the body of animals for example, the position of organ is not random, and the segmentation of the anterior-posterior axis is very regular in many species. However, plant patterns are very peculiar, because they are made of the repetition of similar units in a fractal arrangement and they are established dynamically. To this

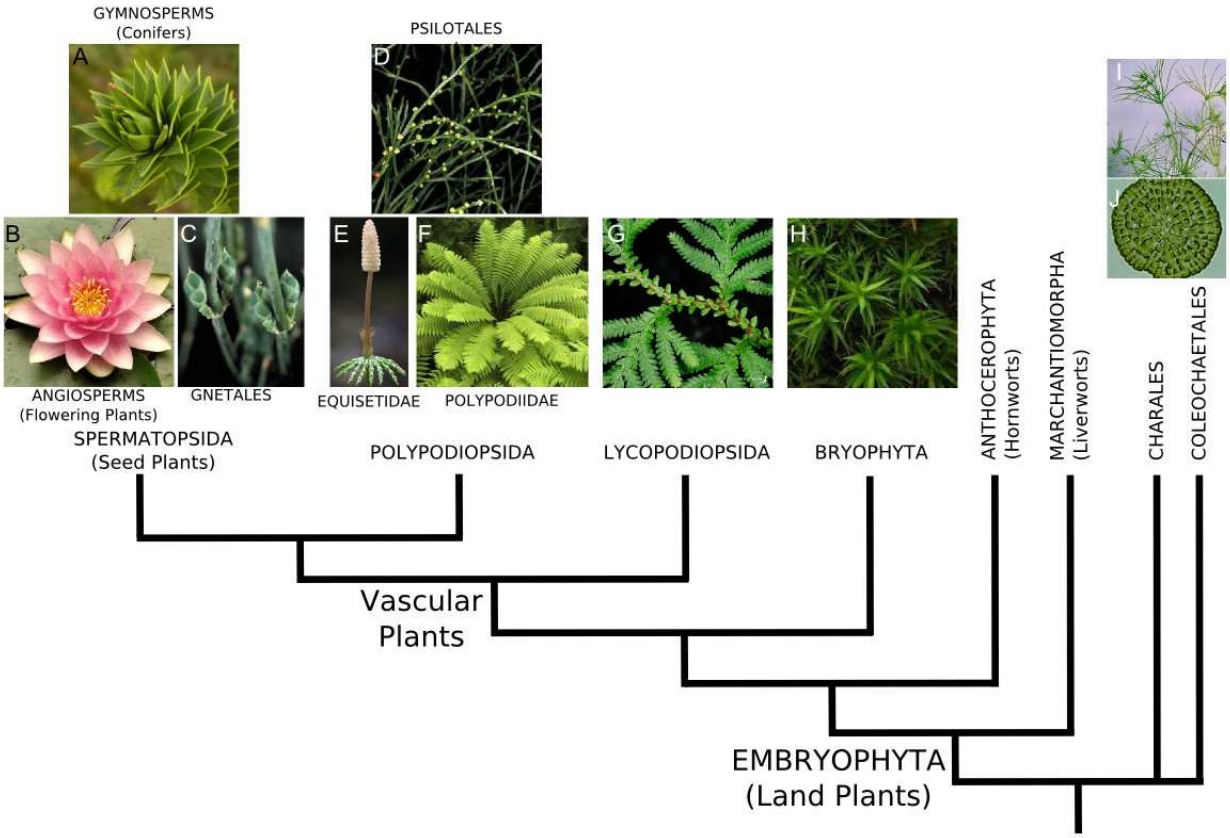

Figure 2: **Phyllotaxis is a feature shared by a vast majority of land plants**. Different examples of plant species belonging to the main phylogenetic groups of land plants (Embryophyta) are shown, with a schematic phylogenetic tree indicating their evolutionary relationships, including two green plant sister groups. Phyllotaxis may have appeared early in the architecture of land plant shoots, since it is also present outside vascular plants, in some Bryophyta species.
(A) *Araucaria sp.*, (B) *Nymphaea adorata* (Water lily) (C) *Ephedra antisyphilitica* (D) *Psilotum nudum* (Whisk fern), (E) *Equisetum pratense* (Horsetail) (F) *Cyatheales sp*. (Tree fern)(G) *Selaginella delicatula* (Spikemosses) (H) *Polytrichastrum formosum* (Moss) (I) *Chara* sp. (J) *Coleochaete*

respect, phyllotaxis has been often compared with the regularity of crystals or proteins aggregates, and “phyllotactic-like patterns” have been also described outside botany, e.g. in polypeptide chains (Frey-Wyssling 1954), or in bubbles floating on a liquid free surface (Yoshikawa et al. 2010). Moreover, in physical experiments, phyllotactic-like spirals were observed in different contexts: in a flux lattice of a superconductor (Levitov 1991b), with ferromagnetic droplets moving in a magnetic field (Douady & Y Couder 1992), with rotating magnets (Nisoli et al. 2009), or with core/shell microstructures self-assembled by controlled cooling (C. Li et al. 2005). These observations as well as the geometrical regularity of phyllotaxis make phyllotaxis quite unique among biological patterns and this raises the question of the specificities and the common points of these patterns between plants and inorganic systems (Shipman et al. 2011). For those reasons, the study of phyllotaxis has attracted scientists from different disciplines, like botanists, biologists, mathematicians, physicists or computer scientists and the history of the research on phyllotaxis is made of significant contributions from both theoretical works and experimental approaches (Adler et al. 1997).

In this introduction, I will review some of the most important contributions to the understanding of phyllotaxis, coming from different disciplines and based on various approaches. In a first part, I will present how the phenomenon of phyllotaxis can be understood at a macroscopic scale, from its scientific description and characterization to the discovery of the rules and principles likely controlling organ spacing in a shoot apical meristem (SAM). In the second part, I will describe the multicellular nature of the SAM, and the complex genetic and signaling networks controlling its behavior. In the third part, I will detail the role of a key regulator of organogenesis and phyllotaxis: the phytohormone auxin. Finally, I will present how other factors may contribute to the formation of the pattern, like mechanical signaling and in particular other hormones. This last point will lead us to underline actual unresolved questions of the field and to precise the objective I have been following during my doctoral studies.

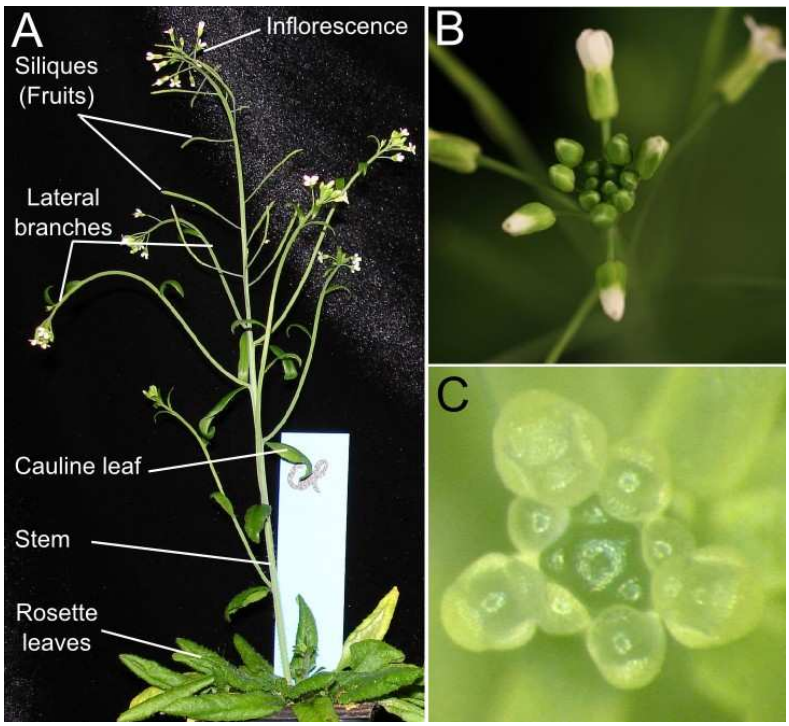

Figure 3: **Shoot Apical Meristems (SAM) produce all the aerial part of seed plants**. The model plant *Arabidopsis thaliana* is shown here. (**A**) Aerial part of a wild type plant of the columbia ecotype. The SAM is reponsible for the production of rosette leaves and, after floral transition, for the production of the stem, cauline leaves, lateral meristems and flowers of the inflorescence. (**B**) Detail of an inflorescence, showing oldest flowers blooming outwards and the highly organized phyllotaxy. (**C**) Dissected meristem: older flowers have been removed to let appear the SAM surrounded by very young floral buds. In those latter, emerging sepals can be seen, which fully cover the floral meristem of the oldest floral on this picture. Adapted from Vernoux *et al*, 2010.

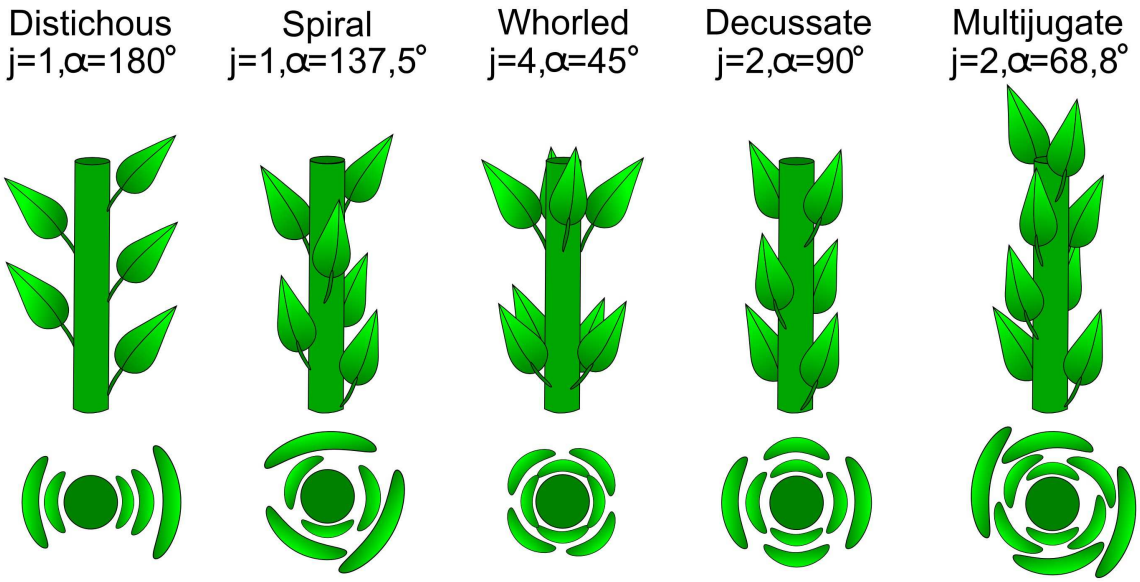

Figure 4: **Major types of phyllotaxis.** This classification takes into account the jugacy (j, the number of organs inserted on the same node in the stem) and the divergence angle (α) between organs in successive nodes. The multijugate type can be seen as a combination of whorled and spiral types and the decussate type as a particular case of multijugate phyllotaxis.

I. Phyllotaxis at a macroscopic scale: interactions between organs in the SAM

I.1. Describing phyllotaxis: the mathematical beauty of plants

A rapid examination of different plants shows that different phyllotactic patterns exist in nature. They are usually classified in 4 different types,(Cris Kuhlemeier 2007; B. Lee, Yu, et al. 2009) depending on the number of organ inserted at each node (termed jugacy) and the divergence angle between organs: distichous, spiral, whorled and multijugate, a mixture of whorls and spirals (figure 4 and figure 5). A first intriguing fact of phyllotaxis is that only this restricted set of arrangement exists among all the universe of possible regular patterns (Hotton et al. 2006). Moreover, spiral phyllotaxis is the most common arrangement (table1, A).

Changes in phyllotaxis are also often observed in the same plant, at different phases of growth. In dicots for example, the small embryo has two opposite cotyledons. Then, the developing seedling often starts with a decussate phyllotaxis (sets of two opposed leaves turn of 90º at each node, figure 4) and then makes rapidely a transition to spiral phyllotaxis, like in *Arabidopsis* (Cris Kuhlemeier 2007). In other species, the change in phyllotaxis is correlated to the transition from the vegetative to the reproductive phase: instead of leaves, the SAM produce flowers with a different phyllotaxis. (Meicenheimer 1982; Meicenheimer 1998; D Kwiatkowska 1995; Dorota Kwiatkowska 2008; D Kwiatkowska & Florek-Marwitz 1999; Meicenheimer & ZAGORSKAMAREK 1989). Finally, flowers which are meristems with a determinate growth, also have a typical phyllotaxis: most of the time, floral organs are inserted on whorls. Hence, a great diversity of phyllotaxis can be produced depending on the type of meristems and its developmental stage. A major challenge is to identify what genetic, developmental or environmental parameters in the SAM can control the type of the pattern.

To further characterize phyllotactic patterns, other quantitative parameters have been introduced in addition to the jugacy and the divergence angle: the plastochron ratio (F. Richards 1951)(the ratio between the distances to the axis center of two consecutive primordia) and the number of contact parastichies (figure 5). Contact Parastichies are spirals that catch the eye in densely packed structures: they are made by joining the closest organs and they define two sets of spirals, turning either clockwise or anti-clockwise. The pair (i,j) counting the number of spirals in each direction

Relative Frequencies of Phyllotactic patterns in Dicots-
Results from different surveys

A

Study	Species	Spiral and multijugate	Whorled exclusively	Mixture
Hutchinson in Meicenheimer, 1998	650	50,6 %	14,7 %	34,7 %

B

Study	Species	Number of Specimens	Fibonacci	Bijugate	Lucas	Accessories Series starting with (1,4,5)
Jean, 1994	650	12500	92 %	6 %	1,5 %	-
Weisse, 1894	*Helianthus annuus L.*	141	131	-	6	-
Schoute, 1938		319	262	9	46	2

Table 1. The survey (A) includes all kind of vascular plants while the surveys in (B) are only restricted to species having a spiral phyllotaxis.

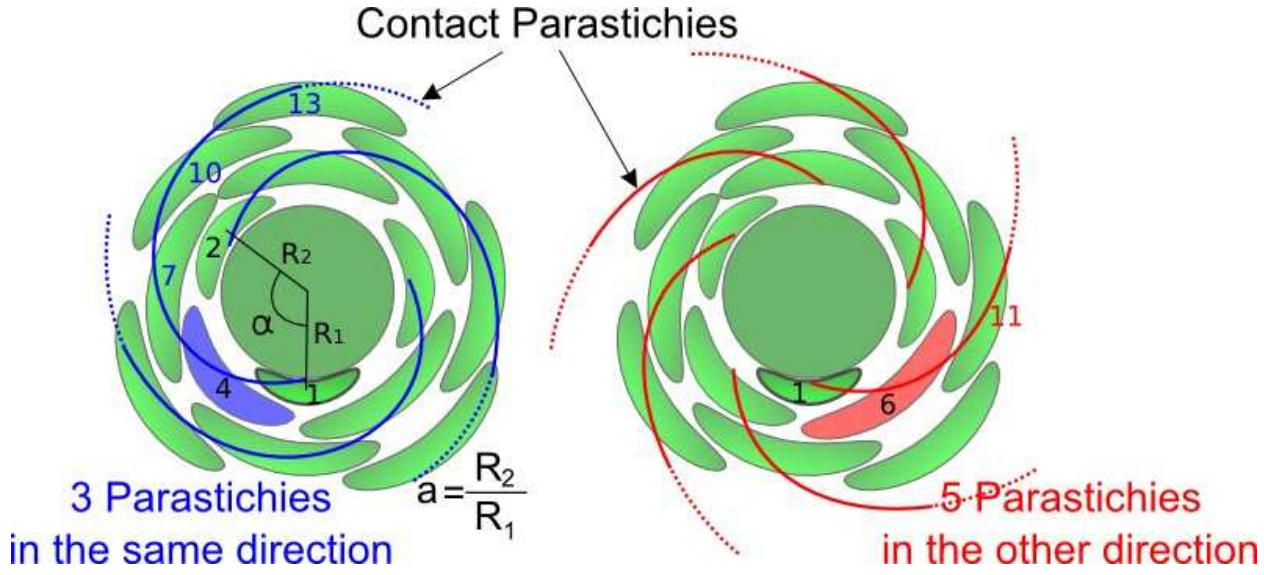

Figure 5: **Definition of some parameters used in the description and quantification of phyllotaxis**. Organs are numbered according to their order of apparition, the younger **α** is the **divergence angle** between successive organs (placed in two different nodes). In regular phyllotaxis, it stays constant at each iteration. $\mathbf{R_n}$ is the distance between the center of the meristem and the center of the organ n. $\mathbf{a}=R_n/R_{n-1}$ is Richard's **plastochron ratio**. α and a are thus sufficient to position a new organ (called primordium) appearing in the structure. The blue and red spirals linking the organs in direct contact are called **contact parastichies**. Two sets of parastichies exist: one winding to the left, the other to the right. The couple (i, j) of parastichies in each set is the **parastichy number**. For a (i,j) parastichy number, the nearest neighbors of a new primordium n are (n+i) and (n+j). In **Fibonacci spiral**, the number of spirals in these two sets are two consecutive numbers of the Fibonacci series. In this example, 3 parastichies turn to the right (blue) and 5 to the left (red), defining a (3,5) Fibonacci spiral.

defines the parastichy numbers. Studying the geometry of phyllotactic patterns, many scientists revealed puzzling mathematical properties hidden in these parameters.

Particular numbers seems to be linked to the description of contact parastichies and divergence angle: the numbers of the Fibonacci sequence and the golden angle, 137.5º, that derives from it. Described first in the 13th century by the Italian mathematician Leonardo Fibonacci, this infinite series is defined as follows: it begins with 0 and 1 and each new term is the sum of the two preceding ones. The sequence is thus <1,1,2,3,5,8,13,21,…> and the ratio of two consecutive terms 2/1, 3/2, 5/3,… tends to a fixed limit $\tau=\sqrt{(5+1)/2}$, the golden number. The golden angle 137.5º is obtained by sectioning a circle according to the golden number (given the formula $360-(2-\tau)$). In the vast majority of plant with a spiral phyllotaxis, the measure of divergence angle gives a similar value which is very close to the golden angle. The reference to the golden angle was first found by expressing the divergence angle as a fraction of a turn (Schimper 1830). Consider a stem of a plant with leaves arranged in spiral, pick up one leaf and find the leaf directly above it, when looking from the top: the mean divergence angle is the ratio between the total rotation in degree around the stem in the ascent from the lower leaf to the upper (several turns can be done) and the number of leaves inserted in between (figure 6). For most plants, the divergence angle in ratio will be a fraction of 2 alternate terms of the Fibonacci sequence: 1/2, 1/3, 2/5, 3/8, etc. However, in real plants, two leaves are never exactly one above the other. Expressing divergence angle as rational numbers could thus appear arbitrary. Yet, the Fibonacci sequence is also present in the parastichy number. Indeed, the numbers of parastichies winding either to the left or to the right are generally two consecutive terms of the sequence (A. Braun 1831; A. Braun 1835). Using lattices, a mathematical representation made of helices on a cylinder or of spirals on a disk, it can be demonstrated that when contact parastichies are Fibonacci numbers, the divergence angle is close to the golden angle and rapidly converges to it as the number of parastichies increases (L. Bravais & A. Bravais 1837). Moreover, other spiral arrangements have been described with similar properties. The Lucas spirals have parastichy number belonging to the sequence <1,3,4,7,11 …>, a Fibonacci-like sequence with starting terms 1 and 3, and a divergence angle converging towards 99°30. Another divergence angle of 77°57 corresponds to the sequence <1,4,5,9,14 …>. Surveys among spiral phyllotaxis indicate that Fibonacci spirals are the most frequent (table 1B). Interestingly, in the same species (e.g. the sunflower, table 1B), various types of spirals can coexist, but Fibonacci spirals are still the most common. This suggests that a mechanism of similar nature is able to

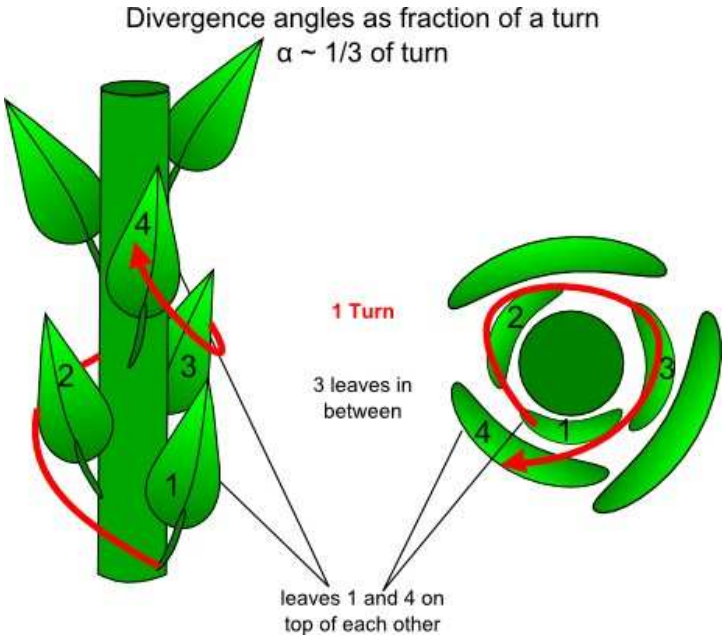

Figure 6: **Expressing the divergence angle as fraction of a turn**. In this example, the divergence angle α is 1/3 of a turn.

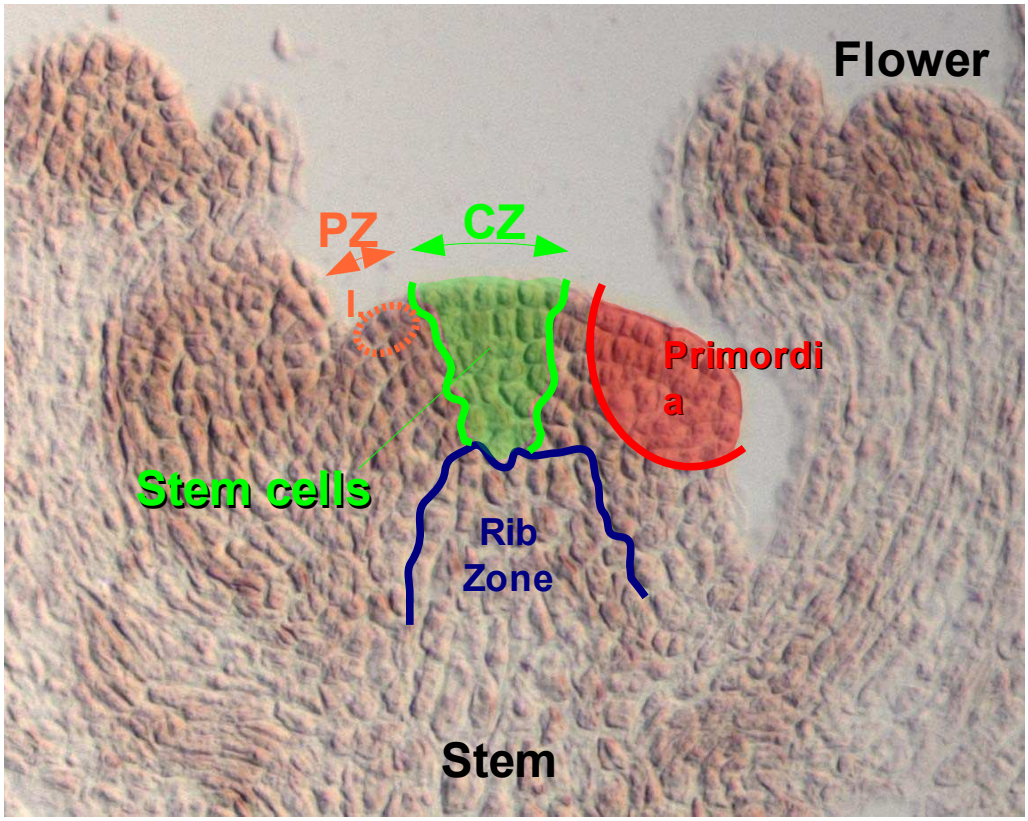

Figure 7: **Functional zonation of the shoot apical meristem**. Longitudinal section of an inflorescence meristem of *Arabidopsis thaliana*. At the meristem summit the central zone (CZ) contains the stem cells, whereas primordia are initiated as initium (I) in the peripheral zone (PZ). The rib zone (RZ) produces the internal part of the stem. Adapted from Vernoux *et al*, 2010.

generate these different patterns, and that some parameters of plant growth favor the Fibonacci arrangements.

The description of phyllotaxis using mathematical laws has been a point of debate for decades. Presented as the design of god before Darwin, the existence of the golden angle and Fibonacci numbers was hard to explain after the elaboration of the evolution theory. Many biologists considered that it was nothing but an irreducible subjectivity and that their use was meaningless for understanding phyllotaxis (J. Sachs 1882). Of course, these works do not provide any explanations for the generation of phyllotaxis. However, they were very helpful for classifying and characterizing phyllotactic patterns and they point out interesting properties of phyllotaxis. Thus, they have motivated an important community of scientists to study phyllotaxis and influenced both theoretical and experimental research.

I.2. Experiments in Phyllotaxis: the model of inhibitory fields in the shoot apical meristem

To understand the ontogeny of phyllotaxis, it is necessary to look more closely to the place where organogenesis takes place: the shoot apical meristem (SAM). This dome-shaped tissue is composed of self-renewing stem cells at the center (figure 7). Bulges called primordia (P) emerge in a stereotypical manner and develop into lateral organs (leaves or flowers for example). A Primordium first appear as a small bump of cells called initium (I), located adjacent to the central stem cell domain, in the so-called peripheral zone. Observing a large number of different meristems, Hofmeister (1868)formulated this phenomenological rule: new primordia appear periodically at the periphery of the meristem in the largest gap between the edges of older primordia. This rule suggests that the position of a new organ depends on interactions with the primordia already there. In mechanistic terms, each primordium would be the source of an inhibitory field that prevents the formation of another organ nearby. Very early, two different natures have been postulated for those fields: they could be either biophysical (Schwendener 1878; Delpino 1883; Airy 1873; P. Green et al. 1996) or chemical (Schoute 1913; F. Richards 1948; Wardlaw 1949b; Wardlaw 1949a).

According to this hypothesis, eliminating a primordium in a meristem should modify the positioning of younger neighbor primordia. To test this, Snow and Snow (1932; 1933) initiated a series of microsurgery experiments in meristems: they isolated a primordium or an initium from the

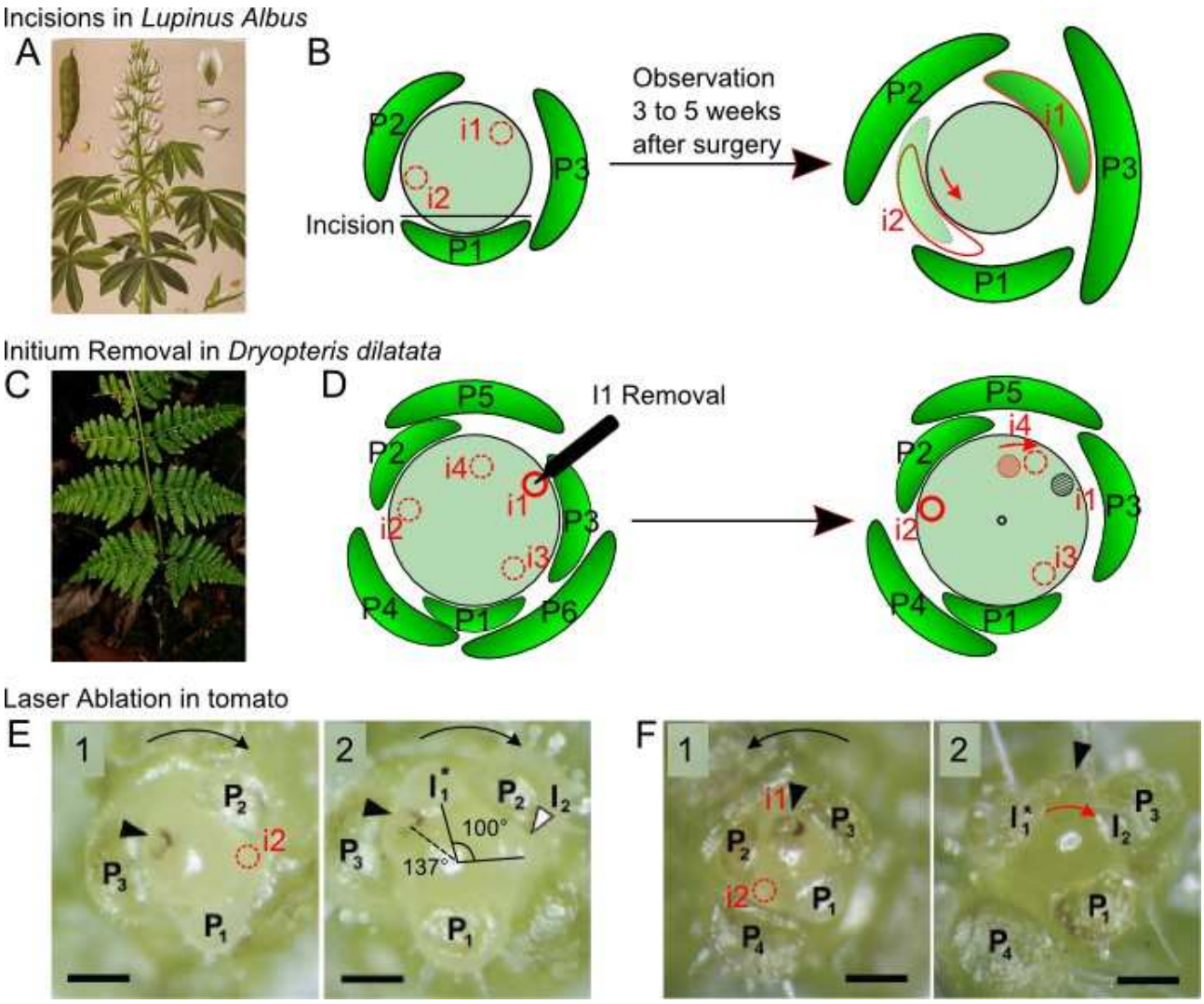

Figure 8: **Experimenting phyllotaxis by microsurgery on meristems**. (**A-B**) Isolation of primordia by tangential incisions (Snow and Snow). (**A**) Drawing of *L. albus*. (**B**) Isolation of P1 results in a shift of the development site of i2 towards P1 (red arrow). (**C-D**) Surgical ablation of initium site (Wardlaw). (**C**) Picture of the fern *D. dilatata*. (**D**) After i1 ablation, i4 develops closer to the ablated site (red arrow). (**E-F**) Laser ablation of initium site in tomato (Reinhardt). The black arrowhead points to the ablated site. Photographs are taken 1 day (1) and 3 days (2) after ablation. (**E**) A new initium (I1*) forms just adjacent to the ablated region, resulting in a altered I1*-I2 divergence angle (smaller in the example of the picture).(**F**) I1* initiates at ectopic positions between I1 and I2, resulting in a reversal of the phyllotactic spiral from an anti-clockwise (back arrows in 1) to a clockwise direction (red arrow in 2). Expected site of I2 in picture 1 is indicated by a dashed red circle. The first situation (E) was observed in 50% of cases, the second (F) in 12% of cases. Pictures adapted from Reinhardt *et al*, 2003.

remainder of the meristem through tangential incisions in *Lupinus albus* (figure 8A,B). They let the plant grow for 3 to 5 weeks, and then observed divergence angles between newly initiated leaves. *Lupinus* have a spiral phyllotaxis of low order (2,3 parastichies). Direct neighbors of an organ n are thus n+2 and n+3 (the 2^{nd} and 3^{rd} organ produced after the organ n), but in this small meristem, n+1 is also close. They always observed that the n+1 was initiated at its expected position, whereas n+2 was displaced towards the isolated organ. This supports the idea that the position of incipient primordia is not prefixed and depends on positional information given by direct neighbors: organs repel the formations of younger organs away from their close vicinity. After the perturbation, the pattern returns quickly to normal divergence angles after a few plastochron (the plastochron is the time separating two organ initiations). This also highlights the robustness of phyllotaxis. Recently, Reinhardt (2005) reproduced these experiments on tomato: this time, they monitor the apparition of new primordia directly in the meristem, just after surgery, to control that the site of initiation was effectively displaced. They confirmed the results of Snow and Snow, demonstrating that organ repositioning was not due to late wounding effects and post-meristematic growth. Tomato has the same (2,3) spiral phyllotaxis as *Lupinus*. However, Wardlaw (1949a) also obtain similar results in a fern, *Dryopteris dilatata*, with a (3,5) spiral phylloyaxis (figure 8C,D): surgically removing I1 led to the displacement of I4 (n+3) towards I1. This shows that the positioning of organ through local interactions with direct neighbors seems to be conserved among vascular plants with different order of the Fibonacci spiral. Reinhardt (2005) also performed precise ablations of incipient I1 using infrared laser beam in tomato (Reinhardt et al. 2005). This modern technique limits the damage of the meristem and let more space in the peripheral zone for new organ initiation. Most of time, a new initium (I1*) arises just adjacent to the ablated region (figure 8E). This is in agreement with the idea that the ablated I1 was inhibiting organogenesis around. After this perturbation, other initia are positioned normally and the spiral restores quickly with normal divergence angles. In some cases, I1* is displaced further away from ablated I1: this time I2 is also misplaced and a new spiral starts in the opposite direction (figure 8F). This observation again demonstrates the stability of spiral phyllotaxis, which can restore once the initial disturbances are overcome.

These first experiments brought convincing data concerning the existence of local interactions between primordia. Another question concerned the periodicity of organ formation: is the plastochron fixed by unknown independent factors or does it emerge from the dynamic interactions between primordia? It is hard to perturb experimentally the plastochron. Yet, Snow and Snow indirectly did it in a microsurgery experiments on *Epibolium* hirsutum (figure 9)(M. Snow & R.

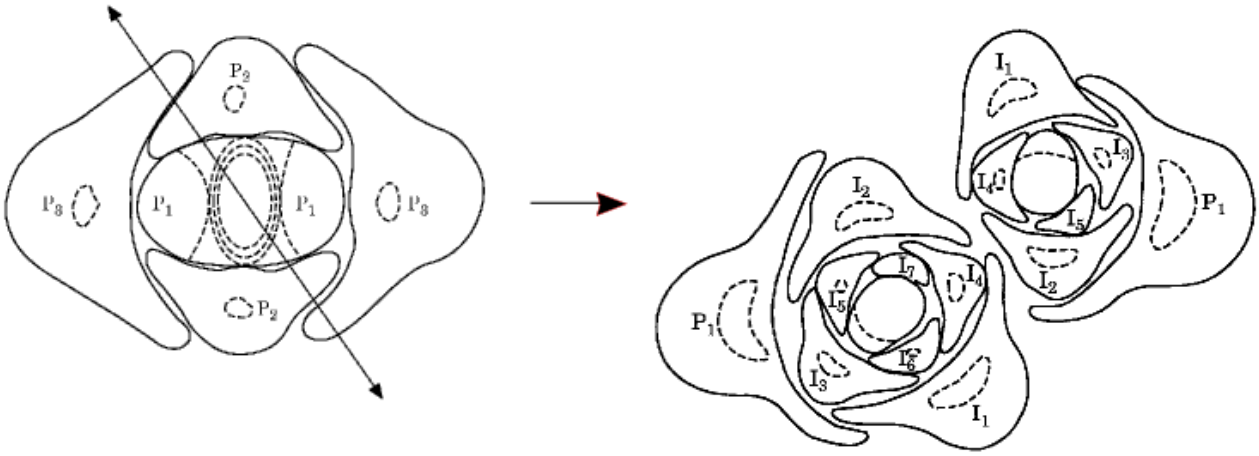

Figure 9: **Switch from a decussate to a spiral phyllotaxis**.i**nduced by microsurgery (Snow and Snow, 1935).** A normal decussate apex of *Epilobium hirsutum* was slitted diagonally along the arrow. Later, the two regenerating halves formed independent meristems which started a spiral phyllotaxis. Adapted from Snow and Snow, 1935.

Snow 1935). This plant has a decussate phyllotaxis: this means that two organs form at the same time (null plastochron) and the two next are initiated one plastochron later. Snow and Snow slitted diagonally the SAM in two halves, by breaking the symmetry imposed by two opposed leaves in a node. Surprisingly, they observed that each part recover as an independent SAM with a spiral phyllotaxis, where only one organ emerges at a time. This suggests that the plastochron is not fixed in a meristem and that the periodicity of organ initiation emerge from the interaction between organs. Moreover, these dynamic interactions may not be constrained by the identity of the meristem (its genetics, its structure, etc.), because the same meristem can produce different patterns after this microsurgical manipulation. Here, the switch between decussate and spiral phyllotaxis was attributed to a change in the initial symmetry (see later the results from modeling, I.3). This with other data (RICHARDS 1951) led them to propose a new rule for phyllotaxis: an new organ simply initiates in the peripheral zone where and when a sufficient space is available for its formation.

Altogether, these experiments strongly support the model of lateral inhibition for organogenesis and the control of phyllotaxis. However, these interactions are only local and they do not explain how complex regular patterns can be created at higher scale, like in a whole inflorescence. A holistic mechanism controlling the global pattern is though hard to conceive. Could the phyllotaxis simply be an emergent property of the local interactions between nascent organs? This is typically the definition a complex system: it is composed of a set of entities interacting together with simple rules and on the whole, it exhibits properties that are not obvious from the properties of the individual parts. However, the emergent behaviors are not obvious, especially when interactions between entities are not linear. Abstract and computational modeling are then very efficient tools to explore the possible outputs of such systems.

I.3. Modeling Phyllotaxis: a dynamic self-iterative process of pattern formation

I.3.1. Understanding the properties of phyllotaxis by theoretical models

Given our previous considerations (I.1 and I.2), relevant models of phyllotaxis should reproduce the follwing properties observed for phyllotaxis:

- Organ positioning generates geometric regular arrangements

- Only a restricted set of regular arrangement exists in nature
- Among them, Fibonacci spirals are the most common
- Patterns can arise *de novo*, from radially symmetric embryo or from new meristems (such as axillary shoot meristems or flowers)
- Patterns must propagate stably during development
- Transition between patterns are frequent, especially between decussate and spiral
- The pattern is robust and can recover from small perturbations

A model however would never be a definite proof that the mechanism implemented is true. Thus, models are often used as a test for particular mechanisms. More generally, they can be used to determine what characteristics of a system are necessary and/or sufficient to reproduce the expected behavior, even if the precise microscopic mechanism is unknown. To this purpose, abstract models are attracting, because they do not require precise cellular and molecular parameters which are most of time not available. Besides, their conclusions can be powerful, since they point out general characteristics compatible with a wide range of microscopic mechanisms. However, they should be interpretable in biological terms so as to provide predictions and fuel further experiments. A fine balance must thus be found between abstraction and realism in models.

Many theoretical models of phyllotaxis have been elaborated since the beginning of the 20th century (Adler et al. 1997). They are all deterministic and can be interpreted as attempts to model self-organization from interacting primordia. What can we learn from them? First, they all reproduce at least some phyllotactic patterns observed in nature, notably Fibonacci spirals. Second, dynamical system models demonstrated that the patterns can be maintained over several iterations. Third, they often provide mathematical formula correlating the different phyllotactic parameters. This suggests important control parameters of phyllotaxis that could be biologically regulated. Four, their important contribution is to suggest possible mechanisms, by implementing different abstract principles coming from geometry, mathematics and physics. We can notably cite models based on basic assumptions like piling of a surface with solids of finite size (Iterson 1907), maximization of the minimum distance between primordia (Adler 1974), minimization of an entropy-like function under some constraints (Jean 1994) maximization of the energy of repulsion (Levitov 1991a; Levitov 1991b) or principle of minimal energy (Douady & Y Couder 1992). However, the principles tested are sometimes hard to translate into biological reality. Biologists expect some rules compatibles with the experimental conclusions of Hofmeister or Snow and Snow. To implement

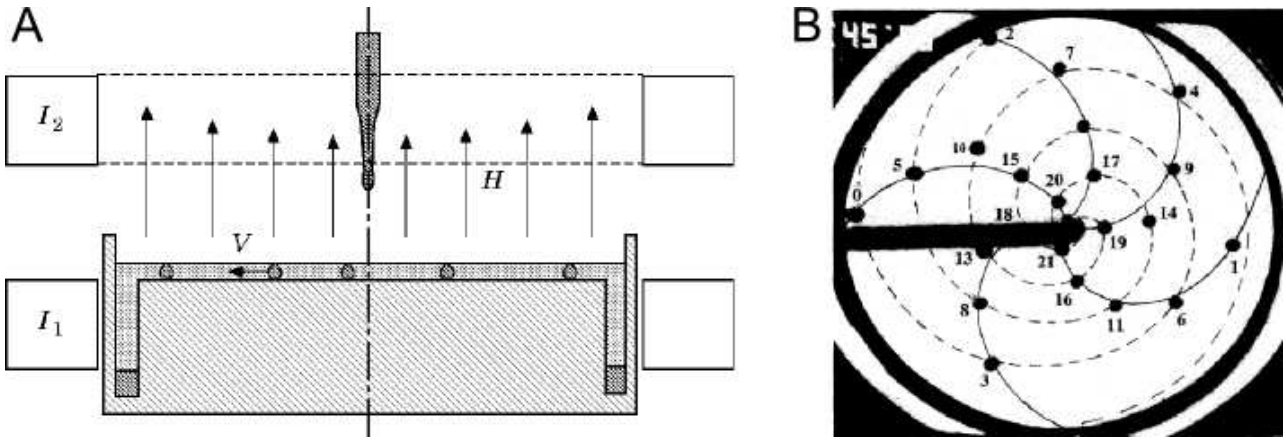

Figure 10: **Modeling Phyllotaxis as a physical dynamical system (Douady and Couder, 1992)**. (**A**). Sketch of the experimental apparatus. Drops of ferrofluid are used to simulate the primordia. The drops fall with a tunable periodicity T at the centre of a horizontal teflon dish The vertical magnetic field H is created by two coils in the Helmholtz position. The dipoles are radially advected with velocity V by the magnetic field gradient (controlled by the currents I_1 and I_2 in the two coils). The drops ultimately fall into a deep ditch at the periphery, designed to prevent accumulation. (**B**) Photograph of an experimental pattern. The drops are visible as dark dots. The tube for the ferrofluid supply partially hides the central truncated cone. The drops are numbered in their order of formation. From Douady S. and Couder Y., 1996a.

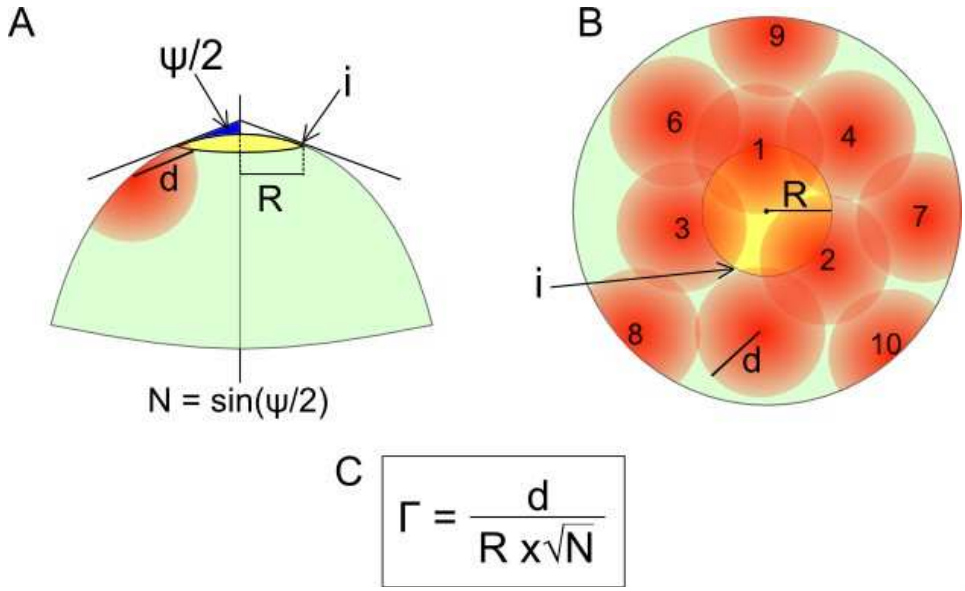

Figure 11: **Modeling organ interactions in meristems (Douady and Couder, 1996)**. (**A**) The meristem shape is simplified into a paraboloid. The peripheral zone where organs are initiated is approximated by the cone tangent to the apex at this level. The central non-organogenetic domain (yellow) is characterized by its radius R. Each primordium emits a repulsive energy (red circle). This energy decreases with distance and the repulsive field is characterized by d, the distance from the organ center where the energy no longer inhibits organogenesis. The parameter N depends on the geometry of the apex (1/N is called the conicity). (**B**) Top view of a meristem (1/N=1, all fields are circular). The repulsive energies from different organs can be added in the peripheral zone. i indicates the place where the next initium will form. (**C**) Phyllotactic patterns generated by the model depend on the control parameter Γ.

these rules in models, approaches based on dynamical systems are pertinent (Hotton et al. 2006). First, they mimic the sequential production of organs (one or several at each step). Second, a deterministic rule governs the position of the new primordium/primordia appearing at each iteration: it can thus be chosen to implement inhibitory fields. Choosing a geometry of the system similar to a growing apex could also be instructive. Modeling dynamical systems requires computing power and these approaches only begun to be used for phyllotaxis in the 80's, and has really been developed during the last two decades e.g. (Williams & Brittain 1984; Schwabe & Clewer 1984; Kunz 1997; Koch et al. 1998; d' Ovidio & Mosekilde 2000; Atela et al. 2002; Hotton et al. 2006). Among those, the work of Douady and Couder (DOUADY & COUDER 1992; Douady & Couder 1996a; Douady & Couder 1996b; Douady & Couder 1996c) is a landmark and it is sometimes considered as a new paradigm in the study of phyllotaxis (Shipman & Newell 2005). We will next detail their work to illustrate how meaningful and instrumental such an approach can be.

I.3.2. The model of phyllotaxis proposed by Douady and Couder supports the Inhibitory fields theory of Snow and Snow.

Douady and Couder focused on the dynamics of the process *per se*. They thus simplified phyllotaxis to a system with iterative apparition of new elements of finite size, representing primordia, in an axisymmetric circular structure, representing the meristem. Old primordia move radially outward with time, this movement representing growth. They then translated in their model either the rule of a fixed plastochron (that they called the Hofmeister'rule, (Douady & Y Couder 1996a) or the rule of non-fixed periodicity (based on Snow and Snow hypothesis, (Douady & Y Couder 1996b) to determine how new organs appear at each iteration. In the Hofmeister rule, primordia arise at a fixed period of time in the largest space available at the apex periphery. The Snow and Snow rule postulates that a new primordium appears where and when the minimal space for primordium is available in the peripheral zone. In both assumptions, the position of a new primordium depends on the space left by the previous ones. This interaction was modeled by repulsive fields surrounding each primordium. A key aspect is that the postulated form of this inhibitory field is compatible with experimental studies and is sufficiently general to be explained by various biological mechanisms. Douady and Couder tested their hypotheses by two methods. First, they used an ingenious physical experiment (Douady & Y Couder 1992; Douady & Y Couder 1996a)(figure 10): they periodically deposited droplets of a ferromagnetic fluid at the center of a

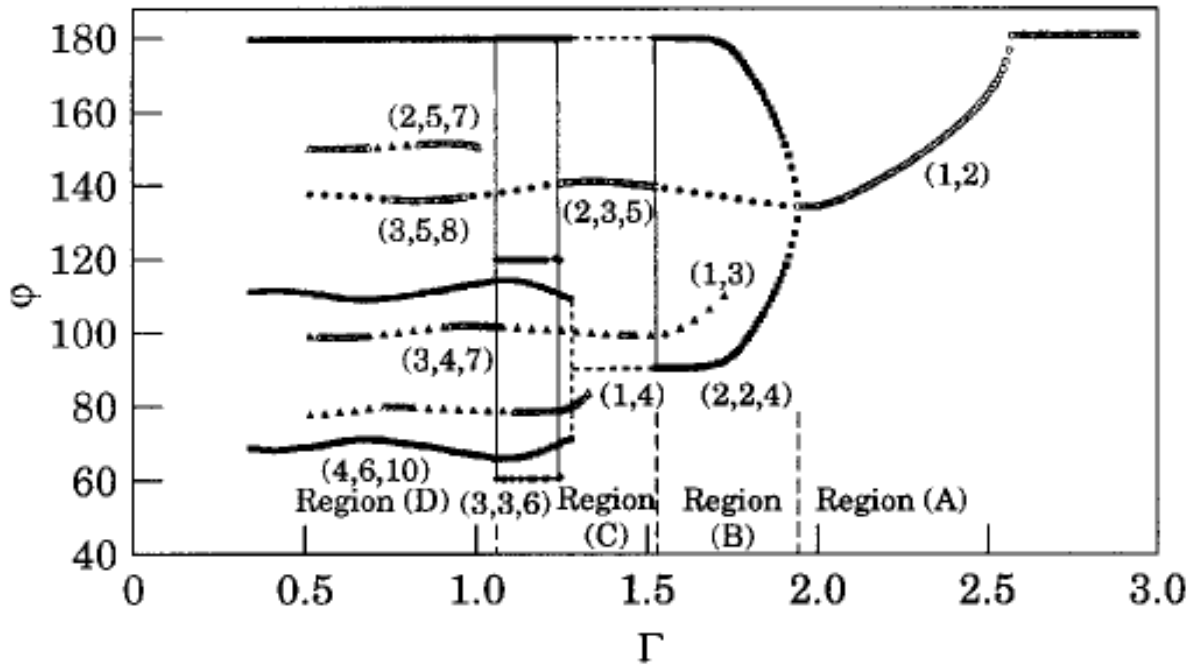

Figure 12: **Phase diagram of phyllotaxis explained by the control parameter Γ (Douady and Couder, 1996c).** The value of the diverge,ce angle φ depends on the value of the parameter Γ. The different region correspond to the existence and co-existence) of different types of phyllotaxis. The Fibonacci branch is continuous in this diagram and converges to the golden angle with successive higher order. Numbers in brackets indicate the number of contact parastichies.

plate submitted to a magnetic field. Each drop, representing a primordium, repels other drops and is also advected to the periphery of the plate by the magnetic field. By imposing the periodicity of the fall of drops, they simulated the Hofmeister's hypothesis. Second, they extended their study with numerical simulations to test both hypotheses (figure 11).

A key result is that they obtained in each case realistic phyllotactic patterns, demonstrating that both hypotheses were sufficient to create a regular self-organization. Beacause of its design, the model they used to simulate the Hofmeister rule could not give whorled or multijugate arrangements (sine only one organ can be made at a time). However, they discover that periodicity could emerge from the dynamics of the system, as postulated by Snow and Snow. The implemented "Snow and Snow" hypothesis could indeed generate all phyllotactic modes, and only these arrangements, as expected for a relevant model. Their model can generate *de novo* patterns or propagate them, and is also robust to small perturbations. From their study, we can conclude that this parsimonious hypothesis is a plausible minimal rule for self-iterative dynamical systems to produce phyllotactic patterns. In other words, if a primordium appears in the peripheral zone when and where the sum of the inhibitory fields of older primordia is below a certain threshold, phyllotactic patterns with global geometry can arise spontaneously from these local interactions.

I.3.3. The lessons from the model: answers, predictions and limits

Apart from the validation of inhibitory fields as a plausible ontogenic principle for phyllotaxis, their study gave also significant results meaningful for a better understanding of the principles underlying the dynamics of phyllotaxis. This can be simply summarized by a phase diagram where all phyllotactic modes (identified by the divergence angle φ in this diagram) are function of a unique control parameter, Γ (figure 12). This phase diagram, first obtained by van Iterson (1907), is now a common result of all deterministic modeling of phyllotaxis (Barabé 2006). In the work of Douady and Couder, Γ is a dimensionless parameter given by $\Gamma=d/\sqrt{N}/R$, where d represents the size of the inhibitory field of a primordium, N the conicity of the meristem and R the size of a central domain where no organ can be initiated (figure 11). Biologically, this domain encompasses the stem cells zone where no organogenesis occurs. The measure of Γ is not really accessible on plants: the actual size of the inhibitory field is unknown and R is also hard to determine. However, it can be shown that $\Gamma=\ln(a)$, where a is the plastochron ratio, which can be measured on plants (F. Richards 1951; Barabé et al. 2009). As a result, phase diagrams provides a link between

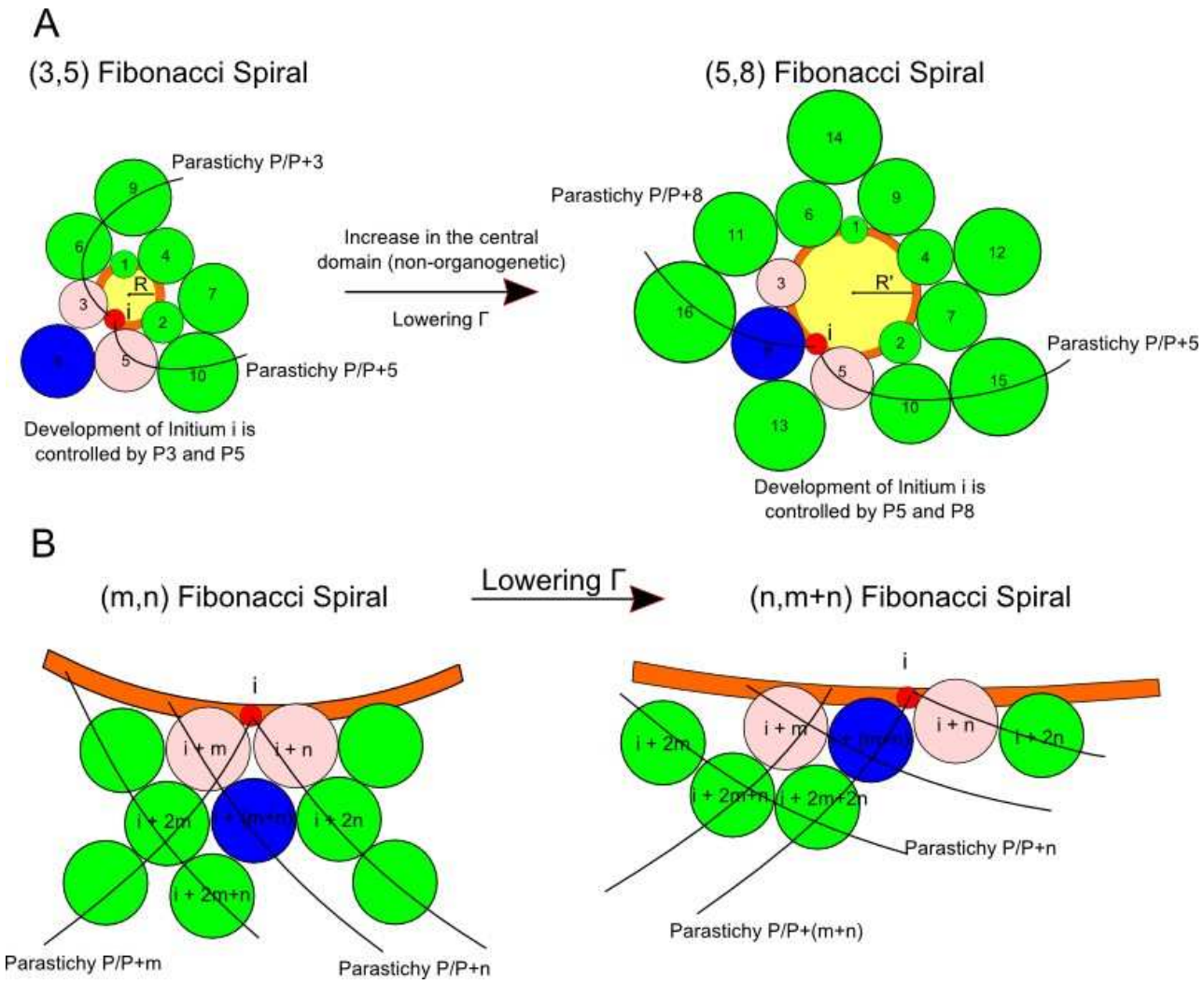

Figure 13: **Geometrical scheme explaining transitions of phyllotaxis in the Fibonacci branch upon decrease of parameter Γ.** (**A**) Transition from a (3,5) phyllotaxis to a (5,8) phyllotaxis. The blue organ become closer to the initium i, defining new direct neighbors and new parastichies. (**B**) Generalization to the transition of a Fibonacci spiral of order (m,n) to order (n, m+n).

observations and models, and here the parameter Γ suggest to study particular biological parameters and processes.

The first lesson is that the topology of the meristem, namely an axisymmetric meristem with a peripheral organogenetic zone surrounding a central non organogenetic domain is important for the generation of phyllotactic patterns. Second, in the diagram, the lower Γ is, the higher the phyllotactic mode (with numerous contact parastichies). In nature, this correlation is indeed observed: plants with a big meristem compared to the size of organ have also higher order phyllotaxis, as seen for example in the sunflower capitulum.

But why are Fibonacci spirals so common in nature?. In plants, measures of plastochron ratio or just meristem size suggest that Γ changes at different phases of growth: it generally decreases when the seedling produces its first leaves, or at the onset of the vegetative to reproductive transition. Many studies showed that these changes in the SAM size correlate with changes in phyllotaxis e.g. (Meicenheimer 1982; Meicenheimer 1998). It can also shrink later, at the end of the reproductive phase (e.g. sunflower). Thus, transition between patterns in a same plant could be due to the evolution of Γ during development. In the phase diagram Γ can follow different branch upon decrease. However, only one brancj is continuous, and it contains the Fibonacci spirals (figure 12). It can be rigorously demonstrated that in theory, transitions are more likely to occur along continuous branches of the phase diagram (Atela et al. 2002), but this property can be explained simply by geometrical diagrams (Douady & Y Couder 1996a)(figure 13). Indeed, this continuity is due to geometric relationships of neighborhood at the periphery of the apex: as Γ decreases, old primordia in the periphery are packed, creating new distances between primordia. In a spiral Fibonacci with (m,n) parastichies, the newly formed initium *i* is closer to organs (*i*-m) and (*i*-n) before Γ change, and gets closer to (*i*-n) and (*i*-(m+n)) after Γ change (figure 13). The presence of older parastichies thus constrains the system to stay on the same branch. Since all seedlings start with high value of Γ, this would explain the prevalence of Fibonacci spirals in plants.

How can we then explain other arrangements? In the diagram, for a given value of Γ, different arrangements are possible in addition to Fibonacci spirals. To understand the selection of a pattern, Douady and Couder identified three factors: compactness of the structure, initial conditions and temporal evolution of Γ, governed by the ontogeny of the plant. They first show that, the most compact structure tends to be selected at steady regimes for a given Γ. They predict that higher conicity of the apex can thus explain decussate or whorled phyllotaxis instead of spiral modes for identical Γ, because it increases the compactness. However, steady regimes sometimes require

several hundred of iterations before reaching the most stable arrangements. In Plants, unstable modes could still exist as transients, because only a limited number of organs are produced over plant lifespan. Moreover, the actual phyllotaxis of a plant is greatly influenced by the initial disposition of organs and the evolution law of Γ. In their model, a quick decrease of Γ could promote the transition towards less frequent branches of the diagram, such as the branch of Lucas spirals. Once on this branch, the system stays on it even upon further decrease of Γ. To test all these predictions, Couder (1998) studied naturally grown sunflowers: he observed that phyllotaxis of leaves around stem is always is of the same type (Fibonacci, Lucas or multijugate) as the phyllotaxis of the capitulum, albeit with less parastichies. This confirms that during the formation of the capitulum and the concomitant decrease of Γ, the organization of phyllotaxis stayed on the same branch. Moreover, he also observed alternative phyllotaxis (Lucas, bijugate or trimerous phyllotaxies), at low frequencies (table 1B). Trying to reproduce *in silico* these alternative patterns using the dynamical system model previously elaborated, he only obtained them for a narrow range of parameters concerning the evolution of Γ, which could explain that they are very rare in nature .

This theoretical work has thus brought significant responses to many questions concerning phyllotaxis. However, some peculiar biological patterns like the ridges and planforms of some cacti cannot be explained by the model (Shipman & Newell 2005). Besides, the authors mainly focused on regular patterns. Although they mention irregular patterns, as those encountered in some plant species, e.g. in magnolia flower (Zagorska-Marek 1994) or in mutant plants (Golz & Andrew Hudson 2002; Barabé 2006), they did not study them in particular. For this reason, Douady and Couder's model cannot be considered as universal. However, it still provides a rich framework to further explore the biology of the phenomenon. Indeed, this model does not identify the underlying physiological processes governing phyllotaxis, but it indicates some rules any candidate mechanism should be compatible with. We list here some biological questions opened by this work:

- In meristem, development of primordia is continuous and not discrete as in the model. However the tissue is segmented by discrete cells. How do these parameters alter the dynamics of the model?
- The emergence of organs, by mobilizing cells from the peripheral zone adjacent to the central domain, modifies continuously the geometry of the apex. How is maintained the stability of the central zone over time? How is controlled the stability of meristem shape (the conicity is predicted to be important by the model)? These questions emphasize that

unlike simplified models, the whole meristem structure is self-organized, and not only the positioning of organs.

- What is the mechanism controlling the apparition of primordia?
- What is the nature of the inhibition between neighboring primordia?

To understand the nature of phyllotaxis at a microscopic scale, it is thus necessary to know the cellular organization of the SAM and to explore the main genetic and developmental regulations controlling its structure, organization and homeostasis. If phyllotaxis emerges from interactions between organs, organs are themselves composed of many cells. The next step is then to analyze how the cells located in different part of the SAM communicate and interact to create a regular pattern and to generate organ interactions. The following sections (II, III and IV) are adapted from a recent review article I wrote under the supervision of T. Vernoux and O. Hamant (Besnard et al. 2011).

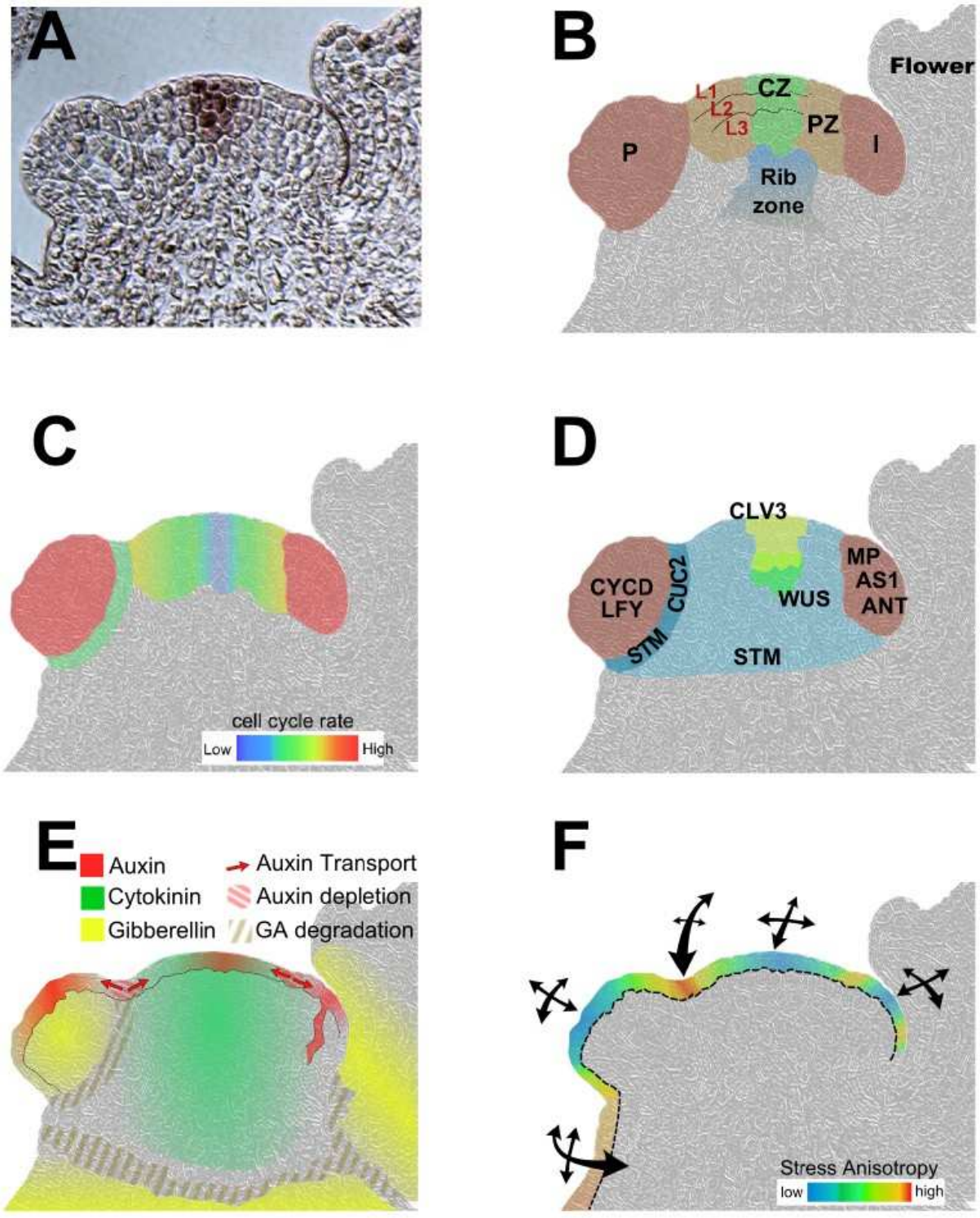

Figure 14: **Structural and functional organization of the SAM in *Arabidopsis thaliana***. (**A**) Longitudinal section of a paraffin-embedded WT SAM of the plant model *Arabidopsis thaliana*, showing an *in situ* hybridization of the CLV3 gene. (**B**) Structural zonation of the SAM, CZ central zone, PZ peripheral zone, P primordium, I Initium, L1–L3 cellular layers. (**C**) Spatial variations of cell cycle rate in the SAM. (**D**) Genetic zonation of the SAM. (**E**) Putative distribution for the three hormones auxin, cytokinin, and gibberellins in the SAM. (**F**) Mechanical stresses in the SAM. The models predict that the L1 is under tension and internal tissues are under compression. Anisotropy of stress varies across the L1 layer; arrows indicate relative strength (by size) and direction of stress anisotropy in different subdomains (see text for details).

II. The SAM at a microscopic scale: signaling in a multicellular object

II.1. Morphogenesis at the SAM: highly dynamic cells produce a stable structure

The structure and function of the SAM have been extensively described (Lyndon 1998; Steeves & Sussex 1989; Traas & Doonan 2001; Ha et al. 2010) and here, we will simply summarize its main features from a morphogenetic perspective.

Different species produces leaves or flowers of very different shape. Even within a given species, the SAM can produce very different organs, depending on the phase of its life cycle, from leaves with various shapes during the vegetative phase, to flowers during the reproductive phase. However, all SAMs in higher plants share a stereotypical common structure: a central often dome-shaped domain surrounded by several emerging organs (figure, 7 and 14A-B). Cells in the meristem proper are considered as undifferentiated, because of a smaller size, a reduced vacuole and an active mitotic cycle. The tissue structure is nonetheless highly organized in the SAM: the outermost cells define one or several continuous surface layers, called the tunica, covering internal tissue, referred as the corpus. These external layers, numbered from the periphery L1 and L2, maintained themselves as sheets thanks to preferential anticlinal cell divisions (figure 14B). Chimera analyses have shown that daughter cells generally remain within the same layer as their mother (Szymkowiak & I. Sussex 1996). Notably, the L1 layer never loses its organization and generates the epidermis of all the aerial part of the plant. The L2 layer usually looses its planar organization at sites of organogenesis due to random directions in cell division planes. In the corpus (also called L3), cell division planes are more random as well.

Mapping the cell division rates in the meristem revealed that a partitioning into functional zones is superimposed to this layered organization (figure 14B-C). First, at the meristem summit, a group of slowly dividing cells defines the central zone (CZ) and ensures meristem maintenance. The CZ contains the stable long-lived stem cells, from which all shoot tissues are ultimately derived after germination, and extends through the tunica layers down to the upper part of the corpus. The CZ is surrounded by stem cell daughters, which are progressively displaced away from the center by the

continuous growth of the structure. Consecutively, these cells enter the peripheral zone (PZ) where organogenesis occurs. In that domain, a restricted number of founder cells considerably increase their proliferation and elongation rate, allowing the formation of the organ primordium. Cells surrounding the primordium adopt a much lower growth rate and a strong anisotropy: they will establish a boundary between the new organ and the meristem. Note that in the ring-shape PZ, only a small subset of cells becomes founder cells. Thus, only a defined number of primordia can arise at the same time, in a precise position, according to the phyllotaxis. Finally, the rib zone is located below the CZ and cells entering this zone produce all the tissues of the stem.

Therefore, despite the dynamics of cell behavior within the SAM, this structure exhibits a remarkably stable organization with well-defined positional information. The SAM is patterned in subdomains of different identities and behaviors, such as the central and the peripheral zone. As mentioned before, this is of great importance for the formation of phyllotactic arrangements. This patterning of the SAM and its homeostasis largely rely on genetic regulations.

II.2. Patterning of the SAM is under genetic control

To investigate the genes underlying the meristem activity, mutants of various model species (mainly *Arabidopsis thaliana*) have been screened for defects in stem cell maintenance, organ initiation, outgrowth, and polarity. Most of these mutants are impaired in transcriptional regulators that are highly conserved in angiosperms. Their expression patterns are often correlated with the histological zonation presented above. In addition, some also define several important functional subdomains. Here, we only describe the main genes characterized in the model plant *Arabidopsis thaliana* (figure 14D).

The integrity of the stem niche relies on an organizing center located below the stem cells and defined by cells expressing the homeobox transcription factor WUSCHEL (T Laux et al. 1996). The activity of *WUSCHEL* (*WUS*) promotes stem cell identity in the cells above (Mayer et al. 1998). Its precise targets are still unknown, even though a recent study demonstrates that it acts as a transcriptional repressor in this function (M. Ikeda et al. 2009). The stem cell subdomain is associated with the expression of the *CLAVATA3* (*CLV3*) gene (Rieu & Thomas Laux 2009)(figure 14A), whose transcription is dependent on *WUS* activity. CLV3 is a secreted peptide, which acts as a non-cell autonomous signal repressing the transcription of *WUS (J C Fletcher et al. 1999; Rojo et al. 2002; T. Kondo et al. 2006)*. This creates a dynamic feedback loop that regulates stem cell

number and is essential for meristem homeostasis (Brand et al. 2000; Schoof et al. 2000). Stem cells are thus not defined by a positive regulator but rather by the transcription of a signaling molecule that eventually represses stem cell identity and its own expression. Other markers for stem cell identity not involved in the *WUS-CLV3* loop have recently been identified (Yadav et al. 2009; Aggarwal et al. 2010) and could lead to the identification of such a positive regulator. Note also that the core *CLV3-WUS* loop is connected to a complex gene regulatory network (Dodsworth 2009; Stahl & Rüdiger Simon 2010; Ha et al. 2010), involving hormone signaling and particularly cytokinin (Leibfried et al. 2005; Gordon et al. 2009), nutrients availability, transcription regulation or chromatin remodeling. The elucidation of the connections between these different regulatory levels is only starting and will certainly fuel further research on stem cell homeostasis in the coming years.

Surrounding the stem cell pool, two antagonistic pathways control cell differentiation in the PZ. First, the maintenance of a meristematic undifferentiated identity requires the action of the homeodomain protein SHOOTMERISTEMLESS (STM) (J A Long et al. 1996; Endrizzi et al. 1996; Michael Lenhard et al. 2002; Gallois et al. 2002) in combination with several members of the CUP-SHAPED COTYLEDON (CUC) family of transcription factors (M Aida et al. 1999). But as soon as cells are recruited in an organ, these meristematic identity genes are switched off by an unknown factor and maintained in a repressed state by organ specific regulators like the MYB transcription factor ASYMMETRIC LEAVES 1 (AS1)(Byrne et al. 2000). The recruitment of founder cells depends on transcription factors belonging to the auxin signaling pathway, like the AUXIN RESPONSE FACTOR 5/MONOPTEROS (Przemeck et al. 1996; Hardtke & T Berleth 1998; Mitsuhiro Aida et al. 2002; Didier Reinhardt, Pesce, et al. 2003; Schuetz et al. 2008).

As an initium starts to emerge, its size, polarity and identity are progressively determined by a complex network of genetic regulation. The organ identity mainly depends on the presence of the transcription factor LEAFY (LFY) which acts as a master switch controlling the organ fate, typically between a leaf and a flower (D Weigel et al. 1992). Many genes are expressed specifically in boundaries. Some of them are necessary for proper organ separation like CUC genes (M Aida et al. 1997; Hibara et al. 2006). Others like *JAGGED LATERAL ORGANS* both interact with genes of the *STM* gene family (the *KNOTTED*-like Homeobox or *KNOX* genes) and auxin transport, and could coordinate the drastic changes in gene expressions occurring between the meristem and developing lateral organs (Borghi et al. 2007). Organ polarity relies on the antagonistic activity of HD-ZIP class III transcription factors (PHAVOLUTA/REVOLUTA/PHABULOSA) promoting

Nature of signals	Molecules involved	Distribution within the SAM	Perception	Cellular effects	Meristem effects
Phytohormones	**AUXIN**	**Polar transport** thanks to PIN efflux carriers, **Diffusion** through the apoplast and symplasm	Plasma Membrane and cell wall : **ABP1** Receptor, Nucleus: F-box **TIR1/AFB** Receptors	Cell wall loosening and **Cell expansion** Inhibition of endocytosis, promotes PIN membrane localization and its auxin efflux, Transcriptional regulation by **ARF** transcription factors, Permissive role on cell division	**Organ founder cell commitment** (instructive signal), Regulation of organ spacing **(Phyllotaxis)**
	CYTOKININ	**Diffusion** through the apoplast and symplasm	Plasma membrane: transmembrane Histidine-kinase receptor **AHK1, AHK2, AHK3**	**Cell division,** Transcriptional regulation by **B-type Response Regulators** and **CRF** Transcription factors	**Stem cell maintenance** Role in early differentiation?
	GIBBERELIC ACID	**Diffusion** through the apoplast and symplasm	Nucleus: **GID1** Receptors	**Cell expansion, Cell differentiation,** Transcriptional regulation	**Organ differentiation** Restrict stem cell activity
	ETHYLENE	**Diffusion** (gas)	Plasma membrane and endoplasmic reticulum: transmembranes Histidine-kinase receptors **ETR1/2, ERS1/2, EIN4**	**Cell elongation, cell differenciation** Transcriptional regulation, e.g. **EIN3**	**Organ differentiation** Restrict stem cell activity (see Hamant *et al.*, 2002)
	BRASSINO-STEROIDS	**Diffusion** through the apoplast and symplasm	Plasma membrane: Transmembrane receptor **BRI1** and coreceptor **BAK1**	**Cell expansion** Transcriptional regulation, e.g. **BIN2**	Control of plant stature and **growth** (see Savaldi-Goldstein and Chory 2008)
	STRIGO-LACTONE	**Diffusion** through the apoplast and symplasm	Nucleus: Not identified yet, Sensing requires the F-Box protein **MAX2**	Not established	Regulation of **shoot branching**: inhibits axillary meristem outgrowth (see Umehara *et al.*, 2008; Gomez-Roldan *et al.*, 2008)
Molecule exchange through plasmodesmata	**Transcription factors e.g. LFY, STM, KNAT1,MP/ARF5...**	**Diffusion** through the symplasm Possible targeted **transport**	Association with DNA cis-regulatory sequences in the nucleus	Control of gene expression	Possible non cell-autonomous signaling: **"fail-safe" mechanism** (e.g. *KNOX* genes) or spatial control of **stem-cell/differentiation balance for MP**
	Small RNAs e.g. ta-siARF from the *TAS3* gene	**Diffusion** through the symplasm	Association with target RNA in the cytoplasm within the **RISC** complex	Degradation and/or translational inhibition of target RNAs	Acts as a morphogen gradient to set ARF3 expression domain and the **dorsi-ventral** polarity of organs
Small diffusing peptide	**CLV3**	**Diffusion** through the apoplast	Plasma membrane: transmembrane receptor **CLV1** and **CLV2/CORYNE** complex	Inhibition of ***WUS*** transcription	Control of stem cell number, **WUS-CLV** regulatory loop
Mechanical stress	**Cell wall components, remodeling proteins, cytoskeleton or transmembrane proteins**	**Tension** across tissues	Not identified yet Wall receptors? Stretch-activated channels? Cytoskeleton?	Impact cortical **microtubule** orientation and **PIN1** polarity, **Cell expansion, Cell anisotropy**	**Growth coordination** Control of **morphogenesis** Robustness in **patterning**

Table 2 Signals involved in cell–cell communication and growth coordination in the SAM (see text for details).

adaxial polarity (i.e. adjacent to the meristem, the dorsal side of the organ) and *KANADI* and *YABBY* genes promoting the abaxial polarity (i.e. away from the meristem, the ventral side of the organ)(Bowman et al. 2002).

Finally, transcription factors like AINTEGUMENTA (ANT) control organ outgrowth and its final size, notably by promoting the expression of the cell cycle gene *CYCD3* (Mizukami & Fischer 2000). The expression patterns of some of these genes are further defined by miRNAs. For example, HD-ZIP class III transcription factors and *CUC* mRNA are known to be targeted by miRNAS (Pulido & Laufs 2010).

Many other genes have been identified as regulators of shoot meristem activity and we refer the reader to recent reviews describing these in further details (Rast & Rüdiger Simon 2008; Husbands et al. 2009; Barton 2010; Ha et al. 2010).

II.3. Signals behind cell-cell communication and growth coordination in the SAM

The SAM is divided in different regions with contrasted gene expressions, identities and cell behaviors. Many evidences, from pioneering microsurgery of meristems (I.2) to modern molecular biology demonstrated that signaling between cells and throughout tissue is responsible for the coordination of these different subdomains (for review see (Golz 2006; Besnard et al. 2011).

A great diversity of molecules, including phytohormones, small peptides, mobile transcription factors, or small RNAs has been involved in SAM function. In addition to these biochemical signals, the role of mechanical signals is emerging as an important contributing factor to the control of meristem biology. A list of those signals is provided in Table 2. Thanks to molecular and genetic studies, we begin to understand the role of these signals in the SAM.

Concerning phyllotaxis and organogenesis, some of these signals have been demonstrated to play a prominent role. The phytohormone auxin is considered to date as the major player in those processes However, new data are now revealing the role of other hormones, notably cytokinins and of mechanical signaling. To understand how these signals function, is is necessary to know some particularities of plant histology and physiology that greatly influence the way these signals are working.

II.4. Specificity of signaling in plants and in the SAM

Nearly all signals are produced and act locally in the SAM, as it is now well established for auxin and cytokinin (reviewed in (Y. Zhao 2008). This accounts for the considerable autonomy of SAM development: even isolated on artificial media, stem cell homeostasis and organogenesis still go on in a very robust and stereotypic manner (reviewed (Steeves & I. A. Sussex 1989). In parallel, long-range effects of phytohormones circulating through the vascular system are also well documented: for example, an acropetal cytokinin flow from the roots is important to sustain shoot growth and development. But in the meristem proper, where no mature vascular system is formed, the local production of cytokinins might be critical to generate differential concentrations, and thus biochemical patterns. It should be noted here that the term “hormones” in plant maybe misleading. If some may have an action at a distance as their animal counterparts, most of them are also characterized by a paracrine action and context-dependent effects. In this respect, they rather resemble animals growth and developmental factors like e.g. Wnt.

Despite their local production, one major bottleneck for the study of signals in plants is the difficulty to precisely assess where they act and to quantify the strength of the signal. For example, no antibody is available for the CLV3 peptide. Its localization is currently inferred from the expression domains of the *CLV3* gene itself and of the CLV1/CLV2 receptors. This issue is even more acute for plant hormones. Indeed, plant hormones usually are small molecules, deriving from simple metabolites (like auxin which is a derivative of tryptophan) and it is hard to define methods to identify the active hormone from the widespread precursor. Furthermore, each hormone is in fact represented by a group of natural chemicals variants of the same molecule, with possibly subtle differences in activity. In addition, many enzymes catalyze reactions that activate or deactivate hormones. For example, in rice and *Arabidopsis*, the local activation of cytokinins by the LOG enzymes in the central zone is essential for stem cell maintenance (Kurakawa et al. 2007; Kuroha et al. 2009). In general, the exact sites of hormone biosynthesis, activation, deactivation and degradation are still poorly documented. As a result, we still ignore the precise localization and concentration of plant hormones at a cellular level. Finally, no measurements of the physical properties throughout the SAM have been reported yet, even though techniques like Atomic Force Microscopy could provide valuable inputs in the future. More generally, the development of new tools to acquire quantitative data on signal localization and intensity will certainly help unraveling the precise mechanisms through which signals coordinate multicellular growth in the SAM

(Vernoux et al. 2011). Despite these shortcomings, we can propose maps of potential signal localization and corresponding signaling intensity in the SAM.(figure 14E and 14F).

Beyond the molecular control of signal production and decay in the SAM, the histological structure of the SAM itself adds another layer of complexity: the extracellular matrix and the presence of an extensive symplasm channel also control the distribution of signals in the tissue.

Extracellular signaling molecules, like hormones and small peptides, are able to travel throughout the cell wall, by the so-called apoplastic way. They are then specifically recognized by membrane-embedded or nuclear receptors and their transduction pathway is rather well documented (Chow & McCourt 2006). Besides, because each cell is mechanically glued to its neighbors, the presence of cell walls provides a simple mean of cell growth coordination. Sharing common walls can also generate physical stress between neighboring cells, and in theory act as a coordinating factor (Hamant & Jan Traas 2010; Boudaoud 2010). Last, plant cells can be connected by tubular channels called plasmodesmata. This complex structure establishes continuity between the cytoplasm of neighboring cells, but also between their plasma membranes and their endoplasmic reticulum membranes. Like gap junctions in animals, these channels allow the passage of ions and metabolites between cells, as well as molecules of various size including hormones, peptides, proteins, or RNAs. The movement of these molecules can obey simple diffusion rules or follow a targeted path (reviewed in (Gallagher & P. N. Benfey 2005). The maximal size of a molecule which flows through plasmodesmata defines its size of exclusion limit (SEL). Interestingly, the SEL can change in space and time and is likely to be developmentally controlled, as shown during embryo development for instance (I. Kim et al. 2005) or flowering (Gisel et al. 2002) in *Arabidopsis*. Sometimes, protein movement can even be restricted to a one-way direction (J.-Y. Kim et al. 2003). All these properties define different symplasmic domains, the size of which depends on the molecules considered.

In meristems, microinjections (Cantrill et al. 2005) and targeted expression of diffusible fluorescent reporters (J. Y. Kim et al. 2002; J.-Y. Kim et al. 2003) has demonstrated extensive communications between cell layers. In contrast, the diffusion from the meristem proper into developing organs was found to be rather limited. As proposed by Kim and Zambryski (2005) a restriction of the SEL may be a general feature accompanying cell differenciation in plants (Cantrill et al. 2005). Many transcription factors important for meristem function, like LFY, STM and KNAT1/BP (a STM paralogue) have been shown to move through plasmodesmata (Sessions et al. 2000; J.-Y. Kim et al. 2003; X. Wu et al. 2003), albeit with different range. Notably, the movement

of the maize orthologue of STM, KNOTTED1, is clearly restricted in a developing leaf, since the movement is only possible from the inner tissues to the L1 layer but is impossible the other way around. This suggests that the meristem, as an immature tissue, is generally more permissive to proteins movements between cells than other tissues in differentiating organs. In view of these data, all transcription factors with partial cytoplasmic localization, unless specifically retained in cells, could thus extend their activity outside the domain where their RNA is transcribed (X. Wu et al. 2003). This idea was recently further supported by the observation that the transcription factor AUXIN RESPONSE FACTOR 5/MONOPTEROS (ARF5/MP), a key regulator of auxin signaling (see below for further details on auxin signaling), establishes a gradient from its site of transcription in the PZ towards the CZ (Z. Zhao et al. 2010). Are these movements required for normal development? A LFY fusion protein that is impaired in its diffusion is not as efficient as wild type LFY to rescue *lfy* loss of function mutants, suggesting that LFY movement in flower is critical for its function (X. Wu et al. 2003). The wide expression domain of STM would suggest that the role of STM movement is secondary. Nevertheless, some authors have proposed that STM mobility could homogenize the concentrations of these meristematic identity genes and acts as a "fail-safe" mechanism to control cell fate in the SAM (J.-Y. Kim et al. 2003). In the case of ARF5/MP Zhao et al (Z. Zhao et al. 2010) convincingly showed that MP regulates transcription in the central zone non-cell autonomously, with a functional impact on stem cell homeostasis.

Very exciting results concerning a putative role of plasmodesmata in growth coordination also came from recent reports on developmental patterning by mobile small RNAs, miRNAs or plant specific ta-siRNA (Chitwood et al. 2009; Carlsbecker et al. 2010). In particular, during leaf polarity establishment, a ta-siRNA moves from its site of biogenesis in the adaxial side of the organ to the abaxial side and creates a gradient that patterns the expression of an abaxial determinant (Chitwood et al. 2009). These pioneering data pave the way for the discovery of other important mobile small RNAs in the SAM. More generally, it highlights the importance of plasmodesmata for the mobility of various cytoplasmic molecules, which could behave as plant non-conventional morphogens.

In summary, cells in a meristem are interconnected by many signals, giving different developmental or environmental cues. Among those these signals, auxin has been shown to be critical for both triggering the developmental program of organ formation and for regulating their correct spacing around the meristem. This is due to special properties of this original signaling molecule that I will detail in the next section.

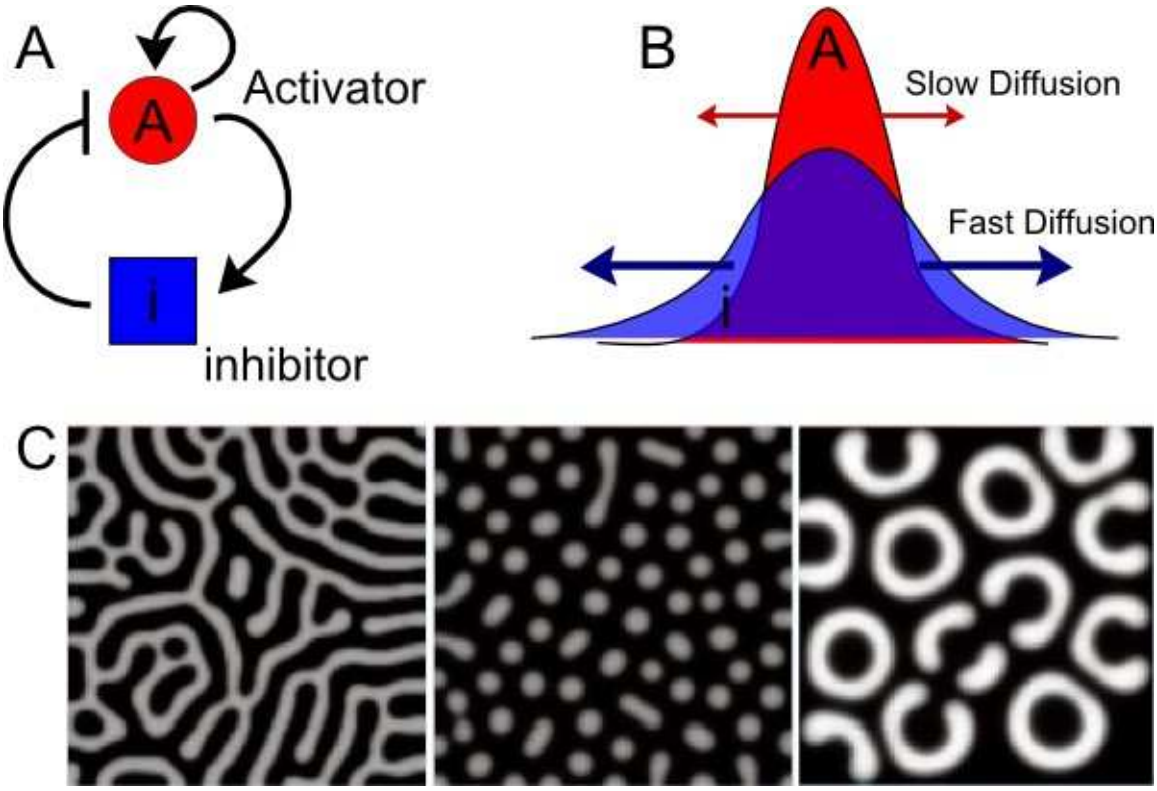

Figure 15: **Reaction-diffusion models explaining the formation of biological patterns**. (**A**) In the system, two molecules are present: an activator A (red) and an inhibitor i (blue). The activator promotes its own production and the production of the inhibitor. i blocks the formation of A (reactions between the 2 molecules). (**B**) In space, the two molecules diffuse with different velocities, generating inhomogeneous concentrations, acting locally in feedback on the reaction. (**C**) With the combination of the two properties (reaction and diffusion), the system can generate autonomously various stable patterns *de novo*. This is because the reaction-diffusion creates a short-range positive feedback and a long-range negative feedback. (Turing patterns from Kondo S. *et al*, 2010)

III. Control of organogenesis and phyllotaxis by dynamic polar auxin transport

III.1. The chemical hypothesis for the nature of inhibitory fields.

The nature of the inhibiting interactions between organs in a meristem has been a long source of debate. Since Schoute (1913), many different chemical models of inhibitory fields have been proposed for phylltaxis (for review, see Adler et al. 1997). These models show that diffusing molecules could create efficient inhibitory fields (Mitchison 1977; Veen & Lindenmayer 1977). Most popular ones were based on Reaction/Diffusion Models (Bernasconi G.P. 1994; Meinhardt et al. 1998), as first proposed by Turing (1952). In this chemical system, an activator and a inhibitor diffuse in the tissue: the activator promotes its own synthesis and the synthesis of the inhibitor, which represses the activity of the activator in feedback. While the activator diffuses slowly, the inhibitor is fast: this difference is sufficient to create various patterns of activator/inhibitor concentrations from an initial homogenous situation, by amplifying and stabilizing small perturbations (figure 15). This mechanism has been shown to be responsible for different patterns in animals and has been a guiding framework in phyllotaxis for decades (S. Kondo & Miura 2010).

To test if a molecule among the various one active in the meristem (table 2) could control phyllotaxis, different experiments using exogenous treatments, notably with phytohormones, have been performed e.g. (Meicenheimer 1981; D Kwiatkowska 1999). However, these assays were often difficult to interpret, notably because the exogenous application of a treatment cannot prove that the molecule tested is necessary in the plant, even if it has a significant effects in the experiment. In the last decade, the main progresses were made thanks to the use of the genetics in *Arabidopsis thaliana*, which helped establishing clearly the major role of auxin. However, the way auxin functions is significantly different from the traditional model of reaction/diffusion, because it largely depends on an active transport of auxin throughout the plant that I will describe first.

III.2. Auxin is polarly transported from cell to cell.

Auxin is both diffusible and transported throughout tissues in defined directions. Early experiments showed that auxin travels in stem from meristems to the base and towards the tip of

roots, following a global shoot-to-root flux. These oriented fluxes are explained by the action of specific auxin efflux carriers. Auxins, like the indo-acetic acid IAA, are weak acids. Depending on the pH of the solution, they can be protonated (IAAH) or ionic (IAA-). This property has fundamental biological consequences, formulated in the "chemio-osmotic model" (Goldsmith et al. 1981). In the acidic environment of the cell wall, auxin is found under its neutral form (IAAH): it can cross biological membranes and enters the cell. This entry is also facilitated by influx carriers, like the Arabidopsis AUX1 and its paralogues LAX1, LAX2, LAX3, as well as PGP4, a member of the multidrug resistance/p-glycoprotein (MDR/PGP) ATP-binding cassette transporters (M. J. Bennett et al. 1996; Marchant et al. 1999; Didier Reinhardt, Pesce, et al. 2003; Terasaka et al. 2005; Bainbridge et al. 2008) In the cytoplasm, whose pH is around 7, IAAH loses a proton and becomes ionized (IAA-). This change has two effects. First, it maintains a gradient of IAAH between the extra- and intracellular compartments, and thus maintains the entry of IAAH into the cell. Second, as it becomes charged in the cytoplasm, anionic auxin loses its ability to cross membranes. It thus absolutely requires efflux carriers to exit the cell, a role played by the members of the PIN-FORMED (PIN) family, as well as as PGP1 and PGP19 (Petrásek et al. 2006).

Interestingly, the PIN proteins generally exhibit a polar localization in each cell, and the predicted direction of auxin efflux at the cell level can be correlated with macroscopic auxin fluxes in tissues like stems and roots. PIN polar localization thus likely dictates the direction of the net flux of IAA- outside the cell (Jirí Friml 2010). PIN polarities show specific supracellular patterns in the SAM (see below, figure 16C) and in various organs (Heisler et al. 2005; Blilou et al. 2005). The auxin signaling reporter DR5 has been used to evaluate whether such patterns could generate local peaks of auxin. Gene transcription in response to auxin is controlled by members of the ARF transcription factors family that are themselves regulated by interaction with the Aux/IAA transcriptional repressors, a class of protein targeted to the proteasome upon perception of auxin (Leyser 2006; Chapman & Estelle 2009). The DR5 reporter drives the expression of a reporter gene (GFP or b-glucuronidase) under the control of a synthetic promoter, consisting of several auxin response elements (AuxRE) bound by the AUXIN RESPONSE FACTORS (ARF) fused to a minimal CaMV35S promoter (Ulmasov et al. 1997). Activation of the DR5 reporter thus corresponds to an induction of auxin transduction that could be expected upon local accumulation of auxin (Ulmasov et al. 1997; Sabatini et al. 1999). Overall, the orientations of PIN proteins correlate most of the time with patterns of DR5 activation and simple and multiple pin mutants as well as transgenic lines with modified PIN polar localizations consistently display disrupted DR5

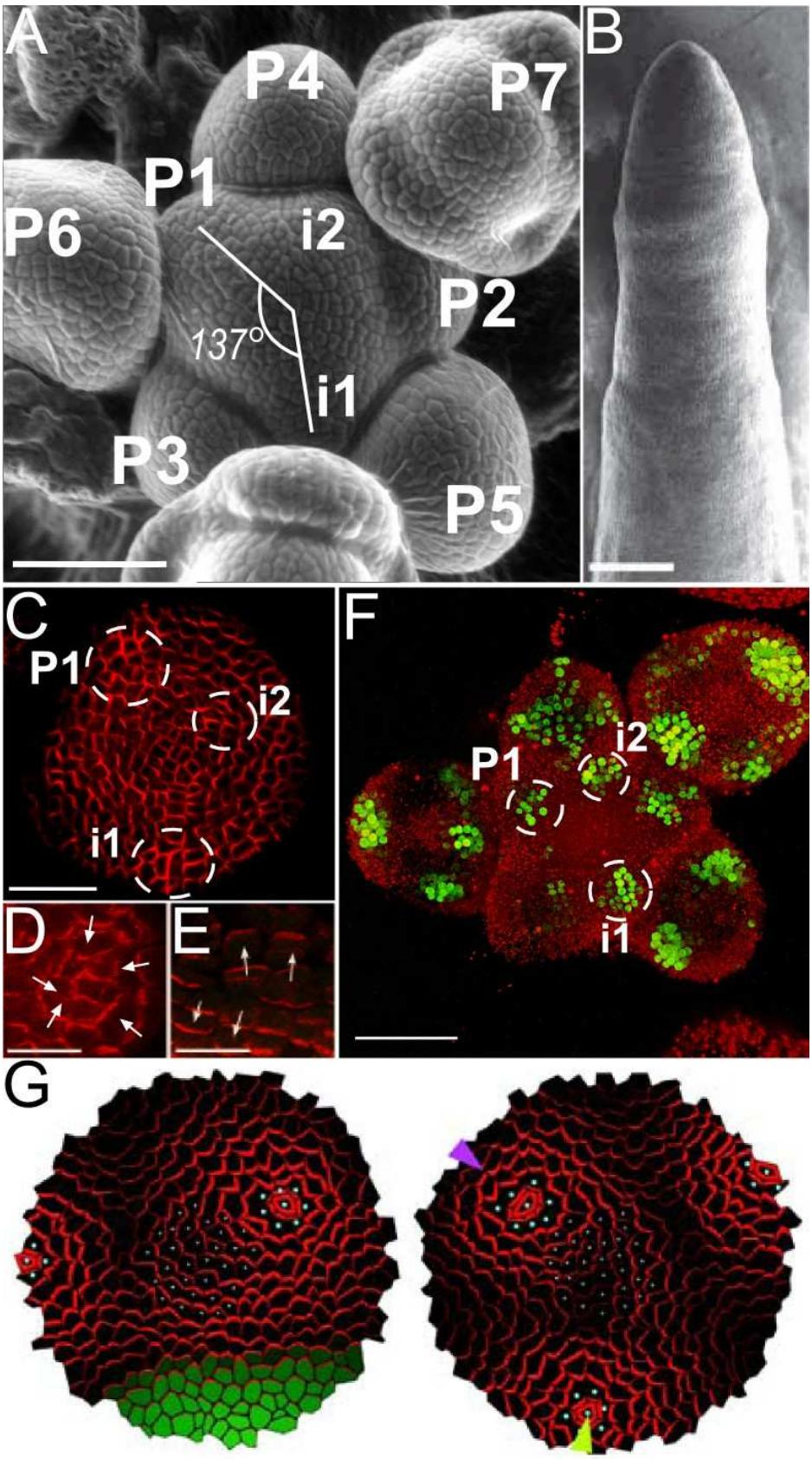

Figure 16: **Polar auxin transport controls organogenesis and phyllotaxis in the SAM**. (**A**) Top view (scanning electron microscopy) of the SAM of *Arabidopsis thaliana* showing the regular spacing of organs with a mean divergence angle close to 137,5°. Primordia (P) are numbered from the youngest P1 to the oldest P7. Initium position (I1, then I2 in the sequence of appearance) is determined although initia are not bulging out (*legend continues p48*)

expression patterns (S Sabatini et al. 1999; Benková et al. 2003; de Reuille et al. 2006; Smith et al. 2006; Wisniewska et al. 2006). Altogether, this demonstrates the key role of PIN proteins for auxin distribution in plants.

III.3. Auxin transport controls organogenesis and phyllotaxis at the shoot apical meristem.

Numerous evidence support a role for auxin transport in organogenesis in the SAM. First, mutants in the PIN1 efflux carrier are unable to produce organs, and generate naked pin-shaped inflorescences (Okada et al. 1991) (figure 16B). This indicates a limiting role for the PIN1 eflux carrier in polar auxin transport at the SAM. In line with this idea, inhibition of auxin transport by drugs like NPA phenocopies the *pin1* phenotype (D Reinhardt et al. 2000). Reinhardt *et al* (2003) further showed that a local application of auxin in the PZ of naked *pin1* meristems or NPA-treated plants can rescue the formation of organs, suggesting that auxin accumulation is necessary and sufficient to trigger organogenesis. What would then be the mechanism responsible for such an accumulation of auxin?

First, auxin carriers of the AUX/LAX family are thought to concentrate auxin in the epidermis (called L1 layer) of the SAM (Didier Reinhardt, Pesce, et al. 2003; Bainbridge et al. 2008). This is consistent with the specific role played by the L1 layer in controlling organogenesis, as evidenced by inhibition of organogenesis following laser ablation of cells in the epidermis (Didier Reinhardt et al. 2005). Second, PIN1 is expressed in the L1 layer throughout the meristem and exhibits concentric and centripetal patterns at sites of emerging organs (Didier Reinhardt et al. 2005; de Reuille et al. 2006) (figure 16, C-E). Analysis of the putative auxin distribution using computer simulations based on observed PIN1 orientations confirm that this cellular transport network likely directs auxin to the sites of organogenesis . Expression of the DR5 reporter in the SAM supports this hypothesis (figure 16F) and live imaging of the SAM identified the induction of DR5 expression as one of the earliest landmark for organogenesis (Heisler et al. 2005). In addition, local biosynthesis of auxin is important to supply the hormone to the pump network: loss of function of YUCCA enzymes, a family of flavin-monooxygenases catalyzing a rate-limiting step in auxin synthesis, further enhances the inhibition of organogenesis in a *pin1* or *aux1* background (Cheng et al. 2007). The different YUCCA genes are expressed in discrete groups of cells in the SAM (Cheng et al. 2006), but it is not clear how this localized auxin production participates to the spatial

Figure 16 (*See page 46*): (**B**) Meristem from the *pin1* mutant shown by electron microscopy: stem cells are maintained while organogenesis is abolished in the periphery (taken from Vernoux et al. 2000). (**C**) Immunodetection of PIN1 efflux carrier in the L1. Note the subcellular polarized localization of the auxin pump that is thought to direct auxin fluxes out of cells and distribute auxin in the whole meristem. (**D**) Concentric PIN1 patterns around predicted new organs are responsible for auxin accumulation in founder cells. Note that PIN1 is up-regulated in these organs, suggesting a positive feedback loop of auxin on the quantity of PIN1 proteins. (**E**) Divergent PIN1 orientations in the boundary domain deplete these areas in auxin (c, d and e are taken from de Reuille *et al*). (**F**) Activity of a nuclear DR5 reporter in a WT SAM, imaged from the top by a confocal microscope. DR5 reports high auxin signaling mediated by ARF transcription factors. Clusters of green nuclei indicate primordium (P1) and allows the identification of early initium (I1 and I2). Plant tissue is colored in red by autofluorescence. g Computer simulation of auxin transport by a model of self-regulatory PIN1 pump network (taken from Stoma *et al*.). This model reproduces PIN1 patterns and is able to generate a correct phyllotaxis: arrows indicate the sequential emergence of two new initium (yellow then magenta). Putative auxin concentrations are indicated in green. Scale bar 50 µm, excepted B (200 µm) and E, F (10 µm)

variation in auxin signaling. Consequently, patterns of auxin accumulation in the SAM are thought to be mainly the results of auxin distribution through the PIN1 network (figure 17A). Note that this original mechanism differs from traditional reaction-diffusion models, where the formation of the pattern requires both the movement of molecules (through diffusion) and local self-enhanced production (figure 15) (Smith 2008).

As auxin is predicted to accumulate at sites of organ emergence, this also suggests that auxin could get depleted in the vicinity of primordia. In addition to its expression in the L1 layer, PIN1 is also expressed in internal layers below incipient organs, in the developing vasculature (Didier Reinhardt, Pesce, et al. 2003; E. M. Bayer et al. 2009). Thus, if auxin is driven into inner tissues through these provascular strands, organs likely behave as sinks. Patterns of auxin depletion around organs would then be equally important because they would define zones where new primordia cannot be produced. The PIN1 carriers network would thus be able not only to control the sites of auxin accumulation but also to determine their relative position, and thus phyllotaxis(Didier Reinhardt, Pesce, et al. 2003)(figure 17A). Note that, this time, the auxin transport-based mechanism is somewhat comparable to reaction-diffusion models because it can generate inhibitory fields. Indeed, in the reaction-diffusion models, two molecules, an activator and an inhibitor, interact and diffuse. Inhibitory fields result from the diffusion of the inhibitor. In the auxin-transport model, only one activator is present: the active transport of auxin generates activation by local accumulation as well as lateral inhibition by depletion around the site of accumulation.

III.4. A self-regulatory network of auxin carriers provides a plausible model for the control of phyllotaxis

The proposed role for auxin transport in both organ formation and organ spacing raises the question of whether such an auxin distribution network can function in a self-regulatory manner, without external factors or inputs. Such a property would require feedbacks between auxin signaling and transport, and accumulating evidences supports such links.

Several studies demonstrated that auxin stimulates its own efflux out of cells by a quantitative control on PIN proteins: it both promotes PIN transcription and triggers the delivery to the plasma membrane of internalized PIN (Paciorek et al. 2005) Up-regulation of PIN can be clearly seen in the incipient primordium in the SAM (Heisler et al. 2005)(figure 16C). Thus auxin increases the

intensity of its own flux in feedback. However, patterns of auxin accumulation and depletion more rely on PIN1 polarity rather than PIN1 quantity. Does auxin also feedback on PIN1 polarity? Two concurrent mechanisms have been proposed and their plausibility was explored using computer modeling approaches. In the first one, PIN1 orients according to the direction of the main auxin fluxes. This flux-based mechanism, first proposed by Sachs (1969) is known as the canalization model because of its ability to progressively drive auxin flows in discrete merging channels between auxin sources and sinks. Experimental evidence indicate that this mechanism could explain vascular strands formation, in leaves (Scarpella et al. 2006) or in stems after wounding (Sauer et al. 2006). In the alternative mechanism, the authors proposed that PIN1 orients towards the cell with the highest auxin concentration, pumping auxin up the gradient. This concentration-based mechanism appears to better fit with the observations in the SAM. It could explain the presence of PIN1 concentric patterns towards the incipient primordium, where auxin concentration is thought to be the highest (figure 16D).

Based on this simple mechanistic framework (auxin increases its own efflux from cells and controls PIN polarization), several computer models have been recently elaborated to test whether such feedbacks could confer self-regulatory properties and explain phyllotaxis (Jönsson et al. 2006; Smith et al. 2006; Stoma et al. 2008; E. M. Bayer et al. 2009). All the tested models were able to reproduce plausible PIN1 polarity patterns as well as various phyllotactic arrangements (figure 16G). The two concurrent hypothesis explaining the influence of auxin on PIN1 polarity, canalization (Stoma et al. 2008) or concentration-based (Jönsson et al. 2006; Smith et al. 2006), are thus equally plausible, according to these computer simulations. Bayer and colleagues (2009)even developed a model combining the two hypothesis, with a concentration-based mechanisms and canalization governing PIN1 polarities in the L1 and internal tissues of the SAM respectively. Taken together, these models provide a demonstration that simple self-regulatory mechanism for polar auxin transport would be sufficient to explain phyllotaxis. They strongly support a scenario in which phyllotaxis is an emerging property of local cell-cell interactions driving PIN1 polarity. While these computer models give conceptual insights into the possible mechanisms operating in a complex system, they also predict that the elucidation of the biological basis for PIN1 polarization likely holds the key to the identification of the actual mechanisms involved in phyllotaxis.

III.5. How do cell perceive auxin and polarize in a multicellular context ?

As discussed above, models of PIN1 polarization postulate the existence of two unknown molecular mechanisms: canalization models require a "flux sensor" while up-the-gradient models incorporate a "concentration sensor" of the neighboring cell. Which molecules could play this role in the SAM ?

Coen *et al.* (Coen et al. 2004) speculate a molecular mechanism to explain how a cell can interpret the direction of a molecular flow: the translocation of the signaling molecule across the membrane could generate a molecular by-product, which would thus accumulate asymmetrically on one side of the membrane. This molecule would keep a record of the net morphogen flow. Differences in its concentration between outer membranes would polarize the cell according to the morphogen's main stream. Sensing a flow rather than concentrations is conceptually attractive, because a concentration is measured at a particular time point, whereas a flux measurement integrates morphogen flow over time, giving robustness to patterning. However, in the context of the SAM, where the auxin transport network is changing each time a new initium is created, the requirement of such a mechanism remains to be investigated. Furthermore, to date, no molecular players have been reported to act as a tally molecule, although pH changes associated to auxin transport across membranes could provide some elements of cell polarization.

On the contrary, very recent results may provide a mechanism by which a cell sense auxin concentrations in its neighbours, or more precisely in the surrounding apoplast.

Many studies have proposed a particular role for one of the first identified receptor of auxin, AUXIN BINDING PROTEIN 1 (ABP1), that is involved in non-transcriptional responses to auxin. ABP1 is present at the plasma membranes and in the cell wall (A. M. Jones & Herman 1993), where it is able to functionally bind auxin, at least in protoplasts (Leblanc et al. 1999; Steffens et al. 2001). Robert and colleagues (2010) have now identified an interesting functional link between ABP1 signaling and PIN1 trafficking. They showed that ABP1 promotes clathrin-dependent endocytosis of PIN1 in the absence of auxin, and that binding of the hormone inhibits this function thus triggering the recycling of the transporters back to the membrane. This is of particular importance, because PIN proteins have been proposed to be primarily delivered evenly to the plasma membrane and subsequently polarized to one cell side through a continuous dynamic endocytic recycling (Dhonukshe et al. 2008). Furthermore, the effect of ABP1 on endocytosis may

account for the positive feedback of auxin on its own flux (Paciorek et al. 2005) ABP1 likely associates with other partners to provide an asymmetry to signaling, as evidenced by the work of Xu and co-workers (2010) that show that cell-cell communication could occur *via* the Rho of Plants (ROP) protein family. In leaves, epidermal pavement cells exhibit interdigitated shapes. ROP2 and ROP6 have been shown to promote the formation of lobes and indentations, respectively and in those cells, PIN1 is polarly localized at the lobes tip. Interestingly, the activation of ROP2 and ROP6 is auxin dependent *via* the ABP1 protein. Assuming differences in sensitivity to auxin between the different ROPs, a cell could sense auxin concentration in its neighbour through very sensitive ABP1/ROP molecular modules. Altogether, these results support a model in which cell polarization depends on auxin perception in the cell wall. However, the precise role of ABP1, ROP signaling pathway and their link with PIN polar targeting to membranes still needs to be clarified. Indeed, ABP1 is unlikely setting alone PIN polarities: ABP1 loss of function does not change PIN1 or PIN2 polarities or DR5 expression patterns, suggesting unchanged auxin gradients in roots (Tromas et al. 2009).

These new findings raise the question of whether a mechanism involving auxin sensing at membranes and local cues for polarization could support either the canalization or the concentration-based model. A recent computational study has made a significant contribution to this issue: Wabnik and collaborators tested whether the modulation of PIN trafficking by an extracellular auxin receptor could lead to tissue polarization in the frame of the canalization hypothesis (Wabnik et al. 2010). In this model, the authors postulated that auxin binding to its receptor in the apoplast (ABP1 being an obvious candidate for such a receptor) immobilize the receptor and triggers inhibition of PIN internalization in the nearest cell, increasing locally the efflux. The strength of auxin signaling is proportional to the amount of bound receptor. Since two neighboring cells compete for auxin receptors in their common walls, this model can lead to an asymmetric PIN internalization in the two facing membranes. In addition, the authors implemented other important biological data, including the effect of auxin on PIN transcription through nuclear signaling and auxin transport through the influx and efflux carriers. Interestingly, this mechanistic framework has the capacity to polarize cells in a tissue with discrete auxin source and sink, which is the typical context of canalization. The authors successfully applied their model to the biological situations of vascular formation in leaves and regeneration in stem, where simulations accurately reproduce observed patterns of PIN polarization as well as auxin distribution.

It is interesting to note that instead of a flux-sensor, it integrates concentration sensors which in turn modulate PIN endorecyling. This is a call for elucidating the molecular basis underlying PIN polarization to understand the coordination of this process at the tissue level. Also, it remains to be shown whether this model could explain organogenesis and phyllotaxis in the SAM, where the context is different. For example, there are no localized auxin sources and multiple organs act as sinks. Stoma *et al.* (2008) already demonstrated that canalization-based model could generate symmetry breaking and reproduce robust phyllotactic patterns at the SAM. It would be then interesting to determine whether the proposed mechanistic framework could formally behave as the hypothetical flux sensor of canalization model and test whether it also functions for phyllotaxis.

The precise mechanism through which auxin allows cell-cell communication and polarization is still an open question. In the coming years this exciting role for auxin perception in the apoplast will certainly inspire further investigations, and may answer whether there is a unifying molecular mechanism explaining auxin-related patterning, from vascular formation to phyllotaxis.

III.6. A possible role for PIN1 efflux carrier phosphorylation in phyllotaxis?

Downstream of the cell-polarizing cues acting in the SAM, several intracellular effectors targeting PIN proteins to correct membranes have been identified, involving transcytosis, endocyclic recycling and the cytoskeleton (for review (Grunewald & Jirí Friml 2010). A striking role for PIN1 phosphorylation has been observed. In particular, mutants of the Seronine/Threonine kinase PINOID produce *pin*-like inflorescences (Christensen et al. 2000), and in this mutant, PIN1 switches from apical to basal membranes (Jirí Friml et al. 2004). Further studies showed that the kinase PID and the phosphatase PP2A antagonistically control a similar apical to basal binary switch in many cell types (Michniewicz et al. 2007). Recently, Huang and coworkers even identified three direct sites of PINOID-phosphorylation in the intracellular loop of PIN1 (Huang et al. 2010). Interestingly, a phosphomimetic version of PIN1 in those three sites has a restored apical localization in shoot epidermis. However, this PIN1 phosphomimetic line, as well as loss-of-phosphorylation PIN1 lines are unable to rescue organogenesis in *pin1* inflorescences. These experiments highlight the importance of reversible phosphorylation of PIN1 for proper organogenesis in the shoot apex. Interestingly, in the boundaries between the meristem and the emerging organ, PIN1 was reported to undergo polar switches (Heisler et al. 2005) and PID is also

expressed at higher levels in boundaries (Christensen et al. 2000). PID may thus play a direct role in these polar switches and contribute to organ separation.

The wealth of experimental data and compelling models concerning auxin support with high confidence the following model: regulated transport of auxin dynamically creates peaks, which then gives an organ acting as a sink, surrounded by depletion fields. However, recent studies have pointed out possible cooperation between auxin and other signals, notably mechanics and other hormones.

IV. Multiple feedback loops integrating mechanical signals and hormonal crosstalk during phyllotaxis

IV.1. Role of Mechanical signals in phyllotaxis

IV.1.1. A biophysical mechanism is not likely at the origin of the phyllotactic pattern.

Before chemical inhibitory fields were postulated, the first hypothesis upon the nature of the mechanism of phyllotaxis was physical. Indeed, the crystal-like regularity of phyllotaxis led many 19th century scientists to think that spiral patterns in plants and outside biology could result from common physical mechanisms. The first explanations given for phyllotaxis were models of contact pressures (Schwendener 1878) and piling of hard disks (Airy 1873). However, since Hofmeister (1868), different observations of meristems indicated that organs do not necessarily touch each other. Furthermore, in the fern *Drypoteris* where organs are cleary not in contact, Wardlaw (1949a) observed perturbations of phyllotaxis following the local surgical ablation of an organ (figure 8, partI). This experiment and other indicated that repelling interactions between organs could not rely on simple steric interactions between emerging primordia.

For a long time, mechanical hypotheses were neglected and chemical models were favored. This was notably due the incapacity of these first physical hypotheses to explain the initiation of an organ. As we saw for chemical models and with auxin in particular, a mechanism must first initiate the pattern by the formation of an organ and then create the regular spacing by lateral inhibition. In the 80's, Green and coworkers revived the interest for mechanical hypothesis with a new mechanism: the buckling of tissue (P. Green et al. 1996). Buckling is an out-of-plane deflection of slender objects or sheets caused by in-plane compression (Jacques Dumais 2007). If the peripheral zone of a meristem experiences a compressive stress, buckling instabilities could create periodic undulations with finite size bumps. Each bump repels its first neighbors, as expected by the inhibitory field theory. Cells in ridges and creases would experience different physical forces which would serve as signals for guiding differentiation and organogenesis. Mathematical modeling showed that buckling can produce various phyllotactic arrangements and could thus be a plausible model for phyllotaxis (P. Green et al. 1996; P. B. Green 1999). This mechanism possesses very

attractive properties compatible with phyllotaxis. Above all, it is very very parsimonious: the positioning signal is also the first agent of morphogenesis (P. Green 1996).

Some biological experiments support this model. An important requirement of the buckling model is that the region where the bumps appear must be under compression. Small cuts in a tissue can reveal mechanical stresses: if the two lips of the cut open, the tissue is under tension, whereas they keep closed under compression. Performing cuts in a sunflower capitulum, Dumais and Steele (2000) showed that the center of the meristem is under tension and the annular region where the pattern appears is effectively under compression. They show that these mechanical stresses are likely due to turgor pressure: after exposure to a hypertonic solution, tensions along the cut lips disappear. They pointed out that the energy of turgor pressure can be extremely high: since plants cells are encased in rigid cellulosic cell walls, pressure inside cells can reach 7 to 10 atmospheres. Based on these observations, they proposed with others the *pressurized shell* model (Selker et al. 1992; STEUCEK et al. 1993; CR Steele 2000). External layers of the meristem (e.g. the epidermis) support most of internal pressure, because internal tissues grow faster and/or because they have thicker walls. With turgor pressure, this results in stresses in the epidermis that depend on the geometry of the apex: if it is dome-shaped, it under tensile stress, if it is saddle-like, it is under compression. Accordingly, the sunflower capitulum is saddle-shaped where primordia are formed. The buckling model also predicts that compressing meristems should perturb the pattern. In compressed sunflower capitulum, Hernandez and Green (1993) observed alterations of phyllotaxis that follow the imposed stresses. The compression even changed the identity of some sunflowers bracts. Green (1996) also triggered the formation of a row of leaves in compressed *graptopetalum* meristems

However, many criticisms have been made to these experiments and to the buckling model in general (Jacques Dumais 2007; Cris Kuhlemeier 2007; Boudaoud 2010). First, compression experiments are ambiguous to interpret: it cannot be ruled out that observed effects are due to a chemical response induced by mechanical stress. Second, only a few meristems have the particular hyperbolic geometry of sunflower capitulum at the periphery. Most meristems are only dome-shaped and the peripheral zone where primordia appear is under tensile stress rather than compression, as predicted by the pressurized shell model. Earlier experiments of meristem cutting in various species led to contrasting results, which can be due to species differences or protocol variations (Dumais & Steele 2000). In *Lupinus albus (M. Snow & R. Snow 1947; M. Snow & R. Snow 1951)*, *Pisum Sativum* (Gulline & R. Walker 1957) and *Dryopteris dilatata* (Wardlaw 1948),

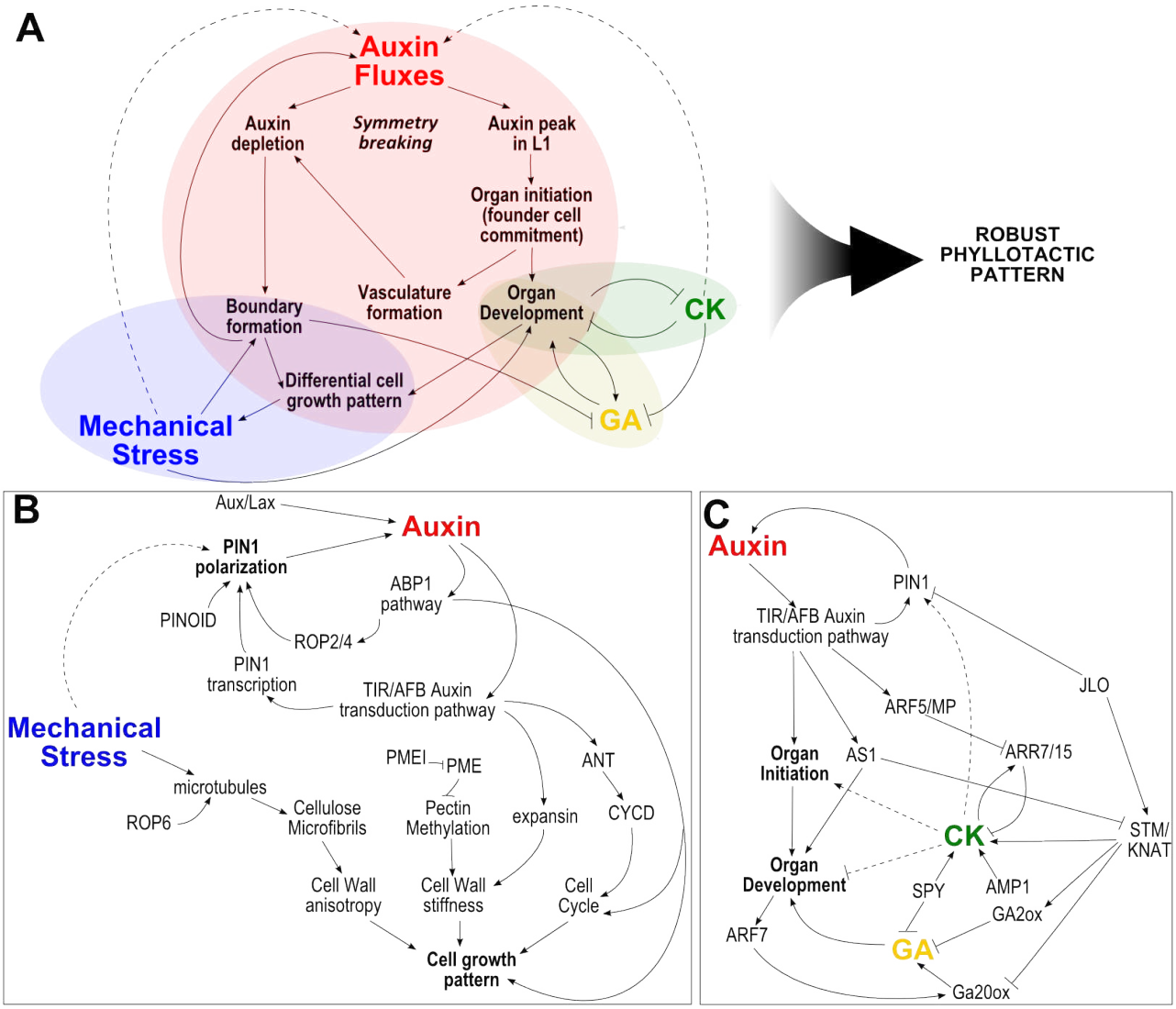

Figure 17: **Signaling network controlling organogenesis in the SAM of Arabidopsis thaliana**. (**A**) Intersection of auxin signaling with cytokinin, gibberellins, and mechanical signaling during organogenesis. The numerous positive and negative feedbacks existing between these pathways may be essential for the robustness of organ development and the control of phyllotaxis. (**B**) Details of the molecular crosstalks between auxin signaling and mechanical signaling controlling cell growth. (**C**) Details of the hormonal crosstalk between auxin, cytokinin, and gibberellin signaling controlling organogenesis

no gaping of cuts were observed at the sites of organogenesis, suggesting compressive stresses. However, gating of cuts in meristems of *Euphorbia lathrys* (M. Snow & R. Snow 1951; Hussey 1973) and more recently in tomato (Didier Reinhardt et al. 2005) confirm that peripheral region is under tension. In *Arabidopsis thaliana*, a recent analysis showed that microtubule orientation is likely controlled by mechanical stresses: their orientations in the peripheral zone also indicate a region under tension (Hamant et al. 2008)(figure 14F). Third, buckling requires a mechanical continuity of the external layer. However, surgical removals of primordia or of large stretches of epidermis only have local effects and organogenesis still goes on in regions with intact epidermis (Didier Reinhardt, Frenz, et al. 2003). Finally, a major limitation to explore the biophysical theory today is the lack of known molecular transduction pathway, that would be necessary for mechanical forces to act as a developmental signal.

For all those reasons, mechanical buckling is not likely the patterning mechanisms that first give a signal for primordium development. However, biophysical mechanisms can still participate in other aspects of morphogenesis.

IV.1.2. A possible cooperation of mechanical signals with auxin?

If mechanical signaling is not the initial signal for pattern formation, it might still be involved during later steps of organogenesis. Assuming that the epidermis has a dominant role in morphogenesis, tissue folding associated with the initiation of a primordium will inevitably affect the mechanical constraints in the meristem, and thus could impact on the position of the subsequent initiation. This theoretical view has later been supported by a series of experiments in the meristem. In particular, the local application of expansins, a cell wall protein which causes stress relaxation, on the meristem has been shown to induce a local outgrowth, followed by a modification of the subsequent phyllotaxis (Fleming et al. 1997). Knowing that expansins have a very local impact on the mechanical properties of the wall, the global impact on architecture would be due to a modification of the pattern of mechanical stress within the meristem. More recently, modification of pectins, and thus cell wall stiffness, by pectin methyl esterases was also able to impact phyllotaxis, consistent with a crucial role of the mechanical properties of the wall in organ formation and positioning (Peaucelle et al. 2008).

Interestingly, auxin is known to promote cell expansion by influencing the mechanical properties of the cell wall. First, auxin can directly or indirectly trigger the expression of cell wall remodeling proteins like expansins (H.-T. Cho & Cosgrove 2002), consistent with the preferential expression of

expansins in incipient primordia in tomato SAM (D Reinhardt et al. 1998). Second, auxin signaling stimulates an active transport of hydrogen ions in the apoplast, lowering the pH of the cell wall. This acidification activates the remodeling proteins (e.g. expansins), allowing the cellulose microfibrils to creep and the cell wall to expand (for review, see (Y. Li et al. 2003).

As seen above, polar auxin transport generates local accumulation of auxin. Then, auxin modifies locally the mechanical properties of cell wall to allow primordium bulging: could these patterns of differential growth and cell wall stiffness in the SAM produce a mechanical signaling that could feedback on auxin transport and SAM patterning? To confirm this hypothesis, we need to know how exactly those constraints are distributed in the SAM and what the molecular targets of such signals in the cell could be.

Because plant cells display high turgor pressure and are encased in a stiff cell wall, they can be viewed as thin shells with internal pressure, a bit like a balloon. Turgor pressure, by pushing on the wall, allows cell expansion and is thus considered as the motor of growth. It is also the source of mechanical signals: regional differences in wall stiffness or turgor pressure can generate gradients of constraints that the cell could in principle interpret as positional information. In the pressurized shell model of plant described above, tension builds up in the epidermis, while inner tissues are under compression (figure 14F), (Kutschera & Niklas 2007). With these assumptions, it is possible to calculate the principal directions of mechanical stress. For instance, on a cylinder-shaped structure, like a stem, mechanical stress is predicted to be twice higher in the circumferential direction than in the axial direction. These calculations on a meristem-like shape predict the presence of a strong tangential stress at the boundary between the emerging organ and the meristem (figure 14F). Interestingly, this direction is parallel to the PIN1 signal on the anticlinal wall, as viewed from the top. The orientation of the microtubular cytoskeleton at the cell cortex facing the outer wall is also parallel to this direction. It has thus been proposed that both PIN1 and the microtubules are able to sense, indirectly, the direction of the main principal stress direction (figure 17B). Cell-based modeling, using mass-spring networks as well as the finite element method show that this assumption is plausible. An array of experiments, involving cell ablation, tissue compression and pharmacological treatments, further support the conclusions of the models (Hamant et al. 2008; Heisler et al. 2010).

Based on these data, one could imagine that mechanical forces cooperate with auxin to establish a supracellular patterns, for instance by reinforcing the directionality of auxin transport (e.g. by targeting PIN1 on the membrane experiencing the highest tensile stress) and by impacting on tissue

morphology and thus on the direction of mechanical forces (figure 17A and B). For this last point, as cortical microtubules control the deposition of the cellulose microfibrils in the cell wall and thus cell anisotropy, the reinforcement of the wall at the boundary could help defining the position of the physical separation between the emerging organ and the meristem in the boundary domain. If the boundary is better defined, the pattern of stress is also reinforced and PIN1 could then acquire its polarity more rapidly or more accurately.

Nevertheless, the contribution of mechanics to patterning in the SAM is still largely debated, notably because, mechanical forces cannot be observed like a morphogen, and because, in contrast to auxin, we currently do not know how a mechanical signal could be perceived and transduced in plant cells. Both pathways could actually be intertwined: a number of effectors of the auxin-dependent cell polarity are potentially involved in the transduction of mechanical stress. For instance, the mechanosensitive Ca^{2+} channel TOUCH3 has been shown to interact with PINOID (Benjamins et al. 2003). Similarly, in yeast, the Rho proteins have been involved in the wall integrity pathway, and thus it is possible that the ROP proteins could actually be activated by both biochemical and biophysical signals. Last, the importance of the vesicle trafficking machinery for PIN1 polarity could be largely under mechanical control, knowing that membrane tension prevents endocytosis and stimulates exocytosis in animal systems (C. E. Morris & Homann 2001).

IV.2. Complex hormonal crosstalks during organogenesis

If the role of mechanical signals in plants is still a matter of debate, hormonal crosstalks have been known to be crucial in plant development and physiology for many years. For example, in angiosperms, changing the ratio between auxin and cytokinin for tissue explants cultured *in vitro* can switch the developmental program to shoot formation if cytokinin activity prevails, to root if auxin signaling is dominant, and to undifferentiated callus if none dominates. However, the precise role of hormonal crosstalk during organogenesis in the shoot apex and their possible role in phyllotaxis only begin to be addressed.

The classical view of hormone balance in the shoot states that high cytokinin (CK) signaling promotes stem cell identity and maintenance in the central zone of the SAM, while high auxin and gibberelic acid (GA) signaling are required for cell differentiation and elongation in organs (Veit 2009)(figure 14E). This hormone pattern and its homeostasis are directly coordinated by master regulators of the SAM identity. Indeed, in the meristem proper, high CK signaling is promoted by

the transcription factors of the *KNOX* family, like *KNAT1* or *STM* (figure 14C). They were shown to promote CK synthesis in the meristem ((Jasinski et al. 2005; Yanai et al. 2005). Conversely, they were also shown to promote the expression of GA deactivating enzyme (GA2ox) at the base of the meristem, either indirectly through CK signaling, or directly by regulating transcription as recently shown in maize (Bolduc & Sarah Hake 2009). The barrier-shaped expression domain of GA2ox likely protects the meristem from the influence of external GA (figure. 14E and figure 17C). KNOX proteins have also been shown to repress directly GA20ox, a key enzyme of GA synthesis, in tobacco and in *Arabidopsis (Sakamoto et al. 2001; Hay et al. 2002)*. Consequently, KNOX action creates a high CK/GA ratio within the meristem. Conversely, overproduction of CK induces the expression of the *KNOX* genes and can rescue the *stm* phenotype (Rupp et al. 1999; Jasinski et al. 2005). Application of GA can suppress the phenotype of several *KNOX* overexpressor lines (Hay et al. 2002). Other hormones promote the same effect, like ethylene, which is able to restrict the expression pattern of the *KNAT2* gene and partially rescue the *KNAT2* overexpressor phenotype (Hamant et al. 2002).

Other pathways redundantly function along with *KNOX* genes like SPINDLY, that both inhibit GA signaling and promote CK responses (Greenboim-Wainberg et al. 2005; Jasinski et al. 2005). Now considering the growing organ, auxin and GA act in synergy this time to promote cell elongation and differentiation. First, auxin controls the activation of proteins like AS1, which repress *KNOX* expression in organs. Second, auxin, through its own signaling pathway (notably ARF7) activates GA biosynthesis genes (*GA20ox*) in leaves (Frigerio et al. 2006). Interestingly, it also promotes the activation of GA2ox enzymes, which catabolize GA, at the boundary of the meristem. Thus, in principle, the spatial pattern of auxin transduction allows auxin to function in synergy with *KNOX* genes at meristem boundaries and with GA in developing organs. Altogether, these results suggest that multiple crosstalks between auxin, cytokinin, GA or ethylene are necessary to precisely control the switch of hormonal balance to allow organ development (Figure 17C).

Recently, studies have brought some elements that refine the binary vision of organ emergence opposed to meristem maintenance (high CK in meristem versus high Auxin and GA in organs). They support a view in which CK would also be required for organ initiation and development (figure 17C).

First, Carabelli *et al.* (Carabelli et al. 2007) showed that CK are necessary for leaf primordium growth, because catabolism of CK by CKX6 can be responsible for primordium growth arrest when

plants are shaded by neighbours. A minimal CK activity must then be necessary to sustain leaf development and the activation of *CKX6* must require auxin signaling. Second, the maize *abphyl1* mutant exhibits a stunning defect in the definition of organ position as the mutant produces two leaves per node instead of one (D Jackson & S Hake 1999). Thus, *abphyl1* mutants exhibit a regular decussate phyllotaxis, whereas wild-type maize have a distichous phyllotaxis: this is to our knowledge the only mutation reported so far that trigger a switch between two regular arrangement of phyllotaxis. *ABPHYL1* encodes a cytokinin RESPONSE REGULATOR, a primary cytokinin response protein that inhibits cytokinin signaling. Consistently, *abphyl1* meristems are bigger (Giulini et al. 2004)and have a higher CK content (B. Lee, Johnston, et al. 2009). However, ABPHYL1 may also have a function in the PZ, in relation with auxin. Its expression is localized in the incipient leaf primordium and requires auxin or its polar transport, as treatment with NPA, an inhibitor of polar auxin transport strongly reduced its transcription. *Abphyl1* SAM also have lower *ZmPIN1* expression and reduced auxin content. Furthermore a short exogenous treatment with CK rapidly induces *ZmPIN1* expression, showing a complex crosstalk between auxin and cytokinin. An interesting model proposed by Lee and collaborators is that lower auxin and PIN1 contents delay leaf initiation: this would lead to an extra growth of the meristem, leaving enough space for the concomitant formation of two organs (B. Lee, Johnston, et al. 2009). This further underlines the crucial role of hormonal balance in the control of the transition from stem cells to organ founder cells.

In *Arabidopsis*, several *spy* mutant alleles exhibit phyllotactic defects, also suggesting a role for the GA/CK balance in organ positioning (Silverstone et al. 2007). Furthermore, the *amp1* mutant, known to have higher CK content, can rescue the loss of organogenesis of the *mp* single mutant (Vidaurre et al. 2007). Consistently, Zhao *et al.* (2010) partially restored organ formation in a *mp* mutant by silencing the Arabidopsis RESPONSE REGULATORS 7 and 15. Similarly to their maize ortholog ABPHYL1, these genes inhibit cytokinin signaling in a feedback loop, suggesting that increased cytokinin signaling promotes organogenesis. The authors also demonstrated a mechanistic framework for this auxin/cytokinin synergy. They found that ARF5/MP directly inhibits ARR15 and excludes its expression from primordia, likely potentiating CK signaling in the PZ. Altogether, these recent findings challenge the former models where CK were important only for stem cell maintenance in the central zone. Consistent with this, a role for CK in cell differentiation has been recently shown in roots (Dello Ioio et al. 2007).

Altogether, these new data suggest that more attention must be paid to hormone interactions and specific competence of target cells to understand the diversity and specificity of developmental responses to a limited number of signals.

In the last 10 years, the field of phyllotaxis research has made an incredible step forward with the identification of plausible biological mechanisms based on precise molecular players. Current explanations of the phenomenon are now centered on auxin transport. As illustrated in this introduction, the SAM is a typical complex system and phyllotaxis is the result of multiple interactions and feedback loops at different levels. The complexity of these interactions raises new questions. In particular, it is not clear what gives the pattern its robustness. It would be also interesting to understand how such an intricate network can evolve to give different phyllotaxis. Beyond that, the integration of the mechanisms governing organogenesis and phyllotaxis with the other processes in the SAM is a major challenge to build a complete model of self-organization for the SAM. However, the precise nature of these crosstalk and their precise function in the formation of the pattern is still elusive. Assuming that the understanding of phyllotaxis cannot be complete with the description auxin biology alone, my research project during my phD was thus motivated by identifying new regulators of organogenesis and phyllotaxis.

V. Objective of my thesis: identifying new regulators of organogenesis and phyllotaxis

V.1. Actual questions in phyllotaxis and possible hypothesis for further research

Thanks to almost two centuries of research, with inputs from botany, developmental biology, mathematics, physics and computational modeling, important principles and mechanisms of phyllotaxis have been discovered. However, these progresses have left unresolved problems and fed new issues. We can summarize the present challenges in phyllotaxis by these three questions:

-What is the precise mechanism of PIN1 polarization in the SAM (This is indispensable to validate that the auxin regulated transport is a self-regulatory system governing phyllotaxis)?

- Why is the mechanism of phyllotaxis so robust?

-How is phyllotaxis influenced by the different signals present in the SAM and the other developmental processes occurring in this tissue?

In fact, these three questions are likely linked. Phyllotaxis is always described as a robust mechanism, and reports in literature mainly mention patterns with a regular arrangement and precise positioning of organs. Theoretical studies have shown that the inhibitory field theory in the context of a growing meristem is a very powerful principle, able *per se* to generate stable patterns. However, considering the proposed biological mechanism, one could wonder whether auxin regulated transport is sufficient to confer robustness to the system. How can we reconcile the dynamic capacity of the PIN1 network to respond to auxin changes with the expected stability of auxin fluxes and distribution? The diverse computational models of auxin fluxes exhibit a narrow range of stability and a tendancy to generate perturbations (Jönsson et al. 2006). This lack of robustness is not likely to be solved by a better tuning of the parameters. However, the model could still be improved, either by eliminating excessive simplifications or by discovering the precise mechanisms of PIN1 polarization. Another problem is experimental: no tools are available today for exploring the robustness of the PIN1 network and the auxin fields: most of auxin transport and signaling mutants make no more organs, precluding any analyses of the perturbed phyllotaxis.

Alternatively, one hypothesis is that additional factors participate in stabilizing phyllotaxis. These factors could impact directly on auxin transport and PIN polarization, but they could also modulate auxin transduction pathway or other unidentified parameters. Mechanical signaling, but also complex hormonal crosstalk are interesting candidates for providing robustness to phyllotaxis.

Furthermore, robustness of phyllotaxis does not rely simply on the mechanism of oranogenesis in the peripheral zone of the SAM. As seen before, the structure of the meristem, its geometry and the size of the central domain containing stem-cells is also critical. The SAM is a very dynamic tissue, able to adapt to a wide range of environmental and physiological conditions. How is this compatible with its homeostasis, notably for the relevant parameters controlling phyllotaxis? In addition, many developmental processes occur in the SAM often with a tight coupling: maintenance of stem cells, genetic patterning of the SAM subdomains, polarity of developing organs, etc. They are all regulated by genetic networks and hormonal pathways that share some overlap with the development of organs and its auxin control. Besides, auxin is known to interact with other hormones in nearly all the developmental situation it is involved. During organogenesis in the SAM, the situation must be similar. The challenge is then to identify these interactions and to understand how they control the self-organization of the tissue and the coordination between different processes.

V.2. Objectives and Strategy developed during my phD

We decided to identify new genes involved in the control of organogenesis and phyllotaxis. Rather than exploring the possible link with mechanics, we initially favored the search of master developmental genes (transcription factors) and hormonal regulators. We were interested in candidates not directly linked with auxin. We chose to work with *Arabidopsis thaliana*, because of the wealth of data available concerning the biology of its SAM and its genome and the possibility to use functional genetics. Two strategies were possible:

-A forward genetic approach based on the identification of mutants with obvious defects in organogenesis and phyllotaxis.

-A reverse genetic approach, based first on the selection of candidate genes.

I first begun my phD project with the second strategy, by selecting *ARABIDOPSIS HISTIDINE PHOSPHOTRANSFER PROTEIN6* (*AHP6),* an inhibitor of cytokinin signaling (Mähönen et al.

2006), as candidate gene (see chapter2 for the detailed reasons of this choice). Since this have given significant results, I dedicated all my thesis to analyze the role of this protein in phyllotaxis.

I will present the results in three parts. First, I will present the characterization of the post-meristematic phenotype of *ahp6* loss of function mutants. In collaboration with statisticians, we developed a new approach to phenotype and analyze perturbations in phyllotaxis. We show that this method is very insightful to predict some mechanisms involved in normal and abnormal phyllotaxis. Notably, our data reveal a strong instability of natural *Arabidopsis* phyllotaxis and our analyses strongly incriminate a defect in the stability of the plastochron. Interestingly, *ahp6* mutants exhibit a specific increase of these perturbations: this suggests that a particular mechanism involving AHP6 limits plastochron instabilities. Second, I explore the role of *AHP6 in planta* and I confirm its role on the stability of the plastochron, notably using live-imaging. Our data confirm that AHP6 is an inhibitor of cytokinin signaling and we discover that it acts through inhibitory fields to control the temporal periodicity of organ formation. We show that AHP6 is activated downstream of auxin and that AHP6 fields likely feedback non cell autonomously on auxin signaling of younger organs. Third, I investigated both the origin of plastochron instabilities and the possible mechanism of AHP6 fields theoretically. Collaborators developed an abstract computational model of phyllotaxis and we explored the capacity of noise to generate realistic perturbations. We tested different hypotheses to propose a plausible model of AHP6 fields effects.

In conclusion, I will discuss the significance of our results and the integration of the mechanism we identified with the previous model of phyllotaxis. This work has raised new questions for phyllotaxis and I will suggest possible directions for future research.

References - Introduction

Adler, I., 1974. MODEL OF CONTACT PRESSURE IN PHYLLOTAXIS. *JOURNAL OF THEORETICAL BIOLOGY*, 45(1), p.1-79.

Adler, I., Barabe, D. & Jean, R., 1997. A history of the study of phyllotaxis. *ANNALS OF BOTANY*, 80(3), p.231-244.

Aggarwal, P., Yadav, R.K. & Reddy, G Venugopala, 2010. Identification of novel markers for stem-cell niche of Arabidopsis shoot apex. *Gene Expression Patterns: GEP*, 10(6), p.259-264.

Aida, M, Ishida, T & Tasaka, M, 1999. Shoot apical meristem and cotyledon formation during Arabidopsis embryogenesis: interaction among the CUP-SHAPED COTYLEDON and SHOOT MERISTEMLESS genes. *Development (Cambridge, England)*, 126(8), p.1563-1570.

Aida, M et al., 1997. Genes involved in organ separation in Arabidopsis: an analysis of the cup-shaped cotyledon mutant. *The Plant Cell*, 9(6), p.841-857.

Aida, Mitsuhiro et al., 2002. Roles of PIN-FORMED1 and MONOPTEROS in pattern formation of the apical region of the Arabidopsis embryo. *Development (Cambridge, England)*, 129(17), p.3965-3974.

Airy, H., 1873. On leaf-arrangement. *Proceedings of the Royal Society*, 21, p.176.

Atela, P., Gole, C. & Hotton, S., 2002. A dynamical system for plant pattern formation: A rigorous analysis. *JOURNAL OF NONLINEAR SCIENCE*, 12(6), p.641-676.

Bainbridge, K. et al., 2008. Auxin influx carriers stabilize phyllotactic patterning. *Genes & Development*, 22(6), p.810-823.

Barabé, D., 2006. Stochastic approaches in phyllotaxis. *CANADIAN JOURNAL OF BOTANY-REVUE CANADIENNE DE BOTANIQUE*, 84(11), p.1675-1685.

Barabé, D., Jeune, B. & Lacroix, C., 2009. Comparison between theoretical and empirical parameters in phyllotaxis: the case of Begonia. *Rivista Di Biologia*, 102(2), p.157-164.

Barton, M.K., 2010. Twenty years on: the inner workings of the shoot apical meristem, a developmental dynamo. *Developmental Biology*, 341(1), p.95-113.

Bayer, E.M. et al., 2009. Integration of transport-based models for phyllotaxis and midvein formation. *Genes & Development*, 23(3), p.373-384.

Benjamins, R. et al., 2003. PINOID-mediated signaling involves calcium-binding proteins. *Plant Physiology*, 132(3), p.1623-1630.

Benková, E. et al., 2003. Local, efflux-dependent auxin gradients as a common module for plant organ formation. *Cell*, 115(5), p.591-602.

Bennett, M.J. et al., 1996. Arabidopsis AUX1 gene: a permease-like regulator of root gravitropism. *Science (New York, N.Y.)*, 273(5277), p.948-950.

Bernasconi G.P., 1994. Reaction-Diffusion Model for Phyllotaxis. *Physica D*, 70.

Besnard, F., Vernoux, T. & Hamant, O., 2011. Organogenesis from stem cells in planta: multiple feedback loops integrating molecular and mechanical signals. *Cellular and Molecular Life Sciences: CMLS*. Available at: http://www.ncbi.nlm.nih.gov/pubmed/21655916 [Consulté juillet 13, 2011].

Blilou, I. et al., 2005. The PIN auxin efflux facilitator network controls growth and patterning in Arabidopsis roots. *Nature*, 433(7021), p.39-44.

Bolduc, N. & Hake, Sarah, 2009. The maize transcription factor KNOTTED1 directly regulates the gibberellin catabolism gene ga2ox1. *The Plant Cell*, 21(6), p.1647-1658.

Borghi, L., Bureau, M. & Simon, Rüdiger, 2007. Arabidopsis JAGGED LATERAL ORGANS is expressed in boundaries and coordinates KNOX and PIN activity. *The Plant Cell*, 19(6), p.1795-1808.

Boudaoud, A., 2010. An introduction to the mechanics of morphogenesis for plant biologists. *Trends in Plant Science*, 15(6), p.353-360.

Bowman, J.L., Eshed, Y. & Baum, S.F., 2002. Establishment of polarity in angiosperm lateral organs. *Trends in Genetics: TIG*, 18(3), p.134-141.

Brand, U. et al., 2000. Dependence of stem cell fate in Arabidopsis on a feedback loop regulated by CLV3 activity. *Science (New York, N.Y.)*, 289(5479), p.617-619.

Braun, A., 1835. Dr. Carl Schimper's Vorträge über die Möglichkeit eines wissen-schaftlichen Verstandnis der Blattstellung, nebstAndeutung de Hauptsächlichen Blattstellungsgesetze undInsbesondere der Neuentdeckten Gesetze der Aneinanderreihungvon Cyclen Verschiedener Maasse. *Flora*, 18, p.145-191.

Braun, A., 1831. Vergleichende Untersuchung über die Ordnung der Schuppen an den Tannenzapfen als Einleitung zur Untersuchung der Blattstellung Überhaupt. *Verhandlungen der Kaiserlichen Leopoldinisch-Carolinischen Akademie der Naturforscher*, 15, p.195-402.

Bravais, L. & Bravais, A., 1837. Essai sur la disposition des feuilles curvisériées. *Annales des Sciences Naturelles Botaniques*, 7, 8, p.42-110; 193-221; 291-348;11-42.

Byrne, M.E. et al., 2000. Asymmetric leaves1 mediates leaf patterning and stem cell function in Arabidopsis. *Nature*, 408(6815), p.967-971.

Cantrill, L.C., Overall, R.L. & Goodwin, P.B., 2005. Changes in macromolecular movement accompany organogenesis in thin cell layers of Torenia fournieri. *Planta*, 222(6), p.933-946.

Carabelli, M. et al., 2007. Canopy shade causes a rapid and transient arrest in leaf development through auxin-induced cytokinin oxidase activity. *Genes & Development*, 21(15), p.1863-1868.

Carlsbecker, A. et al., 2010. Cell signalling by microRNA165/6 directs gene dose-dependent root cell fate. *Nature*, 465(7296), p.316-321.

Chapman, E.J. & Estelle, M., 2009. Mechanism of auxin-regulated gene expression in plants. *Annual Review of Genetics*, 43, p.265-285.

Cheng, Y., Dai, X. & Zhao, Y., 2006. Auxin biosynthesis by the YUCCA flavin monooxygenases controls the formation of floral organs and vascular tissues in Arabidopsis. *Genes & Development*, 20(13), p.1790-1799.

Cheng, Y., Dai, X. & Zhao, Y., 2007. Auxin synthesized by the YUCCA flavin monooxygenases is essential for embryogenesis and leaf formation in Arabidopsis. *The Plant Cell*, 19(8), p.2430-2439.

Chitwood, D.H. et al., 2009. Pattern formation via small RNA mobility. *Genes & Development*, 23(5), p.549-554.

Cho, H.-T. & Cosgrove, D.J., 2002. Regulation of root hair initiation and expansin gene expression in Arabidopsis. *The Plant Cell*, 14(12), p.3237-3253.

Chow, B. & McCourt, P., 2006. Plant hormone receptors: perception is everything. *Genes & Development*, 20(15), p.1998-2008.

Christensen, S.K. et al., 2000. Regulation of auxin response by the protein kinase PINOID. *Cell*, 100(4), p.469-478.

Coen, E. et al., 2004. The genetics of geometry. *Proceedings of the National Academy of Sciences of the United States of America*, 101(14), p.4728-4735.

Couder, Y, 1998. Initial transitions, order and disorder in phyllotactic patterns: The ontogeny of Helianthus annuus. A case study. *ACTA SOCIETATIS BOTANICORUM POLONIAE*, 67(2), p.129-150.

Dello Ioio, R. et al., 2007. Cytokinins determine Arabidopsis root-meristem size by controlling cell differentiation. *Current Biology: CB*, 17(8), p.678-682.

Delpino, F., 1883. Teoria generale della fillotassi. *Alti della R. Università di Genova*, 4, p.1-345.

Dhonukshe, P. et al., 2008. Generation of cell polarity in plants links endocytosis, auxin distribution and cell fate decisions. *Nature*, 456(7224), p.962-966.

Dodsworth, S., 2009. A diverse and intricate signalling network regulates stem cell fate in the shoot apical meristem. *Developmental Biology*, 336(1), p.1-9.

Douady, S. & Couder, Y, 1992. PHYLLOTAXIS AS A PHYSICAL SELF-ORGANIZED GROWTH-PROCESS. *PHYSICAL REVIEW LETTERS*, 68(13), p.2098-2101.

Douady, S. & Couder, Y, 1996a. Phyllotaxis as a dynamical self organizing process .1. The spiral modes resulting from time-periodic iterations. *JOURNAL OF THEORETICAL BIOLOGY*, 178(3), p.255-274.

Douady, S. & Couder, Y, 1996b. Phyllotaxis as a dynamical self organizing process .2. The spontaneous formation of a periodicity and the coexistence of spiral and whorled patterns. *JOURNAL OF THEORETICAL BIOLOGY*, 178(3), p.275-294.

Douady, S. & Couder, Y, 1996c. Phyllotaxis as a dynamical self organizing process .3. The simulation of the transient regimes of ontogeny. *JOURNAL OF THEORETICAL BIOLOGY*, 178(3), p.295-&.

Dumais & Steele, 2000. New Evidence for the Role of Mechanical Forces in the Shoot Apical Meristem. *Journal of Plant Growth Regulation*, 19(1), p.7-18.

Dumais, Jacques, 2007. Can mechanics control pattern formation in plants? *Current Opinion in Plant Biology*, 10(1), p.58-62.

Endrizzi, K. et al., 1996. The SHOOT MERISTEMLESS gene is required for maintenance of undifferentiated cells in Arabidopsis shoot and floral meristems and acts at a different regulatory level than the meristem genes WUSCHEL and ZWILLE. *The Plant Journal: For Cell and Molecular Biology*, 10(6), p.967-979.

Fleming, A. et al., 1997. Induction of leaf primordia by the cell wall protein expansion. *SCIENCE*, 276(5317), p.1415-1418.

Fletcher, J C et al., 1999. Signaling of cell fate decisions by CLAVATA3 in Arabidopsis shoot meristems. *Science (New York, N.Y.)*, 283(5409), p.1911-1914.

Frey-Wyssling, A., 1954. Divergence in helical polypeptide chains and in phyllotaxis. *Nature*, 173, p.596.

Frigerio, M. et al., 2006. Transcriptional regulation of gibberellin metabolism genes by auxin signaling in Arabidopsis. *Plant Physiology*, 142(2), p.553-563.

Friml, Jirí, 2010. Subcellular trafficking of PIN auxin efflux carriers in auxin transport. *European Journal of Cell Biology*, 89(2-3), p.231-235.

Friml, Jirí et al., 2004. A PINOID-dependent binary switch in apical-basal PIN polar targeting directs auxin efflux. *Science (New York, N.Y.)*, 306(5697), p.862-865.

Gallagher, K.L. & Benfey, P.N., 2005. Not just another hole in the wall: understanding intercellular protein trafficking. *Genes & Development*, 19(2), p.189-195.

Gallois, J.-L. et al., 2002. Combined SHOOT MERISTEMLESS and WUSCHEL trigger ectopic organogenesis in Arabidopsis. *Development (Cambridge, England)*, 129(13), p.3207-3217.

Gisel, A. et al., 2002. Leaf-to-shoot apex movement of symplastic tracer is restricted coincident with flowering in Arabidopsis. *Proceedings of the National Academy of Sciences of the United States of America*, 99(3), p.1713-1717.

Giulini, A., Wang, J. & Jackson, David, 2004. Control of phyllotaxy by the cytokinin-inducible response regulator homologue ABPHYL1. *Nature*, 430(7003), p.1031-1034.

Golz, J.F., 2006. Signalling between the shoot apical meristem and developing lateral organs. *Plant Molecular Biology*, 60(6), p.889-903.

Golz, J.F. & Hudson, Andrew, 2002. Signalling in plant lateral organ development. *The Plant Cell*, 14 Suppl, p.S277-288.

Gordon, S.P. et al., 2009. Multiple feedback loops through cytokinin signaling control stem cell number within the Arabidopsis shoot meristem. *Proceedings of the National Academy of Sciences of the United States of America*, 106(38), p.16529-16534.

Green, P.B., 1999. Expression of pattern in plants: combining molecular and calculus-based biophysical paradigms. *American Journal of Botany*, 86(8), p.1059-1076.

Green, P., 1996. Transductions to generate plant form and pattern: An essay on cause and effect. *ANNALS OF BOTANY*, 78(3), p.269-281.

Green, P., Steele, CS & Rennich, S., 1996. Phyllotactic patterns: A biophysical mechanism for their origin. *ANNALS OF BOTANY*, 77(5), p.515-527.

Greenboim-Wainberg, Y. et al., 2005. Cross talk between gibberellin and cytokinin: the Arabidopsis GA response inhibitor SPINDLY plays a positive role in cytokinin signaling. *The Plant Cell*, 17(1), p.92-102.

Grunewald, W. & Friml, Jirí, 2010. The march of the PINs: developmental plasticity by dynamic polar targeting in plant cells. *The EMBO Journal*, 29(16), p.2700-2714.

Gulline, H. & Walker, R., 1957. The regeneration of severed pea apices. *Aust J Bot*, 5, p.129-136.

Ha, C.M., Jun, J.H. & Fletcher, Jennifer C, 2010. Shoot apical meristem form and function. *Current Topics in Developmental Biology*, 91, p.103-140.

Hamant, O. & Traas, Jan, 2010. The mechanics behind plant development. *The New Phytologist*, 185(2), p.369-385.

Hamant, O. et al., 2008. Developmental patterning by mechanical signals in Arabidopsis. *Science (New York, N.Y.)*, 322(5908), p.1650-1655.

Hamant, O. et al., 2002. The KNAT2 homeodomain protein interacts with ethylene and cytokinin signaling. *Plant Physiology*, 130(2), p.657-665.

Hardtke, C.S. & Berleth, T, 1998. The Arabidopsis gene MONOPTEROS encodes a transcription factor mediating embryo axis formation and vascular development. *The EMBO Journal*, 17(5), p.1405-1411.

Hay, A. et al., 2002. The gibberellin pathway mediates KNOTTED1-type homeobox function in plants with different body plans. *Current Biology: CB*, 12(18), p.1557-1565.

Heisler, M.G. et al., 2010. Alignment between PIN1 polarity and microtubule orientation in the shoot apical meristem reveals a tight coupling between morphogenesis and auxin transport. *PLoS Biology*, 8(10), p.e1000516.

Heisler, M.G. et al., 2005. Patterns of auxin transport and gene expression during primordium development revealed by live imaging of the Arabidopsis inflorescence meristem. *Current Biology: CB*, 15(21), p.1899-1911.

Hernandez, L.F. & Green, P.B., 1993. Transductions for the Expression of Structural Pattern: Analysis in Sunflower. *The Plant Cell*, 5(12), p.1725-1738.

Hibara, K.-ichiro et al., 2006. Arabidopsis CUP-SHAPED COTYLEDON3 regulates postembryonic shoot meristem and organ boundary formation. *The Plant Cell*, 18(11), p.2946-2957.

Hofmeister, W., 1868. Allgemeine Morphologie der Gewächse. Dans *Handbuch der Physiologischen Botanik*. W. Engelmann, p. 405–664.

Hotton, S. et al., 2006. The possible and the actual in phyllotaxis: Bridging the gap between empirical observations and iterative models. *JOURNAL OF PLANT GROWTH REGULATION*, 25(4), p.313-323.

Huang, F. et al., 2010. Phosphorylation of conserved PIN motifs directs Arabidopsis PIN1 polarity and auxin transport. *The Plant Cell*, 22(4), p.1129-1142.

Husbands, A.Y. et al., 2009. Signals and prepatterns: new insights into organ polarity in plants. *Genes & Development*, 23(17), p.1986-1997.

Hussey, G., 1973. Mechanical stress in the shoot apices of Euphorbia, Lycopersicon, and Pisum under controlled turgor. *Ann Bot*, 37, p.57-64.

Ikeda, M., Mitsuda, N. & Ohme-Takagi, M., 2009. Arabidopsis WUSCHEL is a bifunctional transcription factor that acts as a repressor in stem cell regulation and as an activator in floral patterning. *The Plant Cell*, 21(11), p.3493-3505.

Iterson, G. van, 1907. *Mathematische und Mikroskopisch-AnatomischeStudien über Blattstellungen nebst Betraschtungen über denSchalenbau der Miliolinen* Jena: GustavFischer.,

Jackson, D & Hake, S, 1999. Control of phyllotaxy in maize by the abphyl1 gene. *Development (Cambridge, England)*, 126(2), p.315-323.

Jasinski, S. et al., 2005. KNOX action in Arabidopsis is mediated by coordinate regulation of cytokinin and gibberellin activities. *Current Biology: CB*, 15(17), p.1560-1565.

Jean, R., 1994. *Phyllotaxis: a systemic study in plant morphogenesis*,

Jones, A. M. & Herman, E.M., 1993. KDEL-Containing Auxin-Binding Protein Is Secreted to the Plasma Membrane and Cell Wall. *Plant Physiology*, 101(2), p.595-606.

Jönsson, H. et al., 2006. An auxin-driven polarized transport model for phyllotaxis. *Proceedings of the National Academy of Sciences of the United States of America*, 103(5), p.1633-1638.

Kim, I. & Zambryski, P.C., 2005. Cell-to-cell communication via plasmodesmata during Arabidopsis embryogenesis. *Current Opinion in Plant Biology*, 8(6), p.593-599.

Kim, I. et al., 2005. Cell-to-cell movement of GFP during embryogenesis and early seedling development in Arabidopsis. *Proceedings of the National Academy of Sciences of the United States of America*, 102(6), p.2227-2231.

Kim, J.Y. et al., 2002. Intercellular trafficking of a KNOTTED1 green fluorescent protein fusion in the leaf and shoot meristem of Arabidopsis. *Proceedings of the National Academy of Sciences of the United States of America*, 99(6), p.4103-4108.

Kim, J.-Y., Yuan, Z. & Jackson, David, 2003. Developmental regulation and significance of KNOX protein trafficking in Arabidopsis. *Development (Cambridge, England)*, 130(18), p.4351-4362.

Koch, A., Bernarsconi, G. & Rothen, F., 1998. Phyllotaxis as a geometrical and dynamical system. Dans *Symmetry in Plants*. Singapore: Jean RV, Barabé D.

Kondo, S. & Miura, T., 2010. Reaction-diffusion model as a framework for understanding biological pattern formation. *Science (New York, N.Y.)*, 329(5999), p.1616-1620.

Kondo, T. et al., 2006. A plant peptide encoded by CLV3 identified by in situ MALDI-TOF MS analysis. *Science (New York, N.Y.)*, 313(5788), p.845-848.

Kuhlemeier, Cris, 2007. Phyllotaxis. *Trends in Plant Science*, 12(4), p.143-150.

Kunz, M., 1997. *Phyllotaxie, billards polygonaux et theorie des nombres*. Switzerland: Université de Lausanne.

Kurakawa, T. et al., 2007. Direct control of shoot meristem activity by a cytokinin-activating enzyme. *Nature*, 445(7128), p.652-655.

Kuroha, T. et al., 2009. Functional analyses of LONELY GUY cytokinin-activating enzymes reveal the importance of the direct activation pathway in Arabidopsis. *The Plant Cell*, 21(10), p.3152-3169.

Kutschera, U. & Niklas, K.J., 2007. The epidermal-growth-control theory of stem elongation: an old and a new perspective. *Journal of Plant Physiology*, 164(11), p.1395-1409.

Kwiatkowska, D, 1999. Formation of pseudowhorls in Peperomia verticillata (L.) A-Dietr. shoots exhibiting various phyllotactic patterns. *ANNALS OF BOTANY*, 83(6), p.675-685.

Kwiatkowska, D, 1995. Ontogenetic changes of phyllotaxis in Anagallis arvensis L. *ACTA SOCIETATIS BOTANICORUM POLONIAE*, 64(4), p.319-325.

Kwiatkowska, D & Florek-Marwitz, J., 1999. Ontogenetic variation of phyllotaxis and apex geometry in vegetative shoots of Sedum maximum (L.) Hoffm. *ACTA SOCIETATIS BOTANICORUM POLONIAE*, 68(2), p.85-95.

Kwiatkowska, Dorota, 2008. Flowering and apical meristem growth dynamics. *Journal of Experimental Botany*, 59(2), p.187-201.

Laux, T et al., 1996. The WUSCHEL gene is required for shoot and floral meristem integrity in Arabidopsis. *Development (Cambridge, England)*, 122(1), p.87-96.

Leblanc, N. et al., 1999. A novel immunological approach establishes that the auxin-binding protein, Nt-abp1, is an element involved in auxin signaling at the plasma membrane. *The Journal of Biological Chemistry*, 274(40), p.28314-28320.

Lee, B., Johnston, R., et al., 2009. Studies of aberrant phyllotaxy1 Mutants of Maize Indicate Complex Interactions between Auxin and Cytokinin Signaling in the Shoot Apical Meristem. *PLANT PHYSIOLOGY*, 150(1), p.205-216.

Lee, B., Yu, S. & Jackson, D, 2009. Control of Plant Architecture: The Role of Phyllotaxy and Plastochron. *JOURNAL OF PLANT BIOLOGY*, 52(4), p.277-282.

Leibfried, A. et al., 2005. WUSCHEL controls meristem function by direct regulation of cytokinin-inducible response regulators. *Nature*, 438(7071), p.1172-1175.

Lenhard, Michael, Jürgens, Gerd & Laux, Thomas, 2002. The WUSCHEL and SHOOTMERISTEMLESS genes fulfil complementary roles in Arabidopsis shoot meristem regulation. *Development (Cambridge, England)*, 129(13), p.3195-3206.

Levitov, L., 1991a. ENERGETIC APPROACH TO PHYLLOTAXIS. *EUROPHYSICS LETTERS*, 14(6), p.533-539.

Levitov, L., 1991b. PHYLLOTAXIS OF FLUX LATTICES IN LAYERED SUPERCONDUCTORS. *PHYSICAL REVIEW LETTERS*, 66(2), p.224-227.

Leyser, Ottoline, 2006. Dynamic integration of auxin transport and signalling. *Current Biology: CB*, 16(11), p.R424-433.

Li, C., Zhang, X. & Cao, Z., 2005. Triangular and Fibonacci number patterns driven by stress on core/shell microstructures (vol 309, pg 909, 2005). *SCIENCE*, 310(5746), p.236-236.

Li, Y., Jones, L. & McQueen-Mason, S., 2003. Expansins and cell growth. *Current Opinion in Plant Biology*, 6(6), p.603-610.

Long, J A et al., 1996. A member of the KNOTTED class of homeodomain proteins encoded by the STM gene of Arabidopsis. *Nature*, 379(6560), p.66-69.

Lyndon, R.F., 1998. *The shoot apical Meristem*, U.K.: Cambridge.

Marchant, A. et al., 1999. AUX1 regulates root gravitropism in Arabidopsis by facilitating auxin uptake within root apical tissues. *The EMBO Journal*, 18(8), p.2066-2073.

Mayer, K.F. et al., 1998. Role of WUSCHEL in regulating stem cell fate in the Arabidopsis shoot meristem. *Cell*, 95(6), p.805-815.

Meicenheimer, R.D., 1982. CHANGE IN EPILOBIUM PHYLLOTAXY DURING REPRODUCTIVE TRANSITION. *AMERICAN JOURNAL OF BOTANY*, 69(7), p.1108-1118.

Meicenheimer, R.D., 1981. Changes in Epilobium phyllotaxy induced byN-1-Naphthylphthalamic acid and a-4-Chlorophenoxyisobutyricacid. *American Journal of Botany*, 68, p.1139-1154.

Meicenheimer, R.D., 1998. Decussate to spiral transitions in phyllotaxis. Dans *Symmetry in Plants*.

Meicenheimer, R.D. & ZAGORSKAMAREK, B., 1989. CONSIDERATION OF THE GEOMETRY OF THE PHYLLOTAXIC TRIANGULAR UNIT AND DISCONTINUOUS PHYLLOTACTIC TRANSITIONS. *JOURNAL OF THEORETICAL BIOLOGY*, 139(3), p.359-368.

Meinhardt, H., Koch, A. & Bernasconi, G., 1998. Models of pattern formation applied to plant development. Dans *Symmetry in Plants*.

Michniewicz, M. et al., 2007. Antagonistic regulation of PIN phosphorylation by PP2A and PINOID directs auxin flux. *Cell*, 130(6), p.1044-1056.

Mitchison, G.J., 1977. Phyllotaxis and the fibonacci series. *Science (New York, N.Y.)*, 196(4287), p.270-275.

Mizukami, Y. & Fischer, R.L., 2000. Plant organ size control: AINTEGUMENTA regulates growth and cell numbers during organogenesis. *Proceedings of the National Academy of Sciences of the United States of America*, 97(2), p.942-947.

Morris, C.E. & Homann, U., 2001. Cell surface area regulation and membrane tension. *The Journal of Membrane Biology*, 179(2), p.79-102.

Mähönen, A.P. et al., 2006. Cytokinin signaling and its inhibitor AHP6 regulate cell fate during vascular development. *Science (New York, N.Y.)*, 311(5757), p.94-98.

Nisoli, C. et al., 2009. Static and Dynamical Phyllotaxis in a Magnetic Cactus. *PHYSICAL REVIEW LETTERS*, 102(18). Available at: http://apps.isiknowledge.com.gate1.inist.fr/full_record.do?product=WOS&search_mode=GeneralSearch&qid=51&SID=Y2CpnCdfn3kKa2b842C&page=1&doc=3 [Consulté juillet 12, 2011].

Okada, K. et al., 1991. Requirement of the Auxin Polar Transport System in Early Stages of Arabidopsis Floral Bud Formation. *The Plant Cell*, 3(7), p.677-684.

d' Ovidio, F. & Mosekilde, E., 2000. Dynamical system approach to phyllotaxis. *PHYSICAL REVIEW E*, 61(1), p.354-365.

Paciorek, T. et al., 2005. Auxin inhibits endocytosis and promotes its own efflux from cells. *Nature*, 435(7046), p.1251-1256.

Peaucelle, A. et al., 2008. Arabidopsis phyllotaxis is controlled by the methyl-esterification status of cell-wall pectins. *Current Biology: CB*, 18(24), p.1943-1948.

Petrásek, J. et al., 2006. PIN proteins perform a rate-limiting function in cellular auxin efflux. *Science (New York, N.Y.)*, 312(5775), p.914-918.

Przemeck, G.K. et al., 1996. Studies on the role of the Arabidopsis gene MONOPTEROS in vascular development and plant cell axialization. *Planta*, 200(2), p.229-237.

Pulido, A. & Laufs, P., 2010. Co-ordination of developmental processes by small RNAs during leaf development. *Journal of Experimental Botany*, 61(5), p.1277-1291.

Rast, M.I. & Simon, Rüdiger, 2008. The meristem-to-organ boundary: more than an extremity of anything. *Current Opinion in Genetics & Development*, 18(4), p.287-294.

Reinhardt, D, Mandel, T & Kuhlemeier, C, 2000. Auxin regulates the initiation and radial position of plant lateral organs. *The Plant Cell*, 12(4), p.507-518.

Reinhardt, D et al., 1998. Localized upregulation of a new expansin gene predicts the site of leaf formation in the tomato meristem. *The Plant Cell*, 10(9), p.1427-1437.

Reinhardt, Didier, Frenz, M., et al., 2003. Microsurgical and laser ablation analysis of interactions between the zones and layers of the tomato shoot apical meristem. *Development (Cambridge, England)*, 130(17), p.4073-4083.

Reinhardt, Didier et al., 2005. Microsurgical and laser ablation analysis of leaf positioning and dorsoventral patterning in tomato. *Development (Cambridge, England)*, 132(1), p.15-26.

Reinhardt, Didier, Pesce, E.-R., et al., 2003. Regulation of phyllotaxis by polar auxin transport. *Nature*, 426(6964), p.255-260.

de Reuille, P.B. et al., 2006. Computer simulations reveal properties of the cell-cell signaling network at the shoot apex in Arabidopsis. *Proceedings of the National Academy of Sciences of the United States of America*, 103(5), p.1627-1632.

Richards, F., 1951. PHYLLOTAXIS - ITS QUANTITATIVE EXPRESSION AND RELATION TO GROWTH IN THE APEX. *PHILOSOPHICAL TRANSACTIONS OF THE ROYAL SOCIETY OF LONDON SERIES*, 235(629), p.509-564.

Richards, F., 1948. THE GEOMETRY OF PHYLLOTAXIS AND ITS ORIGIN. *SYMPOSIA OF THE SOCIETY FOR EXPERIMENTAL BIOLOGY*, 2, p.217-245.

Rieu, I. & Laux, Thomas, 2009. Signaling pathways maintaining stem cells at the plant shoot apex. *Seminars in Cell & Developmental Biology*, 20(9), p.1083-1088.

Robert, S. et al., 2010. ABP1 mediates auxin inhibition of clathrin-dependent endocytosis in Arabidopsis. *Cell*, 143(1), p.111-121.

Rojo, E. et al., 2002. CLV3 is localized to the extracellular space, where it activates the Arabidopsis CLAVATA stem cell signaling pathway. *The Plant Cell*, 14(5), p.969-977.

Rupp, H.M. et al., 1999. Increased steady state mRNA levels of the STM and KNAT1 homeobox genes in cytokinin overproducing Arabidopsis thaliana indicate a role for cytokinins in the shoot apical meristem. *The Plant Journal: For Cell and Molecular Biology*, 18(5), p.557-563.

STEUCEK, G., SELKER, J. & REIF, W., 1993. MECHANICAL FORCES IN THE SHOOT APEX COULD DEFINE SITES OF LEAF PRIMORDIA DEVELOPMENT. *JOURNAL OF CELLULAR BIOCHEMISTRY*, p.36-36.

Sabatini, S et al., 1999. An auxin-dependent distal organizer of pattern and polarity in the Arabidopsis root. *Cell*, 99(5), p.463-472.

Sachs, J., 1882. *Text book of botany* 2e éd.,

Sachs, T., 1969. Polarity and induction of organized vascular tissues. *Ann. Bot. (Lond.)*, 33, p.263.

Sakamoto, T. et al., 2001. KNOX homeodomain protein directly suppresses the expression of a gibberellin biosynthetic gene in the tobacco shoot apical meristem. *Genes & Development*, 15(5), p.581-590.

Sauer, M. et al., 2006. Canalization of auxin flow by Aux/IAA-ARF-dependent feedback regulation of PIN polarity. *Genes & Development*, 20(20), p.2902-2911.

Scarpella, E. et al., 2006. Control of leaf vascular patterning by polar auxin transport. *Genes & Development*, 20(8), p.1015-1027.

Schimper, C., 1830. Beschreibung des Symphytum Zeyheri und seiner zwei deutschen Verwandten der S. bulborum Schimper und S. tuberosum Jacqu. *Geiger's Magazin fuX r Pharmacie*, 29, p.1-92.

Schoof, H. et al., 2000. The stem cell population of Arabidopsis shoot meristems in maintained by a regulatory loop between the CLAVATA and WUSCHEL genes. *Cell*, 100(6), p.635-644.

Schoute, J.C., 1938. (IV) Early bonding whorls. *Recueil des travaux botaniques néerlandais*, 35, p.416-558.

Schoute, J.C., 1913. Beitrage zur Blattstellunglehre. I. Die Theorie. *Recueil de Travaux Botaniques Néerlandais*, 10, p.153-339.

Schuetz, M., Berleth, Thomas & Mattsson, Jim, 2008. Multiple MONOPTEROS-dependent pathways are involved in leaf initiation. *Plant Physiology*, 148(2), p.870-880.

Schwabe, W. & Clewer, A., 1984. PHYLLOTAXIS - A SIMPLE COMPUTER-MODEL BASED ON THE THEORY OF A POLARLY-TRANSLOCATED INHIBITOR. *JOURNAL OF THEORETICAL BIOLOGY*, 109(4), p.595-619.

Schwendener, S., 1878. *Mechanische Theorie der Blattstellungen.*, Leipzig: Engelmann.

Selker, J.M., Steucek, G.L. & Green, P.B., 1992. Biophysical mechanisms for morphogenetic progressions at the shoot apex. *Developmental Biology*, 153(1), p.29-43.

Sessions, A., Yanofsky, M.F. & Weigel, D, 2000. Cell-cell signaling and movement by the floral transcription factors LEAFY and APETALA1. *Science (New York, N.Y.)*, 289(5480), p.779-782.

Shipman, P. & Newell, A., 2005. Polygonal planforms and phyllotaxis on plants. *JOURNAL OF THEORETICAL BIOLOGY*, 236(2), p.154-197.

Shipman, P. et al., 2011. How universal are Fibonacci patterns? *EUROPEAN PHYSICAL JOURNAL D*, 62(1), p.5-17.

Silverstone, A.L. et al., 2007. Functional analysis of SPINDLY in gibberellin signaling in Arabidopsis. *Plant Physiology*, 143(2), p.987-1000.

Smith, R.S., 2008. The role of auxin transport in plant patterning mechanisms. *PLoS Biology*, 6(12), p.e323.

Smith, R.S. et al., 2006. A plausible model of phyllotaxis. *Proceedings of the National Academy of Sciences of the United States of America*, 103(5), p.1301-1306.

Snow, M. & Snow, R., 1932. Experiments on phyllotaxis I - The effect of isolating a pininordium. *PHILOSOPHICAL TRANSACTIONS OF THE ROYAL SOCIETY OF LONDON SERIES*, 221, p.1-43.

Snow, M. & Snow, R., 1933. Experiments on phyllotaxis II - The effect of displacing. *PHILOSOPHICAL TRANSACTIONS OF THE ROYAL SOCIETY OF LONDON SERIES*, 222, p.353-400.

Snow, M. & Snow, R., 1935. Experiments on phyllotaxis Part III - Diagonal splits through Decussate apices. *PHILOSOPHICAL TRANSACTIONS OF THE ROYAL SOCIETY OF LONDON SERIES*, 225, p.63-94.

Snow, M. & Snow, R., 1947. On the determination of leaves. *New Phytol*, 46, p.5-19.

Snow, M. & Snow, R., 1951. On the question of tissue tensions in stem apices. *New Phytol*, p.184-185.

Stahl, Y. & Simon, Rüdiger, 2010. Plant primary meristems: shared functions and regulatory mechanisms. *Current Opinion in Plant Biology*, 13(1), p.53-58.

Steele, CR, 2000. Shell stability related to pattern formation in plants. *JOURNAL OF APPLIED MECHANICS-TRANSACTIONS OF THE ASME*, 67(2), p.237-247.

Steeves, T.A. & Sussex, I.A., 1989. *Patterns in Plant Development* 2e éd., U.K.: Cambridge.

Steffens, B. et al., 2001. The auxin signal for protoplast swelling is perceived by extracellular ABP1. *The Plant Journal: For Cell and Molecular Biology*, 27(6), p.591-599.

Stoma, S. et al., 2008. Flux-based transport enhancement as a plausible unifying mechanism for auxin transport in meristem development. *PLoS Computational Biology*, 4(10), p.e1000207.

Szymkowiak, E. & Sussex, I., 1996. What chimeras can tell us about plant development. *ANNUAL REVIEW OF PLANT PHYSIOLOGY AND PLANT MOLECULAR BIOLOGY*, 47, p.351-376.

Terasaka, K. et al., 2005. PGP4, an ATP binding cassette P-glycoprotein, catalyzes auxin transport in Arabidopsis thaliana roots. *The Plant Cell*, 17(11), p.2922-2939.

Traas, J & Doonan, J H, 2001. Cellular basis of shoot apical meristem development. *International Review of Cytology*, 208, p.161-206.

Tromas, A. et al., 2009. The AUXIN BINDING PROTEIN 1 is required for differential auxin responses mediating root growth. *PloS One*, 4(9), p.e6648.

Turing, A., 1952. The Chemical Basis of Morphogenesis. *Phil. Trans. B.*, 237, p.37-72.

Ulmasov, T., Hagen, G. & Guilfoyle, T.J., 1997. ARF1, a transcription factor that binds to auxin response elements. *Science (New York, N.Y.)*, 276(5320), p.1865-1868.

Veen, A.H. & Lindenmayer, A., 1977. Diffusion mechanism for phyllotaxis: theoretical physico-chemical and computer study. *Plant Physiology*, 60(1), p.127-139.

Veit, B., 2009. Hormone mediated regulation of the shoot apical meristem. *Plant Molecular Biology*, 69(4), p.397-408.

Vernoux, T. et al., 2011. The auxin signalling network translates dynamic input into robust patterning at the shoot apex. *Molecular Systems Biology*, 7, p.508.

Vidaurre, D.P. et al., 2007. AMP1 and MP antagonistically regulate embryo and meristem development in Arabidopsis. *Development (Cambridge, England)*, 134(14), p.2561-2567.

Wabnik, K. et al., 2010. Emergence of tissue polarization from synergy of intracellular and extracellular auxin signaling. *Molecular Systems Biology*, 6, p.447.

Wardlaw, C., 1949a. EXPERIMENTAL AND ANALYTICAL STUDIES OF PTERIDOPHYTES . 14. LEAF FORMATION AND PHYLLOTAXIS IN DRYOPTERIS-ARISTATA DRUCE. *ANNALS OF BOTANY*, 13(50), p.163-&.

Wardlaw, C., 1948. Experimental and analytical studies of PteridophytesXI. Preliminary observations on tensile stress as a factor in fern phyllotaxis. *Ann Bot*, 12, p.97-108.

Wardlaw, C., 1949b. PHYLLOTAXIS AND ORGANOGENESIS IN FERNS. *NATURE*, 164(4161), p.167-169.

Weigel, D et al., 1992. LEAFY controls floral meristem identity in Arabidopsis. *Cell*, 69(5), p.843-859.

Weisse, A., 1894. Neue Beiträge zur mechanischen Blattstellungslehre. *Jahrb. Wiss. Bot.*, 26, p.236-294.

Williams, R. & Brittain, E., 1984. A GEOMETRICAL MODEL OF PHYLLOTAXIS. *AUSTRALIAN JOURNAL OF BOTANY*, 32(1), p.43-72.

Wisniewska, J. et al., 2006. Polar PIN localization directs auxin flow in plants. *Science (New York, N.Y.)*, 312(5775), p.883.

Wu, X. et al., 2003. Modes of intercellular transcription factor movement in the Arabidopsis apex. *Development (Cambridge, England)*, 130(16), p.3735-3745.

Xu, T. et al., 2010. Cell surface- and rho GTPase-based auxin signaling controls cellular interdigitation in Arabidopsis. *Cell*, 143(1), p.99-110.

Yadav, R.K. et al., 2009. Gene expression map of the Arabidopsis shoot apical meristem stem cell niche. *Proceedings of the National Academy of Sciences of the United States of America*, 106(12), p.4941-4946.

Yanai, O. et al., 2005. Arabidopsis KNOXI proteins activate cytokinin biosynthesis. *Current Biology: CB*, 15(17), p.1566-1571.

Yoshikawa, H. et al., 2010. Pattern formation in bubbles emerging periodically from a liquid free surface. *EUROPEAN PHYSICAL JOURNAL E*, 33(1), p.11-18.

Zagorska-Marek, B., 1994. Phyllotaxic diversity in Magnolia Fowers. *Acta Soc. Bot. Poloniae*, 63, p.117-137.

Zhao, Y., 2008. The role of local biosynthesis of auxin and cytokinin in plant development. *Current Opinion in Plant Biology*, 11(1), p.16-22.

Zhao, Z. et al., 2010. Hormonal control of the shoot stem-cell niche. *Nature*, 465(7301), p.1089-1092.

CHAPTER 1

Identification of perturbation patterns in Fibonacci spirals suggest a new role for cytokinin signaling in coordinating space and time in phyllotaxis.

This chapter has been adapted from an article in preparation to be integrated in this manuscript. It corresponds to a work done in close collaboration with mathematicians and modelers.

Most of methods concerning the mathematical analysis and models, which were not relevant with respect to the biological focus of this chapter, were removed from "supplementary information" section and are given as appendices at the end of this chapter.

The following people collaborated to the work presented in this chapter:

Yann Guédon[(1)], Yassin Refahi[(1)], Fabrice Besnard[(2)], Etienne Farcot[(1)], Christophe Godin[(1)], Teva Vernoux[(2)].

[(1)] Laboratoire de Reproduction et Développement des Plantes, CNRS, INRA, ENS Lyon,UCBL, Université de Lyon, 46 Allée d'Italie, 69364 Lyon Cedex 07, France.

[(2)] Virtual Plants INRIA Project Team, UMR DAP, INRIA/CIRAD, Montpellier, France.

Author contributions:

T.V, F.B. designed the project and the biological experiments and F.B. performed the experiments. Y.R., E.F., C.G. and Y.G. designed and performed the analysis of phyllotactic sequences.

ABSTRACT

Vascular plants iteratively produce organs in geometric spatial arrangements called phyllotaxis. Mostly regular, these patterns may exhibit significant perturbations, which have been reported in many species with various type of phyllotaxis. However, no precise characterization of phyllotactic perturbations has been undertaken yet. We thus decided to analyze specifically the perturbations affecting the phyllotaxis of the model plant *Arabidopsis thaliana*. In this typical Fibonacci spiral phyllotaxis, 2 consecutive organs are expected to be separated by a constant divergence angle close to 137.5°, the golden angle. However, we observed short segments of non-canonical angles in sequences of divergence angles measured between flowers. To characterize these perturbations, we designed a pipeline of methods that combines a sub-model representing perturbations patterns (either a variable-order Markov chain or a combinatorial model) with von Mises distributions accounting for measurement uncertainty. We demonstrated that nearly all perturbations could be explained by permutations in the apico-basal order of 2 to 3 consecutive organs along stems. Given the development and the architecture of shoots, the most plausible explanation for these permutations is a problem affecting the coordination between space and time during early organ development in the SAM. Furthermore, we found that null mutants in the cytokinin signaling inhibitor AHP6 strongly enhance the occurrence of permutations, suggesting a role for cytokinin signaling in this process. Moreover, our data highlight the robustness of the spatial positioning in phyllotaxis. Interestingly, nearly 80 years after the pioneering microsurgery experiments of Snow and Snow, we provide novel statistical arguments suggesting that the positioning of a new organ is controlled by its nearest neighbors.

1 Introduction

In vascular plants, the arrangement of leaves, buds and flowers around stems generates regular patterns, called phyllotaxis. Phyllotaxis originates in the tissue located at the tip of branches, the shoot apical meristem (SAM): in the SAM, organs are produced iteratively at very precise positions, determining the final pattern. This tight spatial and temporal control of organogenesis has fascinated many biologist in addition to mathematicians and physicists that have studied phyllotaxis since almost two centuries (Adler et al. 1997).

Most theories explaining the developmental mechanisms behind phyllotaxis are based on the idea that each organ produces an inhibitory field in its surroundings that prevents the formation of a new organ nearby (R. Smith, C Kuhlemeier, et al. 2006). Supported experimentally by pioneering microsurgery experiments in meristems (M. Snow & R. Snow 1932; M. Snow & R. Snow 1933; Wardlaw 1949)or more recently by laser ablations (Didier Reinhardt et al. 2005), the mechanism of local inhibitory fields has been implemented in many models, which showed it was a plausible mechanism for the generation of phyllotaxis. In the last decade, a series of studies have demonstrated the key role played by the phytohormone auxin and strongly suggest that inhibitory fields are created by auxin depletion areas (D Reinhardt et al. 2000; Didier Reinhardt et al. 2003; R. S. Smith, Guyomarc'h, et al. 2006). According to these convincing studies, a network of PIN1 polar trans-membrane pumps directs auxin fluxes throughout the epidermis of the SAM. The self-organized behavior of this network would be able to generate local peaks of auxin concentration, that trigger organ formation (Heisler et al. 2005; de Reuille et al. 2006). Developing organs would then remove auxin from their vicinity, inhibiting the formation of new organs around them. Importantly, several cell-based models relying on these assumptions are able to reproduce the main types of phyllotaxis (Jönsson et al. 2006; R. S. Smith, Guyomarc'h, et al. 2006; Stoma et al. 2008; Bayer et al. 2009; Sahlin et al. 2009).

However, this current biological mechanism remains partially elusive. First the fields of auxin depletion cannot be visualized directly. It is thus difficult to estimate their characteristics (e.g. size, dynamics) and to link them to model predictions. Second, models still need to use several assumptions, like the precise mechanisms of PIN1 polarization (Stoma et al. 2008; Bayer et al. 2009) or the values of several biochemical parameters. Thus, despite the tremendous progress recently brought by system biology approaches, further research is still needed to bridge the gap between models based on inhibitory-field mechanisms and the understanding of molecular and cellular networks controlling phyllotaxis. To contribute to this issue, we propose to analyze the

perturbations that occur naturally in plant phyllotaxis. These perturbed patterns may reveal important properties of the biological mechanism generating phyllotaxis. Notably, their characterization could confirm or infirm model predictions and suggests new assumptions for modeling.

Many studies have reported abnormal phyllotaxis either exhibiting local perturbations of the regular arrangement or more important perturbations with no obvious regularities at all (reviewed in (Jean 1994; Barabé 2006). Moreover, quantification concerning the diversity of phyllotactic patterns has been mostly made at the population scale (see Introduction): how robust the pattern is within a same individual over several iterations of organ formation has not been precisely studied. This question is not trivial to address, notably because the characterization of perturbations requires large samples and dedicated statistical tools, especially if the frequency of perturbations is low compared to regular phyllotaxis. In this respect, it can be helpful to study mutants from model plants in genetics exhibiting obvious perturbations in their phyllotaxis (Barabé 2006; Golz & Hudson 2002). These phyllotactic mutants can first be used to identify new genes involved in the control of phyllotaxis. Moreover, the strongly enhanced frequency of perturbations in phyllotactic mutants helps the statistical characterization of perturbation patterns.

To our knowledge, few studies have tried to analyze both quantitatively and qualitatively the defects in the phyllotaxis of plants (Itoh et al. 2000; Peaucelle et al. 2007; Ragni et al. 2008) and they were impaired by the absence of appropriate tools. Recently, Barabé and Jeune pointed out this lack and first proposed in a series of articles new statistical methods that they applied to the phyllotaxis of the rice mutants *sho1, sho2, sho3* (Barabé & Bernard Jeune 2004; B Jeune & Barabe 2004; B Jeune & Barabe 2006; B Jeune & Barabé 2006; B Jeune & Barabe 2006). Here we propose a new approach, based on the analysis of measures of successive divergence angles in stems of *Arabidopsis thaliana*. This model species exhibit the most widespread type of phyllotaxis found in nature (Cris Kuhlemeier 2007): a Fibonacci spiral, where the divergence angle in regular patterns is close to 137.5°, the golden angle. We analyzed the phyllotaxis of wild-type *Arabidopsis* and of a mutant line exhibiting obvious phyllotactic defects. This line bears a null mutation in the gene encoding the pseudo phosphotransfer protein AHP6 (Mähönen et al. 2006), an inhibitor of cytokinin signaling. We selected this mutant by reverse genetics (see later, chap2) in order to investigate a possible role of cytokinin in the control of phyllotaxis in *Arabidopsis*.

The originality of the proposed approach is that it takes into account the order of organ along the stem in the analysis of the sequences of divergence angles. This information should not be

neglected, since the position of new organs in the SAM is thought to depend on the position of older organs. We thus developed a pipeline of methods to analyze the spatial patterns generated by phyllotaxis and also to infer rules concerning the dynamics of organ formation. Moreover, we used models combining structure with probabilities. Probabilities enable us to identify and characterize complex patterns which cannot be grasped directly from collected data, without knowing or quantifying the underlying biological functions. In this respect, the analysis of complex phyllotactic patterns fits into the general framework of pattern theory (Grenander & Miller 2006). This strategy led us to identify interesting perturbation patterns in Fibonacci spiral phyllotaxis in wild-type as well as in *ahp6* mutant plants. The data presented here question the actual model accounting for phyllotaxis and suggest a new role for cytokinin signaling in the coordination of space and time during phyllotactic pattern formation.

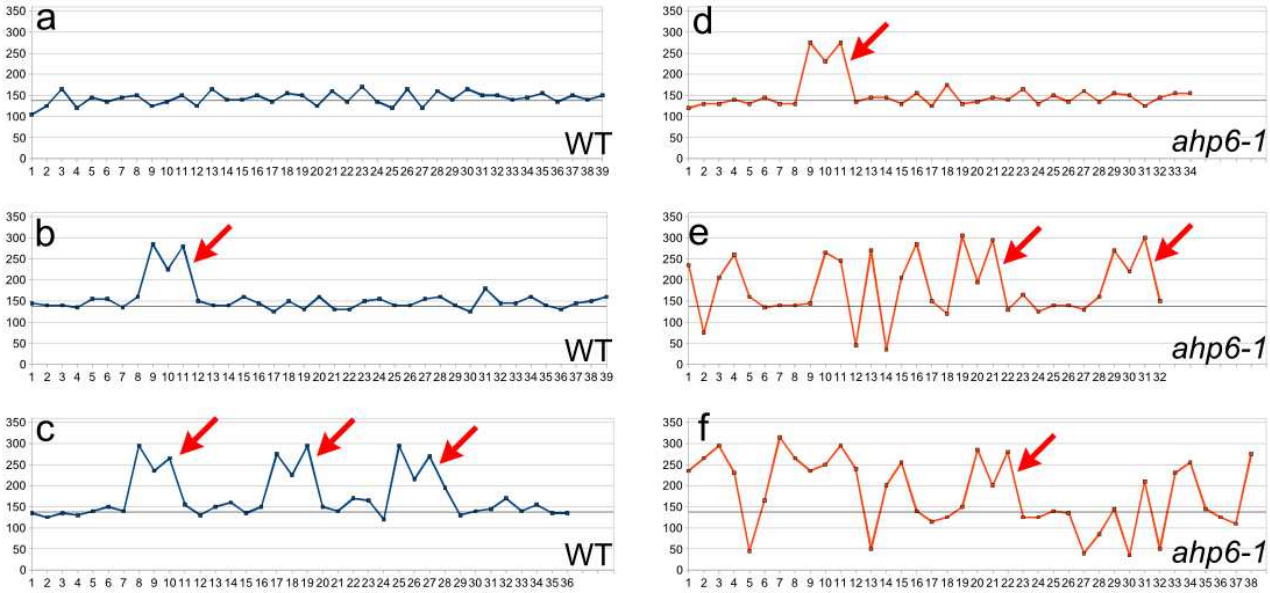

Figure 1: Examples of measured divergence angle sequences in wild-type *Arabidopsis* and *ahp6-1* mutant plants. (a,b,c) WT plants with increasing perturbations, (d,e,f) *ahp6-1* with increasing perturbations. In each diagram the thin black horizontal line indicate 137.5°, the canonical angle of the Fibonacci spiral phyllotaxis. Red arrows indicate a M-shaped perturbation motif recurrent in many sequences.

2 Results

2.1 Measurements of divergence angle sequences between siliques and analysis of spiral orientation.

We measured divergence angles between siliques (*Arabidopsis* fruits) in fully elongated stems in 82 *Arabidopsis* wild-type plants and 89 *ahp6* mutant plants. Angles were measured from the base (first organ produced) towards the top of stems, giving individual sequences of several consecutive angles. The main orientation of the spiral was determined by identifying segments of divergence angles close to the canonical Fibonacci angle of α=137.5° (termed baseline segments). Further precisions are given in the "Supplementary Information" section.

In the measured sample, 39 out of 82 wild-type individuals and 45 out of 89 mutant individuals had a clockwise orientation. Hence, clockwise and counterclockwise spirals occurred in roughly equal proportion in both wild-type and mutant samples. For the wild type, this observation is in accordance with previous results (Beal 1873; Allard 1946). These equal proportions are explained by the fact the spiral originates from an initial symmetry breaking event corresponding to the transition between the decussate phyllotaxis of the seedling and the Fibonacci phyllotaxis of the adult plant. We conclude that in the mutant, the loss of *AHP6* function does not affect this initial symmetry-breaking event.

2.2 Exploratory analysis suggest that both wild-type and *ahp6-1* mutants have structured perturbation motifs

The measured divergence angle sequences generally exhibit baseline segments (the angles fluctuate around of α=137.5º) and were interspersed by segments (i.e. sub-sequences) of non-canonical angles, indicating perturbations of the phyllotaxis (see examples Figure 1). Surprisingly, phyllotaxis of wild-type plants were also significantly perturbed. But as expected, *ahp6-1* plants had many more defects in phyllotaxis, with higher frequencies of non-canonical angles and complex patterns of perturbations (Figure 1)

The angles measured covered almost all the possible values between 0º and 360º. While the global distribution showed highest frequencies around the canonical Fibonacci angle, at least three other classes of divergence angles were apparent, but could not be unambiguously separated (Figure 2). These combined observations suggest that non-canonical angles measured in perturbations are not random and could belong to at least four distinct classes.

Moreover, the sub-sequences of perturbations often seemed highly structured. Particularly, a stereotypical M-shaped motif corresponding approximately to [2α,–α, 2α] was frequently observed in wild-type and even more often in *ahp6-1* mutants (Figure 1, red arrows). This motif can be simply explained by a permutation in the order of insertion on the stem of two consecutive organs, without changing their angular position (Figure S2). It should be noted that a similar M-shaped motif was predicted by theoretical models (Douady & Couder 1996a). However, such a motif was reported only once in a sunflower stem with the Lucas spiral phyllotaxis, a rare arrangement characterized by a canonical divergence angle of 99.5° (Couder 1998).

The occurrence of non-canonical angles and of particular motifs in the sequences suggest that precise patterns of perturbations could be present in our data, like permutations, generating particular divergence angles with possible local dependencies. To test this hypothesis, we decided to analyze our data with statistical tools and a step-by-step approach: we built successively more and more specific models, each model incorporating the deductions made in the previous estimated model. The model explaining the perturbations of phyllotaxis will emerge progressevily, and specific patterns could be identified with a minimum of *a priori* assumptions.

2.3 Identification of permutations patterns in the sequences of measured divergence angles using Hidden Markov Chains (HMC)

To identify patterns in the measured divergence angles sequences, we chose to use hidden-Markov chains (HMC). Markov chain is a stochastic model often used to describe patterns generated by iterative transitions between defined states: in our case, the states would be different divergence angles. Hidden Markov chains are then used because the states of a Markov chain related to divergence angles would not be directly observable for the experimentalist: biological noise and measurement uncertainty modify the value of each "theoretical" angle. The Markov chain is thus hidden and it must be inferred from the sequences of measured angles (Ephraim & Merhav 2002)(see Supplementary Information). To represent the variability of measured divergence angles, we attached to each state of the Markov chain a von Mises distribution. The von Mises distribution is a univariate Gaussian-like periodic distribution for a variable $x \in [0, 360\circ)$ (Mardia & Jupp 2000) At each iteration, the next state can depend only on the previous state (defining a first-order Markov chain) or on more previous states (second-, third-, etc., -order Markov chain). We began our analysis with the first-order. We also made the assumption of stationarity (see Supplementary

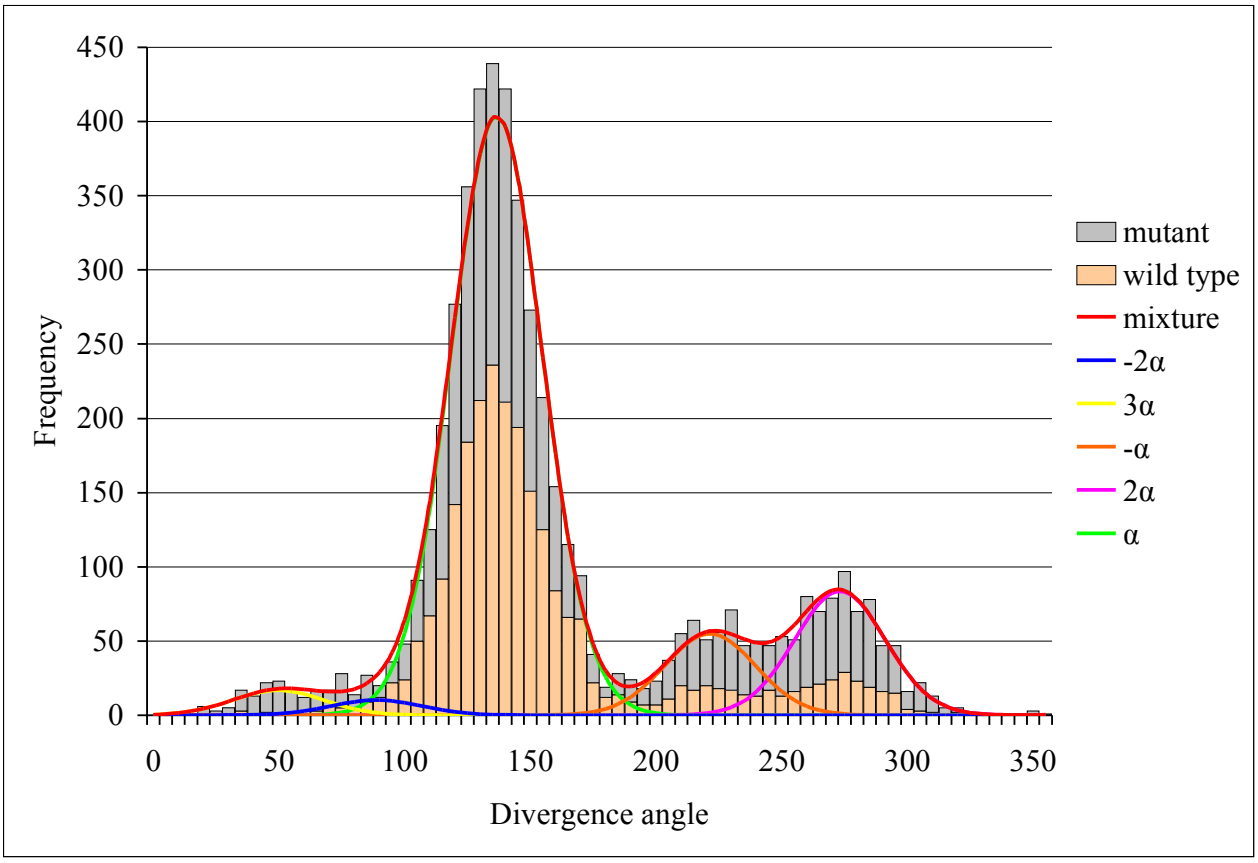

Figure 2: Fit of the divergence angle frequency distribution by the mixture of observation distributions. The fit is visually indiscernible if the observation distributions of the five-state hidden first-order Markov chain are showed instead of the observation distributions of the five-state hidden variable-order Markov chain. Interestingly, the observation distributions associated to the five states of the HMC estimated by the model are centered on values very close to multiples of the canonical angle of Fibonacci spirals (α = 137.5°): α, 2α, 3α, -α, -2α.

	first order				variable order	
	μ	σ	μ ($\sigma = 18.5$)	weight	μ ($\sigma = 18.5$)	weight
α (137.5)	136.5	18.2	136.5	0.71	136.6	0.7
2α (275)	273.3	18.7	273.4	0.14	273.1	0.15
$-\alpha$ (222.5)	221.9	17.7	222.1	0.1	221.5	0.1
3α (52.5)	50.3	20.1	50.8	0.03	49.7	0.03
-2α (85)	80.9	14.3	83	0.02	88.9	0.02
log-likelihood	-17041.3		-17034.4		-16694.3	
BIC	-34339.4		-34282.9		-33705.4	

Table 1: Characteristics of von Mises observation distributions estimated within hidden first-order Markov chains (with different or common concentration parameters) and within a hidden variable-order Markov chain. Since the weights of the different states were similar for the two estimated hidden first-order Markov chains, they are only given one time. Log-likelihoods and BIC values for the three estimated models.

Information for justification, Figure S3). Thus, a stationary (or equilibrium) hidden first-order Markov chain is the most simple model for analyzing sequences of noisy discrete-valued divergence angles. Importantly, it does not rely on any assumption concerning the structure of possible patterns in the divergence angle sequences.

In practice, we pooled in the analysis the measured divergence angle sequences from wild-type and *ahp6* mutants (171 sequences of cumulative length 5220, referred as to the learning sample), assuming that the perturbation patterns was common to the wild-type and the mutant.

We proceeded to a step-by-step identification, deriving model assumptions of the current step from the outputs of the preceding step of analysis. First, the number of possible states for the HMC was selected. The Bayesian information criterion (BIC) favored both a 4-state or 5-state hidden first-order Markov chain model. Interestingly, the 5 states were rather precisely centered on the multiples of the canonical divergence angle α, 2α, -α, (Table 1). The 4 states were centered only on α, 2α, -α and a intermediate angle between 3α and -2α. Assuming that these precise occurrence of 5 multiples of α could be more meaningful, we selected the five-state HMC model. Second, we estimated a five-state hidden first-order Markov chain where the von Mises observation distributions share the same concentration parameter (inverse variance), since the previously estimated von Mises distributions had similar standard deviations. This simplification led to a slight improvement of the the log-likelihood of the model (Table1). Having a robustly estimated five-state hidden first-order Markov chain model from the global learning sample, we next computed for each individual observed sequence the optimally labeled sequence: each measured angle was labeled with five possible values chosen among α, 2α, -α, 3α and -2α. In this way, 161 out 171 sequences were labeled with high confidence (posterior probability of the most probable state sequence > 0.13, Figure S4).

In a last step, we selected the order of the Markov chain depending on the context within the sequence. We thus selected the memories of a variable-order Markov chain (Csiszar & Talata 2005) on the basis of the previously optimally labeled divergence angle sequences (see Supplementary Information and Appendix). First we chose to discard the 10 individuals which were very poorly explained by the estimated hidden first-order Markov chain. The variable-order Markov chain we obtained was a mixed first-/second-order Markov chain where the first-order memory 2α was replaced by the four second-order memories α 2α, 2α 2α, -α 2α, -2α 2α (the memory 3α 2α was not observed) with respect to a simple first-order Markov chain. This means that it was necessary to take into account the divergence angle that precedes 2α to predict accurately the state that follows

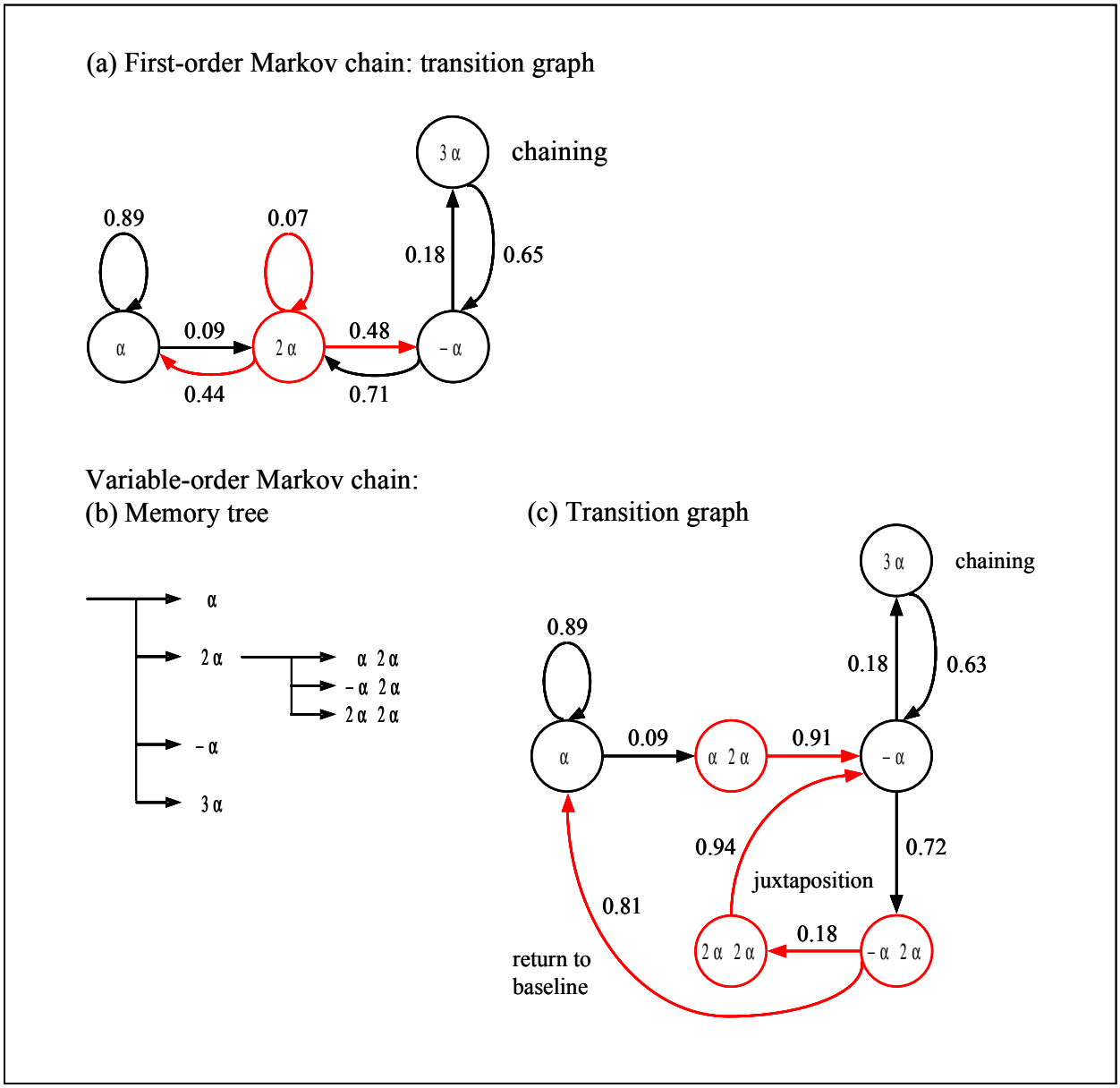

Figure 3: Hidden Markov chains restricted to the modeling of 2-permutations. (a) hidden first-order Markov chain: transition graph of the underlying Markov chain; Hidden variable-order Markov chain: (b) Memory tree; (c) transition graph. In (a) and (c), each vertex represents a possible memory. Possible transitions are represented by arcs. The associated probabilities are noted nearby.

2α. This is illustrated by the graph of transitions of the first-order Markov chain and the mixed first-/second-order Markov chain restricted to the modeling of 4 hidden states (α, 2α, -α, 3α) for sake of clarity (Figure 3).

Most of the selected memories in this graph can be interpreted as permutations in the order of organs along the stem. Indeed, the optimal labeled sequences exhibit perturbed segments that can be interpreted as isolated 2-permutation motif (the [. . . α, 2α, -α, 2α, α, . . .] M-shaped motif), as chaining of 2-permutations ([. . . α, 2α, -α, 3α, -α, 2α, α,. . .]), juxtaposition ([. . . α, 2α, -α, 2α, 2α, -α, 2α, α,. . .]) (Figure 3c), and other optimized labeled sequences involved isolated 3 permutations between the order of 3 organs (3-permutations, e.g. [. . . 3α, -α, - α, 3α, . . .]).

In conclusion, this first step of analysis enables to (i) identify five classes of divergence angles centered on the multiples of the canonical divergence angle α, 2α, -α, 3α, -2α, (ii) estimate a common concentration parameter for the von Mises distributions reflecting measurement uncertainty and (iii) identify a remarkable dependency structure that can be interpreted with regards to the language induced by 2-permutations.

We next wanted to characterize the perturbations patterns in each individual to determine to what extent the permutation hypothesis could explain the individuals sequences and to compare the perturbations between wild-type and *ahp6-1* mutant plants.

2.4 Characterization of permutation patterns using HMC and Combinatorial Mixture models.

Based on the previous model identification steps, we estimated a hidden variable-order Markov chain where the underlying variable-order Markov chain has the memories previously selected and the concentration parameter was common to the five von Mises observation distributions. The optimally labeled divergence angle sequence was computed for each observed sequence using the estimated hidden variable-order Markov chain (including the 10 individuals previously discarded for model selection). Taking the posterior probability as an indicator of confidence (Figure S4), most sequences could be reasonably explained by this model (Table 2). Some sub-sequences poorly explained according to the posterior probability had a strong individual effect, suggesting that other angles than those modeled by the five-state of the HMC could be present in these sequences of some individuals. Within the sequences explained by the model, most could be interpreted as permutations. However, since the HMC model is not constrained *a priori* by the permutation assumption, we also observed 16 occurrences of the memory -2α, 2α, which cannot be generated by

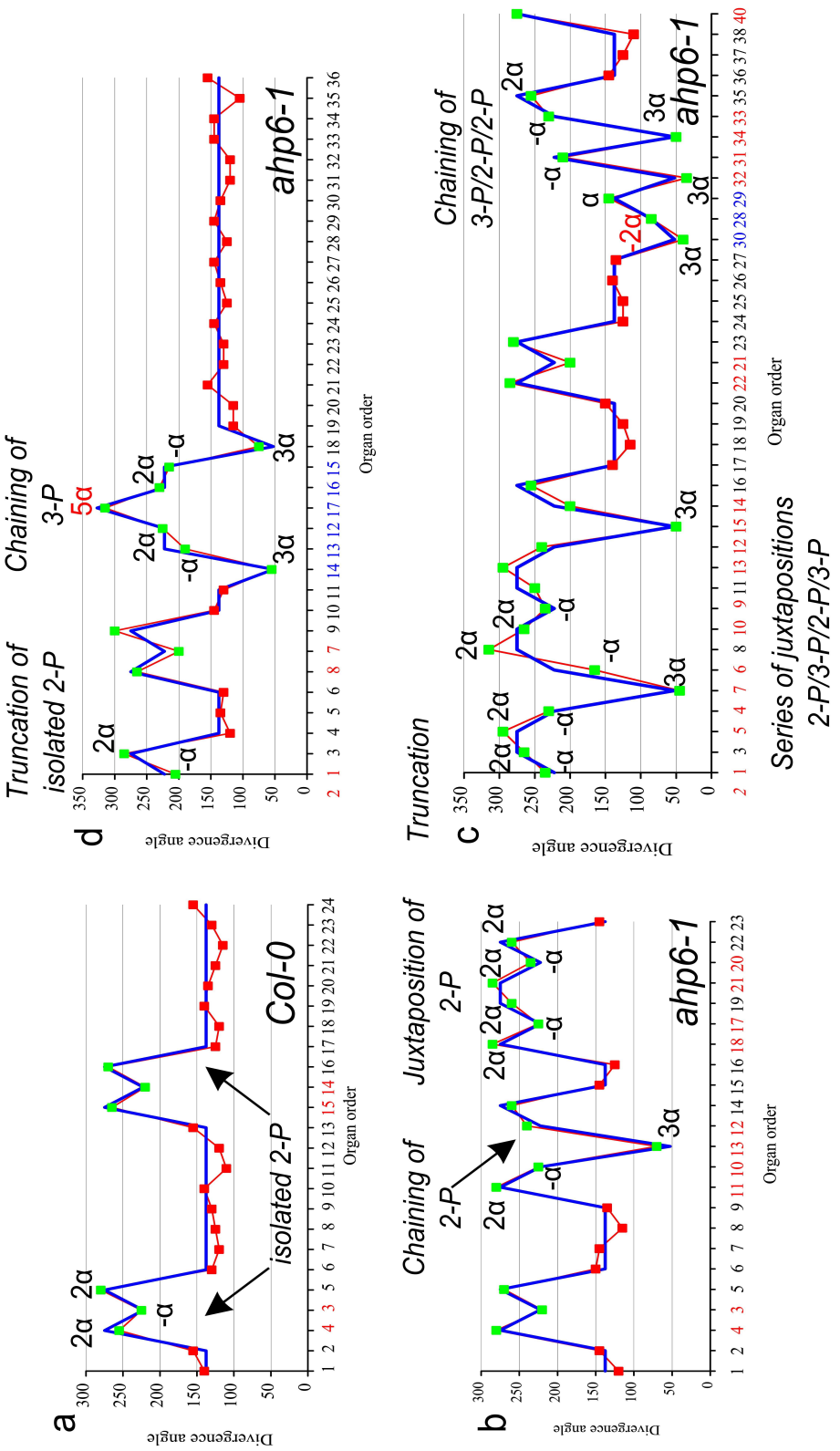

Figure 4: Examples of final consensus optimal labeling of measured sequences. The measured divergence angles are figured by the red squares for canonical angles and green squares for non-canonical angles (excepted α outside baseline segments). The predicted divergence angle sequence is figured in blue. The predicted organ order is given below and permuted organs are in red for 2-Permutation (2-P) and in blue for 3-Permutations (3-P). The sequences are ordered in increasing complexity. Note the occurrence of the rare angles 5α and -2α in c and d.

permutations. However we reasoned that these few unexplained sequences could also be permutations, but that they were too rare to be statistically estimated. A study of the language induced by any possible combination of 2- and 3-permutations indicates that other multiples of α, such as 4α and 5α are possible in complex chaining of permutations, and would thus be expected with a low frequency. However, it was impossible to estimate a seven-state HMC: there is a too big overlap between the von Mises distribution attached to the seven possible states induced by permutations (α, 2α, -α, 3α -2α, 4α, 5α), in conjunction with their very unbalanced respective weights (Figure S5).

Considering that a single model could not have all the desirable properties to model these sequences, we chose to build a second model, based this time on the assumption of permutations, and to build a consensus from the comparison of labeled sequences computed using both models. We designed a combinatorial mixture model (CMM), in which the underlying Markov chain of the hidden Markov model previously used is replaced by a combinatorial model that relies on the assumption that the permutations involved at most 3 successive organs (e.g. [3α -α -α 3α] corresponding to the organ order 3 2 1 4) (Refahi et al. 2011). Von Mises observation distributions centered on the multiples of the divergence angle were attached to the seven "states" α, 2α, -α, 3α, -2α, 4α, 5α. The concentration parameter common to the seven von Mises observation distributions was the concentration parameter estimated within the hidden Markov model. This CMM can thus be viewed as the coupling of a combinatorial model relying on the permutation assumption with an independent mixture model. It can thus model transitions involving multiples of the canonical divergence angle which occur rarely (e.g. 4α, 5α), and it can also model alternative phyllotaxes (e.g. Lucas with a canonical divergence angle of 99.5°). However, its major shortcoming is the risk of predicting very unprobable patterns of permutations despite strong deviations between measured and predicted angles. This is a direct consequence of the important overlap between the von Mises observation distributions (Figure S5). *Since the CMM is not an integrated probabilistic model,* it was not possible to compute a posterior probability to assess the relevance of the optimally labeled divergence angle sequences.

We thus labeled independently each individual sequence with the two models, the five-state hidden variable-order Markov Chain model and the CMM (see Supplementary Information), respectively. When the labeled sequences computed by the two models did not coincide, we made an expert examination of the two labelings to choose the most likely solution (Figure S6). We observed very few mismatches between the optimal labeling of the divergence angle sequences

	5-state HMC		CMM		
	match	mismatch	match	mismatch	consensus
α	3620	21	3579	62	3641
2α	695	5	675	25	700
$-\alpha$	440	6	433	13	446
3α	117	8	120	5	125
-2α	23	10	33	0	33
4α		10	10	0	10
5α		1	1	0	1
total	4895	61	4851	105	4956
?			99	50	149

Table 2: Counts of matches and mismatches between the optimal labeling of the divergence angle sequences using the five-state hidden variable-order Markov chain (HMC), the combinatorial mixture model (CMM) and the final consensus labeling taken as reference (the four Lucas phyllotaxis individuals were excluded from the sample).

	wild type	mutant
No. sequences/No. angles	82/2405	89/2815
% of non-canonical angles	15%	37%
% of unexplained angles	2%	5%
No. individuals, Lucas phyllotaxis	2	2
No. 2-permutations	123	297
No. 3-permutations	3	53

Table 3: Characteristics of the optimally labeled divergence angle sequences using the final consensus. Note that nearly all angles were explained accordingly to the permutations assumption. *ahp6* mutants exhibit a significantly higher proportion of non-canonical angles, which corresponds to a marked increase in the number of 2- and 3 permutations.

given by the two models and the final consensus sequences: this illustrates the complementarity of the two modeling approaches and the strong accordance of the estimated hidden variable-order Markov chain with the permutation assumption.

With this pipeline of methods (Figure S6), we were able to label a very large proportion of the sequences measured for both wild type and the *ahp6* mutant on the basis of the permutation assumption (98% and 95% of explained angles respectively, Table 3). In particular, we labeled 4 individuals assuming a Lucas phyllotaxis (this pattern has a canonical divergence angle of 99.5°). The rare occurrence of the Lucas phyllotaxis in our data set is in accordance with previous reports in sunflower (see in Introduction, table 1). We cannot exclude that the remaining small proportion of non-explained angles could be generated by other types of perturbation, involving different angles or patterns. But the poorly explained angles could also be due to a lack of measurement accuracy or measurement errors. Moreover, the difficulty of measurement increases when successive organs are very close due to non-elongated internodes or when no regular spiral appears on the stem as in highly perturbed individuals. This is often the case in mutant plants (see later section 2.5 and 2.7) and it could thus account for the higher unexplained proportion of angles in *ahp6*.

In previous studies, the authors hypothesized that the perturbations they measured in *Arabidopsis* stems were due to a reversal of the handedness of the generative spiral (Peaucelle et al. 2007). We also tested this assumption, searching for the reversal point after which the divergence angle would fluctuate around 360°-α = 222.5° in baseline segments. This assumption is clearly not supported by the analysis of both wild-type and the mutant sequences. Instead, the proposed permutation hypothesis is supported by the conjunction of (i) the specificity of the permutation assumption, (ii) the high frequencies of the non-canonical angles (Table 3), (iii) the high confidence in the explanation of the observed sequences by the estimated hidden variable-order Markov chain (see the posterior probabilities, Figure S4). This hypothesis thus seems to fit the observed data better that any competing hypothesis that we have been able to consider.

Altogether, our analysis based on mixture models for patterns analysis demonstrated that nearly all the perturbations observed in the measured sequences can be interpreted with high confidence as permutations in the apico-basal order of two to three organs along the stem (Table 3).

2.5 Permutations patterns in *ahp6* mutants are more numerous, longer and more complex.

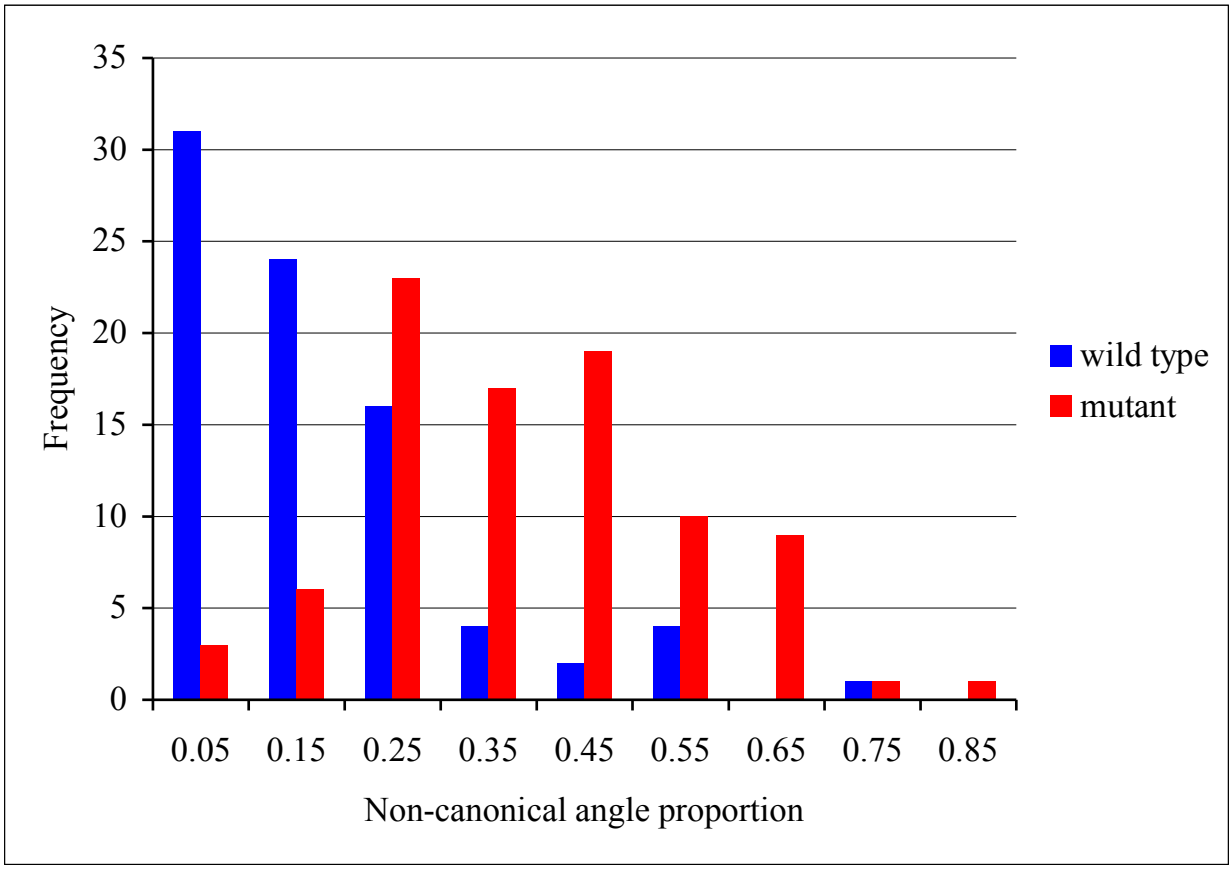

Figure 5: Proportions of non-canonical angles per sequence in wild-type and mutants show overlapping phenotypes. Despite an overlap in the phenotype, the two populations can be separated: individuals having more 30 % of non-canonical angles in their sequences are likely *ahp6-1* mutants, individuals with less than 10% of perturbations are likely wild-type.

Some examples of wild-type and mutant individuals with the optimal consensus labeling are shown in Figure 4. The proportion of non-canonical angles increases from 15% to 37% between the wild type and the mutant (Table 3) and corresponds to a strong increase in the occurrence of 2-permutations and a burst in the occurrence of 3-permutations. Note that, proportionally, 3-permutations increase much more than 2-permutations in the *ahp6* genetic background, suggesting that the developmental defects leading to 3-permutations are very sensitive to the loss of *AHP6* function. However, these global proportions of non-canonical angles hide a great inter-individual heterogeneity within each genotype, with a strong overlap of the two populations (Figure 5). This heterogeneity of the two populations is illustrated by the examples in Figure 1 (compare the perturbed wild-type 1c with mild *ahp6-1* mutant 1d). However, most of the individuals with more than 30% of non-canonical angles were mutant. Conversely, 18 out 82 wild-type plants exhibit perfect sequences fluctuating only around the canonical angle compared to only 1 *ahp6* individual out of 89.

The highly perturbed mutant individuals were characterized by the occurrence of long and complex permuted segments corresponding to the chaining of 2- and 3-permutations (Tables 4 and 5). The permuted segments identified in the measured sequences are listed with their respective frequencies for each genotype in Tables 4 and 5. The close frequencies of the three possible permuted segments corresponding to an isolated 3-permutation (Table 4) suggest that the mechanism generating 3-permutations is affected by randomness. The similar ratios of the frequency of n + 1 chained 2-permutations to the frequency of n chained 2-permutations (16/90 for n = 1 for the wild type and 32/193, 5/32 and 1/5 for n = 1, 2, 3 for the mutant; see Tables 4 and 5) suggest that the chaining of permutations is also random. In addition, we detected all the possible segments produced by a combination of a 2-permutation with a 3-permutation, except one, but they all occur with small frequencies, again suggesting randomness in the chaining.(Table 4).

Finally, it should be noted that we found two Lucas phyllotaxes in each genotype. However, this small number of Lucas individuals precludes the comparison of patterns within individual sequences between the two genotypes. In all cases however, these sequences were highly perturbed (data not shown).

Altogether, these data suggest that *AHP6* limits the number and the complexity of permutations.

2.6 Classification of individuals belonging to different genetic backgrounds confirm the role of *AHP6.*

	organ order	divergence angles	wild type	mutant
2-permutation	2 1 3	2 -1 2	90	193
	3 2 1 4	3 -1 -1 3	1	11
3-permutation	3 1 2 4	3 -2 1 2	1	9
	2 3 1 4	2 1 -2 3		13
total			2	33
2 2-permutations	2 1 4 3 5	2 -1 3 -1 2	16	32
	2 1 5 3 4 6	2 -1 4 -2 1 2	1	1
	2 3 1 5 4 6	2 1 -2 4 -1 2		2
2-permutation and	2 1 5 4 3 6	2 -1 4 -1 -1 3		
3-permutation	3 2 1 5 4 6	3 -1 -1 4 -1 2		1
	2 1 4 5 3 6	2 -1 3 1 -2 3		1
	3 1 2 5 4 6	3 -2 1 3 -1 2		3
total			1	8

Table 4: **Observed permuted segments up to length 6.** These segments are delimited by two splitting points. The divergence angle sequence is the first-order differenced organ sequence. By convention, the origin of the organ sequence is 0 (not indicated). Palindromes (a segment and its reverse in terms of divergence angles are the same) are given at the beginning of each category. A segment and its reverse are then given on two successive rows. Frequencies of segments are given for the wild type and the mutant. Canonical angles α (noted 1) present in perturbed sequences are highlight in yellow. Note that they are always associated with -2α (noted -2) just before or after. This property was useful two estimate their number versus α angles in baseline segments.

	organ order	divergence angles	mutant
3 2-permutations	2 1 4 3 6 5 7	2 -1 3 -1 3 -1 2	5
	3 2 1 6 5 4 7	3 -1 -1 5 -1 -1 3	1
2 3-permutations	2 3 1 6 4 5 7	2 1 -2 5 -2 1 2	1
	3 2 1 6 4 5 7	3 -1 -1 5 -2 1 2	1
	2 1 5 3 4 7 6 8	2 -1 4 -2 1 3 -1 2	1
2 2-permutations and	3 1 2 5 4 7 6 8	3 -2 1 3 -1 3 -1 2	1
a 3-permutation	2 1 4 3 7 5 6 8	2 -1 3 -1 4 -2 1 2	2
	2 3 1 5 4 7 6 8	2 1 -2 4 -1 3 -1 2	1
4 2-permutations	2 1 4 3 6 5 8 7 9	2 -1 3 -1 3 -1 3 -1 2	1
3 2-permutations and a 3-permutation	2 1 4 3 7 6 5 9 8 10	2 -1 3 -1 4 -1 -1 4 -1 2	1

Table 5: Observed permuted segments of lengths from 7 to 10 (Note that some possible segments allowed by the language of 2- and 3-permutations which were not observed are not reported in this table). These segments are delimited by two splitting points. The divergence angle sequence is the first-order differenced organ sequence. By convention, the origin of the organ sequence is 0 (not indicated). Frequencies of segments are given (all these long permuted segments were detected on mutant individuals). Canonical angles α (noted 1) and associated -2α present in perturbed sequences are highlighted in yellow.

To confirm the role of the *AHP6* gene in controlling the permutations of organs, we adopted a classical genetic approach. We selected *ahp6-3,* another independent mutant for *AHP6,* and we also analyzed *ahp6-1* mutants in which a functional AHP6 transgene was introduced (these transgenic *ahp6-1* lines are termed complemented lines). As additional classical controls in genetics, we also selected the trans-heterozygous *ahp6-1/3* line (the direct progeny of a cross between *ahp6-1* and *ahp6-3* parents). These plants bear one null *ahp6-1* allele and one null *ahp6-3* allele, so they have no functional alleles of AHP6. As complemented lines, we used *ahp6-1* plants transformed to express AHP6-GFP or AHP6-HA fusion proteins in the same expression patterns as AHP6 native protein (the fusion with the fluorescent protein GFP and the tag HA was used to visualize the AHP6 protein *in situ* in other experiments). The other *ahp6* mutant lines are expected to exhibit the same phenotype as the *ahp6-1* line (numerous permutations) while complemented lines are expected to exhibit a wild-type phenotype (few permutations) because the transgene should provide a functional version of AHP6.

We then applied a model-based classification approach where for each sequence to be classified, we tested which model among the wild-type and the *ahp6-1* mutant models best explains this sequence. For the building of the wild type and *ahp6-1* mutant models, we adopted the following strategy. The two models share the same memories i.e. (α, $\alpha 2\alpha$, $2\alpha 2\alpha$, $-\alpha 2\alpha$, $-2\alpha 2\alpha$, $-\alpha$, 3α, -2α). This is supported by the selection of the memories on the basis of the state sequence corresponding to the wild-type (respectively mutant) individuals computed using the globally estimated hidden variable-order Markov chain. They also share the same von Mises observation distributions with the common concentration parameter estimated on the basis of the pooled sample of wild-type and mutant individuals (within the globally estimated hidden variable-order Markov chain). On the basis of the wild-type (respectively *ahp6-1* mutant) sample, we applied the EM algorithm where only the transition probabilities were re-estimated. We finally established a threshold at 10^{-2} the lowest transition probabilities in order to avoid misclassification of individuals due to unobserved patterns in the learning samples. For each observed divergence angle sequence to be classified, the likelihood of the wild-type and *ahp6-1* mutant models were computed using the forward or filtering algorithm; see e.g. (Zucchini & MacDonald 2009). Each observed divergence angle sequence was then assigned to the model that best explained it. One difficulty in this classification task comes from the class overlap. The wild-type model is actually nested within the *ahp6-1* mutant model since both wild-type and mutant individuals exhibit permutations, the difference coming essentially from the more frequent occurrence of permutations in the mutant case. Hence, the less perturbed

		HMC	
		wild-type	ahp6-1
Leaning samples	wild-type	73	9
	ahp6-1	21	68
Test samples	ahp6-3	5	9
	ahp6-1-3	5	9
	L91GFP	14	5
	L94GFP	12	3
	T314HA	8	11
	T32HA	11	8

Table 6: Classification of individual sequences of divergence angles into wild-type or *ahp6-1* models. As a test, all individuals of the learning sample that were used two build the two models were classified: some individuals can be misclassified, due to the overlap of the phenotype between wild-type and *ahp6-1* mutant plants. Then individuals from loss of function mutant lines (*ahp6-3* and *ahp6-1/3* mtants) or complemented lines (2 transgenic lines expressing a AHP6-GFP fusion protein and 2 transgenic lines expressing a AHP6-fusion protein) were classified. See text for details.

	wild type			mutant		
	angle	internode	expected	angle	internode	expected
α	2003	100	144.6	1655	140	226.5
α^*	2	1	0.1	37	11	5.1
2α	214	5	15.5	499	46	68.3
$-\alpha$	126	58	9.1	330	120	45.2
3α	20	5	1.4	111	28	15.2
-2α	2	2	0.1	37	21	5.1
4α	1	0	0.1	10	1	1.4
5α				3	0	0.4

Table 7: Non-elongated internodes are more often-associated permuted organs. For each genotype, the number of observed non-elongated internodes for each angle is indicated (α is separated in two classes: α belonging to baseline segments and α* belonging to permuted segments). In the third column is indicated the number of short internodes that would be expected if the traits were independent. The negative angles -α and -2α, which always measure the divergence angle between organs whose order is permuted, and also the angle α* and 3α are significantly associated with non-elongated internodes.

mutant individual can be classified in the wild-type class. This particular class configuration is illustrated by the classification of the individuals used for building the two models where 21 out of 89 *ahp6-1* mutants were misclassified while only 9 out of 82 wild-type individuals were misclassified (Table 6).

Most of the individuals of the other *ahp6* mutant lines (i.e. *ahp6-3* and *ahp6-1/3*) were assigned to the *ahp6-1* model (9 out of 14 in each lines). This result can be considered as significant, since the classification results are biased toward the wild-type model because of the model nestedness. Concerning the complemented lines, most of the plants transformed to express AHP6-GFP were assigned to the wild-type model while the results were not so clear for the plants transformed to express AHP6-HA (Table 6). The fact that not all our transgenic lines had a restored wild-type phenotype is not surprising: there are many biological reasons that could impair the proper expression and function of the AHP6 protein provided by the transgene. For example, insertion of the transgene to silent regions of the genome would compromise its expression, or the function of the protein could be altered due to the fused GFP/HA tag. On the contrary, the capacity of AHP6-GFP to rescue the wild-type phenotype, at least partially, is a strong argument supporting the causal link between *AHP6* loss of function and the increase in permutations.

2.7 A Permutation between two organs is often associated with a non-elongated internode

Since numerous non-elongated internodes can be seen along the stem of *ahp6* mutants (see chapter2, figure 2A), we looked for a statistical link between this phenotype and the permutations. The table 7 details the counts of non-elongated internodes for each of the 7 angles defined by the permutations, in the wild-type and the mutant from the learning sample. Note that we distinguished the angles α appearing in baseline segments and the angle α (noted α*) embedded in permuted segments (see table 4 and 5, angle α highlighted in yellow). Interestingly, the language of 2-and 3-permutations imposes that α* and -2α are always successive angles, which helps the identification of this particular α*. The frequencies of the association of non-elongated internodes with the different angles was clearly not proportional, pointing out an association between non-elongated internodes and the angles -α and -2α and to a lesser extent with with α* and 3α. Within a permuted segment of angles, -α and -2α are always the divergence angles between organs whose order on the stem is reverse to the order they would have without pemutations. For example, if ordered organs [1, 2, 3, 4] are permuted into the [1, **3, 2**, 4] sequence, -α will be the divergence angle measured

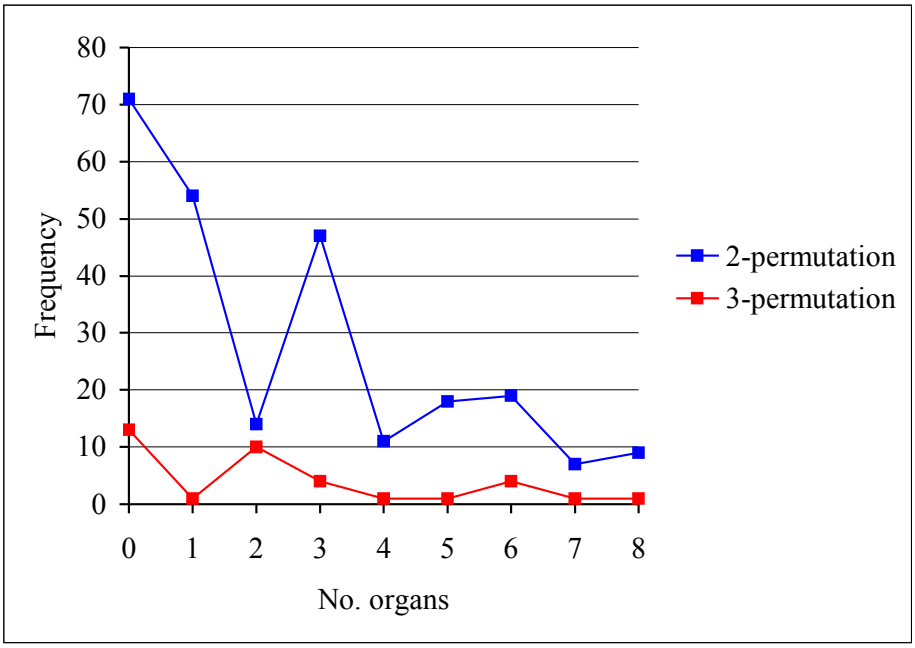

Figure 6: Frequency distributions for the number of successive synchronized organs between two permutations. These runs of organs are distinguished as a function of the permutation that precedes them. The length frequency distribution is highly structured, indicating that a first permutation influences the occurrence of a second over short intervals of synchronized organs. 2- and 3-Permutations restrain differently the

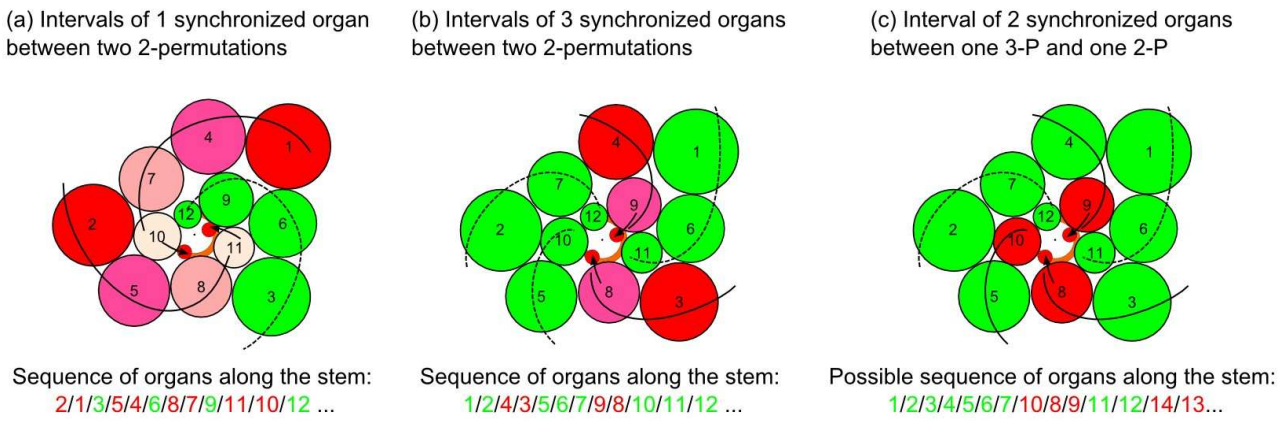

Figure 7: Propagations of permutations over intervals of synchronized organs correlate with contact parastichies. Organs are represented by circles with increasing numbers from older to younger, as expected without permutations. Organs involved in the same event of permutation are colored with the same color (with a red scale according to their age), while synchronized organs are colored in green. The meristem is the central white circle: at its periphery (orange), two small red circles indicate the next organs to form (13 and 14) that will be permuted. The sequence of order of these organs expected along the stem is indicated below each cartoon. Interesting contact parastichies are drawn. The most probable configuration of propagation observed in our data is represented. Note that each time, the parastichies were no organ is permuted (dashed line) is maintained, while permuted organs are found in the same parastichy (plain line), suggesting a transmission of the permutation to the nearest neighbors (arrows).

between the organs [3,2]. There is thus a correlation between a reverse in the order of two organs in the sequence and the absence of the development of the internode in between them. For example, 46% (58/126) in wild-type and 36% (120/330) in *ahp6-1* of internodes between organs ordered in a [...(n+1), n...] order (correspoding to angle -α) are non elongated. Since the association is not strict, this indicates that a permutation is neither sufficient nor necessary to find a short internode (and reciprocally).

2.8 Patterns of propagation of permutation in sequences suggest a role of direct neighbors

As seen above, our analysis suggests that the order of organs within a permutation is random as well as the chaining of 2-permutations. We then wondered whether it was possible to determine a context when a permutation begins or ends. We found no particular context explaining the triggering of a permutation after a baseline segment. However, the triggering of a new permutation is clearly influenced by a former permutation when the baseline segment in between them is short. This is illustrated by the frequency distribution of the length of intervals of synchronized organs between two permuted segments (synchronized organs are those whose order in the measured sequence is the same as expected without permutations). Two situations are observed (Figure 6): intervals of synchronized organs following a 2-permutation or intervals following a 3-permutation (see Supplementary Information for the construction of these frequency distributions).

The resulting distributions revealed that for intervals following a 2-permutation, the length frequency distribution is highly structured with high frequencies for u = 0 (u is the number of synchronized organs in the interval, u = 0 is a chaining of two permutations), u = 1 (juxtaposition of two permuted segments) and u = 3 and comparatively low frequencies for 2 and 4; (Figure 6). For intervals following a 3-permutation, the length frequency distribution seems also highly structured despite the globally lower frequencies with respect to the frequency distribution related to 2-permutations. The chaining of two permutations (u = 0) are relatively frequent while the juxtaposition of two permuted segments (u = 1) seems almost impossible and a canonical angle is required between two permuted segments. In both cases, the interval length frequency distributions differ markedly from geometric distributions which are the unique “memoryless” discrete distribution. Hence, the occurrence of a permutation influences the occurrence of a subsequent permutation at least on the four next positions that follow it and with specific dependencies as function of 2- or 3-permutations.

Using centric representations of meristems, we reproduce the sub-sequences studied above: a first permuted segment, followed by an interval of synchronized organs, followed by a second permuted segment. We observed the existence of particular geometric relationships between organs in the two permuted segments (Figure 7). Interestingly, when the interval length frequency distribution predict a new permuted segment, organs with reverse order in this segment are direct neighbors of organs with reverse order in the former permuted segment. In phyllotactic systems, spirals called contact parastichies can be easily drawn linking direct neighbors (they are often naturally conspicuous in the pattern). The particular geometric relationships observed for organs with reverse order between two permuted segments suggest that the permutation propagates more likely along the contact parastichies. This transmission of permutation between direct neighbors can overcome a return to a normal baseline segment. This correlation is worth to be highlighted, because it is in agreement with the fundamental mechanistic hypothesis for phyllotaxis, stating that the position of a new organ in the structure is determined by its two direct neighbors.

However, in the case of chaining (u = 0, i.e. no synchronized organ is initiated in between permutations), the probability for a new permutation to occur without a return to the baseline is also very high (Figure 6), although the organs involved in the first permutation and the next to come are not located on perturbed contact parastichies (graphic not shown). This could suggest that once a permutation has occurred, the plant is in a state where a subsequent permutation is more likely to happen. In other words, it could be possible that the perturbation that causes the first Larger samples would be needed to further analyze precisely the properties of permutation patterns, notably for complex motifs of which very few were observed (Table 5).

Wild-type and mutant plants had similar interval length frequency distributions (Figure S7). Therefore, whereas the loss of *AHP6* function promote permutations, we conclude that its presence in the wild-type does not reduce their properties of propagation over short intervals of synchronized organs.

2.9 Within baseline segments, the canonical divergence angle is robustly set but can significantly differ from the theoretical golden angle (137.5º)

Apart from the perturbed sub-sequences, we also investigate the properties of the non-perturbed sub-sequences (baseline segments). We first estimated the mean value of the divergence angle of the baseline segments To evaluate the heterogeneity in the population of our learning sample, we

computed the weighted mean absolute deviation between the average baseline segment level for an individual and the canonical angle of 137.5◦. The sample weighted mean absolute deviation is given by

$$\sum_a n_a \left|\overline{x}_a - 137.5\right| / \sum_a n_a,$$

where $\overline{x}_a$ is the mean of the divergence angles within baseline segments and n_a is the cumulative length of the baseline segments for the *a*th individual.

We obtained a mean absolute deviation of 8.1° for the wild-type, 5.7° for the mutant and 7° for the pooled sample (the results are similar if we use as a reference the overall average divergence angle within baseline segments instead of the theoretical angle of 137.5°). It should be noted that the baseline segment effect was slightly larger than this individual effect (results not shown). This result confirm an important inter-individual heterogeneity, which is reflected in part by the concentration parameter estimated for the von Mises distributions (Table 1). The deviation from the expected golden angle indicates a natural range within which a stable Fibonacci spiral establishes a divergence angle in *Arabidopsis thaliana,* with a strong individual effect. This amplitude of this range could be better determined with more accurate measurement tools.

2.10 Exploring local dependencies in baseline segments by sample auto-correlation

Finally, we looked for local dependencies within the baseline segments by studying the auto-correlation between successive angle in the segments (Figure 8). Note that the divergence angles we measured were obtained by subtracting 2 positions of flowers on the protractor (see Supplementary Information): this operation, termed a first-order differencing, can be seen as a linear filter that induces an auto-correlation structure; see (Diggle 1990). In the case of first-order differencing, the induced auto-correlation function is

$$\rho(k) = \begin{cases} 1 & k = 0, \\ -0.5 & k = 1, \\ 0 & k > 1. \end{cases}$$

We observed that the sample auto-correlation functions for the baseline segments were close to the auto-correlation functions induced by first-order differencing a white noise sequence (Figure 8, red line). The sample auto-correlation coefficients which measure the correlation between

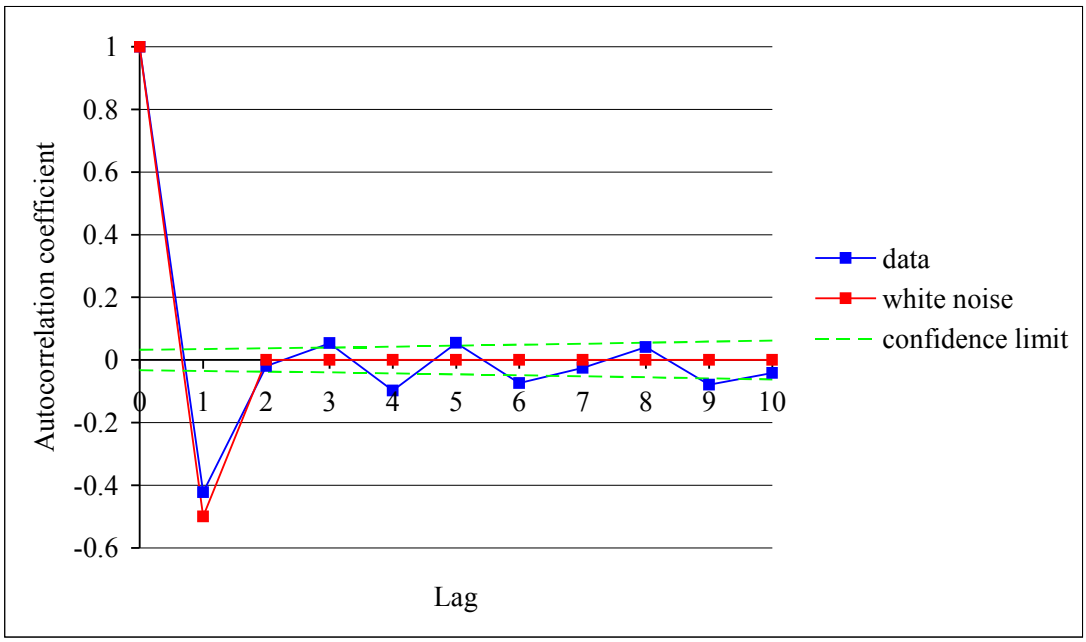

<u>Figure 8</u>: Sample auto-correlation function of divergence angles within baseline segments This auto-correlation is calculated with baseline segments found in both wild-type and mutants plants, with a correction taking into account inter-individual heterogeneity. A lag x indicates the autocorrelation between two organs n and n+x in a baseline segment. The strong negative autocorrelation at lag=1 is induced by the the first-order differencing used for the calculation of divergence angles from measurements and is not biologically relevant. The fluctuation of the auto-correlation function near the confidence limits cannot be considered as statistically significant. However, we noted intriguing potential positive auto-correlations for lag 3, 5 and 8, three Fibonacci numbers corresponding to the number of contact parastichies in *Arabidopsis thaliana.*

divergence angles at different distances apart within baseline segments (pooled sample auto-correlation function) is given by

$$r(k) = \frac{\sum_a \sum_{t=0}^{n_a-k-1} (x_{a,t} - \overline{x}_a)(x_{a,t+k} - \overline{x}_a) / \sum_a (n_a - k)}{\sum_a \sum_{t=0}^{n_a-1} (x_{a,t} - \overline{x}_a)^2 / \sum_a n_a}, \qquad k = 0, 1, \ldots$$

where

$$\overline{x}_a = \sum_{t=0}^{n_a-1} x_{a,t}/n_a$$

is the mean of the divergence angles within the *a*th baseline segment. The baseline segment mean $\overline{x}_a$ can be replaced by the mean of the divergence angles within baseline segments for an individual but not by the overall mean because of the inter-individual heterogeneity of baseline segment levels. The variation of the auto-correlation function stays within the confidence limits for a lag>1, meaning that there are statistically no auto-correlations within baseline segments.

However, it should be noted that we observed a structure in the auto-correlation curve, with positive auto-correlations between one divergence angle and the 3rd, the 5th and the 8th following angle just outside the confidence limits for the two first peaks. The occurrence of these 3 Fibonacci numbers reminds us that *Arabidopsis* phyllotaxis is organized with a (3,5) parastichy number, and perhaps some individuals could be at the intermediary (3,5,8) order. Such positive auto-correlations could mean that each deviation from the mean value of the baseline segment tends propagate along the contact parastichies, as seen for the permutation patterns (see above). However, without strong statistical support, this observation cannot be considered as reliable. Since the fluctuation of the base line is of the same magnitude as the precision of our measurement device, we would need to improve the accuracy of our measurements to demonstrate such property in our sequence.

Moreover, *ahp6* mutants' baseline have the same baseline properties as wild-type, suggesting that *AHP6* loss of function only produce permuted segments that do not affect the properties of the normal regime of phyllotaxis when baseline segments are produced.

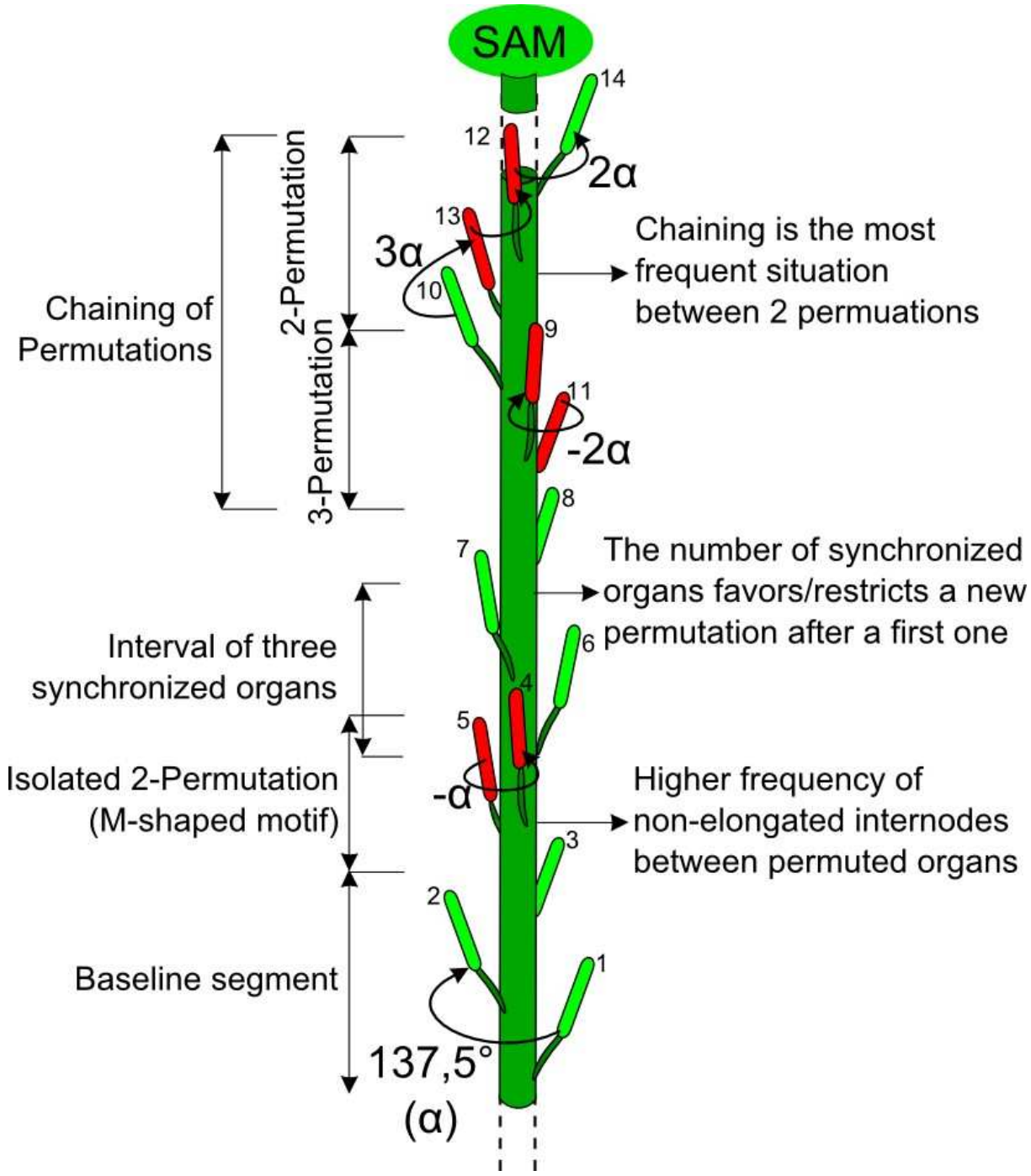

Figure 9: Schematic summary of permutation patterns found in *Arabidopsis* Phyllotaxis. This cartoon of a fully elongated inflorescence stem of *Arabidopsis thaliana* exhibit characteristic permutation patterns measured in plants. Permuted organs are red, synchronized organs are light green. Organs are numbered according to the normal order, from the older to the younger. The five multiples of α (137.5°, the canonical golden angle of Fibonacci spiral) which are most frequently found in sequences are indicated: α, 2α, -α, 3α, -2α. These permutation patterns are most frequent in *ahp6* loss of function mutants. Although observed post-meristematically, these permutations patterns are likely generated earlier in the Shoot Apical Meristem (SAM).

3 Discussion

In this study, we analyzed with a new pipeline of methods the phyllotaxis of the model plant *Arabidopsis thaliana.* Notably, we identified and characterized frequent perturbation patterns of the regular Fibonacci spiral due to permutations in the order of organ along the stem (Figure 9). Interestingly, we found that the loss of function of the cytokinin inhibitor *AHP6* led to an increase in the permutations. Associated to other robust features of the sequences revealed by our analysis, this study provides new data for the understanding of phyllotaxis and question the current models of phyllotaxis. We will first discuss the biological significance of permutations and the possible role of AHP6 related to them. Then we will point some questions raised by our study on the current vision of the developmental mechanism explaining phyllotaxis and we will suggest further possible directions of research.

3.1 Possible origins of Permutations and putative role for *AHP6* functions in *Arabidopsis*.

Thanks to the analysis we developed, nearly all perturbations we observed in *Arabidopsis* post-meristematic phyllotaxis can be considered as permutations in the apico-basal order of organs (here flowers) along the stem. Moreover we demonstrated that this defect is genetically controlled by AHP6, a small pseudo-Histidine-Phosphotransfer protein (pseudo HPt) which has been characterized as an inhibitor of cytokinin signaling (Mähönen et al. 2006). Interestingly, permutations are also present in the wild-type, suggesting that other factors than AHP6 (endogenous or exogenous) could control their occurrence in phyllotaxis. Quantitatively and qualitatively comparing permutations in wild-type and *ahp6* mutants, we found that *AHP6* limits their occurrence and their length, thus maintaining a stable state of the phyllotaxis (Figure 10). This model suggests that AHP6 functions as a stabilizing factor buffering permutations.

Histograms of global divergence angle distribution published in previous studies with the other ecotype Wassileskija (Peaucelle et al. 2007; Ragni et al. 2008) were similar to our data, suggesting the presence of permutations although the authors did not mention it. We propose that permutations are a very common perturbation of the Fibonacci spiral phyllotaxis in *Arabidopsis thaliana*. To our knowledge, it is the second report of permutations in phyllotaxis: Couder (1998) first measured one between the leaves of a sunflower stem having a Lucas spiral phyllotaxis. These observations advocate for more phenotyping in order to determine how frequent these defects are in nature, among plant species belonging to different phylogenetic groups and exhibiting various phyllotaxis.

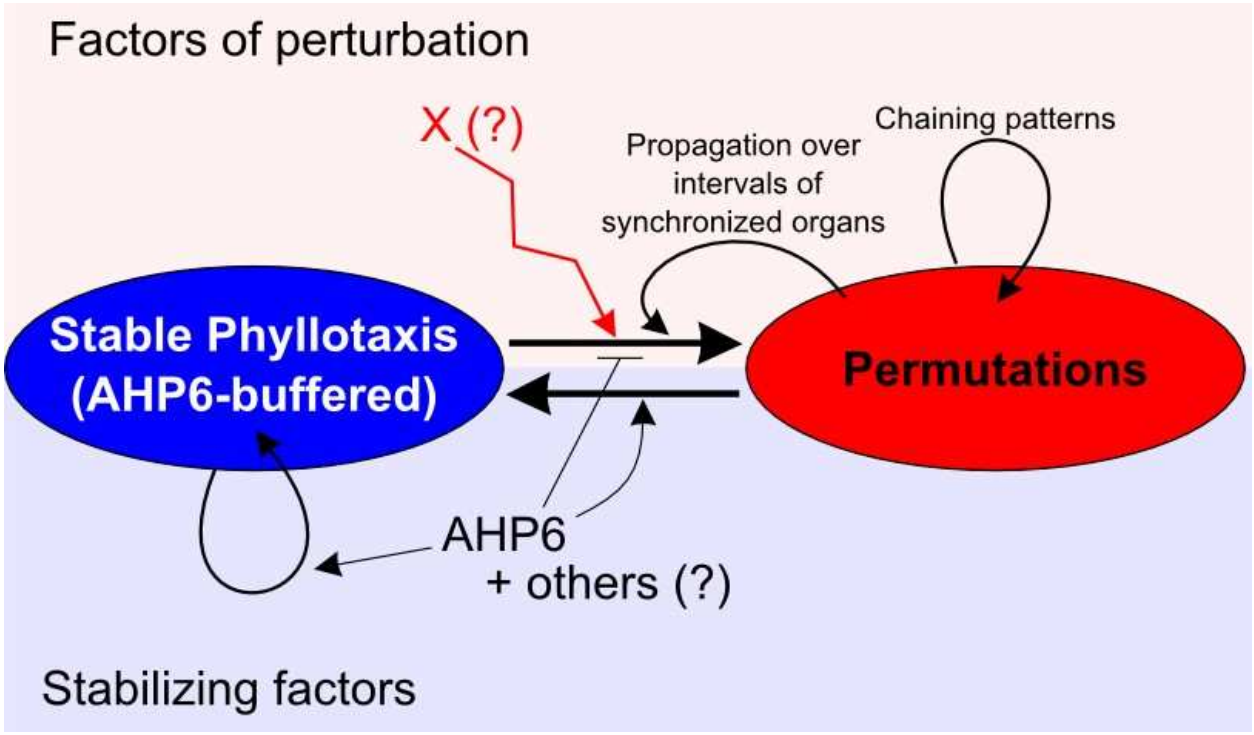

Figure 10: Model of phyllotaxis affected by permutations and putative roles of AHP6. The SAM generally generates stable phyllotaxis but can under certain condition generate permutations. The factors promoting this transition (X) are not known (endogenous? Environment?). Existing permutations favor to a certain extend further permutations (chaining, propagation). AHP6 limits the permutation number and length, potentially by limiting their occurrence (counter-acting X for example), promoting a return to a stable state or both. Other endogenous or exogenous factors could also act together with AHP6. The implications of factors of perturbations independent of AHP6 and the existence of possible redondant stabilizing factors could explain the variable penetrance of *ahp6* phenotype and its overlap with the wild-type.

Where do permutations originate? We measured divergence angles on fully elongated inflorescence stems, while the phyllotaxis is generated in meristems, before internodes elongate. It should be noted that the architecture of the stem is not perturbed by any twisting (figure S7). Pedicels that link flowers to the stem were always normal. Since no defects can be seen in the stem, permutations must appear earlier, in regions close to the meristem or in the meristem proper. Microscopic analysis are thus needed determinate the origin of permutations. However, three possible scenarii can be made:

(1) In the meristem, successive organs could appear with an inverted sequence, but in the right place. Thus the angular position would not be modified, but the time of organ formation would no longer be coupled to its positioning.

(2) In the meristem, the plastochron could be irregular: organs could be initiated in inverted sequences or even at the same time, leading to permutations. In this scenario, time would also be uncoupled from space, but with an additional loss of the regularity of the plastochron.

(3) In the meristem proper, notably in the epidermis, successive flowers would be specified with correct divergence angles and plastochron. However, in their early development, the order of successive flowers would be permuted. For example, the younger flower could grow faster than the older one and would connect lower on the stem, fixing the permutation post-meristematically.

These scenarios are not mutually exclusive and the actual situation could also be intermediate. The interesting common point between them is that they all postulate a decoupling of the timing of organ development with space: at the moment of organ iniation (scenarios1 and 2) or just after (3). This conclusion can be drawn from our data thanks to our protocol of measurement, that collected sequences of divergence angles. Nearly all theories of phyllotaxis postulate the existence of dynamic interactions between older and newly appearing organs at each iteration. Even if we do not know exactly how to correlate post-meristematic order of flowers on the stem with their ontogeny in meristem, the post-meristematic sequences of divergence angles give some clues allowing to reconstruct temporal patterns of development.

It is also worth noting that permuted organs are more associated with non-elongated internodes. Since the internode development occurs after organ initiation, this suggests that permutations, occurring shortly before, could impair internode development. As seen with the scenarios above, the existence of permutation raises questions about the coupling between the specification of the flower

proper on the surface of the meristem and the formation of the internode. To our knowledge, the developmental controls of these couplings have not been elucidated yet.

In conclusion, our results show that time and space are not robustly coupled during early organ development in meristem and that the pseudo-HPt AHP6 participate in maintaining a proper coupling, likely by inhibiting cytokinin signaling. This new role for cytokinin in the phyllotaxis of *Arabidopsis* is interesting given the major role recognized so far for auxin in this process. This is however reminiscent to the situation in maize, where the loss of another cytokinin inhibitor, ABPHYL1, perturbs the phyllotaxis(D Jackson & Hake 1999; Giulini et al. 2004). These similarities raises the question whether crosstalk between auxin and cytokinin in meristem is an important control of the robustness of phyllotaxis in many angiosperm species.

3.2 A body of facts sustaining the theory of local inhibitory interactions between primordia.

In the previous analysis of divergence angle squences, we obtained these different results:

- equal proportion of the orientation of spirals (left or right winding);
- permutations patterns;
- The coexistence of Fibonacci and Lucas phyllotaxis in *Arabidopsis*, Lucas phyllotaxis being rare (4 individuals out of 171).
- a robust and stable divergence angle within spiral. Individual baseline sequences sometimes significantly differ from the golden angle and we measured that stable divergence angles can exist within a natural range of roughly 10° around the golden angle;
- Particular local dependencies within sequences: the intervals of memories controlling the divergence angles correspond to Fibonacci numbers (at least for the propagation of a permutation motif over an interval of synchronized organs and possibly within baseline segments)

These various facts might appear unrelated. However, we realized that they form a coherent body which can be perfectly integrated into the framework of a dynamic system model based on local inhibitory interactions between neighboring primordia in direct contact. This type of model has been remarkably detailed in a series of articles by Douady and Couder (1996a; 1996b; 1996c) and is sometimes considered as a paradigm for phyllotaxis (Shipman & Newell 2005)(see also in Introduction of this manuscript). Briefly, this model propose that the formation of regular patterns of phyllotaxis is a self-organized process that only emerge from the local repulsive interactions of

direct neighbors and the growth of the apex. In other words, the geometry of the pattern at each iteration is determined by the neighboring relationships within the structure. In Fibonacci spirals, the nearest neighbors can be linked by conspicuous spirals called contact parastichies, one set winding to the left and the other to the right. The number of parastichies in each of these sets are consecutive numbers of the Fibonacci series, in which each term is the sum of the two previous one and starting at one (e.g. 1, 1, 2, 3, 5, 8, 13, 21,...). Thus, in a Fibonacci spiral with (i, j) parastichy number, the nearest neighbors of the new organ number *n* are older organs (*n*-i) and (*n*-j). Therefore, in these models, contact parastichies are very important because they propagate the geometry of the phyllotaxis over several iterations. Finally, it can be shown that the initial conditions and the temporal evolution of the structure of the meristem are very important factors conditioning the type of phyllotaxis.

Each of the results listed above can be explained in the framework of this type of models. Firstly, these models explain the equal ratio of left- and right- winding generative spirals by a initial symmetry breaking event when seedlings initiate their first leaves. Secondly, in their simulation, Douady and Couder predicted that permutations in the order of apparition of organs can occur without disrupting the global pattern, as long as parastichies were maintained (1996a; 1996c). Thirdly, the divergence angle between successive organs is not fixed in these models and only reaches precisely the golden angle for perfectly stable regimes, after several iterations. Fourthly, the possible deviation of the divergence angle from the golden angle depends on the number of parastichies: for a phyllotaxis of order (3,5), the expected divergence angle φ by the model is comprised between about $135<\varphi<140^{\circ}$, which is compatible with the mean deviations we observed, given the accuracy of our measures. Finally the core dynamics of the model rely on the relationships between direct neighbors: the local dependencies within a sequence are thus determined by the geometry of the contact parastichies. In our case, this geometry provides a convincing explanation for the pattern of propagation of permutation motifs (Figure 7).

So far, the main experimental data supporting the theory of local inhibitory interactions between neighbors came from studies reporting microsurgery experiments or laser ablation on meristems. These invasive techniques have often been criticized because of possible artifacts. Our approach is completely non invasive and it also supports the model of dynamic local inhibitory interactions. Although the demonstration is not direct, we demonstrated significant statistic dependencies between organs within sequences, revealing the intrinsic dynamics of the system. Our data can thus

be considered as an important support for the theories arguing that local inhibitory interactions between organ is a mechanism explaining phyllotaxis.

Moreover, our data will question current models of phyllotaxis. Although it was shown that they can produce permutations, this property has never been studied properly. It will be interesting to test their capacity to produce realistic patterns of permutations like those we characterized.

3.3 Concluding remarks

Altogether, these results illustrate the relevance of our strategy and the importance of focusing on perturbations to understand both the dynamics of wild-type phyllotaxis and the phenotype of mutants. Focusing also on perturbed phyllotaxis or rare patterns in sunflowers, Couder (1998) quoted Richards (1951): "[…], by a regrettable inversion, the facts of phyllotaxis have frequently been falsified in order to conform with the postulates". Our study advocate again for a more systematic comparison between empirical data and theoretical models. We thus provide a useful pipeline of methods for further research in this direction. Conversely, the questions of the precise role of AHP6 and the origin of permutations will be addressed by experimental data, but models will certainly provide complementary answers.

References - Chapter 1

Adler, I., Barabe, D. & Jean, R., 1997. A history of the study of phyllotaxis. *ANNALS OF BOTANY*, 80(3), p.231-244.

Allard, H.A., 1946. Clockwise and counterclockwise spirality observed in the phyllotaxy of tobacco. *J. Agr. Res.*, 73, p.237-242.

Barabé, D., 2006. Stochastic approaches in phyllotaxis. *CANADIAN JOURNAL OF BOTANY-REVUE CANADIENNE DE BOTANIQUE*, 84(11), p.1675-1685.

Barabé, D. & Jeune, Bernard, 2004. The use of entropy to analyze phyllotactic mutants: a theoretical analysis. *The Plant Cell*, 16(4), p.804-806.

Bayer, E.M. et al., 2009. Integration of transport-based models for phyllotaxis and midvein formation. *Genes & Development*, 23(3), p.373-384.

Beal, W.J., 1873. The phyllotaxy of cones. *Amer. Nat.*, 7, p.449-453.

Couder, Y., 1998. Initial transitions, order and disorder in phyllotactic patterns: The ontogeny of Helianthus annuus. A case study. *ACTA SOCIETATIS BOTANICORUM POLONIAE*, 67(2), p.129-150.

Csiszar, I. & Talata, Z., 2005. Context tree estimation for not necessarily finite memory processes, via BIC and MDL. *2005 IEEE International Symposium on Information Theory (ISIT), Vols 1*, p.755-759.

Diggle, P.J., 1990. *Time Series: A Biostatistical Introduction*, Oxford: Oxford University Press.

Douady, S. & Couder, Y., 1996a. Phyllotaxis as a dynamical self organizing process .1. The spiral modes resulting from time-periodic iterations. *JOURNAL OF THEORETICAL BIOLOGY*, 178(3), p.255-274.

Douady, S. & Couder, Y., 1996b. Phyllotaxis as a dynamical self organizing process .2. The spontaneous formation of a periodicity and the coexistence of spiral and whorled patterns. *JOURNAL OF THEORETICAL BIOLOGY*, 178(3), p.275-294.

Douady, S. & Couder, Y., 1996c. Phyllotaxis as a dynamical self organizing process .3. The simulation of the transient regimes of ontogeny. *JOURNAL OF THEORETICAL BIOLOGY*, 178(3), p.295-&.

Ephraim, Y. & Merhav, N., 2002. Hidden Markov processes. *IEEE TRANSACTIONS ON INFORMATION THEORY*, 48(6), p.1518-1569.

Giulini, A., Wang, J. & Jackson, David, 2004. Control of phyllotaxy by the cytokinin-inducible response regulator homologue ABPHYL1. *Nature*, 430(7003), p.1031-1034.

Golz, J.F. & Hudson, A., 2002. Signalling in plant lateral organ development. *The Plant Cell*, 14 Suppl, p.S277-288.

Grenander, U. & Miller, M.I., 2006. *Pattern Theory, From representation to inference*, Oxford University Press.

Heisler, M.G. et al., 2005. Patterns of auxin transport and gene expression during primordium development revealed by live imaging of the Arabidopsis inflorescence meristem. *Current Biology: CB*, 15(21), p.1899-1911.

Itoh, J.I. et al., 2000. Shoot organization genes regulate shoot apical meristem organization and the pattern of leaf primordium initiation in rice. *The Plant Cell*, 12(11), p.2161-2174.

Jackson, D & Hake, S., 1999. Control of phyllotaxy in maize by the abphyl1 gene. *Development (Cambridge, England)*, 126(2), p.315-323.

Jean, R., 1994. *Phyllotaxis: a systemic study in plant morphogenesis*,

Jeune, B & Barabe, D., 2006. Simulations of transitions from regular to stochastic phyllotactic patterns. *JOURNAL OF BIOLOGICAL SYSTEMS*, 14(1), p.113-129.

Jeune, B & Barabe, D., 2004. Statistical recognition of random and regular phyllotactic patterns. *ANNALS OF BOTANY*, 94(6), p.913-917.

Jeune, B & Barabé, D., 2006. A stochastic approach to phyllotactic patterns analysis. *JOURNAL OF THEORETICAL BIOLOGY*, 238(1), p.52-59.

Jönsson, H. et al., 2006. An auxin-driven polarized transport model for phyllotaxis. *Proceedings of the National Academy of Sciences of the United States of America*, 103(5), p.1633-1638.

Kuhlemeier, Cris, 2007. Phyllotaxis. *Trends in Plant Science*, 12(4), p.143-150.

Mardia, K.V. & Jupp, P.E., 2000. *Directional Statistics*, Chichester: John Wiley & Sons.

Mähönen, A.P. et al., 2006. Cytokinin signaling and its inhibitor AHP6 regulate cell fate during vascular development. *Science (New York, N.Y.)*, 311(5757), p.94-98.

Peaucelle, A. et al., 2007. Plants expressing a miR164-resistant CUC2 gene reveal the importance of post-meristematic maintenance of phyllotaxy in Arabidopsis. *Development (Cambridge, England)*, 134(6), p.1045-1050.

Ragni, L. et al., 2008. Interaction of KNAT6 and KNAT2 with BREVIPEDICELLUS and PENNYWISE in Arabidopsis inflorescences. *The Plant Cell*, 20(4), p.888-900.

Refahi, Y. et al., 2011. A combinatorial model of phyllotaxis perturbations in Arabidopsis thaliana. Dans 22nd Annual Symposium on Combinatorial Pattern Matching. Palermo, Italy.

Reinhardt, D, Mandel, T & Kuhlemeier, C, 2000. Auxin regulates the initiation and radial position of plant lateral organs. *The Plant Cell*, 12(4), p.507-518.

Reinhardt, Didier et al., 2005. Microsurgical and laser ablation analysis of leaf positioning and dorsoventral patterning in tomato. *Development (Cambridge, England)*, 132(1), p.15-26.

Reinhardt, Didier et al., 2003. Regulation of phyllotaxis by polar auxin transport. *Nature*, 426(6964), p.255-260.

de Reuille, P.B. et al., 2006. Computer simulations reveal properties of the cell-cell signaling network at the shoot apex in Arabidopsis. *Proceedings of the National Academy of Sciences of the United States of America*, 103(5), p.1627-1632.

Richards, F., 1951. PHYLLOTAXIS - ITS QUANTITATIVE EXPRESSION AND RELATION TO GROWTH IN THE APEX. *PHILOSOPHICAL TRANSACTIONS OF THE ROYAL SOCIETY OF LONDON SERIES*, 235(629), p.509-564.

Sahlin, P., Söderberg, B. & Jönsson, H., 2009. Regulated transport as a mechanism for pattern generation: capabilities for phyllotaxis and beyond. *Journal of Theoretical Biology*, 258(1), p.60-70.

Shipman, P. & Newell, A., 2005. Polygonal planforms and phyllotaxis on plants. *JOURNAL OF THEORETICAL BIOLOGY*, 236(2), p.154-197.

Smith, R., Kuhlemeier, C & Prusinkiewicz, P, 2006. Inhibition fields for phyllotactic pattern formation: a simulation study. *CANADIAN JOURNAL OF BOTANY-REVUE CANADIENNE DE BOTANIQUE*, 84(11), p.1635-1649.

Smith, R.S., Guyomarc'h, S., et al., 2006. A plausible model of phyllotaxis. *Proceedings of the National Academy of Sciences of the United States of America*, 103(5), p.1301-1306.

Snow, M. & Snow, R., 1932. Experiments on phyllotaxis I - The effect of isolating a pininordium. *PHILOSOPHICAL TRANSACTIONS OF THE ROYAL SOCIETY OF LONDON SERIES*, 221, p.1-43.

Snow, M. & Snow, R., 1933. Experiments on phyllotaxis II - The effect of displacing. *PHILOSOPHICAL TRANSACTIONS OF THE ROYAL SOCIETY OF LONDON SERIES*, 222, p.353-400.

Stoma, S. et al., 2008. Flux-based transport enhancement as a plausible unifying mechanism for auxin transport in meristem development. *PLoS Computational Biology*, 4(10), p.e1000207.

Wardlaw, C., 1949. EXPERIMENTAL AND ANALYTICAL STUDIES OF PTERIDOPHYTES . 14. LEAF FORMATION AND PHYLLOTAXIS IN DRYOPTERIS-ARISTATA DRUCE. *ANNALS OF BOTANY*, 13(50), p.163-&.

Zucchini, W. & MacDonald, I.L., 2009. *Hidden Markov Models for Time Series: An Introduction Using R.*, Boca Raton FL: Chapman & Hall/CRC.

4. Supplementary Information

4.1. Materials and methods

4.1.1. Plants, culture conditions and materials

All the plants studied belong to the same Columbia-0 (Col-0) ecotype, and thus share the same genetic background. *ahp6-1* and *ahp6-3,* respectively EMS and T-DNA insertion null allele of *AHP6* were described previously (Mähönen et al. 2006). Transgenic plants *ahp6-1* x pAHP6::AHP6-GFP were a gift form Y. Helarriutta and generated as described in (Mähönen et al. 2006).

Plants were grown on soil at 20°C in short day conditions (8 h light/16 h darkness) for 4 to 5 weeks to synchronize them before being transferred in long-day conditions (16 h light/8 h darkness).

The plasmid pAHP6::AHP6-HA was generated using the previously described pAHP6::AHP6-GFP plasmid. pAHP6::AHP6 was amplified by PCR and inserted in frame with the HA sequence into a destination vector, using a Gateway® recombination. This plasmid was introduced in *ahp6-1* plants by floral dipping in a *Agrobacterium tumefaciens* culture solution (Clough & Bent 1998).

4.1.2. Measurement protocol

We designed a measurement protocol inspired from previous studies (Peaucelle et al. 2007; Ragni et al. 2008) and built a dedicated device, consisting of a mobile protractor fixed on a vertical structure (Figure S1). The main inflorescence of fully grown *Arabidopsis* plants were placed in the center of the protractor and the angular position of each silique (i.e. *Arabidopsis* fruit) was noted, from bottom to top. We considered the insertion of siliques on the stem, so that possible twisting of pedicels during flower development does not bias the angle value. Sequences always start with the first silique. Last siliques were discarded when internodes were not sufficiently elongated or when the height of the stem exceeds the height of the measurement device. Consequently, perturbation patterns can be truncated at the beginning or at the end of the sequence. We then deduced by first-order differencing the successive divergence angles between pair of consecutive siliques according to the two possible orientations (clockwise or counter-clockwise) of the generative spiral. The orientation of the spiral was determined in an initial exploratory analysis of the divergence angle

sequence mainly by identifying segments of divergence angles close to the canonical Fibonacci angle of α=137.5°(termed baseline segments). In the case of highly perturbed mutant individuals, the optimal labeling of the divergence angle sequence using a previously estimated model was found to be useful for selecting the most likely spiral orientation; see appendix for details. For each divergence angle, the elongated or non-elongated character of the corresponding internode was noted. An internode was considered as non-elongated if its length < 2 mm.

The main analysis was performed on a large sample: we measured 82 wild-type plants of cumulative length 2405 (in number of divergence angles or internodes) and 89 *ahp6-1* mutant plants of cumulative length 2815. Other samples with different plants were also analyzed, they are summarized in table S1.

4.1.3. Stationarity assumption of measured sequences

To validate the stationarity assumption, we computed the pointwise mean directions of divergence angles and the associated standard deviations for the wild type and the mutant (Figure S3). This shows that there were no trend or successive phases along the sequences and that the divergence angle sequences can be considered as roughly stationary. Biologically, this means that the transient phase caused by the transition from decussate to spiral phyllotaxis that occur in seedling is not likely to ovelap with the segment of stem measured. This could be expected because this transition occur very early: more than 30 leaves and 5 to 10 axillary branches are generally produced before the production of the first flower where we started to measure divergence angles. It also suggest that the developmental transition from vegetative to reproductive meristem does not affect the dynamics of phyllotaxis in inflorescence. In the context of our analysis, the stationarity assumption enables to properly model the left-truncation of permutations at the beginning of the sequences.

4.1.4. Extraction of intervals of synchronized organs between permutation

Intervals of synchronized organs were first extracted from the pooled learning samples. The zero value (u=0) for the interval length of synchronized organs corresponds to the chaining of permutations and the corresponding frequencies were extracted from Tables 4 and 5. An interval of length u = 1 corresponds to the juxtaposition of two permuted segments. A length u > 1 corresponds to u − 1 successive canonical angle α outside a permuted segment (since a permuted segment can also include an isolated canonical angle α, see above section 2.7). When the zero value is excluded, the "-1-shifted" frequency distributions are thus the frequency distributions of baseline segment

lengths between two permuted segments. For the category of interval length after a 2-Permutation, we then separated the data from wild-type and *ahp6-1* mutants and we observed the same behavior of the distribution as function of interval length (Figure S7). The occurrences of three permutations in the wild-type were too low to compare intervals following a 3-Permutation between the two genotypes.

Supplementary References – Chapter 1

Clough, S.J. & Bent, A.F., 1998. Floral dip: a simplified method for Agrobacterium-mediated transformation of Arabidopsis thaliana. *The Plant Journal: For Cell and Molecular Biology*, 16(6), p.735-743.

Mähönen, A.P. et al., 2006. Cytokinin signaling and its inhibitor AHP6 regulate cell fate during vascular development. *Science (New York, N.Y.)*, 311(5757), p.94-98.

Peaucelle, A. et al., 2007. Plants expressing a miR164-resistant CUC2 gene reveal the importance of post-meristematic maintenance of phyllotaxy in Arabidopsis. *Development (Cambridge, England)*, 134(6), p.1045-1050.

Ragni, L. et al., 2008. Interaction of KNAT6 and KNAT2 with BREVIPEDICELLUS and PENNYWISE in Arabidopsis inflorescences. *The Plant Cell*, 20(4), p.888-900.

4.2. Supplementary figures

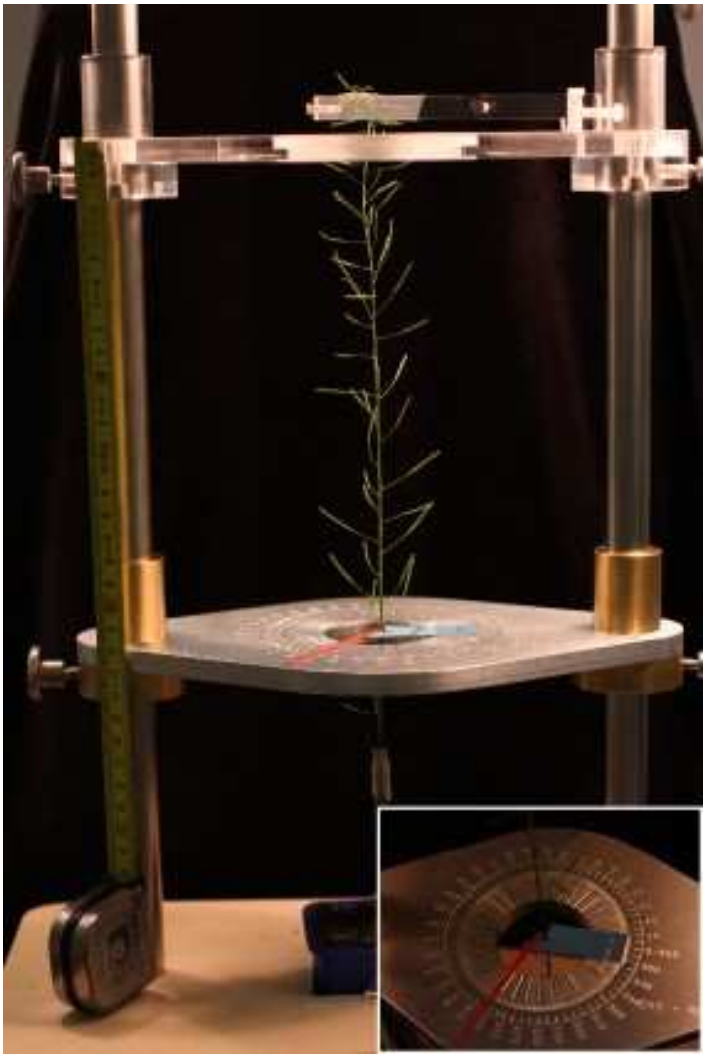

Figure S1: Device used to measure successive divergence angles between siliques (*Arabidopsis* fruit) in fully elongated inflorescence stem. The stem is placed at the center of a mobile protractor (Inset) which is moved from the first silique at the base towards the top. Angular position is noted and divergence angles between successive siliques are calculated according to the direction of the generative spiral (see text for details).

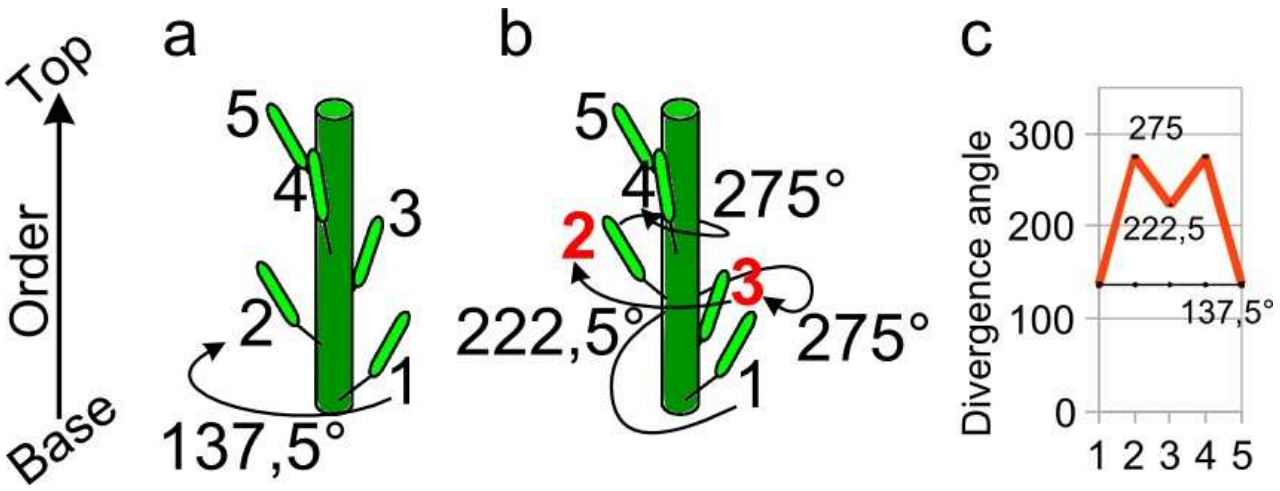

Figure S2: Explanation of the M-shaped perturbation motif by a permutation in the apico-basal order of organ along the stem. Left, the cartoon show a stem with ordered organs and constant canonical divergence angle. Middle, the order of the 2nd silique and the 3rd silique (in red) is switched, but their angular position around the stem stays identical. New successive divegence angles are generated. Right, measuring this new divergence angle sequence from the base to the top generate the stereotypical M-shaped motif.

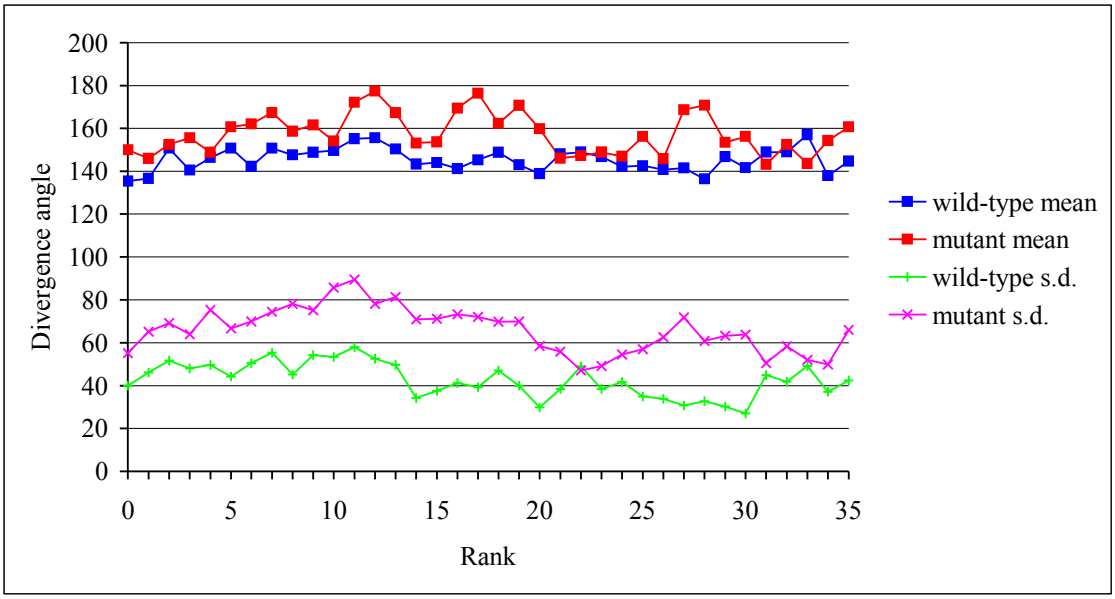

Figure S3: Stationarity of sequences. This graph shows the pointwise mean directions and standard deviations

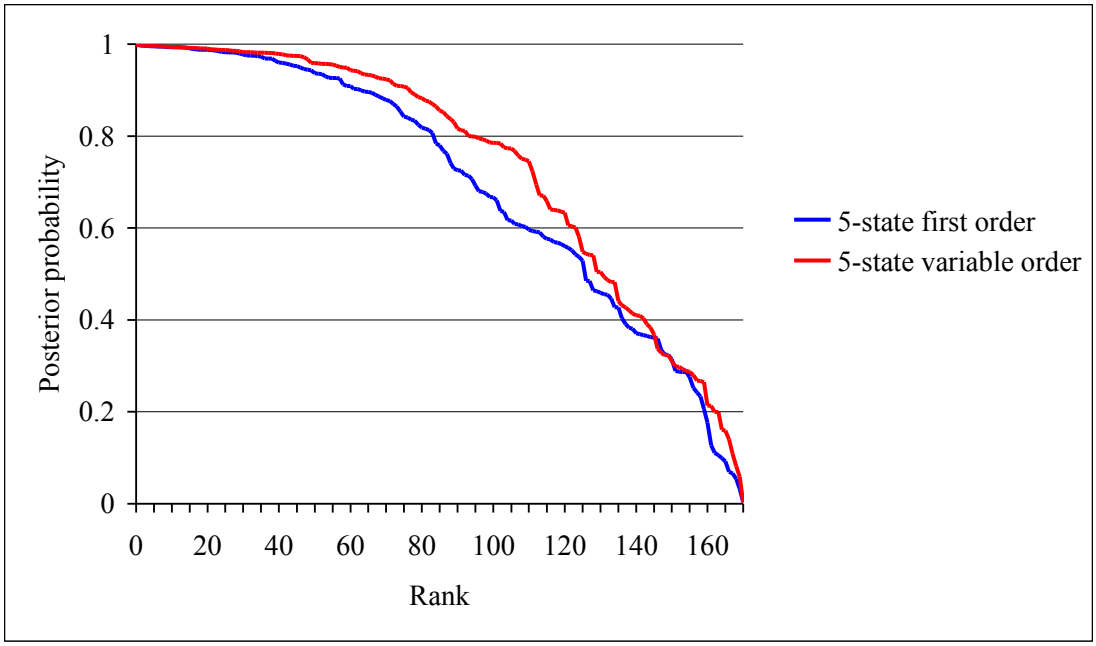

Figure S4: Ranked posterior probabilities of the optimal labelings of the divergence angle sequences computed using the estimated hidden Markov chains. Better posterior probabilities are computed for the 5-state variable-order HMC, indicating a statistcal improvement of the labeling of the sequences.

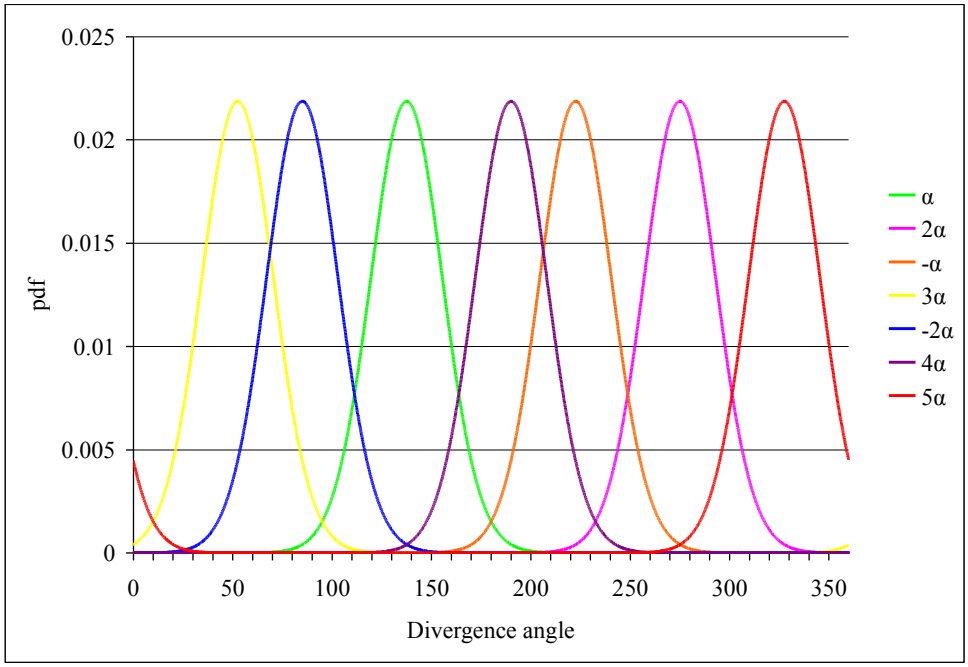

Figure S5: Von Mises observation distributions with common concentration parameter centered on the multiples of the divergence angle. This graph shows the strong overlap between the different distributions. In the data, these different laws have also very different weights: the Von Mises distribution attached to α is very frequent whereas those attached to 4α or 5α are very rare.

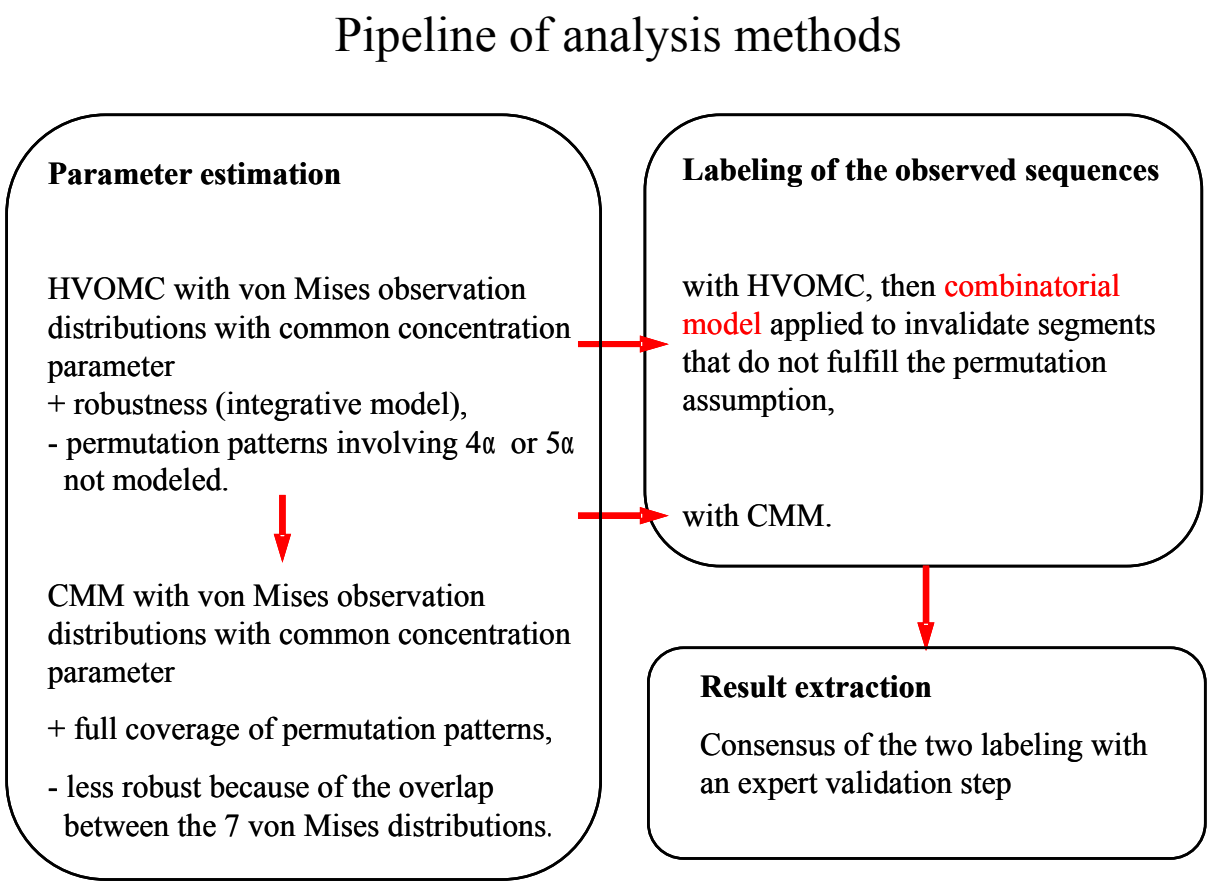

Figure S6: Pipe-line of methods used to analyze the phyllotactic sequences. HVOMC, Hidden-Variable-order Markov Chain; CMM, combinatorial Mixture model. The advantages and the shortcomings of the two models are given.

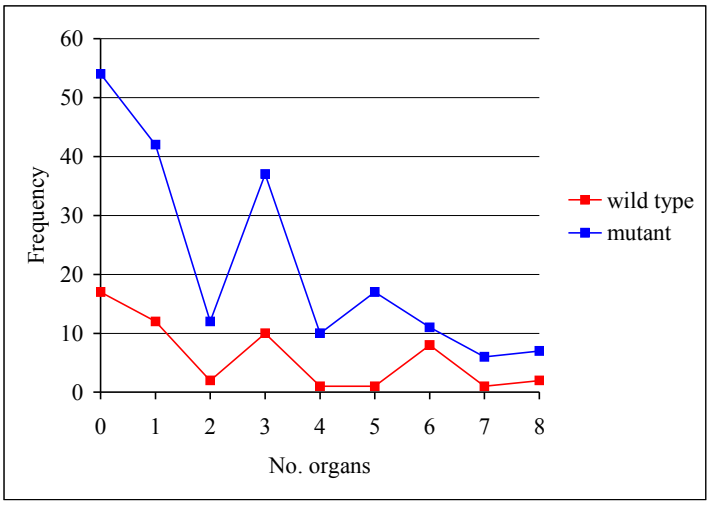

Figure S7: Comparison of the Frequency distributions for the number of successive synchronized organs between two permutations and after a 2-permutation in wild-type and *ahp6-1* mutants.

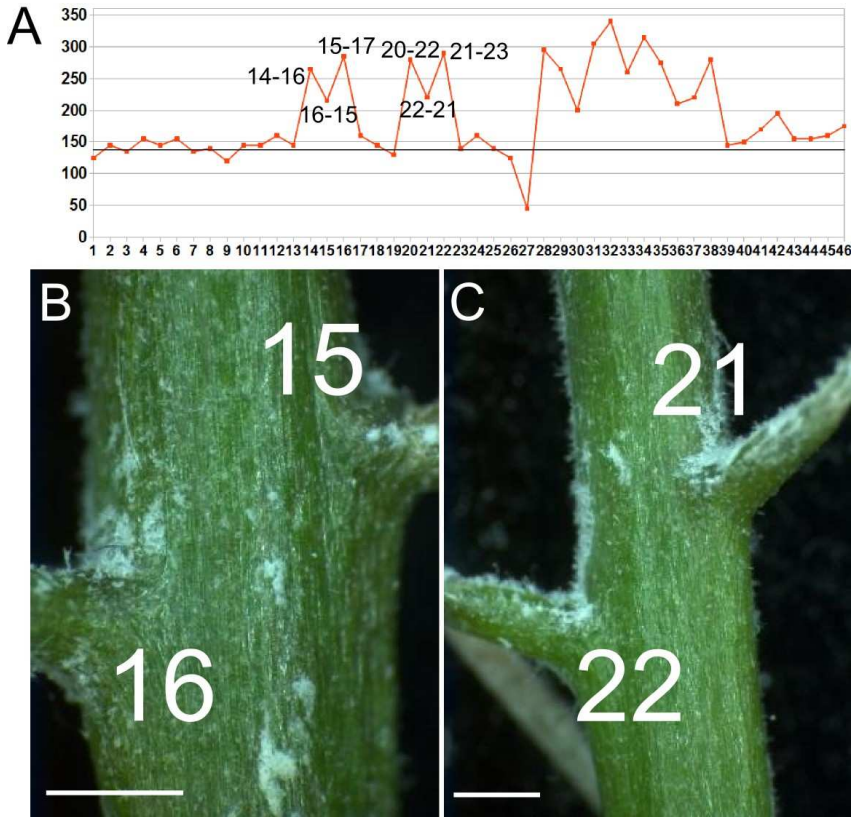

Figure S8: Structure of the stem between permuted organs. (**A**) Divergence angle sequence measured on a *ahp6-1* mutant. Two M-shaped motifs are clearly visible. On top of the graph are indicated for each angle the corresponding number of the two organs. Organs are numbered according to their expected order without permutations. (**B-C**) In the same plant, close view of the internode between the permuted organs 16-15 (B) and 22-21 (C)(the top of stem is oriented towards the top of the picture). The internodes are not elongated (<2mm), but their structure is normal (e.g. no twisting, no morphological alterations). Oidium (white mold) started to develop on this plant at the onset of senescence. Scale bar=1mm.

		N angles	N individuals
Learning sample	WT (Col-0)	2405	82
	ahp6-1	2815	89
test samples	*ahp6-3*	266	14
	ahp6-1/3	266	14
	L91 AHP6-GFP x *ahp6-1*	572	19
	L94 AHP6-GFP x *ahp6-1*	422	15
	L2 AHP6-HA x *ahp6-1*	610	19
	L14 AHP6-HA x *ahp6-1*	625	19

Table S1: Characteristics of the samples studied.

Methods

Definition of (hidden) variable-order Markov chains

In the following, we first introduce high-order Markov chains. Then, variable-order Markov chains and hidden Markov models based on first-order and variable-order Markov chains, which are the stochastic models used in this study, are defined. In the case of an rth-order Markov chain $\{S_t; t = 0, 1, \ldots\}$, the conditional distribution of S_t given $S_0, \ldots, S_{t-1}$ depends only on the values of $S_{t-r}, \ldots, S_{t-1}$ but not further on $S_0, \ldots, S_{t-r-1}$,

$$P\left(S_t = s_t | S_{t-1} = s_{t-1}, \ldots, S_0 = s_0\right) = P\left(S_t = s_t | S_{t-1} = s_{t-1}, \ldots, S_{t-r} = s_{t-r}\right)$$

In our context, the random variable represents theoretical divergence angles and can take the five possible values α, 2α, $-\alpha$, 3α and -2α (or the seven possible values α, 2α, $-\alpha$, 3α, -2α, 4α and 5α). These possible values correspond to the Markov chain states. A J-state rth-order Markov chain has $J^r\,(J-1)$ independent transition probabilities. Therefore, the number of free parameters of a Markov chain increases exponentially with the order. Let the transition probabilities of a second-order Markov chain be given by

$$p_{hij} = P\left(S_t = j | S_{t-1} = i, S_{t-2} = h\right) \quad \text{with } \sum_j p_{hij} = 1.$$

These transition probabilities can be arranged as a $J^2 \times J$ matrix where the row $(p_{hi0}, \ldots, p_{hiJ-1})$ corresponds to the transition distribution attached to the [state h, state i] memory. If for a given state i and for all pairs of states $\left(h, h^{'}\right)$ with $h \neq h^{'}$, $p_{hij} = p_{h^{'}ij}$, i.e. once S_{t-1} is known, S_{t-2} conveys no further information about , the J memories of length 2 [state h, state i] with $h = 0, \ldots, J-1$ can be grouped together and replaced by the single [state i] memory of length 1 with associated transition distribution $(p_{i0}, \ldots, p_{iJ-1})$. This illustrates the principle for building a variable-order Markov chain. In a variable-order Markov chain, the order (or memory length) is variable and depends on the "context" within the sequence.

The memories of a Markov chain can be arranged as a memory tree such that each vertex (i.e. element of a tree graph) is either a terminal vertex or has exactly J "offspring" vertices. In practice, the memories corresponding to unobserved contexts are not included in the memory tree (this is the case for the memory $3\alpha2\alpha$ that was not observed). The memories associated with the J vertices (memories of length $r+1$) deriving from a given vertex (memory of length r) are obtained by prefixing the parent memory with each possible state. For instance, in Figure x, the four second-order memories $\alpha2\alpha$, $2\alpha2\alpha$, $-\alpha2\alpha$ and $-2\alpha2\alpha$ derive from the first-order memory 2α. A transition distribution is associated with each terminal vertex of this memory tree.

Because of the noisy character of the measurements, we built a noisy or hidden Markov model (Ephraim and Merhav, 2002; Zucchini and MacDonald, 2009) based on a variable-order Markov chain. In this hidden Markov model, the non-observable variable-order Markov chain represents the succession of theoretical divergence angles along the axes while the von Mises observation distributions represent measurement uncertainty. A hidden variable-order Markov

chain can be viewed as a two-level stochastic process, i.e. a pair of stochastic processes $\{S_t, X_t\}$ where the "output" process $\{X_t\}$ is related to the "state" process $\{S_t\}$, which is a finite-state variable-order Markov chain, by the observation distributions. The probability density function of the von Mises observation distribution (in degrees) for state j is given by

$$g_j\left(x_t; \mu_j, \kappa\right) = \frac{1}{360 I_0\left(\kappa\right)} \exp\left\{\kappa \cos\left(x_t - \mu_j\right) \frac{\pi}{180}\right\}.$$

where $I_0\left(\kappa\right)$ is the modified zero order Bessel function of the first kind, μ_j the location parameter (analogous to the mean) and κ the concentration parameter (precision or inverse variance) common to the states in the above definition (Mardia and Jupp, 2000). The von Mises distribution, also known as the circular Gaussian distribution, is a univariate Gaussian-like periodic distribution for a variable $x \in [0, 360°)$. The distribution has period 360° so that $g_j\left(x_t + 360; \mu_j, \kappa\right) = g_j\left(x_t; \mu_j, \kappa\right)$. The definition of the observation distributions expresses the assumption that the output process at time t depends only on the non-observable Markov chain at time t.

Selection of the memories of a variable-order Markov chain

The order of a Markov chain can be estimated using the Bayesian information criterion (BIC). For each possible order r, the following quantity is computed

$$\mathrm{BIC}\left(r\right) = 2 \log L_r - J^r \left(J - 1\right) \log n.$$

where L_r is the likelihood of the observed sequences for the rth-order estimated Markov chain, $J^r\left(J-1\right)$ is the number of independent transition probabilities of a J-state rth-order Markov chain and n is the cumulated length of the observed sequences. The principle of this penalized likelihood criterion consists in making a trade-off between an adequate fitting of the model to the data (given by the first term in (A1)) and a reasonable number of parameters to be estimated (control by the second term, the penalty term). In practice, it is infeasible to compute a BIC value for each possible variable-order Markov chain of maximum order $r \leq R$ since the number of hypothetical memory trees is very large. An initial maximal memory tree is thus built combining criteria relative to the maximum order and to the minimum count of memory occurrences in the observed sequences. This memory tree is then pruned, using a two-pass algorithm which is an adaptation of the Context-tree maximizing algorithm (Csiszár and Talata, 2006): a first dynamic programming pass, starting from the terminal vertices and progressing towards the root vertex for computing the maximum BIC value attached to each sub-tree rooted in a given vertex, is followed by a second tracking pass starting from the root vertex and progressing towards the terminal vertices for building the memory tree.

Estimation method and algorithms for hidden variable-order Markov chains

The maximum likelihood estimation of the parameters of a hidden variable-order Markov chain requires an iterative optimization technique, which is an application of the Expectation-Maximization (EM) algorithm (Ephraim and Merhav, 2002; Zucchini and MacDonald, 2009).

Once a hidden variable-order Markov chain has been estimated, the most probable state sequence can be computed for each observed sequence using the so-called Viterbi algorithm. This restored state sequence can be interpreted as the optimal labeling of the observed sequence.

The algorithms for hidden first-order Markov chains directly apply to hidden variable-order Markov chains by the following standard device. A variable-order Markov chain can be viewed as a first-order Markov chain defined on an extended state space corresponding to the possible memories. In the case of a stationary variable-order Markov chain, the implicit initial distribution δ which is the stationary distribution is defined on the possible memories and is directly deduced from the transition probability matrix. The direct application of the EM algorithm to hidden Markov models such that the underlying Markov chain is stationary leads to an M-step which requires a numerical solution for the M-step (Zucchini and MacDonald, 2009) because of the inclusion of a term depending on δ in the function to be maximized for reestimating the transition probabilities. We chose instead to apply a variant of the EM algorithm which is an Expectation Conditional Maximization algorithm (McLachlan and Krishnan, 2008). The transition probabilities are reestimated using standard closed-form solution (i.e. without taking into account $\delta^{(k+1)}$ but instead $\delta^{(k)}$). Then, $\delta^{(k+1)}$ is deduced from the transition probability matrix $P^{(k)}$.

Properties of permuted sequences

Sequences take the form of a concatenation of baseline and permuted segments. A permuted segment is defined as a sub-sequence of divergence angles corresponding to the chaining of 2- or 3-permutations. A permuted segment is either a palindrome or is reversible, that is the reverse of the segment is also a permuted segment (a direct consequence of the fact that a permutation is a reversible operation). The set of permuted segments is prefix free that is a permuted segment cannot be a proper prefix of another one. Because of the reversibility property, the set of permuted segments is also suffix free that is a permuted segment cannot be a proper suffix of another one. A permuted segment is delimited by two splitting points. At a splitting point, the sequence can be split and this does not affect the identification of permutations. The organ rank at a splitting point coincides with the sequence index. The notion of splitting point can be viewed as a deterministic analogue of a regeneration point for a stochastic process. A regeneration point is a time instant at which the future of the process depends only of its state at that instant and is thus independent of its past before that instant. The process is thus reborn at a regeneration point. Within a permuted segment, the organ rank fluctuates around the sequence index, the maximum absolute deviation being $n-1$ where n is the maximum number of permuted organs. The organ rank starts by being above the sequence index (just after the splitting point) and ends by being below the sequence index (just before the splitting point). The language induced by the permutations is a regular language. This is illustrated by the building of the finite automaton corresponding to the language induced by 2-permutations in Figure x. The occurrence of permuted segments of varying length corresponding to the chaining of 2- or 3-permutations justifies the use of hidden Markov models based on variable-order Markov chains. Variable-order Markov chains represent dependencies of varying length induced by the

most frequent permuted segments.

Definition of combinatorial mixture models and sketch of the algorithm for labeling sequences using these models

A combinatorial mixture model can be viewed as a latent structure model where the non-observable component is a deterministic combinatorial model that relies on the assumption that any permutation of organs can occur, provided the permuted organs can be arranged in disjoint bounded blocks of successive organs. In practice, a bound of at most 3 permuted successive organs was adequate for the analysis of the divergence angle sequences, but the model and algorithms were designed in more general terms. Given a positive integer n, we have termed n-admissible the sequences of divergence angles leading to a sequence of organs that are permuted in blocks of length at most n. For a canonical angle α, the angles possibly occurring in an n-admissible sequence were shown to belong to the set $D_n = \{i\alpha \,|\, 1-n \leqslant i \leqslant 2n-1, i \neq 0\}$ (e.g. $D_3 = \{\alpha, 2\alpha, -\alpha, 3\alpha, -2\alpha, 4\alpha, 5\alpha\}$). The set of n-admissible sequences can then be viewed as a regular language on the alphabet D_n, that can be recognized by a finite-state automaton similar to the variable-order Markov chain shown in Figure 3c.

A combinatorial mixture model can be viewed as the coupling of a combinatorial model relying on a permutation assumption with an independent mixture model (McLachlan and Peel, 2000). The probability density function of a mixture of von Mises distributions (in degrees) with common concentration parameter κ (J components corresponding to the possible theoretical angles) is given by

$$f\left(x_t;\theta\right) = \sum_j \eta_j g_j\left(x_t;\mu_j,\kappa\right) = \sum_j \eta_j \frac{1}{360 I_0\left(\kappa\right)} \exp\left\{\kappa \cos\left(x_t-\mu_j\right)\frac{\pi}{180}\right\}.$$

where the parameters are the J weights $\eta_j = P\left(S_t = j\right)$ such that $\sum_j \eta_j = 1$, the J location parameters μ_j and the concentration parameter κ. We assumed that the weights were all equal i.e. $\eta_j = 1/J$ (this uniform distribution assumption is the most neutral assumption). The J location parameters μ_j were the theoretical angles corresponding to the seven states α, 2α, $-\alpha$, 3α, -2α, 4α, 5α while the concentration parameter κ common to the seven von Mises observation distributions was the concentration parameter estimated within the hidden variable-order Markov chain.

Von Mises distributions were used (i) to limit the number of potential labelings of an observed sequence using a quantile or a posterior probability criterion, (ii) to compare alternative labelings of an observed sequence. Von Mises observation distributions were used to define ranges of possible measurements for a given theoretical angle using two alternative criteria, (a) a quantile criterion (e.g. between the 0.005th and the 0.995th quantiles corresponding to a deviation between the location parameter μ_j and a limit of 48.5° with the estimated concentration parameter $\widehat{\kappa}$) that do not take into account the overlap between distributions, (b) a posterior probability criterion that takes into account this overlap between distributions. In this latter case, the range of possible values for state j is such that

$$P\left(S_t = j | X_t = x_t; \theta\right) = \frac{g_j\left(x_t; \mu_j, \kappa\right)}{\sum_i g_i\left(x_t; \mu_i, \kappa\right)} \geq \lambda,$$

where λ is a predefined threshold (typical value 0.05) on the posterior probabilities. This pruning step is very useful for limiting the search space of the combinatorial algorithm (see below) since the support of each von Mises observation distribution is $[0, 360^\circ)$. It should be noted that there were important overlaps between ranges of possible measurements for adjacent angles (e.g., between 2α and $-\alpha$; see Figure 5) and thus a measured angle could be assigned to different theoretical angles (generally 2, rarely 3) leading to a large set of candidate sequences on the alphabet D_n for a given observed sequence.

We designed a branch-and-bound algorithm (Refahi *et al.*, 2011) that, given an observed sequence, returns the set of the n-admissible sequences of theoretical angles. When this set is empty, the algorithm returns a list of n-admissible sub-sequences ending at a splitting points. To perform this construction, the algorithm scans a measured sequence $x = (x_0, \ldots, x_{T-1})$ from left to right, building all n-admissible theoretical angle sequences. A measured angle x_t is labeled as "non-explained" when the algorithm fails at finding an n-admissible sub-sequence of length $t + 1$. A backtracking procedure is then applied to invalidate all the preceding angles up to a splitting point. Finally, thanks to the reversibility property, the exact same series of operations is applied to the reversed sequence $x' = (x_{T-1}, \ldots, x_0)$, leading to another set of n-admissible sub-sequences, non-explained and invalidated angles following the latter. This enables to reject only the angle that has been not explained or invalidated in both directions, and to propose an n-admissible labeling for all other sub-sequences. Alternative labelings of an observed sequence (or of parts of the sequence when some segments cannot be explained) were finally compared on the basis of log-likelihoods

$$\begin{aligned}
& \log P\left(S_0 = s_0, \ldots, S_{T-1} = s_{T-1}, X_0 = x_0, \ldots, X_{T-1} = x_{T-1}; \theta\right) \\
= & \sum_t \log P\left(S_t = s_t, X_t = x_t; \theta\right) \\
\propto & \sum_t \log g\left(x_t; \mu_{s_t}, \kappa\right).
\end{aligned}$$

Appendix. Estimation of a hidden Markov chains with von Mises observation distributions with common concentration parameter κ

At each iteration k, The M-step of the EM algorithm consist of maximizing the different components of the conditional expectation of the complete-data log-likelihood, each term depending on a given subset of θ. For an observed sequence x_0^{T-1}, the component of the conditional expectation of the complete-data log-likelihood corresponding to the von Mises observation distributions is given by

$$\begin{aligned}
&\sum_j \sum_t P\left(S_t = j | X_0^{T-1} = x_0^{T-1}; \theta^{(k)}\right) \log g_j\left(y; \mu_j, \kappa\right) \\
= \;& -T \log 360 + \kappa \sum_j \sum_t P\left(S_t = j | X_0^{T-1} = x_0^{T-1}; \theta^{(k)}\right) \cos\left\{\left(x_t - \mu_j\right) \frac{\pi}{180}\right\} - T \log I_0\left(\kappa\right) \\
= \;& -T \log 360 + \kappa \sum_j \left\{\sum_t P\left(S_t = j | X_0^{T-1} = x_0^{T-1}; \theta^{(k)}\right)\right\} \overline{R}_j \cos\left\{\left(\overline{x}_j - \mu_j\right) \frac{\pi}{180}\right\} - T \log I_0\left(\kappa\right).
\end{aligned}$$

The mean direction $\overline{x}_j$ is solution of the equation

$$\overline{R}_j = \overline{C}_j \cos\left(\overline{x}_j \frac{\pi}{180}\right), \qquad \overline{R}_j = \overline{S}_j \sin\left(\overline{x}_j \frac{\pi}{180}\right),$$

where the mean resultant length is given by

$$\overline{R}_j = \sqrt{\overline{C}_j^2 + \overline{S}_j^2},$$

with

$$\begin{aligned}
\overline{C}_j &= \frac{\sum_t P\left(S_t = j | X_0^{T-1} = x_0^{T-1}; \theta^{(k)}\right) \cos\left(x_t \pi / 180\right)}{\sum_t P\left(S_t = j | X_0^{T-1} = x_0^{T-1}; \theta^{(k)}\right)}, \\
\overline{S}_j &= \frac{\sum_t P\left(S_t = j | X_0^{T-1} = x_0^{T-1}; \theta^{(k)}\right) \sin\left(x_t \pi / 180\right)}{\sum_t P\left(S_t = j | X_0^{T-1} = x_0^{T-1}; \theta^{(k)}\right)}.
\end{aligned}$$

Since $\cos x$ has its maximum at $x = 0$, the reestimated location parameter is $\mu_j^{(k+1)} = \overline{x}_j$.

$$\mu_j^{(k+1)} = \begin{cases}
\frac{\pi}{180} \arctan(\overline{S}_j / \overline{C}_j) & \text{if } \overline{C}_j \geq 0, \overline{S}_j \geq 0, \\
\frac{\pi}{180} \arctan(\overline{S}_j / \overline{C}_j) + 180 & \text{if } \overline{C}_j < 0, \\
\frac{\pi}{180} \arctan(\overline{S}_j / \overline{C}_j) + 360 & \text{if } \overline{C}_j \geq 0, \overline{S}_j < 0.
\end{cases}$$

Differentiating with respect to κ and using $I_0'\left(\kappa\right) = I_1\left(\kappa\right)$,

$$T\left[\sum_j \left\{\sum_t P\left(S_t = j | X_0^{T-1} = x_0^{T-1}; \theta^{(k)}\right)\right\} \overline{R}_j \cos\left\{\left(\overline{x}_j - \mu_j\right) \frac{\pi}{180}\right\} - A\left(\kappa\right)\right].$$

Hence,

$$\kappa^{(k+1)} = A^{-1}\left(\sum_j \left\{\sum_t P\left(S_t = j | X_0^{T-1} = x_0^{T-1}; \theta^{(k)}\right)\right\} \overline{R}_j \cos\left\{\left(\overline{x}_j - \mu_j\right)\frac{\pi}{180}\right\}\right),$$

where $A(\kappa) = I_0(\kappa)/I_1(\kappa)$.

Chapter 2

Study of the role of AHP6 at the shoot apical meristem of *Arabidopsis thaliana*

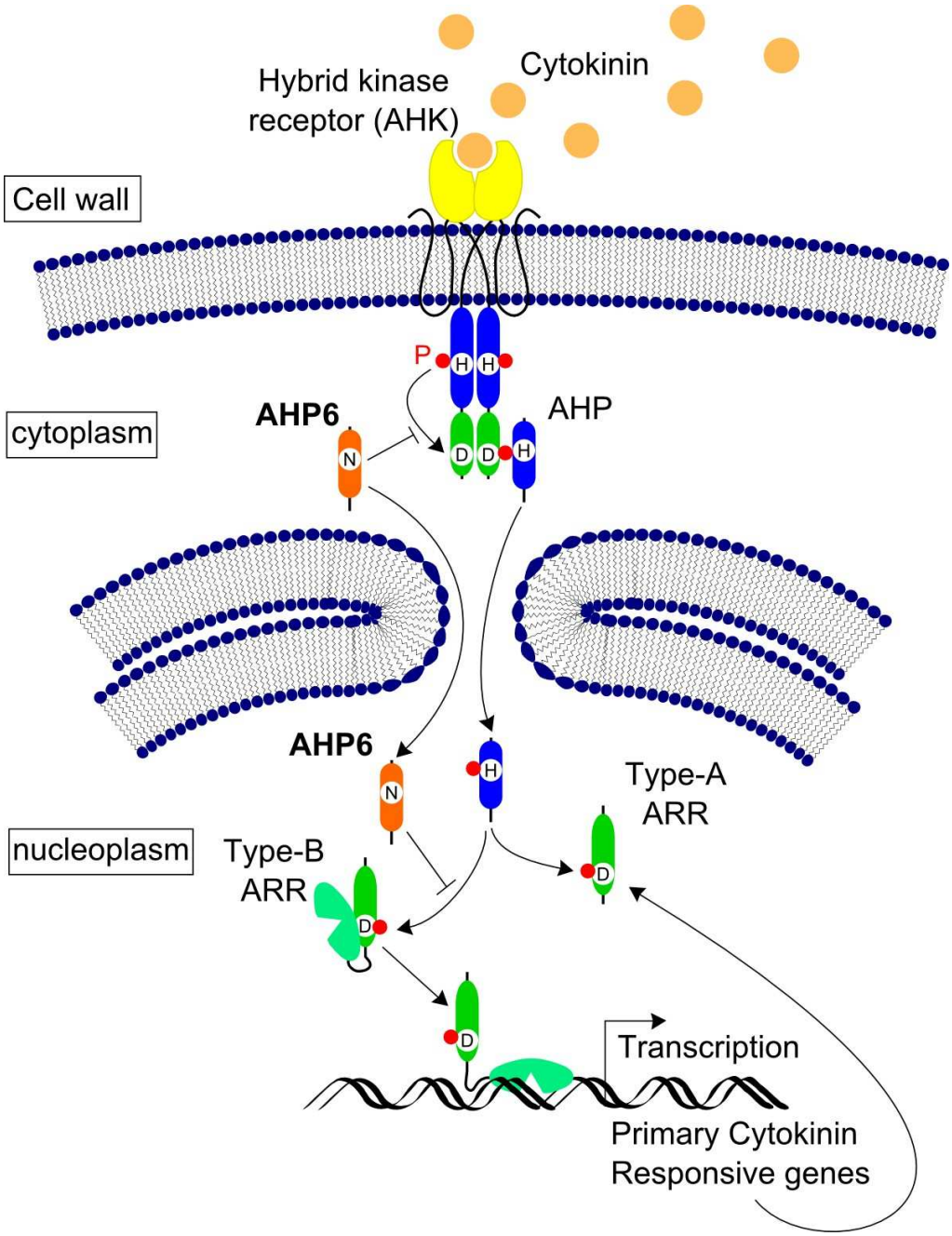

Figure 1: AHP6 is a pseudo Histidine-Phosphotransfer protein (pseudo HPt) that inhibits cytokinin signaling. The cytokinin signaling pathway is a multistep phosphorelay system, involving successive transfers of phosphate (red dots) between Histidine (H)-containing phosphotransfer protein (blue) and Aspartate (D)-containing acceptors (green). In the extracellular space, the binding of cytokinins (small adenine-derived molecules) to Hybrid-Kinase receptors (AHK1-3) triggers the auto-phosphorylation of the AHK on its own phosphotransfer domain and the cascade starts. Functional AHP shuttles between the cytoplasm and the nucleus, where they transmit the phosphoryl group to type-A or type-B Response Regulators (ARR). Phosphorylated type-B ARR, which have a DNA-binding domain, activate transcription. The cytokinin signaling inhibitors type-A ARR likely compete with type-B ARR for phosphate transmission from AHP and would act as phosphate sink. Genetically, AHP6 functions as a cytokinin signaling inhibitor and has been shown *in vitro* to inhibit phosphorelay between the two domains of an Hybrid Kinase and from AHP to type-B ARR. Unlike type-A ARR, AHP6 transcription is not induced by cytokinin.

Introduction

In chapter 1, we have demonstrated the role of *AHP6* in the control of the robustness of phyllotaxis. More specifically, we have shown that AHP6 limits the occurrence of permutations in the order of organs along the stem. Rapid examination of stem exhibiting permutations in *ahp6* mutants indicated that the permutations should arise early in the inflorescence bud or even in the meristem (see Chap1, figure 8). A meristematic origin was very probable, since available data on AHP6 indicated an expression in meristems ((Mähönen et al. 2006; Yadav et al. 2009).

We therefore examined the phenotype of *ahp6* mutant plants at cellular resolution, in order to (i) identify the precise origin of permutations and (ii) determine the role of AHP6 in organ formation and phyllotaxis establishment. AHP6 is a pseudo Histidine-Phosphotransfer Protein pseudo HPt, that has been characterized as an inhibitor of cytokinin signaling in roots. It is thought that this small cytoplasmic protein inhibits different steps of the phosphorylation cascade triggered by cytokinin, notably at the level of the membrane receptors (the ARABIDOPSIS HYBRID KINASE, AHK) and at the level of cytokinin-responsive transcription factors, the type-B ARABIDOPSIS RESPONSE REGULATORS (type-B ARR; see figure 1). One of our goals was thus to establish when and where altered cytokinin signaling was causing the phenotype. Moreover, since auxin is the key hormone regulating phyllotaxis described so far, we looked for possible crosstalk between auxin and cytokinin.

In a first part, I will present evidences showing that AHP6 controls the plastochron regularity in the peripheral zone of the meristem, by establishing inhibitory fields of cytokinin signaling that function in crosstalk with auxin-induced organogenesis. In a brief second part, I will present additional results from a genetic study of AHP6 interaction with genes involved in auxin transport. In particular, we found that the protein kinase PINOID which is known to regulate the polarity of the PIN1 auxin efflux carrier, acts in synergy with *AHP6* to control the robustness of phyllotaxis and flower development.

I. Cytokinin inhibitory fields provide robustness to the temporal patterns of phyllotaxis

This section is an updated version of an article submitted in april 2011.

The following people collaborated to the work presented in this chapter:

Fabrice Besnard[1], Yassin Refahi[2], Benjamin Marteaux[1], Géraldine Brunoud[1], Valérie Morin[1,4], Pierre Chambrier[1], Jonathan Legrand[1,2], Etienne Farcot[1], Coralie Cellier[1], Pradeep Das[1], Anthony Bishopp[3], Ykä Helariutta[3], Christophe Godin[2], Jan Traas[1], Yann Guédon[2] and Teva Vernoux[1]

[1] Laboratoire de Reproduction et Développement des Plantes, CNRS, INRA, ENS Lyon, UCBL, Université de Lyon, 46 Allée d'Italie, 69364 Lyon Cedex 07, France.

[2] Virtual Plants INRIA Project Team, UMR DAP, INRIA/CIRAD, Montpellier, France.

[3] Institute of Biotechnology/Department of Biosciences, University of Helsinki, FIN-00014, Finland.

[4] Present address: UMR CNRS 5534, Université Claude Bernard Lyon I, Bâtiment Gregor Mendel, 16 rue Raphaël Dubois, 69622 Villeurbanne, France

Author contributions:

T.V. designed the project. T.V, F.B., J.T. and Y.H. designed the biological experiments. F.B, T.V., V.M., P.C., G.B., B.M., C.C., P.D. and A.B. performed the experiments. J.L. performed the microarray data analysis. Y.R., E.F., C.G. and Y.G. designed and performed the analysis of phyllotactic sequences. T.V., F.B. and J.T. wrote the manuscript with input from the other authors.

ABSTRACT

Plant organs are initiated at the shoot apex in precise spatio-temporal patterns that define phyllotaxis, the geometric arrangement of organs on the stem. It has been proposed that an inhibitory fields produced by organs might control these patterns, but such fields have never been observed. We show here that intercellular movement of the *Arabidopsis* Phosphotransfer Protein 6 (AHP6) generates inhibitory fields of cytokinin signaling in the shoot apex and controls phyllotaxis. More specifically, we found that the AHP6-based hormonal fields create spatial differences in cytokinin signaling capacities that impose a temporal sequence on organ initiation. We have thus identified a previously unrecognized mechanism by which an inhibitory field controls specifically the periodicity of organ initiation at the shoot apex.

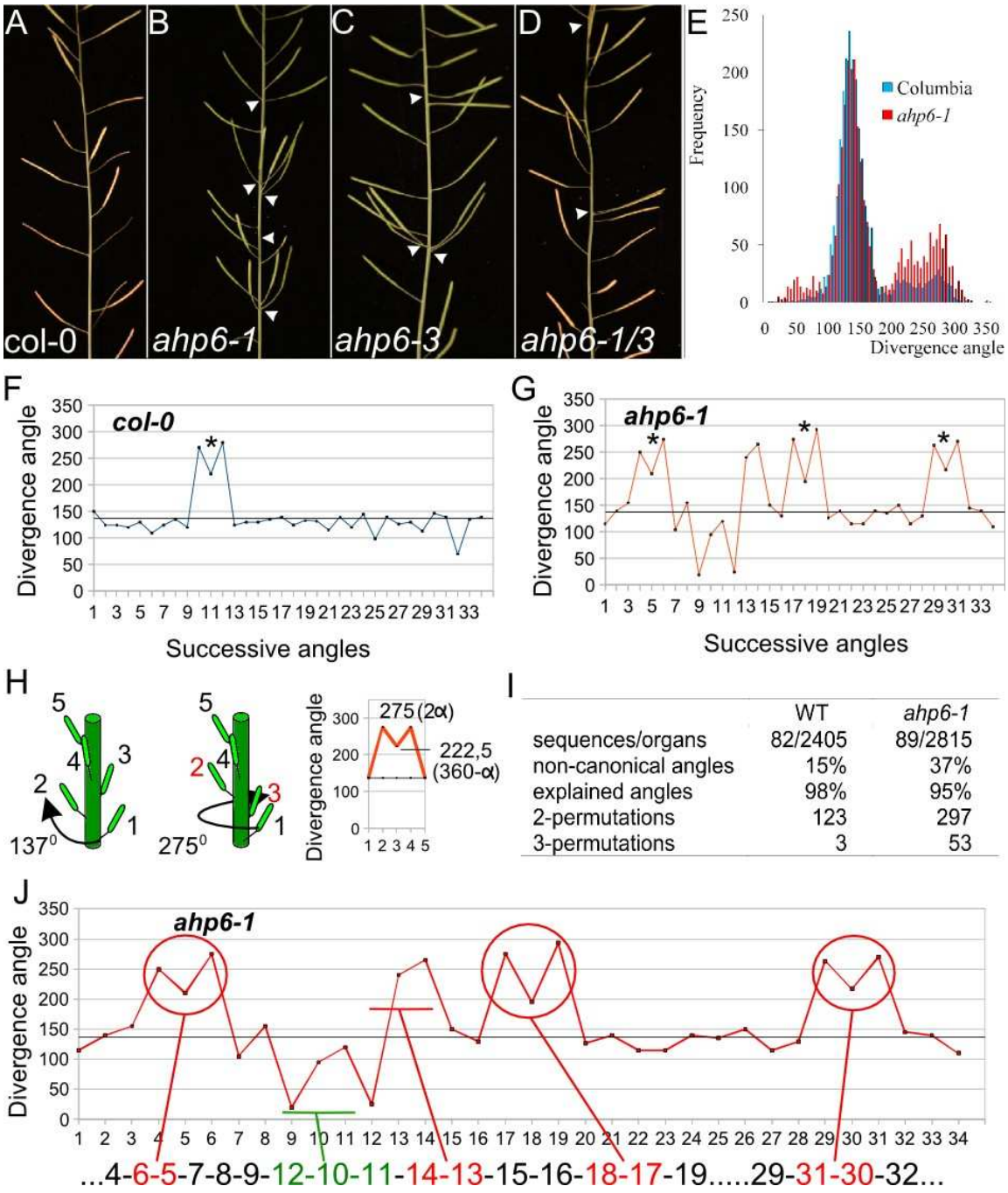

Figure 2: *AHP6* regulates phyllotaxis. (**A-D**) Architecture of the inflorescence stem of wild-type (**A**), *ahp6-1* (**B**), *ahp6-3* (**C**) and *ahp6-1*/*ahp6-3* trans-heterozygous plants (**D**). Phyllotactic perturbations are indicated (arrowheads). (**E**) Distribution of divergence angles observed in wild-type (82 plants) and *ahp6-1* (89 plants). (**F,G**) Representative divergence angle sequence for wild-type (**F**) and *ahp6-1* (**G**). The M-shaped divergence angle sequences are indicated (stars). (**H**) Theoretical explanation of the M-shaped angle sequence by permutation in the order of insertion of two siliques on the stem. The usual insertion order (left), the one obtained by this permutation (centre) and the angle sequences obtained in the two situations are shown. (**I**) Summary table of optimally labeled divergence angle sequences by the stochastic and combinatorial model (see methods). (**J**) Explanation of the representative *ahp6-1* angle sequence shown in (G) by the permutation hypothesis.

1. Results and discussion

A model for phyllotaxis formulated almost a century ago (Schoute 1913) proposes that the sites of new organ initiation at the shoot apical meristem (SAM) are determined by the combined effect of inhibitory fields produced by existing organs, and thus form at a position where the sum of the inhibitory effects is the lowest (Veen & Lindenmayer 1977; Mitchison 1977; Douady & Couder 1996; R. Smith, C Kuhlemeier, et al. 2006). Recent data indicate that polar transport of the plant hormone auxin in the SAM could indirectly create an inhibitory field. A network of polarly localized PIN-FORMED1 (PIN1) efflux carriers has been shown to control accumulation of auxin at the site of organ initiation and to trigger organogenesis (Vernoux et al. 2000; D Reinhardt et al. 2000; Didier Reinhardt et al. 2003; Heisler et al. 2005; de Reuille et al. 2006). Analysis of PIN1 polarities in the SAM suggest that polar auxin transport could also lead to concomitant depletion of the hormone around organs and would then create inhibitory fields by removal of the activator of organ initiation (R. S. Smith, Guyomarc'h, et al. 2006; de Reuille et al. 2006; Jönsson et al. 2006; R. S. Smith, Guyomarc'h, et al. 2006; Stoma et al. 2008; Bayer et al. 2009). However direct evidence for the existence of these fields in the SAM is still missing and inhibitory fields have never been observed so far in plants.

Cytokinins (CK) form another family of hormones implicated in the regulation of phyllotaxis, albeit through probable modulation of the size of the stem cell niche in the meristem (D Jackson & Hake 1999; Giulini et al. 2004) Accordingly, regulators of both CK biosynthesis and signaling are expressed at the center of the meristem (Leibfried et al. 2005; Kuroha et al. 2009; Gordon et al. 2009). However, by re-analyzing recent transcriptomic data for different domains of the *Arabidopsis* SAM (Yadav et al. 2009), we identified *AHP6* as the only gene encoding a CK signaling element up-regulated specifically in aerial lateral organs (Fig. S1, S2A). AHP6 acts as an inhibitor of CK signaling, by impairing the intracellular phosphorylation cascade triggered upon CK perception (Mähönen et al. 2006). *In situ* hybridization further demonstrated that *AHP6* is specifically expressed in lateral organs, starting from the earliest stages (Fig. S2B-H; see also Fig. 3A,B).

To investigate a putative role for AHP6 in phyllotaxis, we analyzed shoot architecture in the null mutants *ahp6-1* and *ahp6-3* (Mähönen et al. 2006). Wild-type *Arabidopsis* plants, like the majority of higher plants, display spiral phyllotaxis, in which consecutive organs are generally initiated at a canonical angle close to 137.5º (noted as a; Fig. 2A). By contrast, both *ahp6* mutants analyzed and the *ahp6-1*/*ahp6-3* trans-heterozygote showed obvious modifications in organ arrangements along

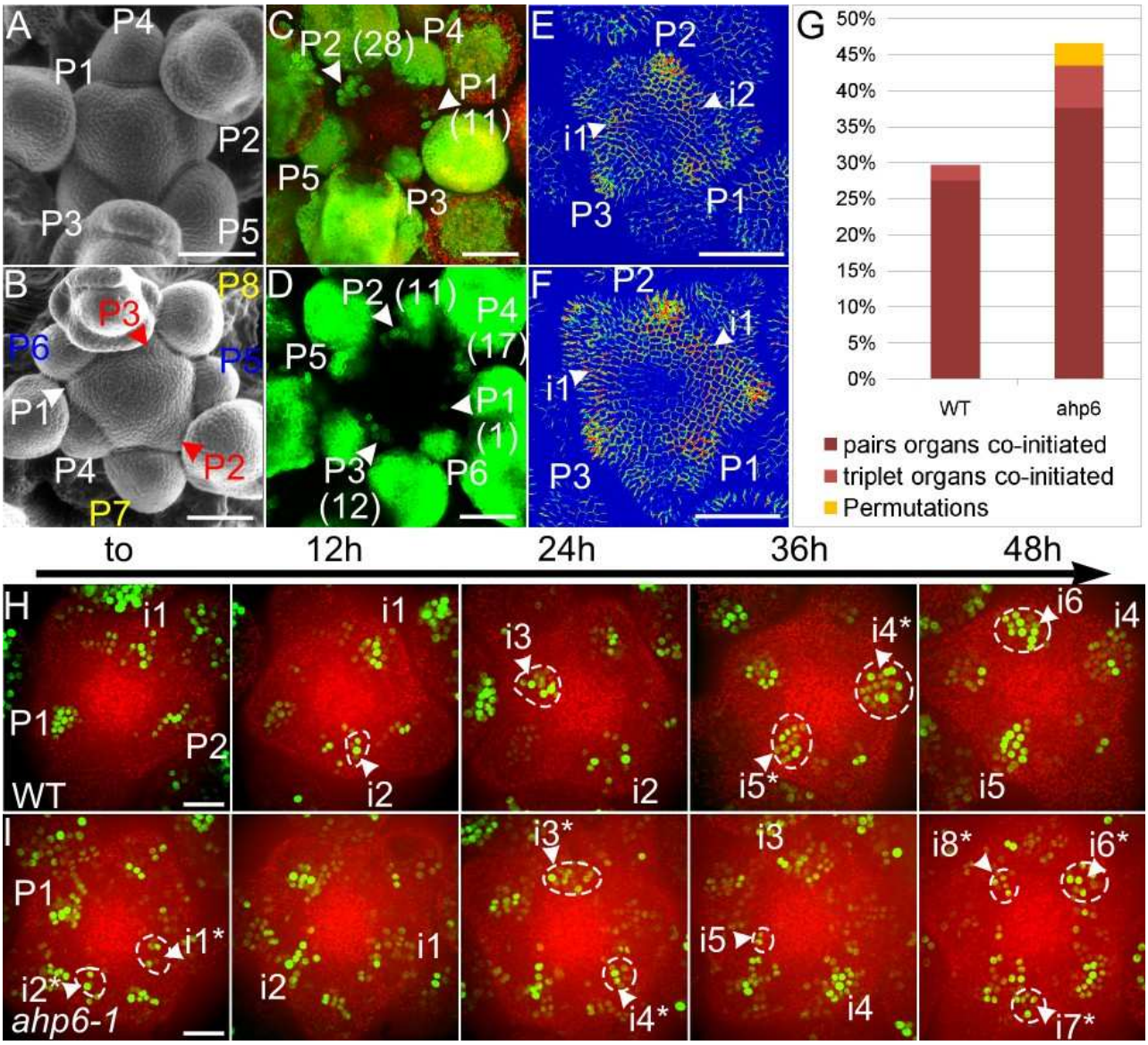

Figure 3: ***AHP6*** **regulates the periodicity of organ initiation at the shoot apical meristem.** (**A-F**) Analysis of wild-type (A,C,E) and *ahp6-1* (B,D,F) meristems using scanning electron microscopy (A,B), *pLFY::GFP* (C,D) and *PIN-GFP* (E,F). The primordia (P) have been numbered from the youngest to the oldest and the *initia* from the oldest to the youngest following standard nomenclature. Letters of identical colors indicate organs at apparent identical developmental stages in (B). GFP is in green in (C,D) and the number of cells present in the younger organ initia expressing *pLFY::GFP* are indicated in brackets. Images are represented in range indicator palette for easier visualization and the younger initia showing an upregulation of *PIN1-GFP* are indicated (arrowheads) in (E,F). (**G-I**) Time-course analysis of *DR5::VENUS* expression. Quantification of organ co-initiations and permutations for 20 wild-type and 33 *ahp6-1* meristems are represented in (G). Representative kinetics of *DR5::VENUS* (Green) expression in wild-type (H) and *ahp6-1* (I) meristems are shown. Co-initiated organs are marked by stars. (C-F, H, I) are projections of confocal serial sections. Autofluorescence is in red. Scale bar is 50 µm in (A-F) and 20 µm in (H,I)

the stem (Fig. 2B-D). We also observed supernumerary petals and sepals in flowers (Fig. S3), suggesting that AHP6 regulates phyllotaxis throughout shoot development.

To determine whether the phyllotactic perturbations in *ahp6* mutants were structured or not, we next measured the sequence of angles between successive organs (divergence angles) on the inflorescence stems of a large population of *ahp6-1* and wild-type plants. This analysis confirmed the presence of a large increase in the amount of non-canonical divergence angles in mutant plants when compared to wild-type (Fig. 2E). Strikingly, an M-shaped motif corresponding approximately to the angle sequence 2α, 360-α, 2α appeared much more frequently in *ahp6* than in wild-type sequences (Fig. 2F-H). This motif, originally observed in sunflowers (Couder 1998), could theoretically arise if the order of insertion of two consecutive organs along the stem were permuted (Fig. 2H). The perturbations in *ahp6* phyllotaxis could therefore result from combinations of such permutations along the stem. To test this hypothesis, we applied a stochastic and combinatorial model to analyze both *ahp6* and wild-type phyllotactic sequences (see Methods). Our analysis showed that over 95 % of the non-canonical angles observed could be explained by the permutation hypothesis in both wild-type and *ahp6* plants (Fig. 2I, J, Fig. S4). These quantifications further demonstrated an increase by 2.4 fold and 17.6 fold of permutations involving 2 and 3 organs, respectively, in *ahp6* mutants compared to wild-type (Fig. 2I). Altogether, our data strongly support a role for *AHP6* in controlling the order of organ positioning along the stem, but not their angular position around the stem.

Since *AHP6* is expressed in the meristem, we reasoned that permutations in the order of organ initiation at the SAM would explain *ahp6* phyllotactic defects. We thus used scanning electron microscopy to compare the structure of wild-type and *ahp6* meristems. The spatial organization of the organs clearly followed the expected phyllotaxis in wild-type meristems (Fig. 3A). Consecutive organs were easily discernable by their size increase and morphogenetic features. In contrast, although the relative positioning of primordia appeared unaffected in *ahp6* meristems and no obvious permutations were visible, the respective order of organs was hard to determine (Fig. 3B). We observed pairs or triplets of young organs at quasi-identical developmental stages in most *ahp6* meristems and this was confirmed using a *pLEAFY(LFY)::GFP* flower-specific marker line (Deveaux et al. 2003) (Fig. 3C, D). Since the size of the stem cell niche was not affected by the *ahp6* mutation (Fig. S5), our data indicate that *AHP6* directly regulates either organ initiation or growth at the SAM.

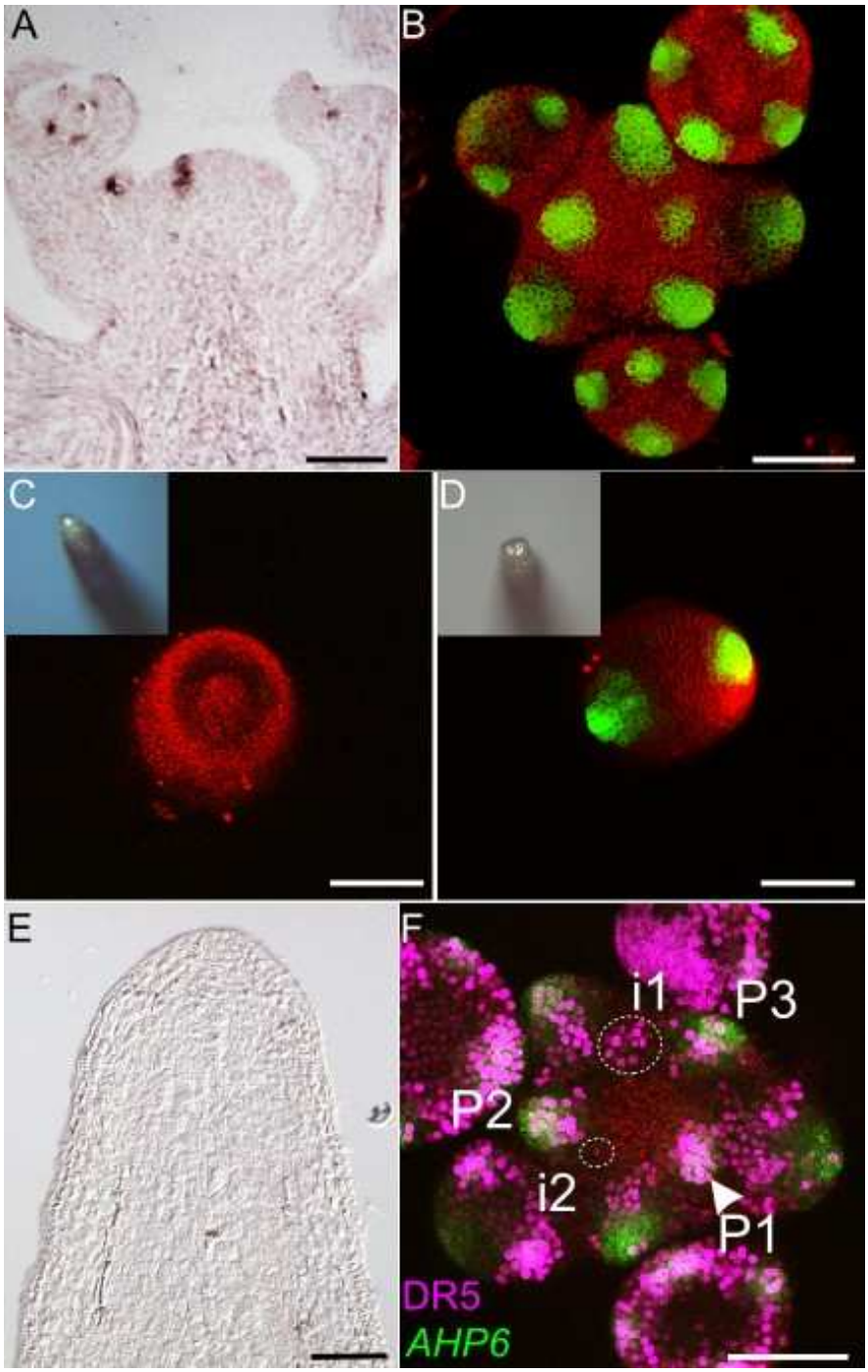

Figure 4: ***AHP6*** **is activated downstream of auxin during organ initiation.** (A,B) Expression of *AHP6* in the inflorescence meristem visualized using *in situ* hybridization (A) or a *pAHP6::GFP* (green) reporter (B). (C,D) Reversible effect of chemical inhibition of polar auxin transport on *AHP6* expression: expression of *pAHP6::GFP* at the SAM in wild-type plants germinated on NPA (C); recovery of *pAHP6::GFP* expression after transfer to NPA-free medium (D). (E) Expression of *AHP6* in an *mp* pin-like meristem visualized using *in situ* hybridization. (F) Co-visualization of *pAHP6::GFP* (green) and *DR5::VENUS* (magenta). The arrowhead indicates the younger primordium showing a co-expression of *pAHP6::GFP* and *DR5::VENUS*. A median section in the meristem is shown in (A,E). Projections of confocal serial sections are shown in (B-D, F). Autofluorescence is in red. Scale bar: 50 μm.

The recruitment of the organ founder cells, the earliest step in organ initiation, correlates with an activation of auxin signaling that triggers an upregulation of *PIN1* transcription and the activation of the synthetic auxin inducible *DR5* reporter (Benková et al. 2003; Heisler et al. 2005; de Reuille et al. 2006; R. S. Smith, Guyomarc'h, et al. 2006). To determine whether *AHP6* directly controls organ initiation, or alternatively regulates organ growth after initiation, we analyzed expression of a PIN1-GFP fusion (Heisler et al. 2005) in *ahp6* meristems. Compared to the wild type, we observed an increase in the number of sites of *PIN1* upregulation (Fig. 3E, F), suggesting concomitant organ initiation in *ahp6* meristems. To further characterize organ initiation and investigate a possible effect on auxin signaling, we next used live imaging to follow a nuclear-localized version of *DR5* (*DR5::VENUS*) (Heisler et al. 2005) over several days in *ahp6* meristems. The dynamics of *DR5::VENUS* expression revealed that loss of *AHP6* resulted mostly in a strong increase in the concomitant emergence of two to three new initia and also in permutations in the order of organ initiation at a low frequency (8 out of 255 initiation events; Fig. 3G-I, Fig. S6). The relative positions of organs were again unaffected by the *ahp6* mutation. Since the rate of organ initiation was comparable in wild-type and *ahp6* (Fig. S7), our results show that AHP6 controls the temporal sequence of organ founder cell recruitment and the stability of the plastochron. As we only occasionally observed permutations in the sequence of organ initiations in *ahp6* meristems (Fig. 3G), this also strongly suggests that the final architecture of *ahp6* mutant inflorescences results from organ co-initiations at the SAM, allowing organ outgrowth to occur *a posteriori* in a different order than in the wild-type.

To clarify the link between auxin and CK in organogenesis at the SAM, we next investigated the role of these two hormones in the spatio-temporal control of *AHP6* transcription in the SAM. Organ initiation is triggered by auxin and is also accompanied by a down-regulation of the *SHOOTMERISTEMLESS* (*STM*) meristem identity gene (Heisler et al. 2005). As *STM* directly activates CK biosynthesis (Yanai et al. 2005; Jasinski et al. 2005), *STM* down-regulation could lower CK levels during organ initiation. Furthermore, since *AHP6* is repressed by CK in the root (Mähönen et al. 2006), both CK and auxin could control *AHP6* expression. Exogenous treatment with CK and misexpression of *STM* did not alter *AHP6* expression (Fig. S8), showing that *AHP6* is activated independently of CK levels in the SAM. On the contrary, blocking organogenesis with the auxin transport inhibitor NPA reversibly inhibited the expression of a *pAHP6::GFP* reporter that recapitulates *AHP6* expression pattern (Fig. 4A-D). *AHP6* expression in the SAM was also lost in *monopteros* (*mp*), a mutant in a major regulator of auxin signaling (Fig. 4A,E). By co-localizing

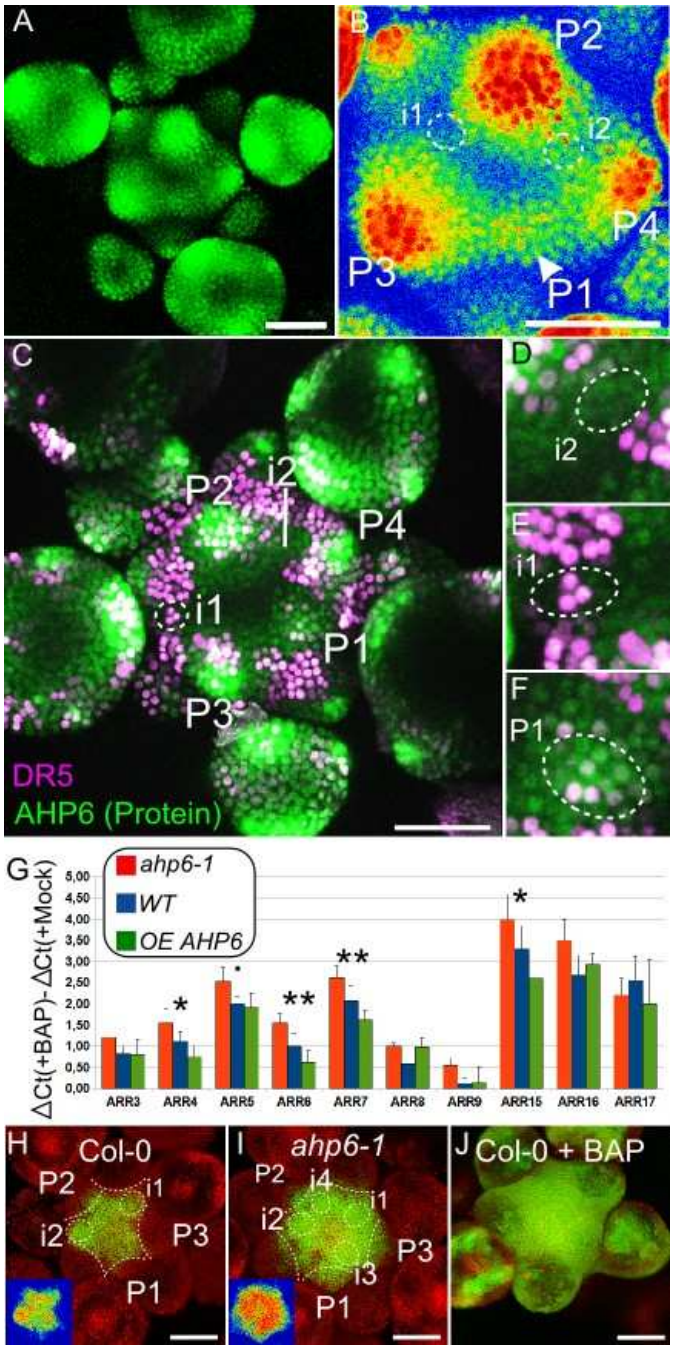

Figure 5: AHP6 acts non-cell autonomously by generating cytokinin-inhibitory fields in the shoot apical meristem. (**A,B**) Expression of *pAHP6::AHP6:GFP* in the inflorescence apex. A close-up of the SAM is shown in (A) using range indicator palette representation to highlight the graded distribution in fluorescence level and the differences in protein levels between i1 and i2 initia. (**C-F**) Co-visualization of *pAHP6::AHP6:GFP* (green) and *DR5::VENUS* (magenta) using confocal spectral microscopy. The position of presumptive i2 is indicated. A close-up of i2, i1 and P1 is shown in D, E and F respectively. (**G**) Real-time RT-PCR analysis of *AHP6* levels on the induction *ARRs* by cytokinins. Induction was compared between plantelets treated with 100 nM BAP or mock for 24H. Wild-type, *ahp6-1* and *35S::AHP6* (OE AHP6) plantelets were used. Error bars indicate standard errors, significant p-values are 0.05<·<0.1; *<0.05. **<0.005 (**H-J**) Expression of *pARR15::GFP* in wild-type (H,J) and *ahp6-1* (I) inflorescence apices. The meristem in (J) has been treated with 1 µM cytokinin (BAP) for 24 h. The insets in (H,I) show a close-up of the meristem in range indicator palette illustrating the differences in fluorescence level. Projections of confocal serial sections are shown. Autofluorescence is in red in (H-J). Scale bar: 50 µm.

pAHP6::GFP and *DR5::VENUS* using spectral confocal microscopy, we were further able to show that *AHP6* is activated one to two plastochrons after *DR5* activation (Fig. 4F). We therefore conclude that *AHP6* is activated downstream of auxin signaling, as it is the case in the root vasculature (Bishopp et al. 2011). However, since *AHP6* expression is unaffected CK, this points out interesting differences in auxin-CK crosstalk mediating by AHP6 in root vasculature specification and during organ initiation at the shoot apex. The activation of AHP6 occurs with a temporal delay of one to two plastochrons and requires both an active auxin transport and *MP*. Consistent with this, it has been shown that *MP* regulates several additional CK signaling components in the SAM (Zhao et al. 2010) and that in seedlings, *AHP6* is downregulated in *mp* mutants or upon brief induction of the dexamethasone-inducible GR-bodenlos inhibitor (Schlereth et al. 2010; Bishopp et al. 2011). Although the activation could be direct or indirect, all these data identify *AHP6* as an early auxin response gene in organ initiation.

The temporal delay between *DR5* and *AHP6* activation (Fig. 4F), together with the fact that *AHP6* acts on the earliest steps of organ initiation (Fig. 3), led us to hypothesize that *AHP6* could act non-cell autonomously in setting the temporal sequence of organ initiation. We therefore used a functional *pAHP6::AHP6-GFP* translational fusion (Mähönen et al. 2006) (Fig. S9) to analyze the distribution of the protein in the SAM. Strikingly, the AHP6-GFP protein fusion exhibited graded distributions centered on primordia and extending largely beyond their boundaries, indicating a movement of the protein outside of the organ primordia (Fig. 5A,B). Co-visualization of AHP6-GFP and *DR5::VENUS* further showed that movement of AHP6 in the SAM resulted in a differential accumulation of AHP6 in the two youngest initia (i1 and i2; Fig. 5C-F). Indeed only the very youngest initium (i2) accumulated significant levels of AHP6 (Fig. 5C,D; see also Fig. 4B). The role of *AHP6* in inhibiting CK signaling (Mähönen et al. 2006) suggested that this could creates differential CK signaling capacities between the first initium to emerge (higher CK signaling) and the following one (lower CK signaling). To investigate this hypothesis, we compared CK signaling capacities between wild-type, *ahp6* mutants and plants over-expressing *AHP6* under the *35S* promoter (Fig. 5G). This analysis showed that in seedlings, the level of *AHP6* modulated negatively the induction of 5 out 10 primary cytokinin response genes *ARR4*, *5, 6, 7* and *15*. All these ARR are expressed in the SAM (To et al. 2004; Leibfried et al. 2005; Müller & Sheen 2008). see also Fig S2A). Since a strong effect was observed with *ARR15* and since the expression of these gene is normally excluded from the developing organs (Zhao et al. 2010), we analyzed the expression of a GFP reporter for this gene (Müller & Sheen 2008) in *ahp6* mutants. When compared to wild-type,

pARR15::GFP was strongly up-regulated in *ahp6* meristems: its expression extended into primordia and also in the entire peripheral zone, covering the sites of new organ initiation. (Fig. 5H,I). AHP6 is therefore required to restrict *ARR15* to the centre of the meristem and to exclude it from primordia by buffering CK signaling. Consistently, exogenous CK application triggered ectopic activation of *pARR15::GFP* in wild-type meristems and flowers (Fig. 5J). To conclude, AHP6 acts non-cell autonomously on organ initiation by generating CK signaling inhibitory fields through movement of the protein in the SAM.

Taken together, our data suggest that fields of AHP6 create a differential CK signaling competence between the two youngest organ initia and regulate the timing of their emergence. Consistent with this idea, endogenous cytokinin signaling is active in young initia, as indicated by the co-expression of the CK-inducible synthetic reporter *TCS::GFP* (Müller & Sheen 2008) with *DR5::VENUS* (Fig. S10A-D). This expression increased with the age of the initium, demonstrating a progressive activation of CK signaling during the earlier steps of organ initiation. This progressive activation was abolished in *ahp6* mutants, since TCS::GFP expression was strongly activated in all putative initia of the peripheral zone (fig S10E-F). To test the effect of this ectopic activation of cytokinin signaling on organ initiation, we treated DR5::GFP expressing meristems with exogenous CK, at a concentration that did not affect stem cell maintenance (Gordon et al. 2009) This caused *DR5::GFP* expression patterns to expand in the periphery of both inflorescence and floral meristems, in a similar manner to *ahp6* mutants (Fig. S11A,B). Together, these results suggests that in absence of AHP6 proteins, higher CK signaling activity acts in a positive feedback on auxin signaling in the peripheral zone, likely indirectly promoting organ initiation (Fig S12). In conclusion, our results suggest an original mechanism for coupling time and space during formation of reiterative structures that is radically different from the clock-driven mechanisms identified in both plants and animals (Lewis 2008; Moreno-Risueno et al. 2010). The periodicity of organ initiation at the SAM appears to be regulated by conversion of the spatial information provided by CK signaling inhibitory fields into a stable temporal sequence of organogenesis (Fig. S12). In contrast our data indicate that the position of new organs is fixed independently of *AHP6*, most likely by the putative auxin-based inhibitory fields (Jönsson et al. 2006; R. S. Smith, Guyomarc'h, et al. 2006). The spatio-temporal pattern of organogenesis at the SAM, and thus the architecture of the shoot, would therefore be controlled by two hormonal inhibitory fields, one sufficient for positioning the initia and the other required for a precise temporal sequence.

Acknowledgements. We thank M. Heisler, B. Müller, R. Sablowski, J. Kieber and V. Pautot for sharing materials; A. Miyawaki for VENUS; C. Chamot and C. Lionnet (PLATIM) for help with confocal microscopy; S. Chamot for help with live imaging; C. Gauthier and A. Laugraud (PRABI, Université Lyon I) for help with statistical analyses; Xavier Jaurand (Pi2) for help with the SEM; Y. Couder for advice on phyllotaxis analysis; O. Hamant, A. Boudaoud, V. Mirabet, C. Scutt for comments on the manuscript; all the present and former members of the Meristem and Biophysics team for support. T.V. was supported by the Human Frontier Science Program Organization (CDA 0047/2007 HFSPO) and the Agence National de la Recherche (AuxFate ANR-07-JCJC-0115); J.T., T.V. and Y.H. by a transnational EraSysBio Grant (iSAM); F.B. by a predoctoral grant of the French Ministry of Research; Y.R. by an CJS grant from INRA.

References – Chapter II, Part I.

Bayer, E.M. et al., 2009. Integration of transport-based models for phyllotaxis and midvein formation. *Genes & Development*, 23(3), p.373-384.

Benková, E. et al., 2003. Local, efflux-dependent auxin gradients as a common module for plant organ formation. *Cell*, 115(5), p.591-602.

Bishopp, A. et al., 2011. A Mutually Inhibitory Interaction between Auxin and Cytokinin Specifies Vascular Pattern in Roots. *Current Biology: CB*, 21(11), p.917-926.

Couder, Y., 1998. Initial transitions, order and disorder in phyllotactic patterns: The ontogeny of Helianthus annuus. A case study. *ACTA SOCIETATIS BOTANICORUM POLONIAE*, 67(2), p.129-150.

Deveaux, Y. et al., 2003. The ethanol switch: a tool for tissue-specific gene induction during plant development. *The Plant Journal: For Cell and Molecular Biology*, 36(6), p.918-930.

Douady, S. & Couder, Y., 1996. Phyllotaxis as a dynamical self organizing process .3. The simulation of the transient regimes of ontogeny. *JOURNAL OF THEORETICAL BIOLOGY*, 178(3), p.295-&.

Giulini, A., Wang, J. & Jackson, David, 2004. Control of phyllotaxy by the cytokinin-inducible response regulator homologue ABPHYL1. *Nature*, 430(7003), p.1031-1034.

Gordon, S.P. et al., 2009. Multiple feedback loops through cytokinin signaling control stem cell number within the Arabidopsis shoot meristem. *Proceedings of the National Academy of Sciences of the United States of America*, 106(38), p.16529-16534.

Heisler, M.G. et al., 2005. Patterns of auxin transport and gene expression during primordium development revealed by live imaging of the Arabidopsis inflorescence meristem. *Current Biology: CB*, 15(21), p.1899-1911.

Jackson, D & Hake, S., 1999. Control of phyllotaxy in maize by the abphyl1 gene. *Development (Cambridge, England)*, 126(2), p.315-323.

Jasinski, S. et al., 2005. KNOX action in Arabidopsis is mediated by coordinate regulation of cytokinin and gibberellin activities. *Current Biology: CB*, 15(17), p.1560-1565.

Jönsson, H. et al., 2006. An auxin-driven polarized transport model for phyllotaxis. *Proceedings of the National Academy of Sciences of the United States of America*, 103(5), p.1633-1638.

Kuroha, T. et al., 2009. Functional analyses of LONELY GUY cytokinin-activating enzymes reveal the importance of the direct activation pathway in Arabidopsis. *The Plant Cell*, 21(10), p.3152-3169.

Leibfried, A. et al., 2005. WUSCHEL controls meristem function by direct regulation of cytokinin-inducible response regulators. *Nature*, 438(7071), p.1172-1175.

Lewis, J., 2008. From signals to patterns: space, time, and mathematics in developmental biology. *Science (New York, N.Y.)*, 322(5900), p.399-403.

Mitchison, G.J., 1977. Phyllotaxis and the fibonacci series. *Science (New York, N.Y.)*, 196(4287), p.270-275.

Moreno-Risueno, M.A. et al., 2010. Oscillating gene expression determines competence for periodic Arabidopsis root branching. *Science (New York, N.Y.)*, 329(5997), p.1306-1311.

Mähönen, A.P. et al., 2006. Cytokinin signaling and its inhibitor AHP6 regulate cell fate during vascular development. *Science (New York, N.Y.)*, 311(5757), p.94-98.

Müller, B. & Sheen, J., 2008. Cytokinin and auxin interaction in root stem-cell specification during early embryogenesis. *Nature*, 453(7198), p.1094-1097.

Reinhardt, D, Mandel, T & Kuhlemeier, C, 2000. Auxin regulates the initiation and radial position of plant lateral organs. *The Plant Cell*, 12(4), p.507-518.

Reinhardt, Didier et al., 2003. Regulation of phyllotaxis by polar auxin transport. *Nature*, 426(6964), p.255-260.

de Reuille, P.B. et al., 2006. Computer simulations reveal properties of the cell-cell signaling network at the shoot apex in Arabidopsis. *Proceedings of the National Academy of Sciences of the United States of America*, 103(5), p.1627-1632.

Schlereth, A. et al., 2010. MONOPTEROS controls embryonic root initiation by regulating a mobile transcription factor. *Nature*, 464(7290), p.913-916.

Schoute, J.C., 1913. Beitrage zur Blattstellunglehre. I. Die Theorie. *Recueil de Travaux Botaniques Néerlandais*, 10, p.153-339.

Smith, R., Kuhlemeier, C & Prusinkiewicz, P, 2006. Inhibition fields for phyllotactic pattern formation: a simulation study. *CANADIAN JOURNAL OF BOTANY-REVUE CANADIENNE DE BOTANIQUE*, 84(11), p.1635-1649.

Smith, R.S., Guyomarc'h, S., et al., 2006. A plausible model of phyllotaxis. *Proceedings of the National Academy of Sciences of the United States of America*, 103(5), p.1301-1306.

Stoma, S. et al., 2008. Flux-based transport enhancement as a plausible unifying mechanism for auxin transport in meristem development. *PLoS Computational Biology*, 4(10), p.e1000207.

To, J.P.C. et al., 2004. Type-A Arabidopsis response regulators are partially redundant negative regulators of cytokinin signaling. *The Plant Cell*, 16(3), p.658-671.

Veen, A.H. & Lindenmayer, A., 1977. Diffusion mechanism for phyllotaxis: theoretical physico-chemical and computer study. *Plant Physiology*, 60(1), p.127-139.

Vernoux, T. et al., 2000. PIN-FORMED 1 regulates cell fate at the periphery of the shoot apical meristem. *Development (Cambridge, England)*, 127(23), p.5157-5165.

Yadav, R.K. et al., 2009. Gene expression map of the Arabidopsis shoot apical meristem stem cell niche. *Proceedings of the National Academy of Sciences of the United States of America*, 106(12), p.4941-4946.

Yanai, O. et al., 2005. Arabidopsis KNOXI proteins activate cytokinin biosynthesis. *Current Biology: CB*, 15(17), p.1566-1571.

Zhao, Z. et al., 2010. Hormonal control of the shoot stem-cell niche. *Nature*, 465(7301), p.1089-1092.

2. Supporting Information

2.1. Material and Methods

4.1.1. Plant material and growth conditions

The *ahp6-1, ahp6-3, pLFY::GFP, pWUS::GFP, pAHP6::GFP, pPIN1::PIN1-GFP, pAHP6::AHP6-GFP, pARR5::GFP, pARR15::GFP, 35S::STM-GR* lines have been described (Mähönen et al. 2006; Deveaux et al. 2003; Benková et al. 2003; Müller & Sheen 2008; Yanai et al. 2005; Gallois et al. 2002) and are all in Columbia (Col-0) except *pLFY::GFP* and *pWUS::GFP* (Ws) and *35S::STM-GR* (Ler).

Previously described plasmids (Müller & Sheen 2008; Heisler et al. 2005) were introduced in Col-0 plants by floral dipping (Clough & Bent 1998) to generate the *DR5::VENUS, STM-VENUS* and *TCS::GFP* line. Plants were grown on soil at 20°C in short day conditions (8 h light/16 h darkness) for 4 to 5 weeks to synchronize them before being transferred in long-day conditions (16 h light/8 h darkness). Reversible inhibition of organ initiation *in vitro* using NPA was performed as described(Olivier Grandjean et al. 2004). For induction of 35S::STM-GR by Dexamethasone, two consecutive treatments were done at a 6 h difference as described 35 and the plants were observed 26 h after the second treatment.

2.1.2. In situ *hybridization, microscopy and live imaging*

Scanning Electron Microscopy and RNA in situ hybridization were performed as described (T Vernoux et al. 2000) using full-length probes amplified by PCR. Microscope observations were done either on a LSM-510 laser-scanning confocal microscope (Zeiss, Jena, Germany), a confocal spinning disc DMI400 microscope (Leica, Germany) or a SP5 spectral detection confocal Microscope (Leica, Germany).

Images were processed under image J (http://rsbweb.nih.gov/ij/). Serial sections were used to count the number of cells expressing *pLFY::GFP* in the younger primordia. Culture and imaging of living SAMs expressing *DR5::VENUS* was performed as described previously (Fernandez et al. 2010) except for adding 555 nM N6-Benzyladenine (BAP; Duchefa) in the culture medium. The meristems were allowed to recover for 12h before starting imaging every 12h for 72h. 20 wild-type and 33 *ahp6-1* meristems were analysed. New primordia were scored as co-initiated when they

Target Gene	Primer	sequence
AHP6	AHP6_qPCR2_F	CCGCAACCTTAGATTATTGTTGAT
	AHP6_qPCR2_R	CCCTACGAGCACCAATGC
TCTP	TCTPQ5	CACCCAGCTCAGCGAAGAA
	TCTPQ3	CATGCATACCCTCCCCAACAA
ARR3	ARR3-qPCR1-F	AGGAAACAAACGGAAGCTGA
	ARR3-qPCR1-R	ATCGAGGATGTGGCTGAGAG
ARR4	ARR4-qPCR1-F	GTCATCGAGAGATTGCTTCGT
	ARR4-qPCR1-R	ACGCCATCCACTATCTACCG
ARR5	ARR5_qPCR2_F	TCAGAGAACATCTTGCCTCGT
	ARR5_qPCR2_R	ATTTCACAGGCTTCAATAAGAAATC
ARR6	ARR6-qPCR1-F	GAACATTTTGCCTCGTATTGATAG
	ARR6-qPCR1-R	CGAGAGTTTTACCGGCTTCA
ARR7	ARR7_qPCR2_F	TCATCTGAGAACATCTTACCTCGT
	ARR7_qPCR2_R	TTCACCGGTTTCAACAAGAAT
ARR8	ARR8-qPCR1-F	ACGTTCCTGCAAGAATCTCC
	ARR8-qPCR1-R	GGTTTCAACTTGGTAAGATCAGC
ARR9	ARR9-qPCR1-F	ACGTTCCTGCAAGAATCAGC
	ARR9-qPCR1-R	CAGCCAATCTTACTGGTTTCAA
ARR15	ARR15_qPCR2_F	GAGAACATACAACCTCGTATAGAACAA
	ARR15_qPCR2_R	GCTAATTTCACCGGTTTTAGCA
ARR16	ARR16-qPCR1-F	AAAGTGAAGCAGGAGTCATCA
	ARR16-qPCR1-R	CATTTGTTTATGCGAGTAGGAA
ARR17	ARR17-qPCR1-F	ATTCCTACCCGCATCAACAA
	ARR17-qPCR1-R	GATAGTTTCAGTGGCTTCTGCAT

Table S1: Sequences of primers used in real-time quantitative PCR.

exhibited similar number of VENUS-positive nuclei at a new time-point. Chemical treatments were done by immersion of the apices in water supplemented with BAP at the indicated concentrations.

4.1.3. Real-Time quantitative RT-PCR experiments

Protocol, proceedings and analysis were design to comply to standards of qRT-PCR defined previously (Udvardi et al. 2008; Rieu & Powers 2009). Col-0, *ahp6-1*,and *35S::AHP6* seedlings were grown *in vitro* on vertical plates on a Murashige and Skoog (MS) medium with 1%sucrose and 1% agarose for 6 days and then transferred to plates containing the same medium supplemented with 100 nM BAP or a mock solution for 6 hours (data not shown) and 24hours. A Similar amount of plants were collected and RNA was extracted with the Spectrum Plant Total RNA kit (SIGMA) , DNAse treated (Turbo DNA-free kit ; Ambion), reverse-transcribed using RevertAid Reverse transcriptase (FERMENTAS) with 1µg of total RNA ().

A matrix of 6,25ng of total cDNA was used in 20 µL PCR reactions. PCR were run on StepOnePlus™ Real Time PCR System (Applied Biosystems) with FastStart Universal SYBR Green Master (ROCHE). In all experiments, three biological replicates of each sample type were tested, and reactions were carried out with three technical (PCR) replicates. Absence of genomic DNA and primer dimers was confirmed by water control samples and by examination of dissociation curves. Expression data were normalized using the expression of the TCTP gene (*At3g16640*), after verification with Bestkeeper©(Pfaffl et al. 2004). Primer pair efficiencies were estimated by analysis of the amplification curves with the StepOnePlus™ software and the average efficiency of the dilution series on a plate (which was always > 1.95) was used in calculations. For statistical analysis of qPCR data, reference-gene corrected threshold cycle (Ct) values were used. These were obtained by converting the Ct values to relative quantities, which were corrected with the calculated normalization factors (see above) and were back-transformed to Ct values. Relative expression of target gene in a sample was calculated as the difference between corrected Ct of the target gene and the corrected Ct of the TCTP reference gene (ΔCt). The effect of the treatment was calculated as the difference between the ΔCt in the BAP-treated samples and the mock-treated samples (ΔΔCt). Statistical significance of the results was tested using an analysis of variance (ANOVA).

2.1.4. Microarray data analysis

Expression estimates were calculated from the raw cell files (Yadav et al. 2009);obtained from ArrayExpress) using gcRMA (Wu et al. 2004). Statistical testing for differential expression between the different datasets was performed with LIMMA (Wettenhall & Smyth 2004). Correction for

multiple testing was done by computing Q-values (Storey & Tibshirani 2003). These analyses were done under R using Bioconductor packages (www.bioconductor.org). By fixing the false discovery rate (FDR) to 1, we identified the following number of genes differentially expressed: FILp-CLV3p: 1379; FILp-WUSp: 1165; CLV3p-WUSp: 1357. Genes affected by protoplasting16 (592 genes identified) were not considered in the analysis.

4.1.5. Measures of phyllotactic sequences and models used for characterization of permutation patterns

See chapter 1.

Supplementary references – ChapII, Part I

Benková, E. et al., 2003. Local, efflux-dependent auxin gradients as a common module for plant organ formation. *Cell*, 115(5), p.591-602.

Clough, S.J. & Bent, A.F., 1998. Floral dip: a simplified method for Agrobacterium-mediated transformation of Arabidopsis thaliana. *The Plant Journal: For Cell and Molecular Biology*, 16(6), p.735-743.

Deveaux, Y. et al., 2003. The ethanol switch: a tool for tissue-specific gene induction during plant development. *The Plant Journal: For Cell and Molecular Biology*, 36(6), p.918-930.

Fernandez, R. et al., 2010. Imaging plant growth in 4D: robust tissue reconstruction and lineaging at cell resolution. *Nature Methods*, 7(7), p.547-553.

Gallois, J.-L. et al., 2002. Combined SHOOT MERISTEMLESS and WUSCHEL trigger ectopic organogenesis in Arabidopsis. *Development (Cambridge, England)*, 129(13), p.3207-3217.

Grandjean, Olivier et al., 2004. In vivo analysis of cell division, cell growth, and differentiation at the shoot apical meristem in Arabidopsis. *The Plant Cell*, 16(1), p.74-87.

Heisler, M.G. et al., 2005. Patterns of auxin transport and gene expression during primordium development revealed by live imaging of the Arabidopsis inflorescence meristem. *Current Biology: CB*, 15(21), p.1899-1911.

Mähönen, A.P. et al., 2006. Cytokinin signaling and its inhibitor AHP6 regulate cell fate during vascular development. *Science (New York, N.Y.)*, 311(5757), p.94-98.

Müller, B. & Sheen, J., 2008. Cytokinin and auxin interaction in root stem-cell specification during early embryogenesis. *Nature*, 453(7198), p.1094-1097.

Pfaffl, M.W. et al., 2004. Determination of stable housekeeping genes, differentially regulated target genes and sample integrity: BestKeeper--Excel-based tool using pair-wise correlations. *Biotechnology Letters*, 26(6), p.509-515.

Rieu, I. & Powers, S.J., 2009. Real-time quantitative RT-PCR: design, calculations, and statistics. *The Plant Cell*, 21(4), p.1031-1033.

Storey, J.D. & Tibshirani, R., 2003. Statistical significance for genomewide studies. *Proceedings of the National Academy of Sciences of the United States of America*, 100(16), p.9440-9445.

Udvardi, M.K., Czechowski, T. & Scheible, W.-R., 2008. Eleven golden rules of quantitative RT-PCR. *The Plant Cell*, 20(7), p.1736-1737.

Vernoux, T et al., 2000. PIN-FORMED 1 regulates cell fate at the periphery of the shoot apical meristem. *Development (Cambridge, England)*, 127(23), p.5157-5165.

Wettenhall, J. & Smyth, G., 2004. limmaGUI: A graphical user interface for linear modeling of microarray data. *BIOINFORMATICS*, 20(18), p.3705-3706.

Wu, Z. et al., 2004. A model-based background adjustment for oligonucleotide expression arrays. *JOURNAL OF THE AMERICAN STATISTICAL ASSOCIATION*, 99(468), p.909-917.

Yadav, R.K. et al., 2009. Gene expression map of the Arabidopsis shoot apical meristem stem cell niche. *Proceedings of the National Academy of Sciences of the United States of America*, 106(12), p.4941-4946.

Yanai, O. et al., 2005. Arabidopsis KNOXI proteins activate cytokinin biosynthesis. *Current Biology: CB*, 15(17), p.1566-1571.

2.2. Supplementary Figures

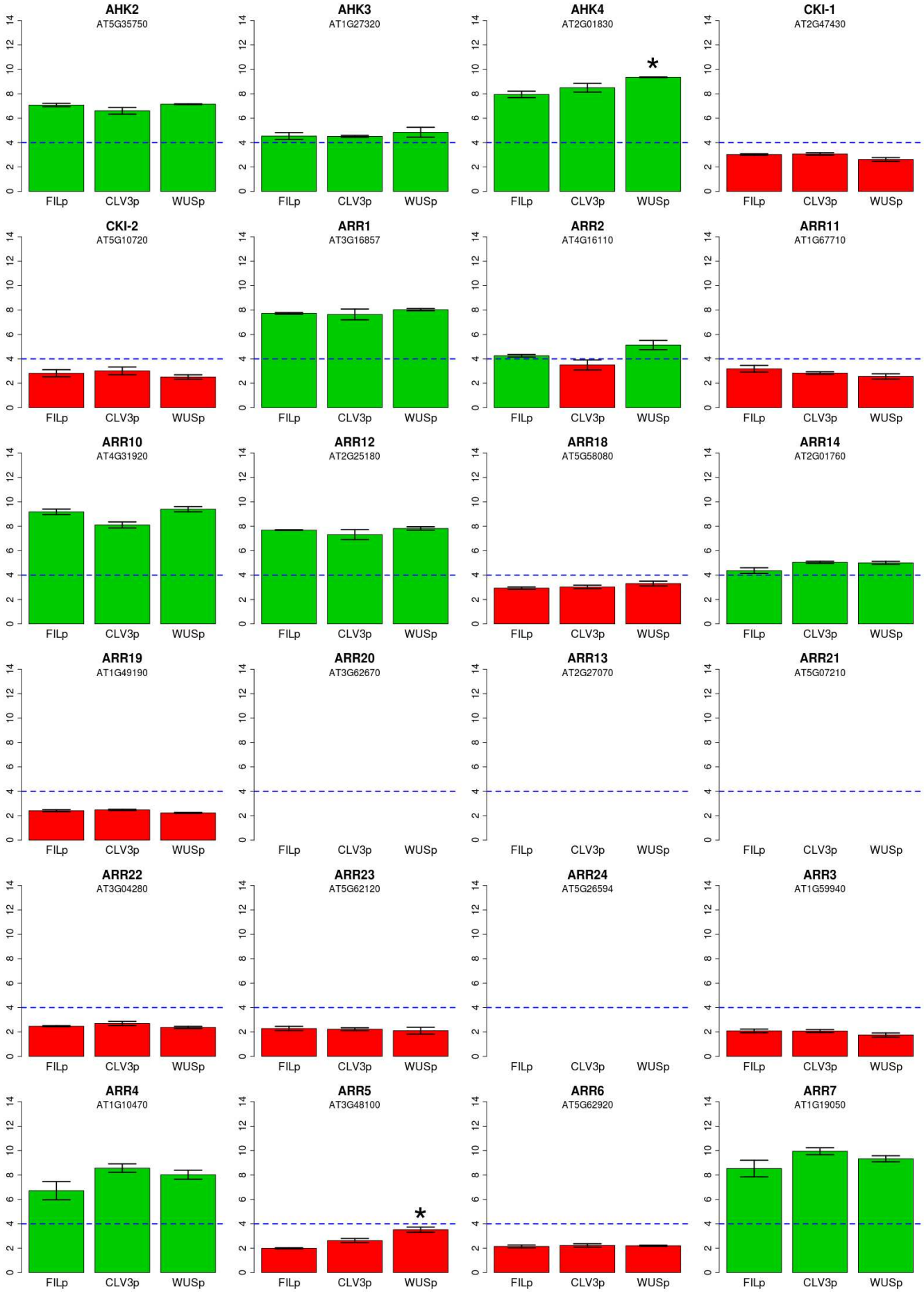

Figure S1 (1/3)

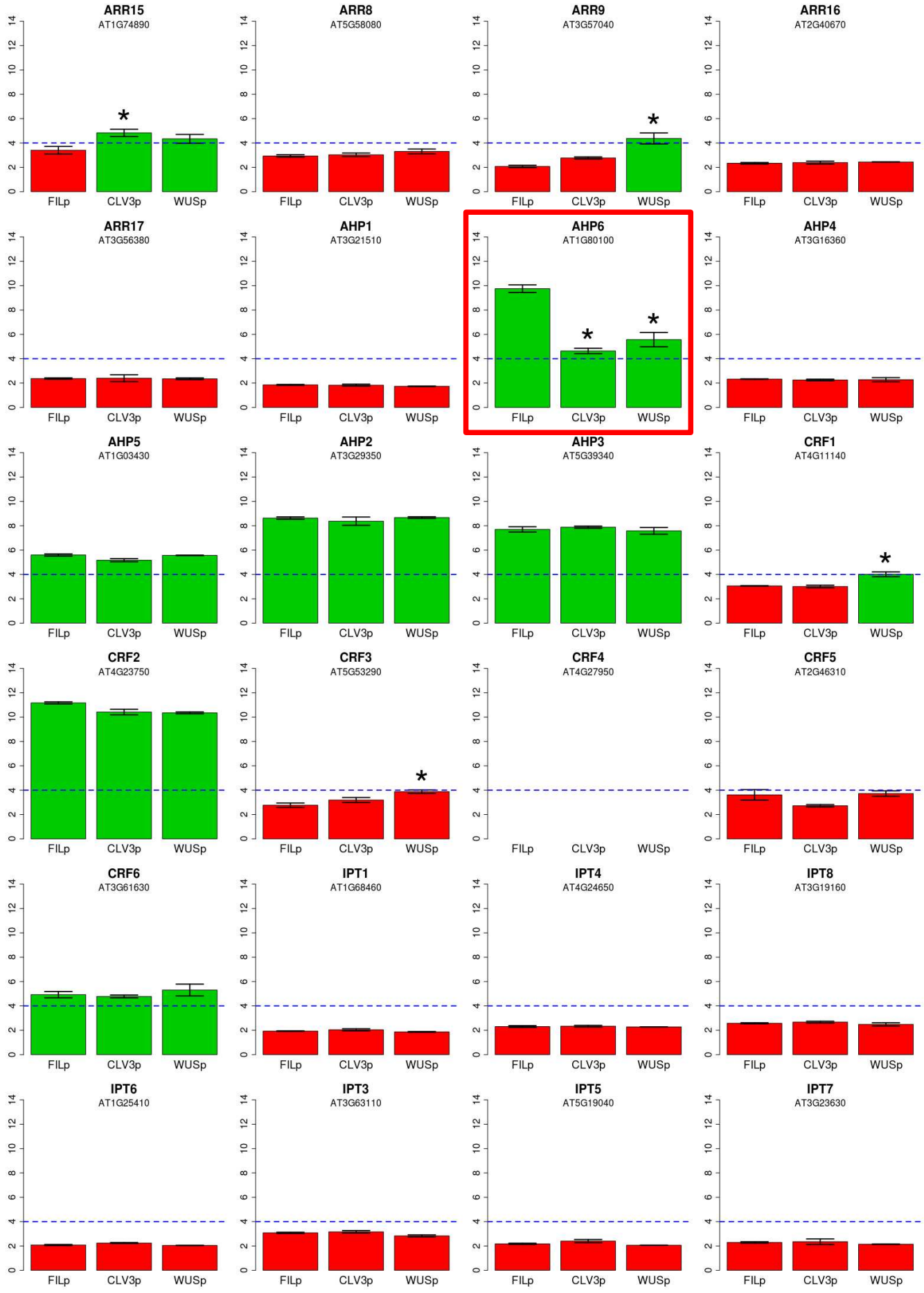
ARR15
AT1G74890
ARR8
AT5G58080
ARR9
AT3G57040
ARR16
AT2G40670
ARR17
AT3G56380
AHP1
AT3G21510
AHP6
AT1G80100
AHP4
AT3G16360
AHP5
AT1G03430
AHP2
AT3G29350
AHP3
AT5G39340
CRF1
AT4G11140
CRF2
AT4G23750
CRF3
AT5G53290
CRF4
AT4G27950
CRF5
AT2G46310
CRF6
AT3G61630
IPT1
AT1G68460
IPT4
AT4G24650
IPT8
AT3G19160
IPT6
AT1G25410
IPT3
AT3G63110
IPT5
AT5G19040
IPT7
AT3G23630
FILp
CLV3p
WUSp

Figure S1 (2/3)

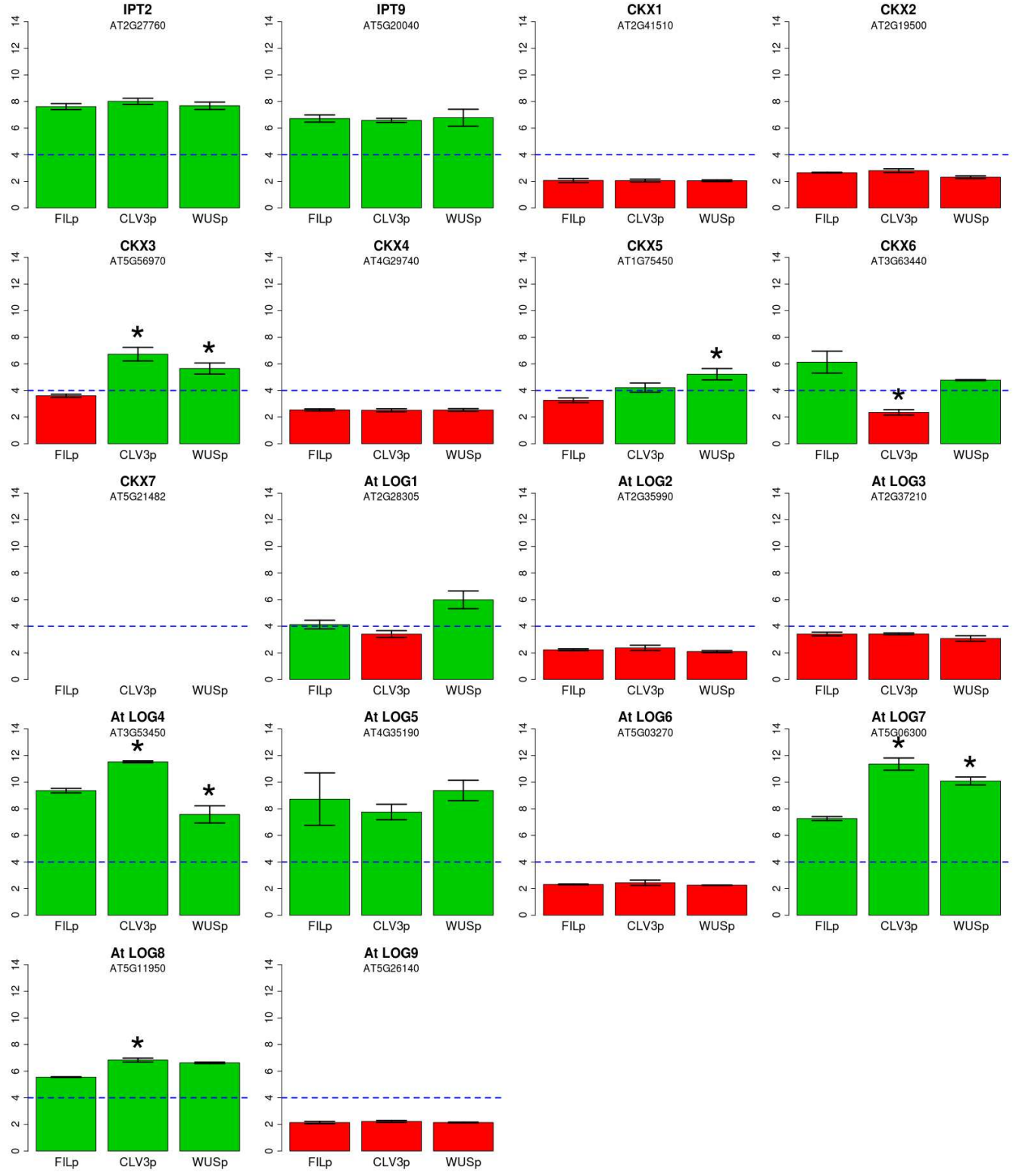

Figure S1 (3/3). Expression of the regulators of cytokinin signalling and biosynthesis in the different domains of the shoot apical meristem. Normalized values of expression were calculated from previously published microarray datasets (Yadav et al., 2009; see main text) obtained from the *FILAMENTOUS FLOWER* (FIL) domain in the lateral organs, and from the *CLAVATA3* (CLV3) and *WUSCHEL* (WUS) domains at the centre of the meristem. The dashed lines represent the background level of expression. Differential expression between the FIL domain and the WUS or the CLV3 domain was systematically tested. The stars indicate when expression is statistically different in the WUS and/or CLV3 domains compared to the FIL domain. The Diagram corresponding to *AHP6* is outlined by a red square.

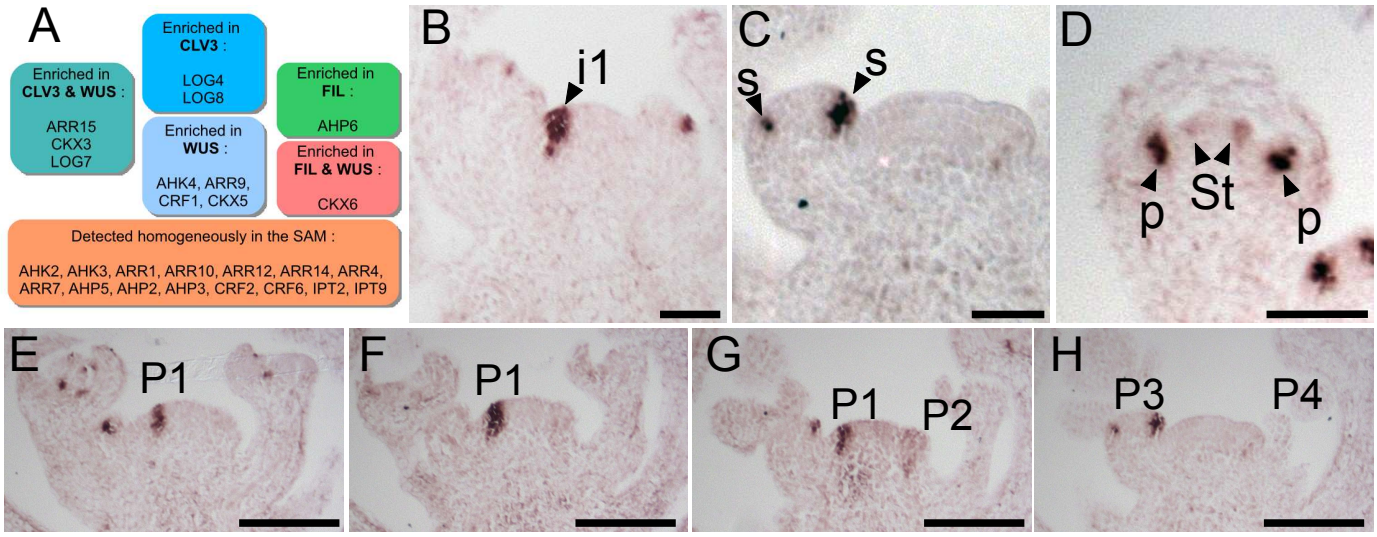

Figure S2. *AHP6* is a regulator of cytokinin signalling that is specifically enriched in lateral organs. (A) Summary of the expression profiles of the regulators of cytokinin signalling deduced from the Yadav dataset (see Supplementary Fig. 2). (B-H) Analysis of *AHP6* expression pattern in the inflorescence using RNA *in situ* hybridization. The arrowheads in (B-D) points at expression in the organ initium (B), the sepal initia (C) and the petals and stamens initia (D). A serial section is shown in (E-H) to illustrate the organ-specific expression. s: sepal; p: petal; st: stamen. Scale bar: 20 µm in (B-D) and 50 µm in (E-H).

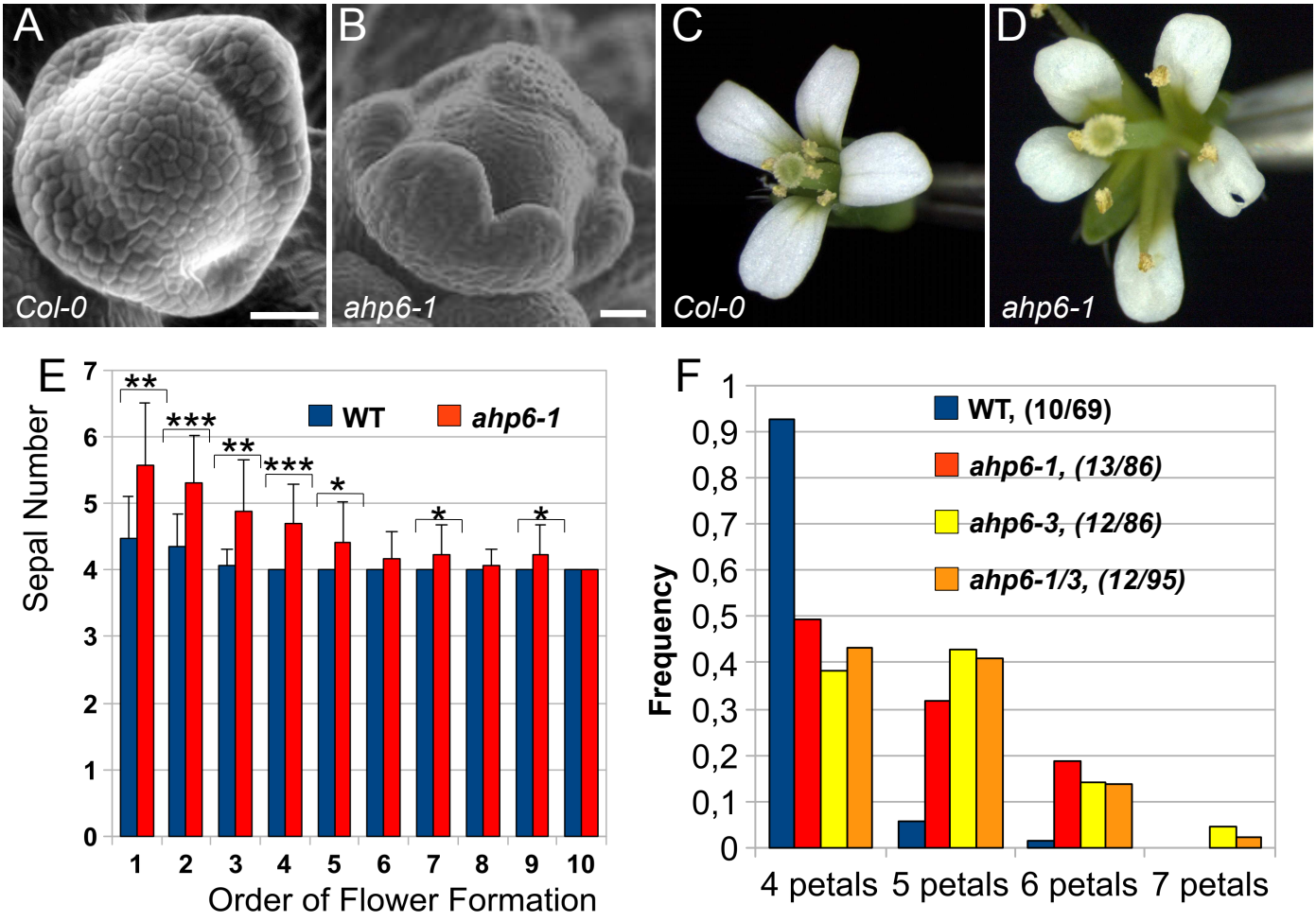

Figure S3. *AHP6* regulates floral phyllotaxis. (A,B) Electron microscopy of wild-type (A) and *ahp6-1* (B) stage 3 flowers showing defects in sepal numbers. (C,D) Mature flowers of wild-type (C) and *ahp6-1* (D) showing defects in petal numbers. (E) Quantification of sepal numbers in wild-type and *ahp6-1*. Error bars represent standard deviations. Differences that are statistically significant are indicated (student t-test: $p<5\%$ (*), $p<5.10^{-3}$ (**), $p<5.10^{-4}$ (***). 122 and 166 flowers were analyzed for wild-type and *ahp6-1* respectively. (F) Petal numbers in wild-type, *ahp6-1*, *ahp6-3* and *ahp6-1*/*ahp6-3*. The number of plants and total flowers analyzed are indicated in parenthesis. Scale bar: 20 µm.

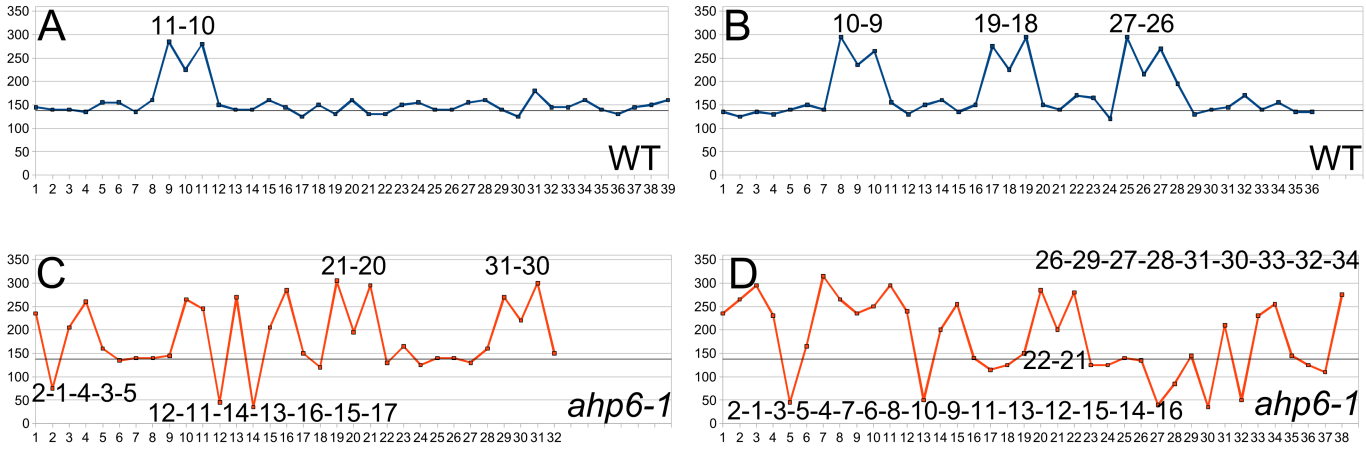

Figure S4. Explanation of the deviations from the canonical phyllotactic sequences by the permutation hypothesis. Significant examples of angle sequences explained by permutation in the order of silique insertions on the stem. The permutations explaining the motifs are indicated.

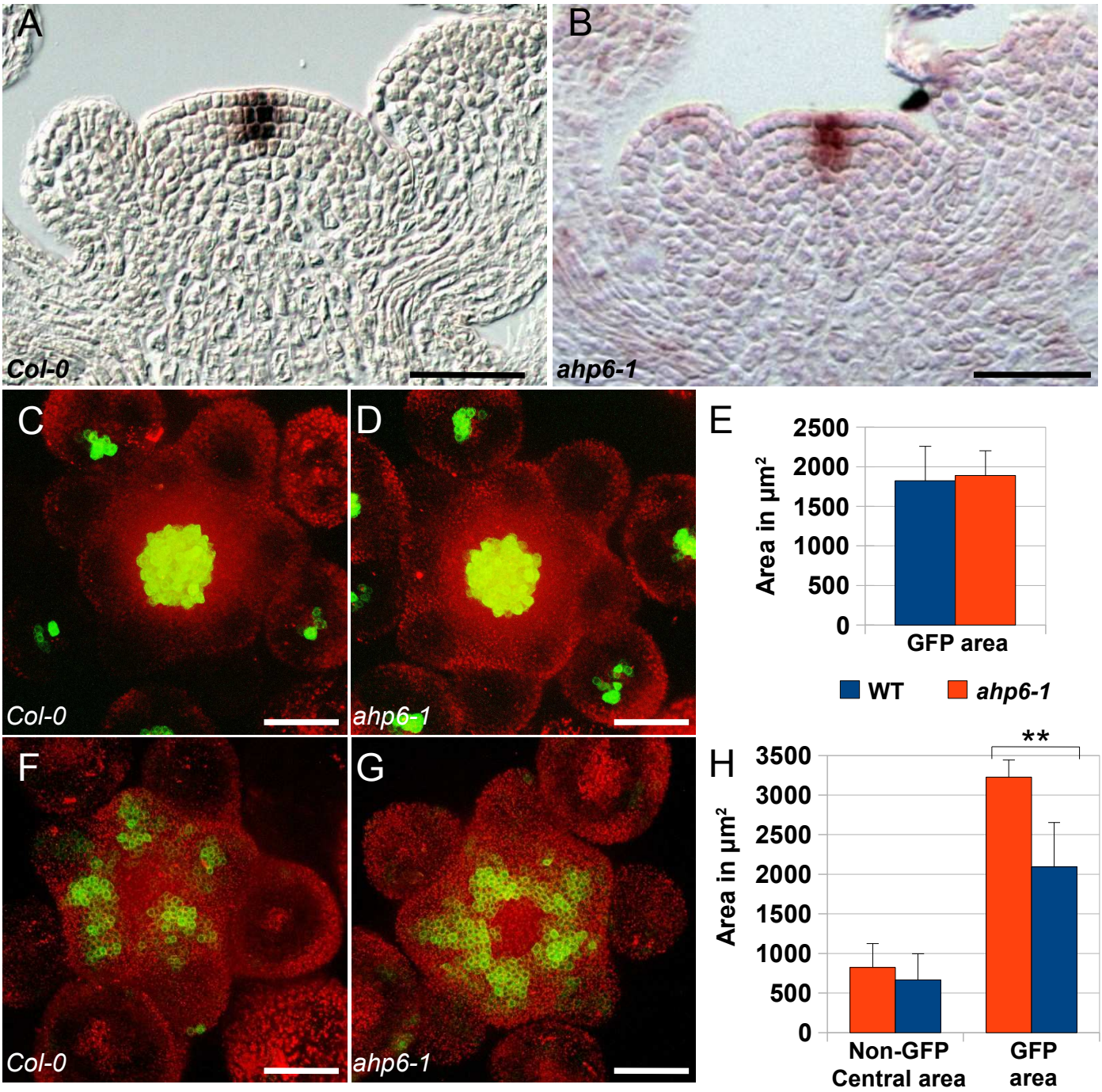

Figure S5. The size of the stem cell niche is not affected by the *ahp6* mutation. (A,B) The size of the expression domain of the *CLV3* stem cell marker is identical in wild-type (A) and *ahp6-1* (B). *CLV3* expression was analyzed by RNA *in situ* hybridization. A median section is shown. (C-E) The expression of *pWUS::GFP* is not affected by the *ahp6-1* mutation. A representative confocal image (projection) for wild-type (C) and *ahp6-1* (D) is shown. The area of the *WUS* domain was quantified using images from 3 wild-type and 9 *ahp6-1* meristems. (F-H) The size of the central area not expressing *pDR5::GFP* is not affected by the *ahp6-1* mutation. A representative confocal image (projection) for wild-type (F) and *ahp6-1* (F) is shown. The area of the peripheral GFP domain and of the central non-GFP domain was quantified using images from 9 wild-type and 5 *ahp6-1* meristems. While the GFP positive area increases significantly in *ahp6-1* ($p<5.10^{-4}$; student t-test), the area of the non-GFP central domain is not affected by the mutation. This further suggests that the size of the central zone is not affected by the *ahp6* mutation. Error bars indicate standard deviations. Scale bar: 50 µm.

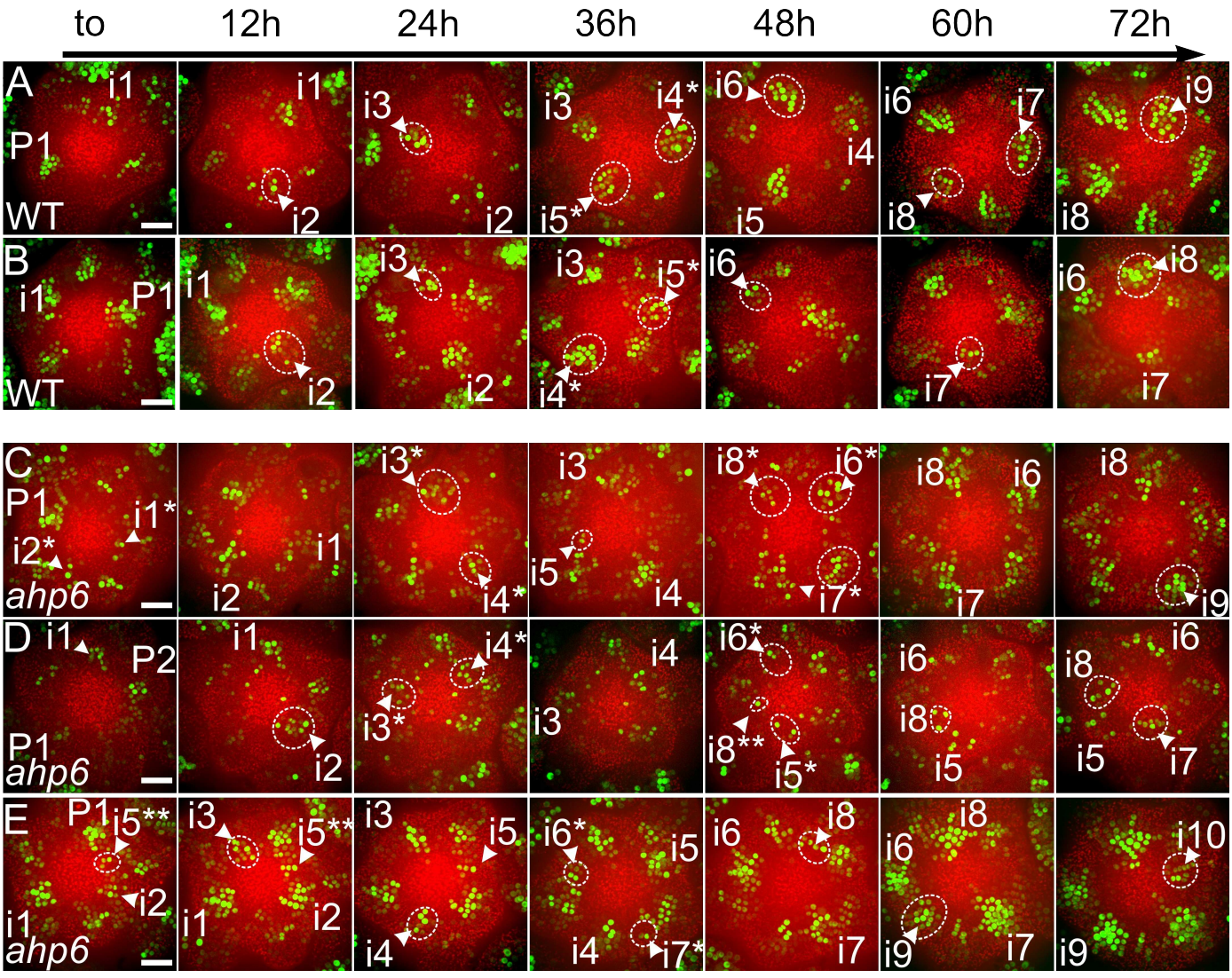

Figure S6. *AHP6* regulates the temporal sequence of *DR5::VENUS* activation at the shoot apical meristem. Live meristems expressing *DR5::VENUS* were followed over 72 h. Representative time-courses are shown. (A,B) Wild-type meristems. (A) corresponds to the time-course shown in part in Fig. 2h. (C-E) *ahp6-1* meristems. (C) corresponds to the time-course shown in part in Fig. 2I. The co-initiated organ initia are indicated with a star. The double stars in (D,E) indicate initia that arise in a non-canonical order (permutations). i: initium; P: primordium. Scale bar: 20 µm.

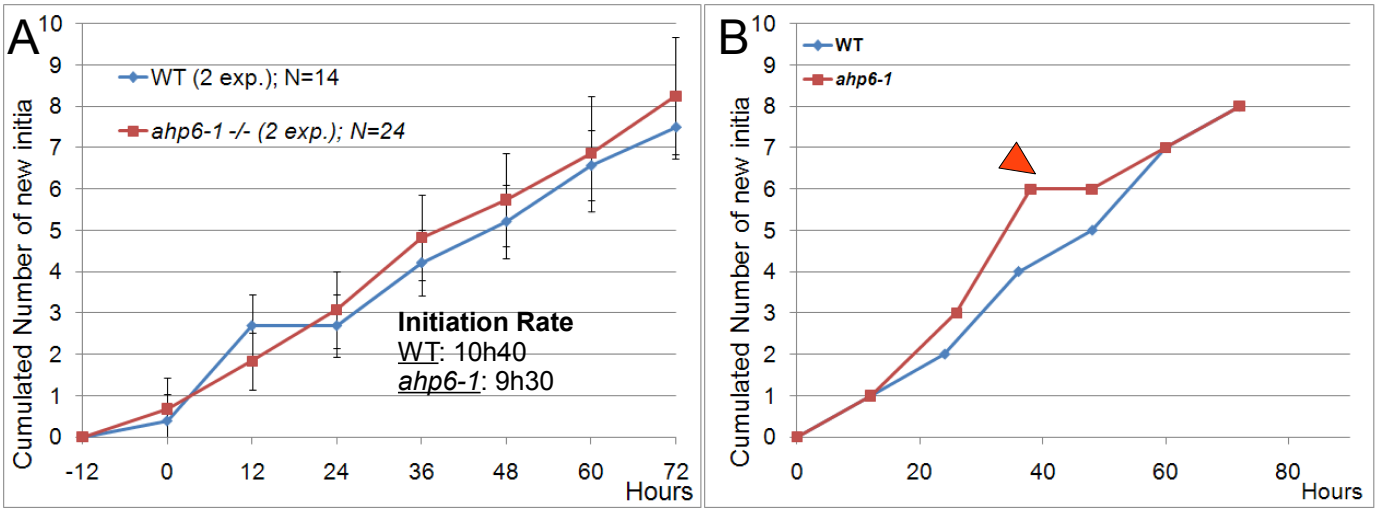

Figure S7. *AHP6* does not affect the mean rate of organ initiation but rather the stability of the plastochrone. (A) Cumulative number of initia produced over time as counted from live imaging of *DR5::VENUS* in the meristem. Values obtained from 2 replicate experiments out of 3 are represented. One experiment was not used due to slight differences in the timing of acquisition. The mean rate or plastochrone over the 72h period was calculated from these curves using a linear regression and is indicated on the figure. (B) The stability of the plastochrone is regulated by *AHP6*. Cumulative organ numbers are represented over time for a wild-type and an *ahp6-1* individual. The *ahp6* mutant dynamics shows a plateau (arrow) just after a burst of production detected at 36 h (note the deviation from the wild-type profile).

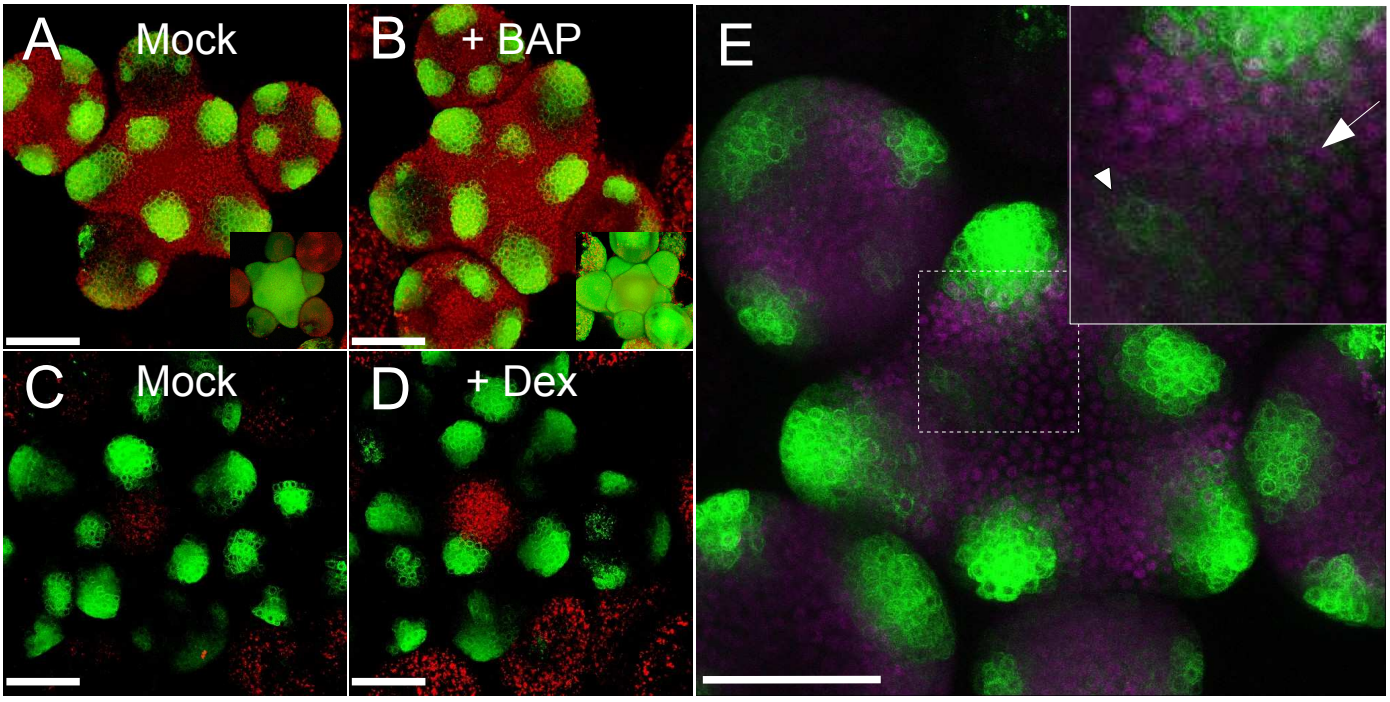

Figure S8. *AHP6* expression is regulated independently of cytokinins in the shoot apical meristem. (A,B) Expression of *pAHP6::GFP* is not modified upon cytokinin treatment (1 µM BAP for 48 h). GFP is in green, autofluorescence in red. Insets show cytokinin inducible *pARR5::GFP* control. Note the strong increase in fluorescence upon cytokinin treatment (C-E). *AHP6* is regulated independently of STM. Expression of *pAHP6::GFP* is not modified by inducible ectopic expression of *STM* (C,D). 35S::STM-GR plants were induced by dexamethasone (Dex) treatment. Co-visualization of STM-VENUS (pink) and *pAHP6::GFP* (green) (E) further demonstrates that *STM* and *AHP6* are co-expressed in organ initia and in organ frontiers (arrowhead and arrow in inset, respectively). Scale bar: 50 µm.

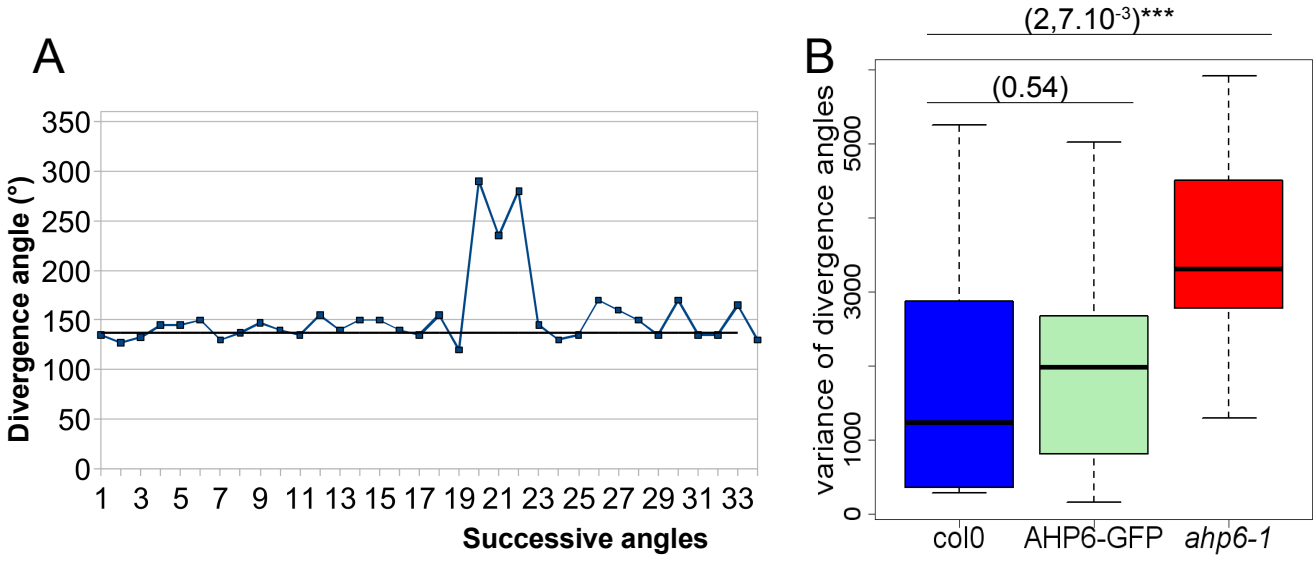

Figure S9. The *pAHP6::AHP6-GFP* construct complements *ahp6* phyllotaxis phenotype. Divergence angle sequences of *ahp6* mutants expressing *pAHP6::AHP6-GFP* were obtained to test the functionality of the construct. A representative angle sequence is shown in (A), showing a single M-shaped motif similarly to wild-type. The *pAHP6::AHP6-GFP* construct reduces the number of non-canonical angles to frequency similar to wild-type as shown in (B). The Box-plots in (B) shows a similar variance of angles between the wild-type (N=19 plants) and *pAHP6::AHP6-GFP* plants (N=15), whereas the variance of *ahp6-1* (N=18) is significantly higher (the p-values of the non-parametric kruskal-wallis test are indicated above the population tested).

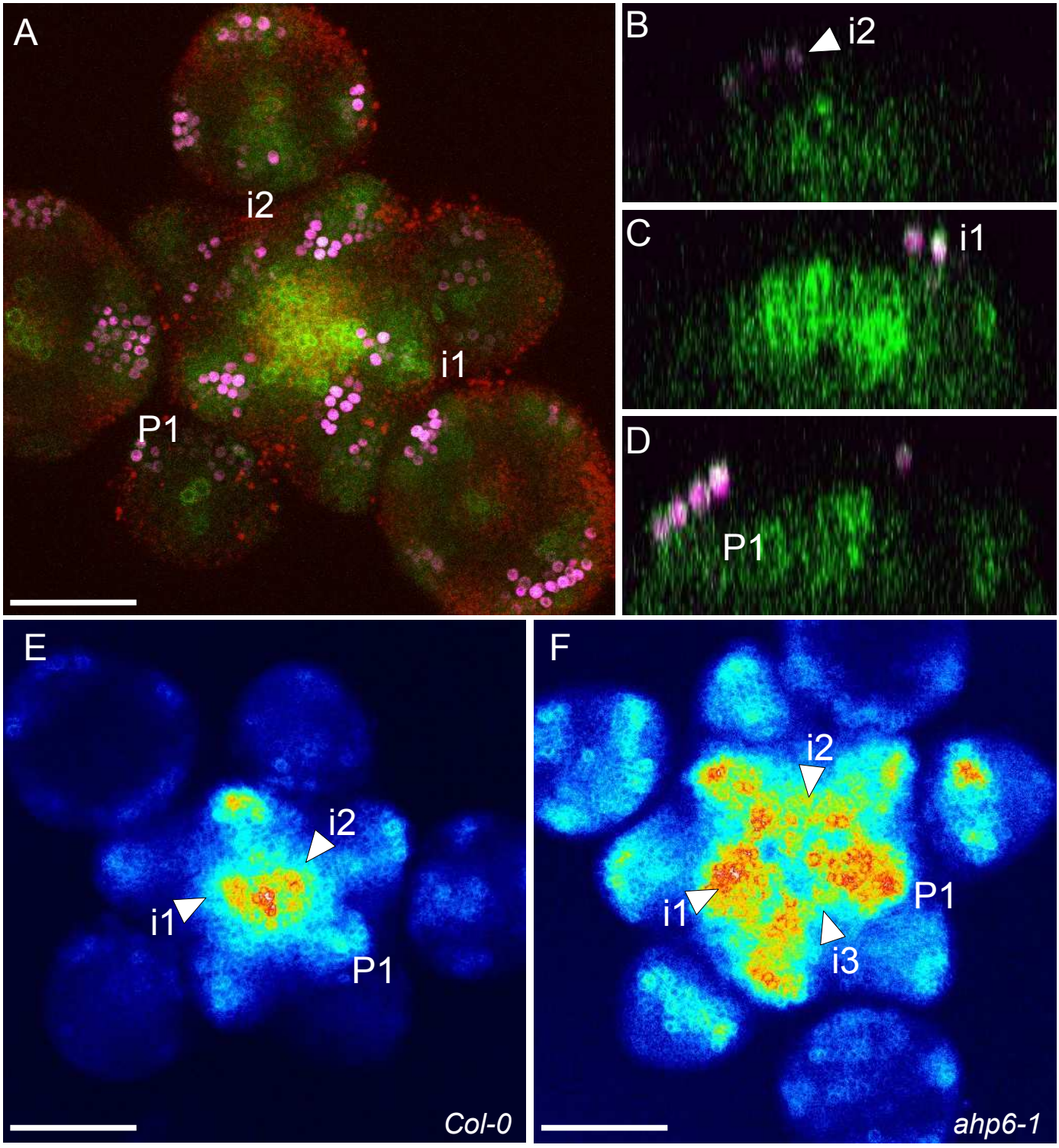

Figure S10. *AHP6* imposes a progressive activation of Cytokinin signalling activation in initia. To evaluate the activity of the cytokinin signalling pathway during organ initiation, we co-localized *DR5::VENUS* (pink) and the cytokinin-inducible *TCS::GFP* (green) reporter (A-D). A projection of a representative meristem is shown in (C) and demonstrate co-activation of *DR5::VENUS* and *TCS::GFP* in the initia and primordia. (B-D) show reconstructed medial longitudinal sections in i2 (arrowhead in B), i1 (C) and P1 (D) from the meristem shown in (A). Note that the expression of *TCS::GFP* is weak in i2 and increases significantly in i1 and P1, suggesting a progressive upregulation of TCS during organ initiation. (E-F) Comparison of *TCS::GFP* expression pattern in wild-type (E) and *ahp6-1* (F) meristem, using a range indicator palette, showing the strong ectopic activation of cytokinin signalling in the initia and a partial loss of the progressive increase in cytokinin signalling between successive initia. Scale bars: 50 μm.

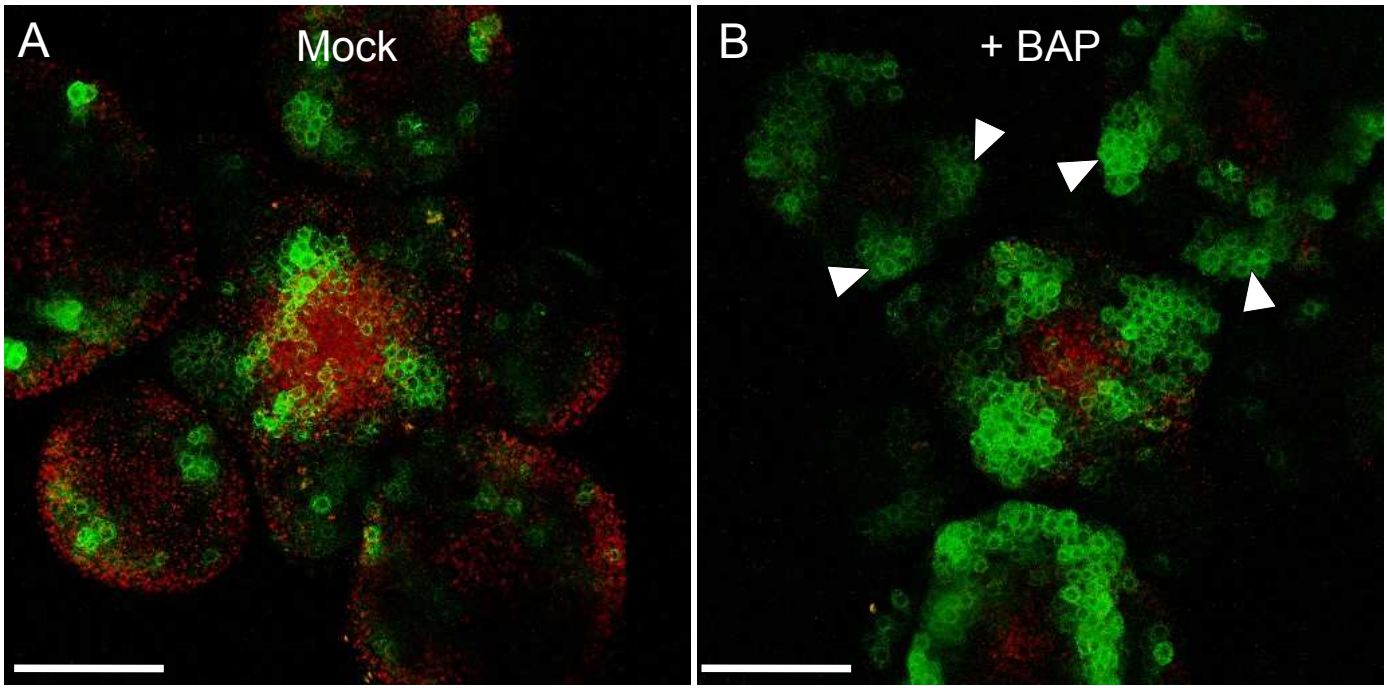

Figure S11. Exogenous cytokinin treatment increases auxin signaling in organogenetic zones of the meristem. The effect of exogenous cytokinin (1 μM BAP for 48 h) on expression of *DR5::GFP* (green; A,B) was tested. This treatment induced an expansion of the DR5::GFP domain in the meristem and the flowers in the sites of organ initiation, further suggesting that the potential for an organ to initiate is promoted by higher cytokinin signalling activity. Note that the treatment induces the formation of two auxin maxima at the site of the adaxial sepal (arrowheads), which could phenocopy the supernumerary sepals seen in *ahp6* mutants (Fig S3). Scale bar: 50 μm.

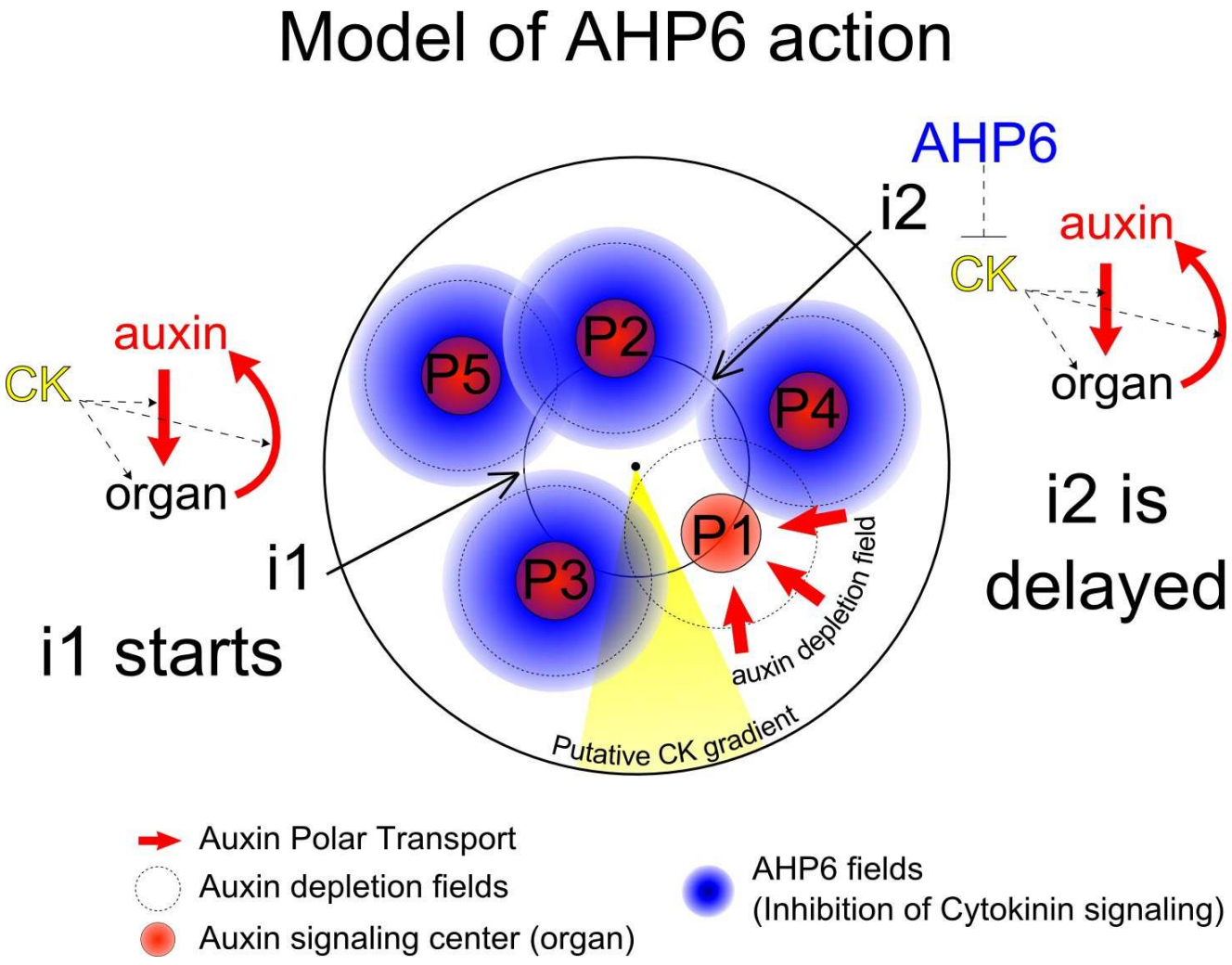

Figure S11. Model of the control of the organ initiation temporal sequence by AHP6 inhibitory fields at the shoot apical meristem. The shoot apical meristem has been schematically represented by the larger circle and the central circle represents the central zone. New initia arise just at the boundary of the central zone, where cytokinin signalling starts to decrease (yellow gradient). Organ initiation is triggered by an auxin signaling maxima (red disk). Their position is set by auxin depletion fields (dashed circles) created by dynamic auxin transport (red arrows). In older primordia, *AHP6* transcription is activated one plastochrone after activation of auxin signalling during organogenesis. The resulting pattern of AHP6 fields creates differential cytokinin signaling context in the peripheral zone: it inhibits CK signalling in the area of the presumptive I2 initium, thus delaying its initiation, but not in the area of I1.

II. Genetic Interactions of *AHP6* with the protein kinase PINOID, a regulator of polar auxin transport.

The occurrence of co-initiations of organs in the SAM of *Arabidopsis thaliana* raises the question of the coupling between space and time during organogenesis. In accordance with the model of Snow and Snow (M. Snow & R. Snow 1962; Douady & Couder 1996)and as proposed by Smith *et al*. (2006), Jönsson *et al.* (2006) and Barbier de Reuille *et al.* (2006), the spacing mechanism generated by auxin depletion fields alone should in theory be able to generate a regular plastochron as well. However, our data, presented in the previous chapter suggested that an additional mechanism based on cytokinin-signaling inhibitory fields of AHP6 is necessary to stabilize the plastochron. Interestingly, the radial positioning of organs is never affected in *ahp6* mutants, indicating that the defects observed in the timing of organ emergence do not perturb the site where organs are specified. Organ founder cells are specified by an accumulation of auxin resulting from dynamic polar transport, followed by rapid auxin signal transduction (Heisler et al. 2005). Thus one could hypothesize that neither auxin transport nor the first auxin signaling events in founder cell specification are affected by mis-regulation of cytokinin signaling in *ahp6* mutants. This seemed, however, contradictory to our data suggesting that cytokinin signaling triggers a positive feedback on auxin signaling in the peripheral zone of the SAM (see Chapter2, fig S10 and S11).

To resolve these discrepancies, we have begun to characterized genetic interactions between *ahp6* mutants and mutants affected in auxin transport. Although this work is still in progress, we have obtained preliminary results identifying particular relationship between *AHP6* and the protein kinase *PINOID* (*PID*) that regulates the polarity of PIN proteins by direct phosphorylation (Christensen et al. 2000; Friml et al. 2004; Michniewicz et al. 2007; Huang et al. 2010) (See also in Introduction). We will discuss here interesting hypotheses that can be formulated from these first results and we will propose further analyses.

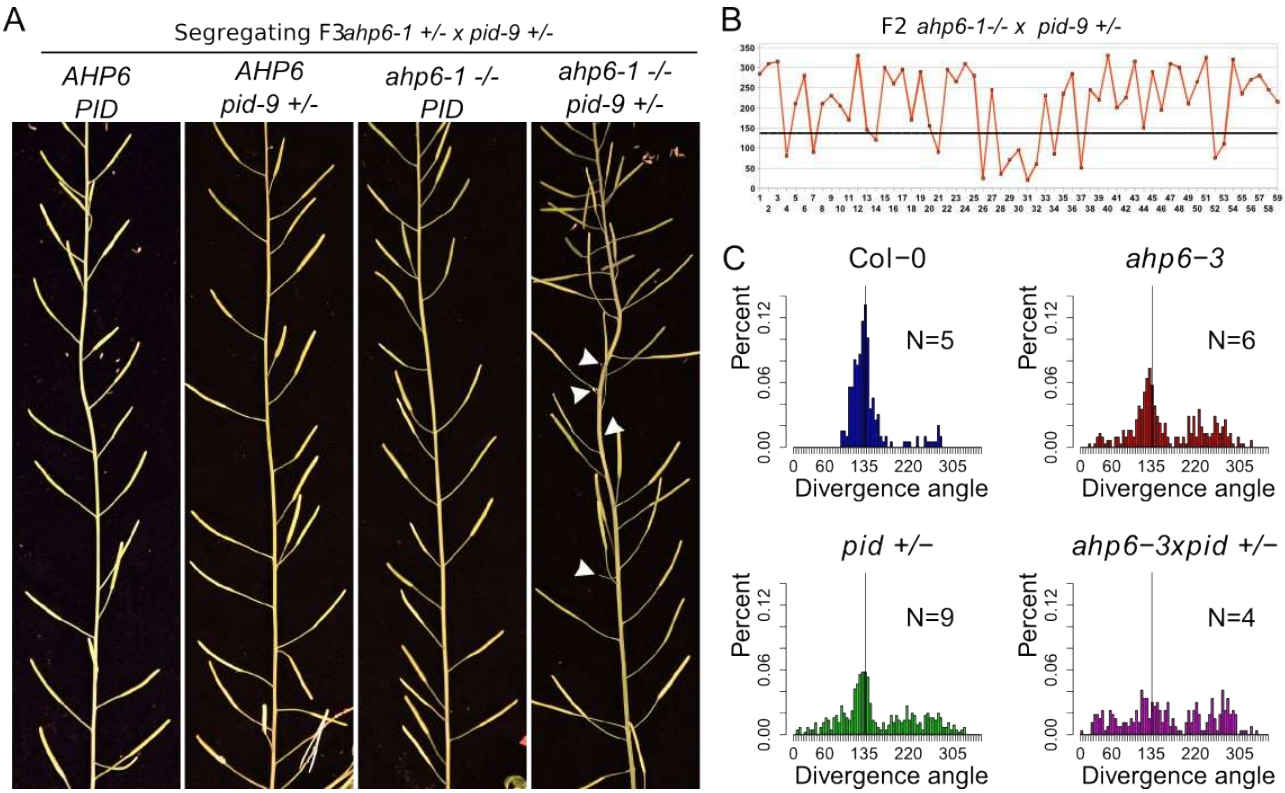

Figure 6: **Strong phyllotaxis defects of *ahp6 x pid-9 +/-* plants suggest a synergy between AHP6 fields and the dynamics of auxin transport in the control of phyllotaxis**. (**A**) Phyllotaxis in the progeny of a F3 *ahp6-1+/- x pid-9 +/-* line. Strong perturbations are seen in *ahp6-1 -/- x pid-9 +/-* plants. Arrows indicate aborted flowers (see figure 7).(**B**) A representative sequence of divergence angle measured in a *ahp6-1 x pid-9 +/-* mutant, showing strong perturbations. (**C**) Histograms of divergence angles measured in plants resulting from a cross between *ahp6-3* mutants and *pid-9* +/- plants. Genotypes and size of the sample (number of individuals) are given in each panel; the vertical bar indicates 137.5°, the canonical golden angle of Fibonacci spirals.

segregating F2 and F3 ahp6-1+/- x pid-9 +/- population				
	col-0	*pid-9 +/-*	*ahp6-1*	*ahp6-1 x pid-9 +/-*
mildly perturbed Phyllotaxis	5	8	5	2
Perturbed Phyllotaxis	0	4	3	15

Table 1: The progeny of a F2 or a F3 a*hp6-1 +/- x pid-9 +/-* line was divided in two classes of phyllotactic phenotype by a qualitative observation and the genotype of each plant was established. The penetrance of the phenotype was markedly enhanced in plants having a *ahp6-1 +/- x pid-9 +/-* genotype.

1. Results and discussion

1. Genetic interactions between *AHP6* and *PINOID* in the control of phyllotaxis.

ahp6 mutants were crossed with *pin1* and *pid* mutants, which are both impaired in polar auxin transport. *PIN1* and *PINOID* genes encode respectively a transmembrane auxin efflux transporter and a protein kinase that regulates PIN1 polar localization. Null mutants for those genes have a naked inflorescence resulting from loss of organ initiation (Okada et al. 1991; Christensen et al. 2000). This phenotype was unchanged in *ahp6-1 x pin1-6* and various allelic combination of *ahp6 x pid* double mutants. This indicates that *PIN1* and *PID* are epistatic on *AHP6*, in accordance with the fact that *AHP6* is activated downstream of organ initiation (chapter 2, part II). While no particular phenotype was noticed in *ahp6-1 -/- x pin1-6 +/-* plants, *ahp6-1-/- x pid-14+/-* plants had very strong destabilization of the phyllotaxis (figure 6). We observed that plants obtained from a cross between the Columbia (Col-0) and Wassilewskaya (WS) ecotypes had much more phyllotactic defects. To avoid problems due to ecotype interbreeding, we selected the *pid-9* allele in Col-0 (Christensen et al. 2000) and we systematically genotyped the progeny of plants with a*hp6-1 +/- x pid-9 +/-* and a*hp6-3 +/- x pid-9 +/-* genotypes, respectively. We confirmed a strong destabilization of phyllotactic sequences in *ahp6-/- x pid+/-* (table 1; figure 6A,B), which was markedly increased compared to individual *ahp6* sequences (see chapter 1, figure 1, 4; chapter2, figure 2). Besides, nearly all individuals of this genotype exhibited such strong perturbations, compared to the partial penetrance of *ahp6*. Interestingly, *pid-9 +/-* plants seem to have a perturbed phyllotaxis, in the same phenotypical range as *ahp6* mutants (figure 6C). Further quantifications and analyses are required to determine whether the strong destabilization observed in *ahp6 x pid+/-* plants is caused by a synergistic rather than an additive interaction. Moreover, perturbations observed in the divergence angle sequences of *ahp6 x pid+/-* plants are not very stereotypic which raises the possibility that other perturbations than permutations are present in these sequences. Following organ initiation by live-imaging in these plants will help determining whether the plastochron is affected, and also whether the divergence angle is modified.

The activity of PID in the SAM is thought to be crucial to control the polarity of PIN1 proteins (Friml et al. 2004), which can change rapidly during the self-reorganization of the pump network following organ initiation. A reversal of PIN1 polarity is for instance visible in the boundary of organs (Heisler et al. 2005). We suggest here that PID heterozygotes have a reduced dynamics of

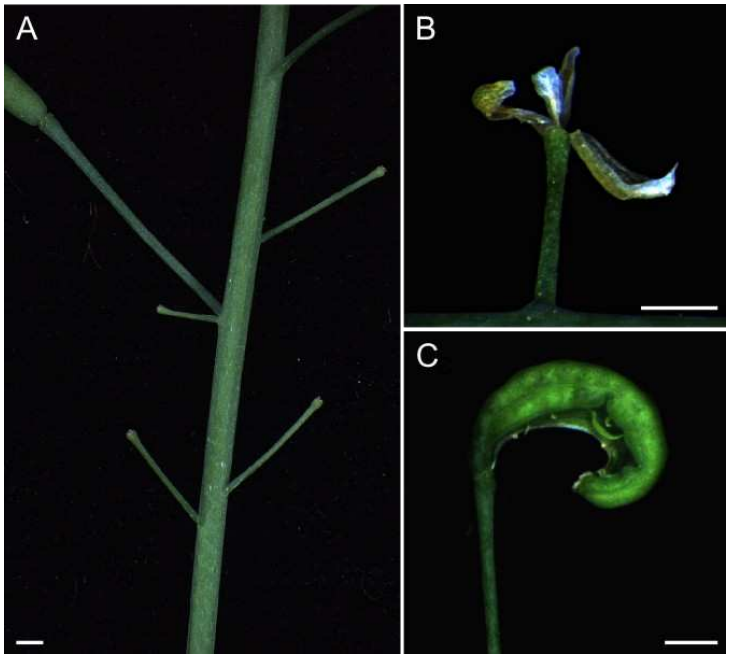

Figure 7: **Synergistic interaction of PINOID and AHP6 in floral and carpel development**. Pictures from *ahp6-1 -/- x pid-9 +/-* plants showing (**A**) multiple abortion of flowers on a stem (naked pedicels are still present) (**B**) detail of an aborted flowers with only 3 sepals, 1 petal and (**C**) a open ovary due to problem of carpel fusion. Scale bar = 1 mm.

PIN1 polarity establishment. This could account for the defect of phyllotaxis observed in *pid-9+/-* mutants. If these defects are characterized as permutations, this would suggest that an intact auxin import machinery would be required to set a regular plastochron. In other words, the auxin network could also possess its own mechanism regulating plastochron stability, apart from cytokinin signaling inhibitory fields. Moreover, if the strong phenotype of *ahp6-/- x pid+/-* is caused by concomittant initiations, the synergistic interaction between *AHP6* and *PID* would indicate a partial functional redundancy of auxin fields and AHP6 fields to control the regularity of the plastochron (Pérez-Pérez et al. 2009). Finally, if the divergence angle is also modified, this would indicate that in certain condition, the plastochron variability could be so important that organ positioning would no longer be stable.

2. Synergistic interaction of *PINOID* and *AHP6* in flower and carpel development.

In addition to the enhanced phyllotactic defects, *ahp6 x pid+/-* plants had many aborted flowers on the stem (figure 6A, 7A). Closer examinations revealed that these flowers produced a normal pedicel, but less sepals and petals than in wild-type flowers and no whorls of reproductive organs, indicating a premature termination of the flower meristem (figure 7A, B). In some flowers, problems in gynoecium development were observed, including abnormal carpel numbers (data not shown) or failure of carpel closure (figure 7C). In flowers, *AHP6* is expressed in sepals, petals and stamen initia and flowers of *ahp6* mutants have sometimes additional sepals and petals. PINOID is thought to ensure the same role in the floral meristem as in the shoot meristem. Thus, the unexpected phenotype of *ahp6 x pid+/-* flowers might reveal different roles of these genes in the floral meristem, such as a positive control on meristem maintenance. Moreover, these additional roles in the floral meristem could be explained by the existence of different crosstalk between auxin and cytokinin in comparison to the SAM and by the presence of additional regulators of the expression these two genes and of the activity of their proteins.

2. Materials and Methods

All the mutants used in this section and their references are described in the following table.

Culture conditions were the same as mentioned previously (chapter II, I.2).

Mutant	reference
ahp6-1	(Mähönen et al. 2006)
ahp6-3	(Mähönen et al. 2006)
pin1-6	(T Vernoux et al. 2000)
pid-14 (or pid-7.1.2.6)	(Furutani et al. 2004)
pid-9	(Christensen et al. 2000)

ahp6-1 allele, which contains a single substituion baise pair (C>T) was genotyped using a dCAPS (derived Cleaved Amplified Sequence Polymorphism, (Michaels & Amasino 1998)), with the primers indicated below. A DNA fragment of 185 pb was amplified by PCR, digested using PstI, loaded on a 3% agarose gel and separated by electrophoresis. *ahp6-1* fragments are not digested, while other alleles are digested, causing a down shift of ~20 pb. DNA from the *ahp6-3* allele was amplified by PCR using the LBb1a primer (SALK), matching the left border of the T-DNA (pROK2) insertion. *pid-9*+/- plants were genotyped by amplifying the resistance gene for the herbicide BASTA. *pid-14* allele was genotyped using a dCAPS (*pid-14* PCR fragments are digested by , and down shifted of ~20 pb compared to other alleles after electrophoresis run on a 3% agarose gel). *pin1-6* has been generated by T-DNA mutagenesis (T Vernoux et al. 2000). However, we found that the mutation was not caused by the T-DNA insertion, but by the insertion of a transposon in the coding sequence of *PIN1* (Chambrier P., unpublished results). We screened the presence of this insertion in genomic DNA with a triplex PCR, mixing in the reaction primers that match both wild-type sequence and transposon sequence, according the following proportions:

1µl ADN (30ng)
4µl tampon 5X
0.1µl GoTaq
0.2µl dNTP à 20mM each
1µl primer F1 (*PIN1*) from 10µM stock
0.3µl primer R1 (transposon) from 10µM stock
1µl primer R2 (*PIN1*) from 10µM stock
12.4µl H2O
20µl

allele	Primer	sequence	Tm
ahp6-1	F	5'-CGA GCA GTT CTT GCA GCT TCT G-3'	53°
	R	5'-CGT ATA CAT TTT GGA ACC AAA CAA C-3'	53°
ahp6-3	F (matching *AHP6* 5'UTR)	5'-AAGCAAGACCTGTTCACATTAG-3'	58°
	R (LBb1a)	5'-ATTTTGCCGATTTCGGAAC-3'	58°
pid-9 (BASTA gene)	F	5'-GCGGTCTGCACCATCGTCAACCACTACATC-3'	60°
	R	5'-ACGTCATGCCAGTTCCCGTGCTTGAA-3'	60°
pid-14 (7.1.2.6	F	5'-AAGAGACGGGTTGGTTCTAAAGTT-3'	60°
	R	5'-GACCTCTCTCTATGCTCCGACTCA-3'	60°
pin1-6	F	5'-CATGGCGTTAAACCCAAGAATAATAGCTT -3'	58°
	R1 (matching the transposon)	5'-TTAGCAGATTGTCGGTTTCAAGCCTC -3'	58°
	R2 (PIN1 stop)	5'-TCATAGACCCAAGAGAATGT-3'	58°

references – Chapter II, part II

Christensen, S.K. et al., 2000. Regulation of auxin response by the protein kinase PINOID. *Cell*, 100(4), p.469-478.

Douady, S. & Couder, Y., 1996. Phyllotaxis as a dynamical self organizing process .2. The spontaneous formation of a periodicity and the coexistence of spiral and whorled patterns. *JOURNAL OF THEORETICAL BIOLOGY*, 178(3), p.275-294.

Friml, J. et al., 2004. A PINOID-dependent binary switch in apical-basal PIN polar targeting directs auxin efflux. *Science (New York, N.Y.)*, 306(5697), p.862-865.

Furutani, M. et al., 2004. PIN-FORMED1 and PINOID regulate boundary formation and cotyledon development in Arabidopsis embryogenesis. *Development (Cambridge, England)*, 131(20), p.5021-5030.

Heisler, M.G. et al., 2005. Patterns of auxin transport and gene expression during primordium development revealed by live imaging of the Arabidopsis inflorescence meristem. *Current Biology: CB*, 15(21), p.1899-1911.

Huang, F. et al., 2010. Phosphorylation of conserved PIN motifs directs Arabidopsis PIN1 polarity and auxin transport. *The Plant Cell*, 22(4), p.1129-1142.

Jönsson, H. et al., 2006. An auxin-driven polarized transport model for phyllotaxis. *Proceedings of the National Academy of Sciences of the United States of America*, 103(5), p.1633-1638.

Michaels, S.D. & Amasino, R.M., 1998. A robust method for detecting single-nucleotide changes as polymorphic markers by PCR. *The Plant Journal: For Cell and Molecular Biology*, 14(3), p.381-385.

Michniewicz, M. et al., 2007. Antagonistic regulation of PIN phosphorylation by PP2A and PINOID directs auxin flux. *Cell*, 130(6), p.1044-1056.

Mähönen, A.P. et al., 2006. Cytokinin signaling and its inhibitor AHP6 regulate cell fate during vascular development. *Science (New York, N.Y.)*, 311(5757), p.94-98.

Okada, K. et al., 1991. Requirement of the Auxin Polar Transport System in Early Stages of Arabidopsis Floral Bud Formation. *The Plant Cell*, 3(7), p.677-684.

Pérez-Pérez, J.M., Candela, H. & Micol, J.L., 2009. Understanding synergy in genetic interactions. *Trends in Genetics*, 25(8), p.368-376.

de Reuille, P.B. et al., 2006. Computer simulations reveal properties of the cell-cell signaling network at the shoot apex in Arabidopsis. *Proceedings of the National Academy of Sciences of the United States of America*, 103(5), p.1627-1632.

Smith, R.S. et al., 2006. A plausible model of phyllotaxis. *Proceedings of the National Academy of Sciences of the United States of America*, 103(5), p.1301-1306.

Snow, M. & Snow, R., 1962. A THEORY OF REGULATION OF PHYLLOTAXIS BASED ON LUPINUS ALBUS. *PHILOSOPHICAL TRANSACTIONS OF THE ROYAL SOCIETY OF LONDON SERIES*, 244(717), p.483-&.

Vernoux, T et al., 2000. PIN-FORMED 1 regulates cell fate at the periphery of the shoot apical meristem. *Development (Cambridge, England)*, 127(23), p.5157-5165.

Chapter 3

Modeling noise and robustness in phyllotactic systems

I. Introduction

In the two previous chapters, we identified and characterized a frequent perturbation in the Fibonacci spiral of *Arabidopsis thaliana*: the occurrence of simultaneous initiations of two to three organs in the meristem, which likely cause the permutation of their order of insertion along the stem. In our culture conditions, up to 25% of organs can be co-initiated in the wild-type *Columbia* background (chapter 2, figure 3). Interestingly, we found that the plastochron could be even more irregular in the absence of the cytokinin signaling inhibitor AHP6. Our data suggest that this small protein establishes fields whose patterns imposes a delay to the development of the younger initia of a co-initiated pair or triplet of organs, thus stabilizing *a posteriori* the pace of the plastochron (chapter 2, figure S12).

These findings raise many questions. Firstly, we have not identified the origin of the plastochron irregularity: since this defect is also significantly present in the wild-type, *AHP6* loss would not be the primary cause, but would only reveal the extent of the perturbations when this correcting mechanism is absent. Secondly, it was necessary to clarify why the plastochron irregularities we observed do not perturb the radial pattern of organ positioning and thus, how space and time are coupled in phyllotacic systems. Thirdly, the plausibility of the proposed correcting mechanism for AHP6 needed to be tested. As phyllotaxis is a complex system involving the interactions of different organs, the emerging pattern is not intuitive and simple assumptions can surprisingly lead to unexpected results.

In parallel to our biological experiments, we thus developed in collaboration with modelers from our Department a complementary heuristic approach based on abstract models of phyllotaxis. We chose to use a dynamical system model based on inhibitory fields, because these models have been shown to reproduce many properties of phyllotactic systems. Besides, they enable to test different hypotheses and to explore a wide range of parameters.

Inspired by the biological results and the literature, we first tested possible origins for co-initiation: we investigated the role of noise on different parameters and we also explored the influence of continuous variations of parameters imposed by the developmental evolution of plants. Since we obtained different classes of defects, notably plastochron irregularity, we could test in a second step various hypotheses for a correcting mechanism based on inhibitory fields produced by organs. We identified a set of requirements that we could compare to the characteristics of observed AHP6 fields. This study also indicate interesting predictions that will orient our future biological

experiments. Beyond the scope of AHP6, our study highlights the variable robustness of phyllotaxis in space and time. It also gives an insight on possible effects of noise on regular developmental patterns and on the mechanisms that can exist to buffer the natural stochasticity.

II. Noise and robustness in phyllotaxis

This article is the version of an article submitted in august2011 to Proceedings of the National Academy of Sciences of the United States of America.

The authors of this work are:

Vincent Mirabet[1], Fabrice Besnard[2], Teva Vernoux[1] and Arezki Boudaoud[21]

[1] Laboratoire Joliot-Curie, CNRS, ENS, Université de Lyon, 46 Allée d'Italie, F-69364 Lyon Cedex 07, France

[2] Laboratoire de Reproduction et Développement des Plantes, CNRS, INRA, ENS Lyon, UCBL, Université de Lyon, 46 Allée d'Italie, 69364 Lyon Cedex 07, France.Virtual Plants INRIA Project Team, UMR DAP, INRIA/CIRAD, Montpellier, France.

Author contributions:

F.B., A. B., V.M. and T.V. designed the project. A. B. and V.M designed the model and V. M. performed the simulations and the exploration of the model. A.B. and V.M. wrote wrote the manuscript with input from the other authors.

ABSTRACT

A striking feature of vascular plants is the regular arrangement of lateral organs on the stem, known as phyllotaxis. Common phyllotactic patterns can be described using spirals, numbers from the Fibonacci sequence and the golden angle. This rich mathematical structure, along with the experimental reproduction of phyllotactic spirals in physical systems, has led to a view of phyllotaxis focusing on regularity. This raises questions about the effect on phyllotaxis of the natural, stochastic variability of organisms as well as about how stochasticity might be regulated. Here we address these questions theoretically using a dynamical system of interacting sources of inhibitory field. Previous work has shown that phyllotaxis can emerge deterministically from the self-organization of such sources and that inhibition is primarily mediated by the depletion of the plant hormone auxin through polarized transport. We incorporated stochasticity in the theoretical model and found three main classes of defects in spiral phyllotaxis — the reversal of the handedness of spirals, the concomitant initiation of organs and the occurrence of distichous angles — and we investigated whether a secondary inhibitory field filters out defects. Our results are consistent with available experimental data, predict the main source of stochasticity during organogenesis and provide a framework for the analysis of phyllotactic mutants. We propose that secondary fields associated with organ initiation, such as other biochemical signals or mechanical forces, are important for the robustness of phyllotaxis. More generally, our work sheds light on how a target pattern can be achieved within a noisy background.

shoot apical meristem — plant development — stochastic dynamical systems — pattern formation — Fibonacci patterns

1. Introduction

Lateral organs (leaves and flowers) are initiated as primordia near the shoot apex yielding a regular arrangement on the stem known as phyllotaxis. Two main phyllotactic patterns are observed : whorled — many primordia emerge simultaneously, and spiraled — a single primordium is initiated at a time. Spiral phyllotaxis features two sets of conspicuous spirals (the parastichies) rotating either clockwise or anti-clockwise, so that the numbers of spirals in each set are often two consecutive numbers of the Fibonacci sequence (1, 1, 2, 3, 5, 8, 13…) ; moreover, the angle (viewed from the apex) between two consecutive organs, known as the divergence angle, is often strikingly close to the golden angle, which is about 137.5°. This mathematical beauty has attracted a stream of mathematicians, computer scientists and physicists along with botanists and plant biologists, see for instance (Jean 1994; Adler et al. 1997; Cris Kuhlemeier 2007) for reviews. A number of mathematical models enabled the prediction of spiral phyllotaxis from the interactions between primordia : physical interactions included optimal packing, e.g. (Levitov 1991) and mechanical forces, e.g. (Green et al. 1996; Shipman & Newell 2005), while biochemical interactions included a reaction-diffusion Turing-like spacing mechanism (Turing 1952; Bernasconi G.P. 1994; Meinhardt 2004) or the production of an inhibitor by each primordium preventing initiation in its vicinity (Veen & Lindenmayer 1977; Mitchison 1977). In all these studies, phyllotactic spirals emerged from the self-organization of interacting primordia, as also shown by more abstract dynamical models (Douady & Y Couder 1992; 1996a; 1996b; 1996c; Atela et al. 2002; Hotton et al. 2006; R. Smith, C Kuhlemeier, et al. 2006). The concept of self-organization was also supported by the observation of phyllotactic-like spirals in physical experiments with ferromagnetic droplets (Douady & Y Couder 1992), self-assembled solidified microstructures (Li et al. 2005), rotating magnets (Nisoli et al. 2009), or bubbles floating on a surface (Yoshikawa et al. 2010). Therefore, careful biological experiments were needed for the identification of the primary mechanism of phyllotaxis (D Reinhardt et al. 2000; Didier Reinhardt et al. 2003; Heisler et al. 2005): the accumulation of the plant hormone auxin in incipient primordia (initium) through a self-enhancing polar transport, so that auxin depletion plays the role of an inhibitory field. This was further supported by the simulation of cell-based models (R. S. Smith, Guyomarc'h, et al. 2006; Jönsson et al. 2006; de Reuille et al. 2006; Stoma et al. 2008; Sahlin et al. 2009) in which phyllotaxis emerges from cell-cell interactions.

Altogether, this body of work is underpinned by an ideal, deterministic view of phyllotaxis, in which regular patterns can be reproduced by theoretical models. Nevertheless, living organisms are

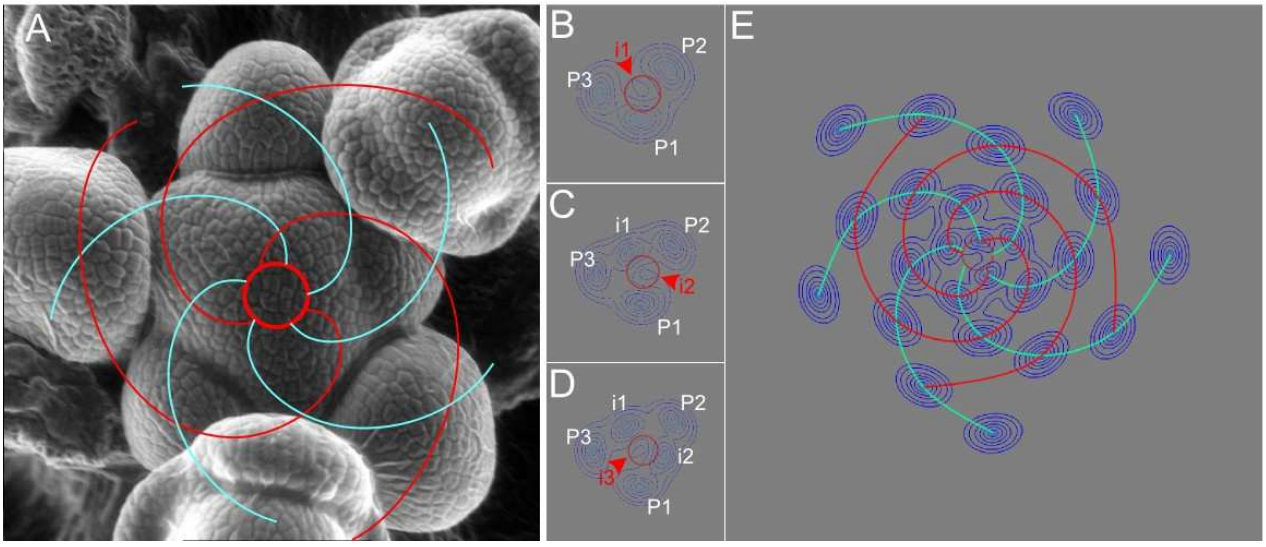

Figure 1: **Phyllotaxis, from observations to an abstract model**.(**A**) Scanning electron microscopy picture of the apex of an inflorescence stem of Arabidopsis thaliana (ecotype Columbia-0) showing the contact spirals (parastichies); the numbers (3 in red and 5 in turquoise) of spirals with a given handedness are two consecutive numbers from the Fibonacci sequence. (**B-D**) A simulation sequence. Organ primordia (P, numbered from the youngest P1 to the oldest P3) are sources of an inhibitory field (of which the contour lines are shown); primordia are formed as initium (i1, i2 and i3 in the sequence of apparition) on a competent circle (in red) and, because of growth, move away radially; a new initium is formed when and where inhibition falls beyond a threshold. (**E**) Example of a resulting pattern after 26 primordia have formed (the red circle has the same size as in **B-D**)

variable and observations indicate that phyllotaxis is also variable (Jean 1994), that permutations between organs can occur (Y Couder 1998), while divergence angles appear variable in Arabidopsis thaliana (Peaucelle et al. 2007; Ragni et al. 2008; Prasad et al. 2011), and almost random in mutants of Arabidopsis (Peaucelle et al. 2007; Prasad et al. 2011) or of rice (Itoh et al. 2000; Jeune & Barabe 2004). In addition, auxin cell-based models of phyllotaxis are liable to show a noisy output (R. S. Smith, Guyomarc'h, et al. 2006; Jönsson et al. 2006). More generally, the importance given to stochastic variability in organismal development is growing (Oates 2011; Lander 2011). In plants, stochasticity can be either reflected in development, as in the variability of cell size in the epidermis of sepals (Roeder et al. 2010), or filtered out, as in the robust establishment of the identity of floral organs (Alvarez-Buylla et al. 2008). This raises the question of the effects of stochasticity on phyllotaxis. In order to address this question, we incorporated stochasticity in the dynamical system introduced by Douady and Couder (1996b), which implements the rules deduced by Snow and Snow from their surgical experiments (M. Snow & R. Snow 1932; 1933; 1962). Such a stochastic model was also alluded to in (R. Smith, C Kuhlemeier, et al. 2006), but no systematic study was performed. We chose this abstract model as it combines the recapitulation of most known phyllotactic modes while being simple enough to enable a comprehensive exploration of the space of parameters (Chickarmane et al. 2010). Doing so, we found that stochasticity yields stereotypical alterations of the phyllotactic pattern, which depend on the source of randomness. Finally, inspired by work on noise in the primary patterning of the fruit fly embryo (Gregor et al. 2007; Erdmann et al. 2009; Morishita & Iwasa 2009; Okabe-Oho et al. 2009), we investigated whether a secondary inhibitory field could modulate the number of phyllotactic alterations.

2. Results

2.1. The role of noise

We started from the dynamical system introduced in (Douady & Y Couder 1996b) which implements the rules stated by Snow and Snow (1962), and we incorporated two different sources of noise in this dynamical system. The main hypotheses of the deterministic model are as follows (see Materials and Methods for details). (i) The average stem apex has an axisymmetric shape. (ii) Organ primordia are formed at the periphery of the apex, on a competent circle of radius R (termed CZ for Central Zone), and, because of growth, they move away with a radial velocity V, which we

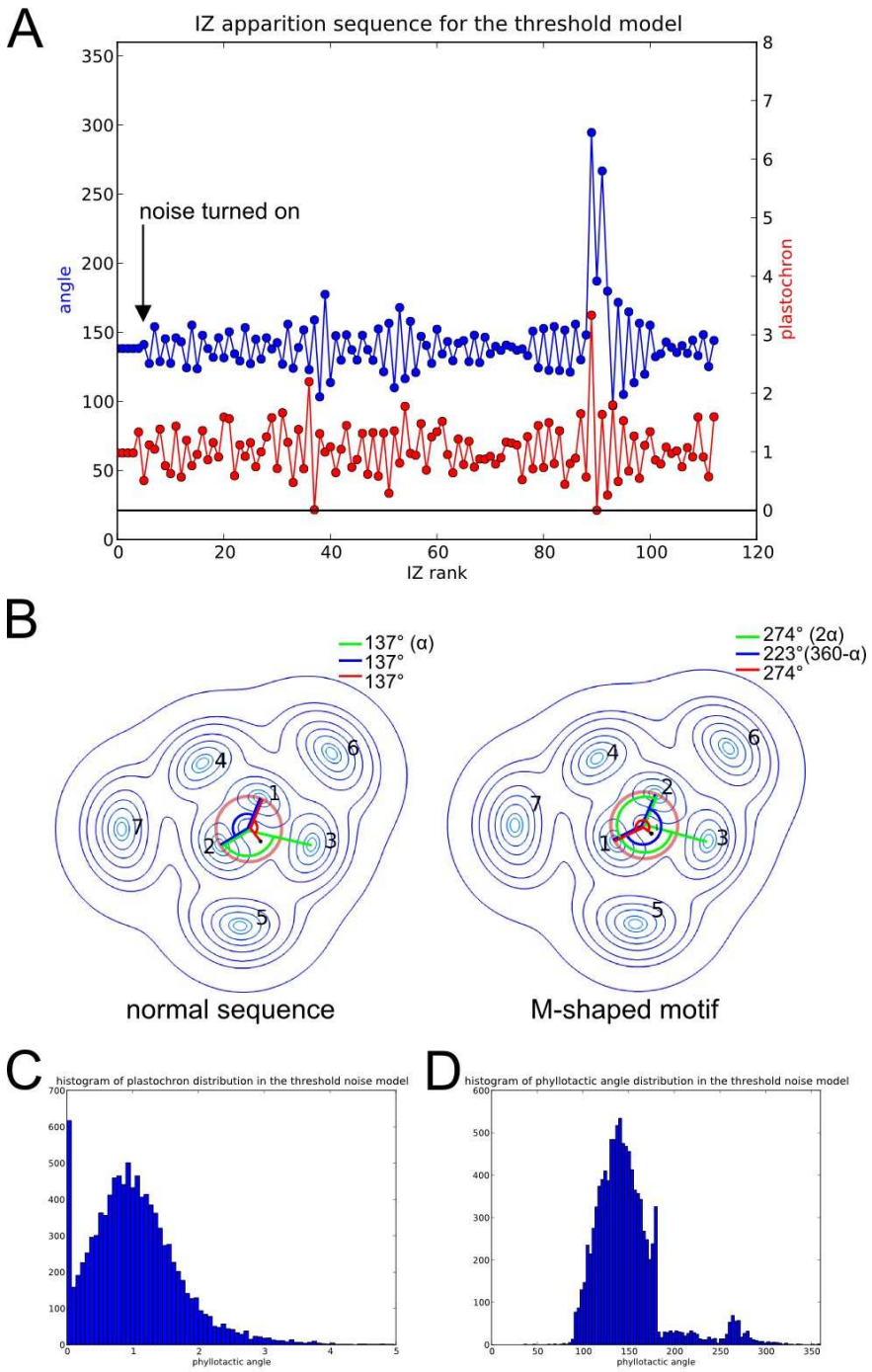

Figure 2: **The model with noise on the threshold for organ initiation.** (**A**) A typical sequence of angles and plastochrons (time delay between consecutive initiations); the simulation is started with no noise; M-shaped angle sequences correspond to concomitant inititations (vanishing plastochron). (**B**) Schematic explaining the origin of M-shaped sequences (same representation as in Fig. 1B-E). A vanishing plastochron implies two equivalent initia, which are ranked at random. This either yields a sequence of divergence angles close to the golden angle (left panel) or a M-shaped sequence of the type (α; 2α; 360-α ; 2α; α). (**C**) Histograms of plastochrons showing a peak at zero corresponding to concomitant initiations. (**D**) Histogram of divergence angles (N ~15000 angles) showing a peak close to the golden angle ~137°, and smaller peaks close to 180° (transient distichous phyllotaxis) and 274° (reflecting M-shaped sequences). *(Please refer later to the published version of this article for precise indication of simulation parameters)*

assume here to be constant. (iii) Each primordium is a source of inhibition (termed IZ, for Inhibition Zone) over a region of diameter *d* and the steepness of gradient of inhibition is also a parameter of the model. (iv) A new primordium (initium) is initiated on the competent circle at the location and at the time such that the sum of the inhibitory fields generated by all previous primordia gets below a threshold *E*. (v) The apex has the shape of a cone and distances are computed on the cone. The angle of the cone was chosen according to the shape of *Arabidopsis thaliana* apex.

A typical simulated sequence is shown in Fig. 1B-D: the inhibition field generated by older primordia in the competent circle decreases as primordia move away, an initium is formed at the place and and the time such that inhibition falls below the threshold. This process is repeated leading to a periodic initiation and the spatial establishment of a spiral phyllotactic pattern. The main control parameter of this model is the ratio of the range of inhibition *d* to the radius of the competent circle *R*. As this ratio is decreased, the phyllotactic mode undergoes a transition from distichous (divergence angles of 180°) to spiral (and also whorled) phyllotaxis of higher and higher order. We note that the model implements local inhibitory interactions between primordia, as an abstract representation of auxin-based biological mechanisms at play. Neither the periodicity nor the spatiality of initiation are prescribed; they emerge from the self-organization of the system instead.

a) Threshold noise

Organs are initiated when the inhibitory field falls below the threshold *E*. The cellular response to this field can be variable which is equivalent to this threshold being variable. Therefore we first assumed that, before each initiation, the threshold is defined randomly according to a Gaussian distribution. Noise intensity then corresponds to the ratio between the width of the Gaussian (noted σ_E) and its mean. In order to ensure a well-defined underlying phyllotactic pattern, simulations are started with no noise until convergence to left-handed spiral phyllotaxis (parastichies 3,5), and noise is then turned on.

Typical angle and time delay sequences are shown in Fig. 2A. The effect on plastochrons, i.e., the time delay between two initiations events, is striking: fluctuations are large and the plastochron even vanishes, corresponding to the concomitant initiation of two, and, more rarely, three organs (Fig. 2A). Accordingly, the histogram of plastochrons also has a maximum at zero delay (Fig. 2C, see also Fig S1).

This raises an issue about organ sorting and more precisely about defining which of the concomitantly initiated organs is the older so as to compute the divergence angle. In view of the

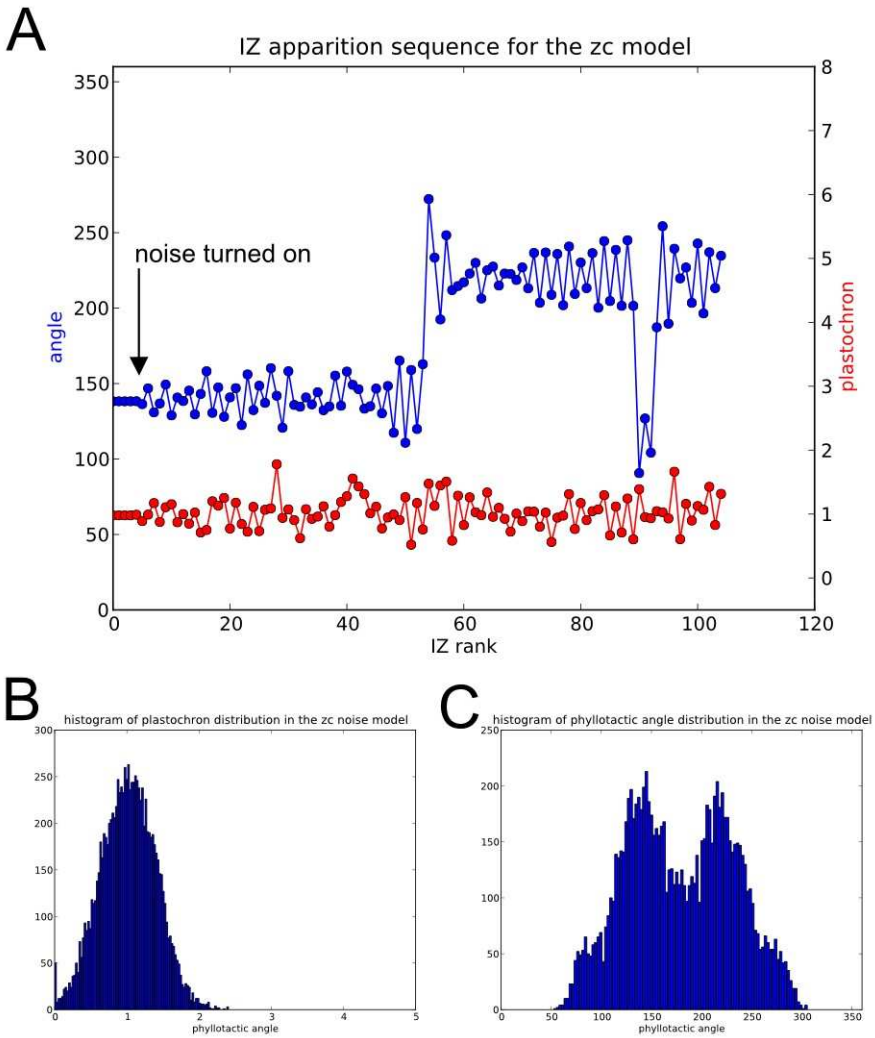

Figure 3: **The model with noise on the size of the competent circle.** (**A**) A typical sequence of angles and plastochrons; the simulation is started with no noise; a handedness reversal is clearly visible. (**B**) Histograms of plastochrons. (**C**) Histogram of divergence angles (N ~15000 angles) showing peaks corresponding to either handedness: α=137 and α=274. Simulation parameters, see Mirabet V. *et al*, in prep.

equivalence between these organs, we pick their order at random. The sequence of divergence angles shows fluctuations around the golden angle (Fig. 2A, D). The concomitant initiation of two organs corresponds to characteristic M-shaped patterns, i.e., sequences close to (α, 2α ,360−α, 2α ,α), where α is the golden angle (Fig 2B, C). Consequently, the histogram of angles has a high peak close to α and smaller peaks close to 2α and 360−α (Fig 2D). It is noteworthy that these M shaped sequences were observed on sunflower (Y Couder 1998), reflecting a permutation of the order of organs with respect to a regular sequence. Consequently, the simple addition of noise in the model can reproduce observed alterations. Another visible alteration is a number of divergence angles close to 180 degrees, corresponding to a transient distichous phyllotaxis. This alteration was recently observed in the *plt3 plt5 plt7* multiple mutant of *Arabidopsis* (Prasad et al. 2011).

We then investigated more systematically the space of parameters (also see Supplementary Figure S1-S3). The main variations in behavior arise when noise is increased (Fig. 4A-E, FigS1). Low noise only adds a small variability to angles and to plastochrons (Fig 4A, B, respectively and see also Fig S1). Concomitant initiations and transient distichous phyllotaxis appear for a noise strength of about 20%, and increase gradually above (fig 4 C, D). It has been shown that the parameter Γ, which is the ratio of inhibition range (IZ) to the competent circle size (CZ), is the most important parameter controlling the type of phyllotactic pattern generated by the system (Douady & Y Couder 1996b). Changing this parameter only affects the proportion of concomitant initiations and transient distichous phyllotaxis (Fig S2, A-B and S3, A-B). Obtaining the same results for other model parameters (data not shown), we conclude that these two alterations are the main components of the effect of threshold noise.

b) Size noise

A second source of stochasticity variability is the activity of apex, which could be reflected either in the size of the competent circle or in the range of inhibition. As only the ratio of these two lengths is important, we chose to model a noise in the size of the competent circle: following each inititiation, the radius is redefined randomly following a Gaussian distribution. Accordingly, noise intensity is quantified as the ratio of the width of this distribution (σ_R) to the radius of the competent circle.

Typical sequences of divergence angles and plastochrons are shown in Fig. 3A. M-shaped angle sequences are associated with vanishing plastochron, while a few angles also occur indicating a transient distichous mode. In contrast with the threshold noise (Fig. 2A), an important observation

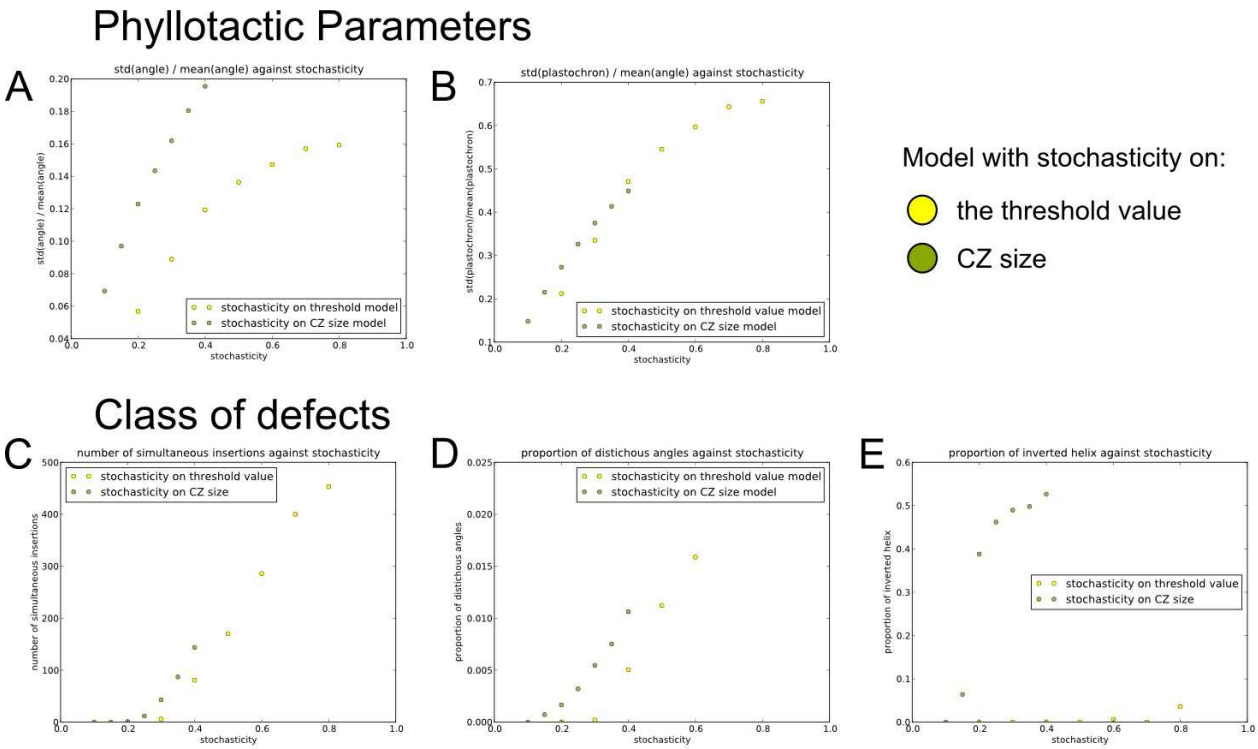

Figure 4: **Alterations as a function of noise strength**, σ_E/E or σ_R/R according to the type of noise. (**A**) Standard deviation of angle normalized by the average angle. (**B**) Standard deviation of plastochron normalized by average plastochron. (**C**) The proportion of concomitant initiations. (**D**) Proportion of distichous angles. (**E**) Proportion of handedness reversals.

is that the handedness of the spiral is occasionally reversed. This is reflected by a relatively high peak in the histogram of angles around the opposite of the golden angle, i.e., 360−α=223° (Fig 3C). We then investigated systematically the effect of increasing noise intensity on observed patterns (Fig 4). At low intensity, divergence angles and plastochrons have a small variability (Fig. 4A, B, respectively; see also Fig S1). At about 10%, transient distichous patterns and handedness reversals appear (Fig. 4 C, E, respectively) and their number increase with noise (FigS1 C, D). Concomitant initiations occur above about 25% (Fig 4D). Again, changes in model parameters such as Γ only affect the proportion of these defects (Fig S2 and S3). Overall, size noise yield a third type of alterations, handedness reversal; concomitant initiations and distichous angles also occur, but less frequently. Spiral reversals have been obtained following laser ablation on tomato meristems (Didier Reinhardt et al. 2005), but apparently, they have not been observed in naturally grown plants. We thus propose that the noise on threshold is more realistic (but see Discussion). In particular threshold noise reproduces the M-shaped sequences of angles that were observed on sunflower (Y Couder 1998). In the following, we will assume that it is the main source in the system.

2.2. Correcting noise

Available experimental data demonstrate that some mutations make phyllotaxis more irregular than in wild type plants, e.g. (Itoh et al. 2000; Peaucelle et al. 2007; Prasad et al. 2011; Ragni et al. 2008; Müller et al. 2006). This suggests the existence of processes regulating noise in phyllotaxis: either indirectly through e.g. changes in the radius of the competent zone and the range of inhibition between primordia, or directly by playing on the level of noise and its interpretation. In the first case, differences between mutant and wild type would be explained within the framework developed above. However, previous work in development suggests that it is often more efficient to control noise by adding appropriate feedbacks or additional modules to filter noise (Lander 2011). In this framework, we sought to propose mechanisms that could regulate noise in phyllotaxis, by adding another layer of control to the model discussed above.

a) Possible scenarios

We categorized the level of controls into three classes. (i) Before initiation. (ii) During initiation. (iii) Post-initiation. In the first class, the outcome would be a reduction in the level of noise introduced in the dynamical. Auxin signalling could play such a role by filtering fluctuations

(Vernoux et al. 2011). In the present framework, this trivially amounts to changing noise strength. In the second and third class, a primordium cannot 'know by itself' whether it emerged at the 'correct' time and position, because this information is relative to the other primordia. In other words, mechanisms of the last two classes cannot be primordia-autonomous. In a different context, studies on the primary patterning of the fruitfly (Gregor et al. 2007; Okabe-Oho et al. 2009; Erdmann et al. 2009; Morishita & Iwasa 2009) also proposed that a second field (a second transcription factor) plays a role in noise regulation, but this work cannot readily be transposed to phyllotaxis. In plants, observations indicate that, in addition to auxin, hormones such as cytokinins (Giulini et al. 2004) or gibberellins (Maksymowych & Erickson 1977), as well as mechanical forces (Hamant et al. 2008) have an impact on phyllotaxis. It has even been proposed that that mechanics cooperates with auxin (Newell et al. 2008; Heisler et al. 2010). Therefore, the existence of secondary fields playing a role in phyllotaxis is not unrealistic.

As auxin is the primary patterning field in phyllotaxis, it seems unlikely that a secondary field acts at the same level as auxin (second class). We nevertheless investigated this possibility by defining a second inhibitory field having similar properties to the first, but with different parameters (range and amplitude). Organs were initiated whenever the sum of the two inhibitions fell below a threshold. To our surprise, we found that, even in the absence of noise source, this resulted either in a chaotic-like phyllotaxis or in regular patterns that have never been observed in nature (data not shown, see later Mirabet V., *et al*, in prep.). We could rationalize the occurrence of chaotic-like phyylotaxis as follows: each field favors one phyllotactic mode with a given organ spacing and if these two fields differ then the two spacings are in general incommensurate and the situation is akin to the impossible matching of two crystals with different spatial periodicities. Therefore, we discarded the second class.

b) Post-initiation noise correction

We then turned to the third class, where noise correction must act on an intrinsic property of a primordium after it has been intiated. In our framework, each primoridium is endowed with a spatial position and an age (the time since its initiation). Modifying the position would not have any effect on M-shaped patterns as primordia are ranked according to age. Hence we focused on a model where the physiological age is changed post-initiation according to the age of closer primordia (Initia are formed according to the dynamical system with threshold noise.) More precisely, we considered a secondary field of range , assumed to be steep so that it is either 1 within

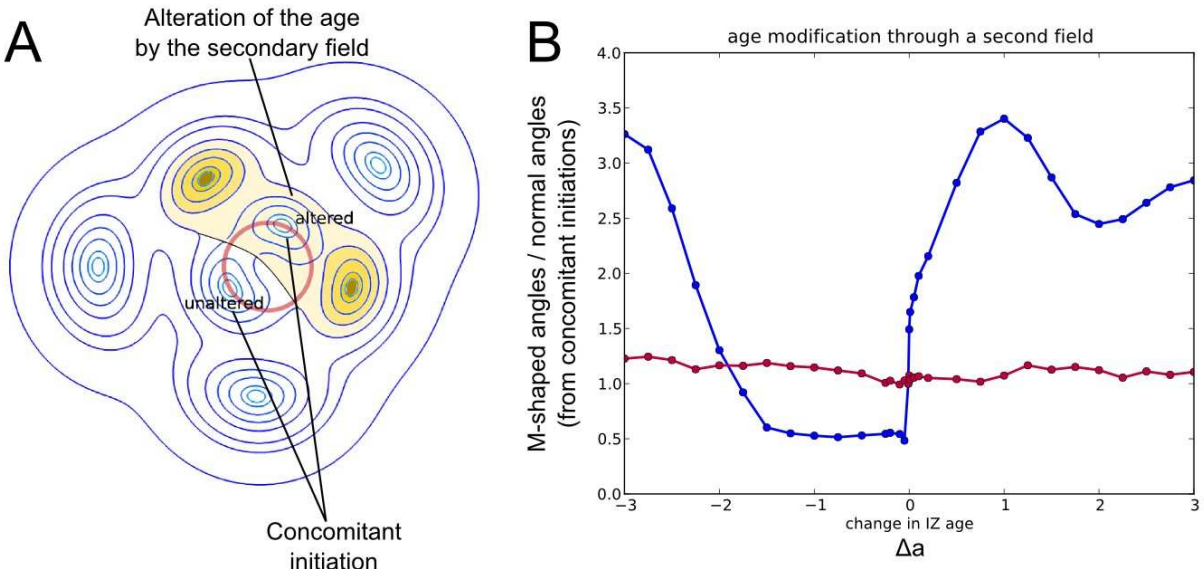

Figure 5: **Noise correction by a secondary field**. (**A**) After a time T2 following initiation, each organ generates a secondary field of range d2 (colored). When formed, an initium may be influenced by the secondary field. If so, its age is shifted by an amount Δa. This results in a differential age shift between initia appearing concomitantly. (**B**) Relative variation in the number of M-shaped motifs resulting from concomitant initiations as a function of the age shift Δa. Two sets of parameters for the secondary fields are shown: T2=3 and d2 =1 (red), or T2 =1 and d2 =1.3 (blue). While the first set does not enable the secondary field to modify the number of M-shaped motifs, the second set allows the secondary fields to lower the number of M-shaped motif for a wide range of Δa values.

its range and 0 beyond (see Materials and methods), and turned on as a source from each primordium with a time delay T2 after its initiation. We took the simpler form of action on an initium: if the secondary field is non zero at the point of initiation, then the physiological age is incremented with a value Δa, which can be either positive or negative, making this primordium 'older' or 'younger' respectively.

The sequences and histograms were similar to the threshold noise model with no secondary field. However the proportion of alterations differed. We investigated quantitatively the parameter space (see Supplementary Figure 4) and found that the secondary field has an effect when its range d2 is close to the primary range *d* but larger and when the delay is close to the average plastochron. Figure 5B shows the proportion of M-shaped patterns as a function of the increment in age Δa. The number of alterations is decreased if $\Delta a<0$, i.e. if the initium is made 'younger' when it feels the secondary field. For a wide range of values of the shift in age, the number of M-shaped sequences is decreased by a factor of 2. Consequently, a secondary field playing on the differential between organs can improve the regularity of a noisy phyllotactic model.

3. Discussion

We investigated the impact of noise on phyllotaxis starting from a deterministic model whereby primordia are sources of an inhibitory field (Douady & Y Couder 1996b), which can be viewed as an abstract representation of the underlying auxin-based dynamics. Initia are formed on a competent circle when the sum of inhibitory fields falls below a given threshold and then the primordia move away due to growth. In this model, the temporality and spatiality of organ initiation and positioning emerge from the self-organization of the system. This model reproduced most known types of phyllotaxis (Douady & Y Couder 1996b; 1996c)and we used it in the range of parameters roughly corresponding to the spiral phyllotaxis observed in *Arabidopsis*, the main parameter being the ratio of the range of inhibition to the radius of competent circle (Γ).

Most previous research on phyllotaxis focused on its mathematical regularity, and most studies on the variability of phyllotaxis dealt with the quantification of the relative frequencies between various patterns across different species e.g. (Jean 1994; Meicenheimer 1998)or within a same species, e.g. in sunflower (Weisse 1894; Schoute 1938; Y Couder 1998). However, from a developmental point of view, many observations indicate a variability in phyllotactic patterns within a same plant, notably in various mutant plants (Y Couder 1998; Peaucelle et al. 2007; Ragni et al.

2008; Itoh et al. 2000; Prasad et al. 2011). In these plants, a higher stochasticity of the developmental parameters controlling phyllotaxis could account for transient or more sustained deviations of the phyllotaxis from the expected regular pattern. Indeed, different sources of stochastic variability can be envisaged, and four of them are discussed hereafter. (i) The discrete nature of the cellular template makes the positioning of an initium according to a given divergence angle only achievable within the precision of a cell radius, as observed in cell-based simulations of auxin transport (R. S. Smith, Guyomarc'h, et al. 2006; Jönsson et al. 2006; Stoma et al. 2008). The amplitude of the corresponding noise is however generally expected to be small : in the small *Arabidopsis* cell radius is about 5% of the radius of the competent circle. We did not consider this type of noise because its amplitude is too small to induce the type of alterations presented above. (ii) The level of inhibition can be noisy as recent work suggests that auxin fluctuates in the shoot apex (Vernoux et al. 2011).(iii) The sensitivity of cells to the signal can be noisy as cellular response can be variable (Oates 2011; Lander 2011). We integrated these last two sources in a noise on the threshold for initiation. (iv) The activity of the apex can be noisy, which would have an impact on the effective radius of the generating circle and/or the range of inhibition. As only the ratio, Γ, of these two lengths is important, we modeled a noise on the size of the generating circle.

We simulated two sources of noise, on the threshold for initiation threshold and on the size of the generating circle. We found that noise leads to stereotypical alterations: (i) fluctuations of the divergence angles and plastochrons around their deterministic values; (ii) transient distichous pattern with angles of 180°; (iii) concomitant initiations corresponding to M-shaped sequences of angles; and (iv) reversal of the handedness of the phyllotactic pattern. These last three types of alterations correspond to an exploration of phyllotactic modes that are neighbors to the spiral mode: distichous for (ii); whorls for (iii); and the spiral with the other handedness for (iv). The proportion of the different alterations varies with the source of noise and its strength. M-shaped sequences are visible in sunflower (Y Couder 1998), angles of 180° occur in a mutant of *Arabidopsis (Prasad et al. 2011)*, while it seems that reversals are not observed in nature. (A caveat is that long sequences of angles might be required to make sure that a reversal has occurred.) A possible explanation for a smaller importance of size noise is that the radius of the competent circle (or the range of inhibition) is determined by the behavior of all cells in the apex (respectively the primordium) which leads to some averaging of cellular noise, while the noise on threshold is a local property defined by the behavior of the few cells that define an initium. Consequently, we favor the noise on threshold as the main source of stochasticity in the shoot apex.

It has been previously argued (Douady & Y Couder 1996a; 1996c; Y Couder 1998) that M-shaped sequences can arise due to a continuous decrease in time of the parameter Γ. This decrease would for instance correspond to the transition from the small vegetative apex to the larger reproductive apex. As it appeared that our simulations were highly sensitive to numerical precision, we re-examined these early conclusions (see Supplementary Figure S5). We found M-patterns to occur only for fast drops in Γ such that the number of parastichies changes within a plastochron ; these variations of Γ are within the range of noise investigated above. When we reduced the numerical precision, which is somehow equivalent to adding noise in the system, M-shaped patterns occurred more frequently (for the higher order parastichies). We therefore concluded that the phyllotactic system is more sensitive to noise when Γ varies in time. This might add another layer of complexity in the interpretation of phyllotactic observations.

We then investigated how the noise on threshold might be corrected. A pre-filter corresponds simply to a modulation of the level of noise. Other filters require the propagation of information from older primordia to an initium or to a primordium. Such a transfer of information might be provided by other hormones (Maksymowych & Erickson 1977; Giulini et al. 2004)or by mechanical signals (Hamant et al. 2008). Therefore we sought whether a secondary field can reduce alterations: a field acting on the same level as the primary field seems unlikely; a field acting post-initiation should play on the age of primordia. We assumed that each primordium that is old enough is a source of the secondary field and that initia sensing this field have their physiological age shifted. This shift may reflect a slowing down or an acceleration of the initiation of primordia or of the emergence of organs. If the shift is negative (primordia slowed down), then the number of M-shaped sequences of angles is largely reduced. Our secondary field differs from the one introduced in the dynamical system of (R. Smith, C Kuhlemeier, et al. 2006)to stabilize whorled phyllotaxis, as, there, the two fields have the same spatial dependance. Reaction-diffusion phyllotactic models also used a secondary field (Bernasconi G.P. 1994) to add memory to the system, which turns out be a pre-filter. Our secondary field has more resemblance to proposals made for the early development of the fruitfly embryo (Gregor et al. 2007; Erdmann et al. 2009; Okabe-Oho et al. 2009) at a smaller scale: the diffusion of the secondary transcription factor Hunchback between nuclei would smooth out the interpretation of the noisy gradient of the primary transcription factor Bicoid. In our case, noise reduction is achieved when an initium is made younger if surrounded by young primordia. Therefore our secondary field corresponds to some averaging of age information between neighboring organs.

The present study yields a framework for the analysis of phyllotactic mutants, as various correspondences can be drawn between nature of noise, level of control, and alterations of phyllotaxis. The different layers reflect the complexity of development: inhibitory interactions between primordia emerge from auxin-based cell-cell interactions, phyllotaxis emerges from primordium-primordium inhibitory interactions, a secondary field corrects the phyllotactic pattern by feeding back on cell-behavior. Such a feedback may help achieving a target pattern in a noisy environment and thus provide a general concept in developmental systems biology.

4. Supplementary Information

4.1. Supplementary figures

See Fig S1 to S5 on left pages (even numbers, pp 274- 280).

4.2. Materials and Methods

Important note: missing information (XXX) will be available in Mirabet V. et al, in prep.

a) Deterministic model

We reimplemented the model of Douady and Couder Douady1996p4192 assuming that (i) the stem has the shape of a cone and distances are computed on the cone; (ii) initia are formed on a circle of radius *R* and then move away with a constant radial velocity *V*; (iii) each primordium is a source of inhibitory field that is function of the distance *r* to the primordium,

$$I_{\alpha,d}(r) = \frac{(\tanh(\alpha r/d))^{-1} - 1}{(\tanh \alpha)^{-1} - 1},$$

α measures the steepness of the field and *d* its range, the inhibitory field is the sum of the sources due to all existing primordia; (iv) a new primordium appears on the competent circle when and where the total inhibition becomes lower than a threshold *E*. Typical value of the cone angle, R, V, α and E have been chosen to correspond to the situation in *Arabidopsis thaliana.*

The dynamical system was implemented in Python. The time of initiation is found using a standard Scipy solver, by solving for when the minimum of the inhibition on the circle falls below the threshold. Then a new primordium is created and the process is repeated. We chose to achieve a

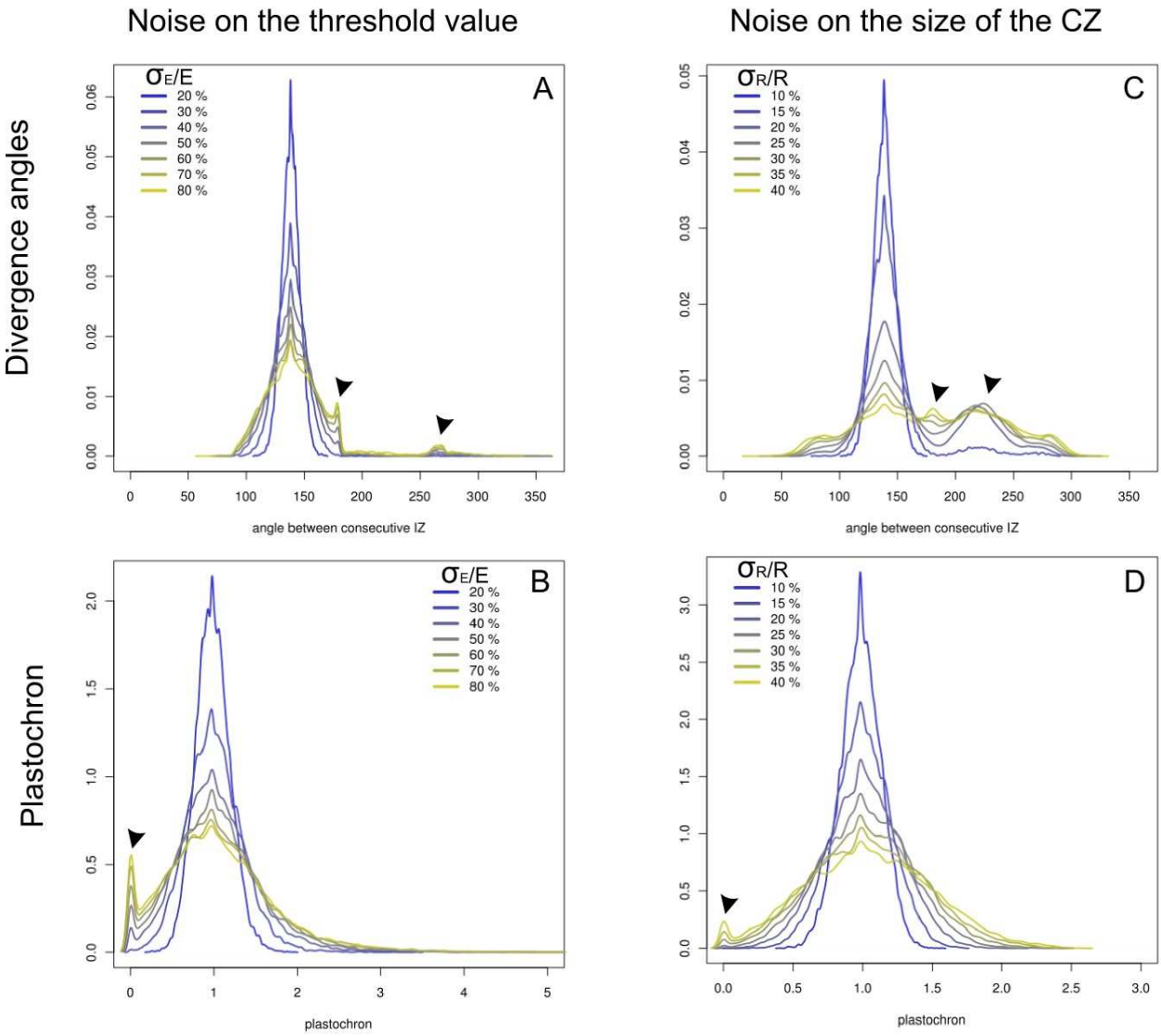

Figure S1: **Alterations of divergence angle and plastochron as a function of noise strength**. Noise strength is either σ_E/E in the threshold noise model (A,B) and σ_R/R in the size noise model (C,D). Curves corresponding to increasing noise are plotted on the same graph for divergence angle (A,C) ad plastochron (B,D). In the threshold noise model, arrowheads point to (A) the divergence angles corresponding to distichous phyllotaxis (180°) or M-shaped motifs (274°) and (B) to vanishing plastochron. In the size noise model, arrowheads point to (C) the divergence angles corresponding to distichous phyllotaxis (180°) or to spiral of reverse handedness (223°) and (B) to vanishing plastochron.

precision on time of XXX and on space of XXX. A typical sequence of XXX is generated in XXX hours on a computer XXX.

b) Model with noise

We added two sources of noise in the model, on the threshold of initiation and on the radius of the competent circle. In each case, the threshold (resp. the radius) is re-defined following each initiation from a random variable of Gaussian distribution of mean E (resp. R) and standard deviation σ_E (resp. σ_R).

In order to avoid errors on the measurement of the handedness of the phyllotactic pattern, we started each simulation with no noise imposing left-handed spiral. Once the simulation has reached a steady state we turned on noise and started the recording of the sequences of angles and plastochrons.

When noise was large enough, we frequently observed a vanishing plastochron. In that case, concomitant initia are equivalent and so we defined their order of apparition at random.

c) Secondary field

After a delay T_2 (of the same magnitude as the plastochron) after initiation, each primordium becomes a step-like source of inhibition of range (of the same magnitude as d), of the form $I_{\alpha=\infty,d2}(r)$ (having the values 0 if $r > d2$ and $+\infty$ if $r < d2$); the secondary field is the sum of all the contributions of primordia. Initia are formed according to the primary field, but their age is shifted by a value Δa if the secondary field value at the position of inhibition is non zero. Primordia are then ranked according to their corrected age.

ACKNOWLEDGMENTS. We are grateful to B. Landrein and O. Hamant for fruitful discussions.

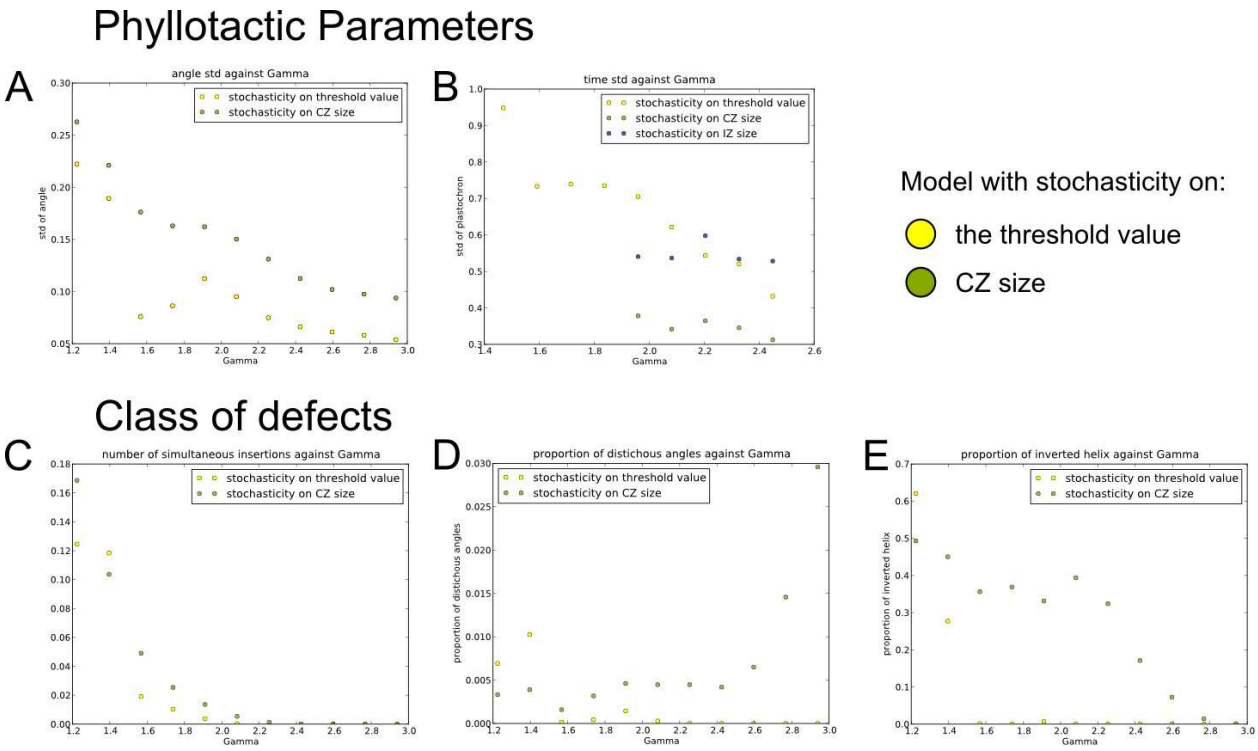

<u>Figure S2</u>: **Alterations as a function of Γ (ratio of inhibition range to competent circle size)** (**A**) Standard deviation of angle normalized by the average angle. (**B**) Standard deviation of plastochron normalized by average plastochron. (**C**) The proportion of concomitant initiations. (**D**) Proportion of distichous angles. (**E**) Proportion of handedness reversals. In general, low Γ values enhance the defects of the two sources of noise, but they do not abolish the difference between the defects generated by the two sources of noise. In particular, reversal of the handedness of the spiral remains a typical defect of the size noise model for values ranging from $1.6<\Gamma<3$. The strength of the noise in each model is fixed for all these simulations.

References – Chap III

Adler, I., Barabe, D. & Jean, R., 1997. A history of the study of phyllotaxis. *ANNaLS OF BOTANY*, 80(3), p.231-244.

Alvarez-Buylla, E.R. et al., 2008. Floral morphogenesis: stochastic explorations of a gene network epigenetic landscape. *PloS One*, 3(11), p.e3626.

Atela, P., Gole, C. & Hotton, S., 2002. A dynamical system for plant pattern formation: A rigorous analysis. *JOURNAL OF NONLINEAR SCIENCE*, 12(6), p.641-676.

Bernasconi G.P., 1994. Reaction-Diffusion Model for Phyllotaxis. *Physica D*, 70.

Chickarmane, V. et al., 2010. Computational morphodynamics: a modeling framework to understand plant growth. *Annual Review of Plant Biology*, 61, p.65-87.

Couder, Y, 1998. Initial transitions, order and disorder in phyllotactic patterns: The ontogeny of Helianthus annuus. A case study. *ACTA SOCIETATIS BOTANICORUM POLONIAE*, 67(2), p.129-150.

Douady, S. & Couder, Y, 1992. PHYLLOTAXIS AS A PHYSICAL SELF-ORGANIZED GROWTH-PROCESS. *PHYSICAL REVIEW LETTERS*, 68(13), p.2098-2101.

Douady, S. & Couder, Y, 1996a. Phyllotaxis as a dynamical self organizing process .1. The spiral modes resulting from time-periodic iterations. *JOURNAL OF THEORETICAL BIOLOGY*, 178(3), p.255-274.

Douady, S. & Couder, Y, 1996b. Phyllotaxis as a dynamical self organizing process .2. The spontaneous formation of a periodicity and the coexistence of spiral and whorled patterns. *JOURNAL OF THEORETICAL BIOLOGY*, 178(3), p.275-294.

Douady, S. & Couder, Y, 1996c. Phyllotaxis as a dynamical self organizing process .3. The simulation of the transient regimes of ontogeny. *JOURNAL OF THEORETICAL BIOLOGY*, 178(3), p.295-&.

Erdmann, T., Howard, M. & ten Wolde, P.R., 2009. Role of spatial averaging in the precision of gene expression patterns. *Physical Review Letters*, 103(25), p.258101.

Giulini, A., Wang, J. & Jackson, D., 2004. Control of phyllotaxy by the cytokinin-inducible response regulator homologue ABPHYL1. *Nature*, 430(7003), p.1031-1034.

Green, P., Steele, C. & Rennich, S., 1996. Phyllotactic patterns: A biophysical mechanism for their origin. *ANNALS OF BOTANY*, 77(5), p.515-527.

Gregor, T. et al., 2007. Probing the limits to positional information. *Cell*, 130(1), p.153-164.

Hamant, O. et al., 2008. Developmental patterning by mechanical signals in Arabidopsis. *Science (New York, N.Y.)*, 322(5908), p.1650-1655.

Heisler, M.G. et al., 2010. Alignment between PIN1 polarity and microtubule orientation in the shoot apical meristem reveals a tight coupling between morphogenesis and auxin transport. *PLoS Biology*, 8(10), p.e1000516.

Heisler, M.G. et al., 2005. Patterns of auxin transport and gene expression during primordium development revealed by live imaging of the Arabidopsis inflorescence meristem. *Current Biology: CB*, 15(21), p.1899-1911.

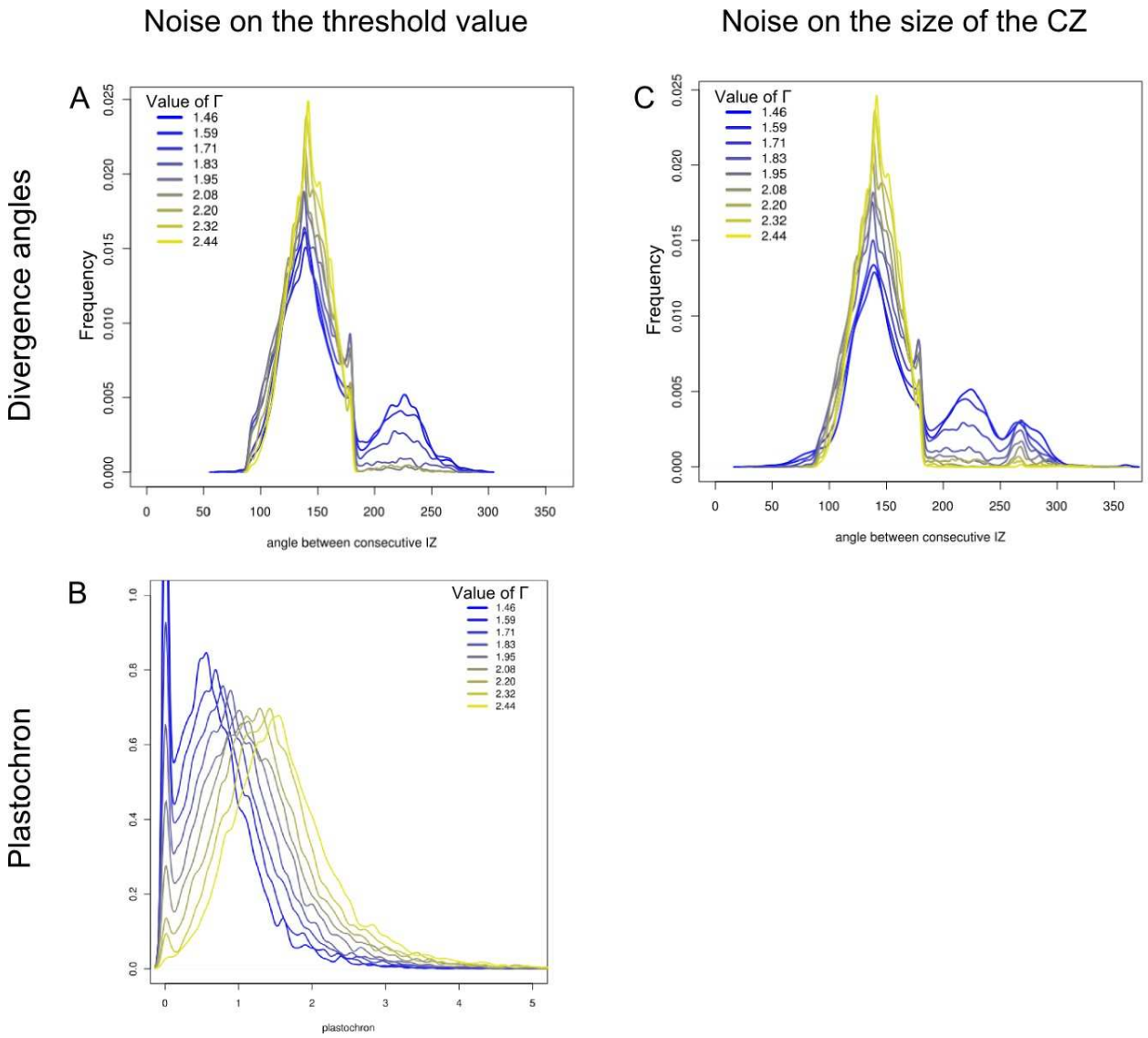

<u>Figure S3</u>: **Alterations of divergence angle and plastochron as a function of Γ.** Different values of Γ are tested with either the threshold noise model (A,B) or the size noise model (C). Curves corresponding to increasing Γ are plotted on the same graph for divergence angle (A,C) and plastochron (B). Low value of Γ enhances the defects produced by the two sources of noise. The strength of the noise in each model is fixed for all these simulations.

Hotton, S. et al., 2006. The possible and the actual in phyllotaxis: Bridging the gap between empirical observations and iterative models. *JOURNAL OF PLANT GROWTH REGULATION*, 25(4), p.313-323.

Itoh, J.I. et al., 2000. Shoot organization genes regulate shoot apical meristem organization and the pattern of leaf primordium initiation in rice. *The Plant Cell*, 12(11), p.2161-2174.

Jean, R., 1994. *Phyllotaxis: a systemic study in plant morphogenesis*,

Jeune, B. & Barabe, D., 2004. Statistical recognition of random and regular phyllotactic patterns. *ANNALS OF BOTANY*, 94(6), p.913-917.

Jönsson, H. et al., 2006. An auxin-driven polarized transport model for phyllotaxis. *Proceedings of the National Academy of Sciences of the United States of America*, 103(5), p.1633-1638.

Kuhlemeier, Cris, 2007. Phyllotaxis. *Trends in Plant Science*, 12(4), p.143-150.

Lander, A.D., 2011. Pattern, growth, and control. *Cell*, 144(6), p.955-969.

Levitov, L., 1991. FIBONACCI NUMBERS IN BOTANY AND PHYSICS - PHYLLOTAXIS. *JETP LETTERS*, 54(9), p.546-550.

Li, C., Zhang, X. & Cao, Z., 2005. Triangular and Fibonacci number patterns driven by stress on core/shell microstructures (vol 309, pg 909, 2005). *SCIENCE*, 310(5746), p.236-236.

Maksymowych, R. & Erickson, R.O., 1977. Phyllotaxis in xanthium shoots altered by gibberellic Acid. *Science (New York, N.Y.)*, 196(4295), p.1201-1203.

Meicenheimer, R.D., 1998. Decussate to spiral transitions in phyllotaxis. Dans *Symmetry in Plants*.

Meinhardt, H., 2004. Out-of-phase oscillations and traveling waves with unusual properties: the use of three-component systems in biology. *PHYSICA D-NONLINEAR PHENOMENA*, 199(1-2), p.264-267.

Mitchison, G.J., 1977. Phyllotaxis and the fibonacci series. *Science (New York, N.Y.)*, 196(4287), p.270-275.

Morishita, Y. & Iwasa, Y., 2009. Accuracy of positional information provided by multiple morphogen gradients with correlated noise. *Physical Review. E, Statistical, Nonlinear, and Soft Matter Physics*, 79(6 Pt 1), p.061905.

Müller, R. et al., 2006. Dynamic and compensatory responses of Arabidopsis shoot and floral meristems to CLV3 signaling. *The Plant Cell*, 18(5), p.1188-1198.

Newell, A., Shipman, P. & Sun, Z., 2008. Phyllotaxis: Cooperation and competition between mechanical and biochemical processes. *JOURNAL OF THEORETICAL BIOLOGY*, 251(3), p.421-439.

Nisoli, C. et al., 2009. Static and Dynamical Phyllotaxis in a Magnetic Cactus. *PHYSICAL REVIEW LETTERS*, 102(18). Available at: http://apps.isiknowledge.com.gate1.inist.fr/full_record.do?product=WOS&search_mode=GeneralSearch&qid=51&SID=Y2CpnCdfn3kKa2b842C&page=1&doc=3 [Consulté juillet 12, 2011].

Oates, A.C., 2011. What's all the noise about developmental stochasticity? *Development (Cambridge, England)*, 138(4), p.601-607.

Okabe-Oho, Y. et al., 2009. Stable, precise, and reproducible patterning of bicoid and hunchback molecules in the early Drosophila embryo. *PLoS Computational Biology*, 5(8), p.e1000486.

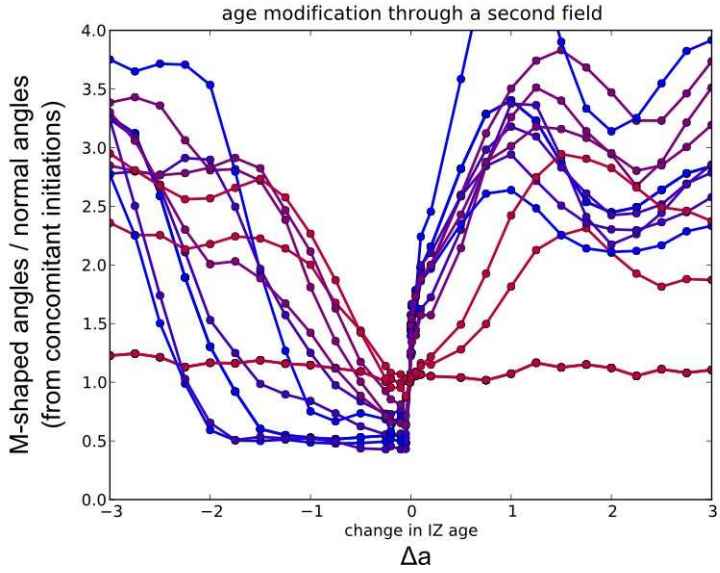

Figure S4: **Correcting effect of the secondary field depends on both its size (d2) and its delay of activation T2.** Each curve corresponds to a different combination of d2 and T2. The range of values are 0<T2<3 and 1.2<d2<1.6 (ratio to d) and curves are colored from blue (low T2) to red (high T2). Curves of the same color share the same T2 value with different d2. When the secondary field is turned on too late (about 3 plastochrons after initiation), the correcting effect is abolished. The size of the secondary field must be a bit larger than d.

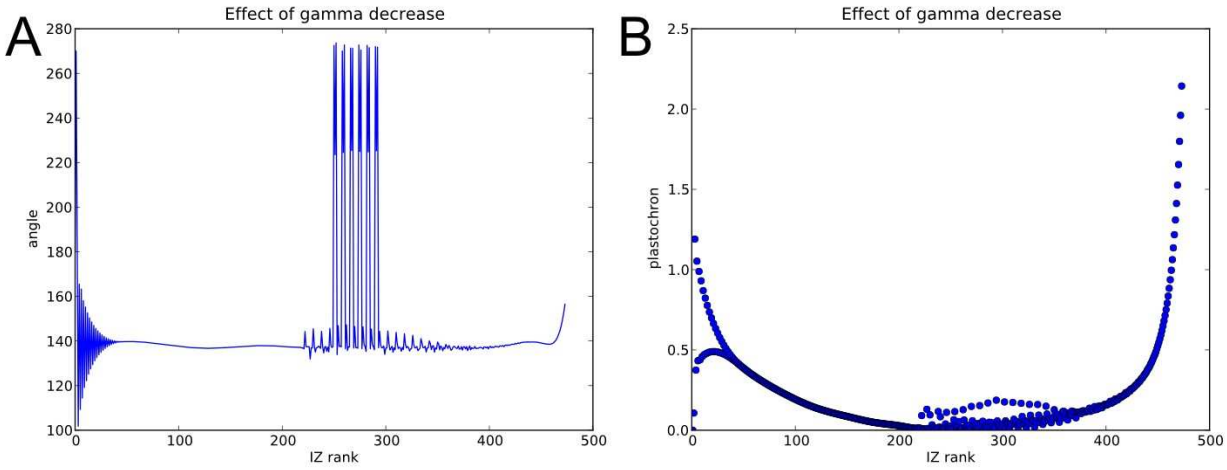

Figure S5: **Fast decrease of Γ creates M-shaped motif and null plastochrons.** (A) Upon a fast drop in the value of Γ, the divergence angle stabilizes around the golden angle after a transient instability. However, a new sequence of M-shaped motif appears later, indicated residual perturbations. (B) Variation of the plastochron upon continuous variation of Γ. We reproduced here the simulation of Douady S. and Couder Y., 1996c, Fig.9: Γ first decreases and then increases again, as seen during the development of a sunflower capitulum. The plastochron follows the variations of Γ. For low Γ values, the plastochron is close to zero and sometimes vanishes due to its variability (it is not a fixed parameter of the model). These alterations of the plastochron are highly sensitive to numerical precision.

Peaucelle, A. et al., 2007. Plants expressing a miR164-resistant CUC2 gene reveal the importance of post-meristematic maintenance of phyllotaxy in Arabidopsis. *Development (Cambridge, England)*, 134(6), p.1045-1050.

Prasad, K. et al., 2011. Arabidopsis PLETHORA Transcription Factors Control Phyllotaxis. *Current Biology: CB*, 21(13), p.1123-1128.

Ragni, L. et al., 2008. Interaction of KNAT6 and KNAT2 with BREVIPEDICELLUS and PENNYWISE in Arabidopsis inflorescences. *The Plant Cell*, 20(4), p.888-900.

Reinhardt, D, Mandel, T & Kuhlemeier, C, 2000. Auxin regulates the initiation and radial position of plant lateral organs. *The Plant Cell*, 12(4), p.507-518.

Reinhardt, Didier et al., 2005. Microsurgical and laser ablation analysis of leaf positioning and dorsoventral patterning in tomato. *Development (Cambridge, England)*, 132(1), p.15-26.

Reinhardt, Didier et al., 2003. Regulation of phyllotaxis by polar auxin transport. *Nature*, 426(6964), p.255-260.

de Reuille, P.B. et al., 2006. Computer simulations reveal properties of the cell-cell signaling network at the shoot apex in Arabidopsis. *Proceedings of the National Academy of Sciences of the United States of America*, 103(5), p.1627-1632.

Roeder, A.H.K. et al., 2010. Variability in the control of cell division underlies sepal epidermal patterning in Arabidopsis thaliana. *PLoS Biology*, 8(5), p.e1000367.

Sahlin, P., Söderberg, B. & Jönsson, H., 2009. Regulated transport as a mechanism for pattern generation: capabilities for phyllotaxis and beyond. *Journal of Theoretical Biology*, 258(1), p.60-70.

Schoute, J.C., 1938. (IV) Early bonding whorls. *Recueil des travaux botaniques néerlandais*, 35, p.416-558.

Shipman, P. & Newell, A., 2005. Polygonal planforms and phyllotaxis on plants. *JOURNAL OF THEORETICAL BIOLOGY*, 236(2), p.154-197.

Smith, R., Kuhlemeier, C & Prusinkiewicz, P, 2006. Inhibition fields for phyllotactic pattern formation: a simulation study. *CANADIAN JOURNAL OF BOTANY-REVUE CANADIENNE DE BOTANIQUE*, 84(11), p.1635-1649.

Smith, R.S., Guyomarc'h, S., et al., 2006. A plausible model of phyllotaxis. *Proceedings of the National Academy of Sciences of the United States of America*, 103(5), p.1301-1306.

Snow, M. & Snow, R., 1962. A THEORY OF REGULATION OF PHYLLOTAXIS BASED ON LUPINUS ALBUS. *PHILOSOPHICAL TRANSACTIONS OF THE ROYAL SOCIETY OF LONDON SERIES*, 244(717), p.483-&.

Snow, M. & Snow, R., 1932. Experiments on phyllotaxis I - The effect of isolating a pininordium. *PHILOSOPHICAL TRANSACTIONS OF THE ROYAL SOCIETY OF LONDON SERIES*, 221, p.1-43.

Snow, M. & Snow, R., 1933. Experiments on phyllotaxis II - The effect of displacing. *PHILOSOPHICAL TRANSACTIONS OF THE ROYAL SOCIETY OF LONDON SERIES*, 222, p.353-400.

Stoma, S. et al., 2008. Flux-based transport enhancement as a plausible unifying mechanism for auxin transport in meristem development. *PLoS Computational Biology*, 4(10), p.e1000207.

Turing, A., 1952. The Chemical Basis of Morphogenesis. *Phil. Trans. B.*, 237, p.37-72.

Veen, A.H. & Lindenmayer, A., 1977. Diffusion mechanism for phyllotaxis: theoretical physico-chemical and computer study. *Plant Physiology*, 60(1), p.127-139.

Vernoux, T. et al., 2011. The auxin signalling network translates dynamic input into robust patterning at the shoot apex. *Molecular Systems Biology*, 7, p.508.

Weisse, A., 1894. Neue Beiträge zur mechanischen Blattstellungslehre. *Jahrb. Wiss. Bot.*, 26, p.236-294.

Yoshikawa, H. et al., 2010. Pattern formation in bubbles emerging periodically from a liquid free surface. *EUROPEAN PHYSICAL JOURNAL E*, 33(1), p.11-18.

CONCLUSIONS AND PERSPECTIVES

Contents

I.DISCUSSION OF OUR RESULTS.....289
I.1.AHP6 inhibitory fields: a new mechanism controlling the robustness of temporal patterns in Arabidopsis phyllotaxis.....289
1.1.Plastochron instabilities supports the « Snow and Sow » hypothesis and are likely the cause of post-meristematic permutations in phyllotaxis.....289
1.2.co-initiations can be explained by stochasticity and other factors in the frame of theoretical models of phyllotaxis.....291
1.3.AHP6 controls specifically the rhythmicity of the plastochron by a mechanism involving cytokinin inhibitory fields.....295
1.4.Importance of plastochron regularity in the control of the segmented architecture of shoots.....301
I.2.Auxin inhibitory fields: new insights on the spacing mechanism controlling phyllotaxis....303
2.1.New arguments supporting the existence of local inhibitory fields.....303
2.2.New predictions concerning the auxin fields in the SAM.....305
I.3.Other inhibitory fields ? Proposition of a model with multiple hierarchical fields.....309
I.4.A new role for cytokinin in organogenesis reveals the complexity of hormonal crosstalk controlling development.....311
I.5.Why has a mechanism evolved that limits co-initiations in phyllotaxis?.....313
II.PERSPECTIVES.....319
II.1.Phenotyping phyllotaxis in different plants.....319
II.2.Exploring the molecular network behind the effect of AHP6 fields and the auxin-cytokinin crosstalk.....321
II.3.Exploring the auxin fields by new experimental and modeling approaches.....323

In the most commonly accepted mechanism explaining phyllotaxis, local repulsive interactions between primordia control the formation of the pattern. Available biological data support the idea that this repulsion is mediated by chemical inhibitory fields generated by polar auxin transport in the epidermis of the meristem. So far, most of the attention has been paid to the spatial patterns of phyllotaxis. While the system is also largely controlled by its dynamics, the temporal patterns generated by iterative organ production have been less studied. In my work, I have discovered a previously unknown mechanism of coordination between space and time in phyllotactic patterns, based on hormonal inhibitory fields. This result suggests that robustness in phyllotaxis is controlled at different levels and it opens new directions for research.

I. DISCUSSION OF OUR RESULTS

I.1. AHP6 inhibitory fields: a new mechanism controlling the robustness of temporal patterns in *Arabidopsis* phyllotaxis.

Looking for spatial perturbations in the phyllotaxis of *Arabidopsis ahp6* mutants, we ended up with the characterization of temporal instabilities. The plastochron can be defined by two different parameters: its mean length and its regularity. While different genes were identified as regulators of plastochron length in different species (Lee, Yu, et al. 2009), we identified for the first time a biological mechanism controlling plastochron regularity.

1.1. Plastochron instabilities supports the « Snow and Sow » hypothesis and are likely the cause of post-meristematic permutations in phyllotaxis.

The originality of our works was to combine a post-meristematic and a meristematic analysis of phyllotaxis. This led us to establish that (i) perturbations in the phyllotaxis of *Arabidopsis thaliana* could be explained by permutations in the position of organs along the stem (see chapter 1) and (ii) that these permutations were likely due to simultaneous initiations of pairs or triplets of organs in the meristem (see chapter 2). Notably, time-laps live imaging of auxin signaling clearly shows that the plastochron is irregular in wild-type and even more in *ahp6* mutants, suggesting that the time between consecutive organ initiations is not fixed (chapter 2). This is in contradiction with the Hofmeister hypothesis (as defined by Douady and Couder (1996a), see Introduction) and rather

supports the “Snow and Snow” hypothesis (see Introduction): an organ likely forms where and when it is possible. Hereafter, I will use the term permutations to refer to the post-meristematic phenotype and co-initiation to refer to simultaneous initiation of organs in the meristem.

The observation of co-initiations - or even inverted order of organ formation in meristem, could question the theory explaining phyllotaxis. Since the pattern emerge from interactions between organs, one could wonder that changing the order of apparition of organs does not disrupt totally the phyllotaxis. However, as shown by most of the dynamical system models, the new appearing organ in a regular spiral is not positioned by the preceding organ, but by the inhibitory fields of its nearest neighbors. Those latter are found along the contact parastichies. Co-initiations can thus theoretically occur as long as they don't perturb the dynamically important contact parastichies, which keep a “memory” of the geometry of the pattern at each iteration. This explains that Douady and Couder could observe “permutations” in the two models they used (see (1996a) figure 5b and 11; (1996c) figure 9). Note that in their case, the permutations were said to come from inverted order of organ formation, although they also showed that this happened when the plastochron is reduced. Anyway, dynamical system models showed that an important property of a mechanism involving local inhibitory fields is to create robust patterns in space (contact parastichies and the divergence angle are stable) but not necessarily in time. The observation of co-initiations in SAM is thus fully consistent with the frame given by these models.

1.2. co-initiations can be explained by stochasticity and other factors in the frame of theoretical models of phyllotaxis.

Although these abstract models were able to generate permutations, the parameters and the conditions which could promote co-initiations have not been fully explored. Moreover, the limitations in the number of parameters required in these models and their broad biological meaning is a key advantage for this kind of exploratory study. Since it corresponds tou our xperimental data, we chose to use the second model established by Douady and Couder (1996b): a dynamical system based on local inhibitory fields with the “Snow and Snow” hypothesis (see chapter 3). For the sake of clarity, we will call this type of model “S&S” model hereafter.

In the “S&S” model, the positions of organs and their inhibitory fields are computed iteratively at each steps and new organs are formed where and when it is possible. In simple spiral phyllotaxis (the jugacy is equal to 1), no co-initiations should occur: the displacement of inhibitory fields away from the generative ring should allow only one emergence at a time. However, if there are small

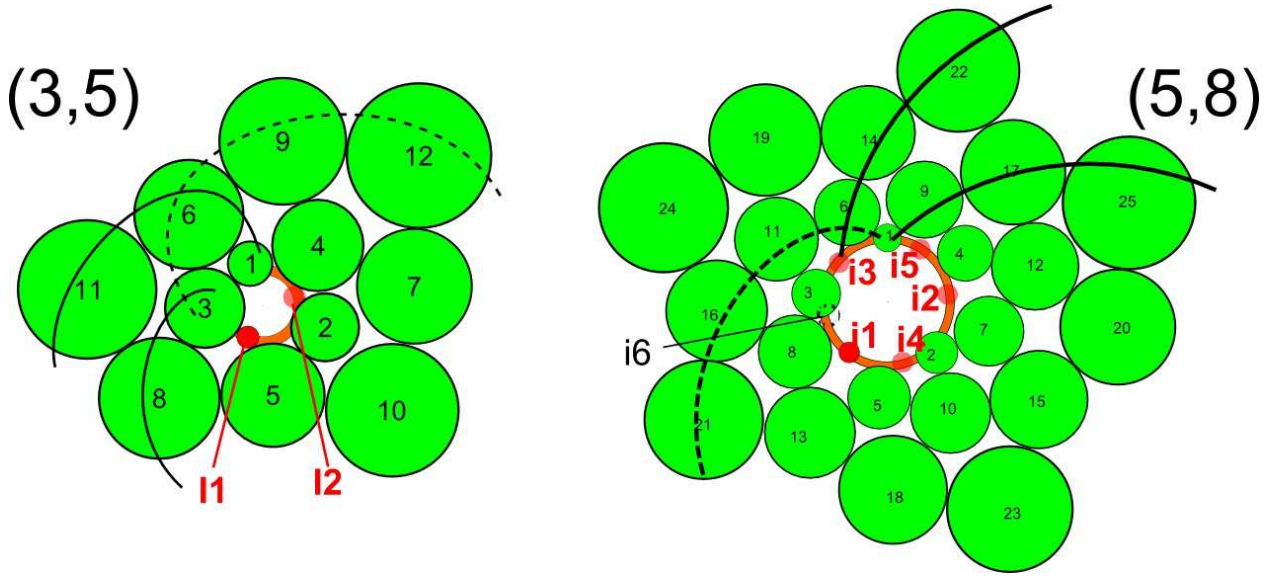

Figure 1: **The number of possible co-initiations is likely constrained by the ratio of organ size to meristem size**. Schematic drawings of meristems (top-view) with Fibonacci spiral of increasing order (parastichy number 3,5 on the left; 5,8 on the right. Primordia are represented by green circles and numbered according to their age, from the younger to the oldest. The peripheral zone is colored in orange and new initia, which could be co-initiated, are indicated by red circles. They are numbered from the first expected to emerge (i1). The maximum number of simultaneous initiations (2 on the left and 5 on the right in this example) is limited by the girth of the peripheral zone relative to the size of primordia and initia.

geometric imperfections in the position of inhibitory fields, this can create a particular configuration where two organs have “enough space” to emerge at the same time (meaning that two sites are at the same level of activation above the threshold of organ formation at the same time point), or even in a slightly inverted sequence.

We hypothesized that these defects could be generated by a certain level of noise in the system. It is widely accepted that natural, stochastic variability is inevitable in living organisms. However, it is still unclear how biological systems cope with this noise and how its effects are filtered to produce final robust outputs, like developmental patterns. We found that noise affecting a spiral phyllotaxis could lead to different defects: co-initiations, but also reversal of the handedness of the spiral and short segments of distichous phyllotaxis. Interestingly, we found that the source of noise determines the type of the most probable perturbations: our study suggests that co-initiations are not due to noise on the size of the field and indicate that noise on the threshold of activation is a potential candidate instead.

However, it is still possible that other sources of noise could produce co-initiations. Divergence angle sequences obtained *in silico* with threshold noise do not fully mirror the sequences we measured in quantity and in quality: the model never generated as much perturbations as in our data (15% and 37% of non-canonical in the wild-type and mutant respectively) and co-initiations of three organs were very rare in simulations. Moreover, although it is hard to definitely exclude the presence of short segments of distichous phyllotaxis in the measured sequence, the pipeline of methods used for their analysis did not detect any of them. Thus, since our theoretical exploration was not fully comprehensive, its main lesson is that co-initiations define a particular class of phyllotactic perturbations that likely relies on precise parameters of the system.

Before our analysis, Douady and Couder (1996a; 1996c) observed permutations upon continuous decrease of the control parameter Γ (Γ indicates the ratio between the size of the inhibitory field of organs and the size of the central non organogenetic zone. See Introduction, figure 11) This transition could represent the increase in the meristem size during development of many plants, for instance during vegetative to reproductive transition when changes in phyllotaxis have been reported for different species (D Kwiatkowska 1995; Dorota Kwiatkowska 2008; Meicenheimer 1982; Meicenheimer 1998). We recapitulated their findings and found that the faster the transition occurred and the bigger its amplitude was, the more numerous were the co-initiations (Chapter 3, figure S5). Moreover noise and temporal evolution of Γ could have additive effect. However, in *Arabidopsis*, the transition of phyllotaxis occurs when the seedling initiates its first leaves, and

rosette and inflorescence spiral phyllotaxis have the same (3,5) order, indicating that no significant transition of Γ occurs at the vegetative-to-reproductive transition. Moreover, the stationarity of the sequences we measured (chapter 1) suggest that the initial phyllotactic transition in seedling does not affect the phyllotaxis of inflorescence. To further clarify this point, it would be particularly interesting to scrutinize the presence of permutations (and co-initiations if possible) in plants exhibiting a fast and important change in meristem size associated with a change in phyllotaxis.

As Douady and Couder, we also found that permutations occurred more frequently in high order spiral phyllotaxis associated with low Γ values (plants with a big meristem-to-organ ratio). In our study, these conditions were more sensitive to noise, notably because their plastochron is short: it can thus more easily decrease to zero (Chapter 3, figure S2, S3 and S5). This tendency of bigger meristems to make more permutations can also be explained by a geometric diagram (figure1): there are more possible sites for organ initiation when organs (and their inhibitory fields) are small compared to the girth of the generative ring. Their sequential apparition thus requires a very precise positioning and coordinated displacement of all organs and small perturbations can easily produce a co-initiation. This diagram also indicates that the number of organs involved in co-initiation is restricted by the geometry of the system: it is roughly equal to the number of initia fitting around one turn of the generative ring (360°). If more organs were co-initiated, the contact parastiches would no longer be preserved and the spatial pattern of phyllotaxis would be disrupted.

To summarize, “S&S” models provide a theoretical explanation for co-initiations. While this mechanism is self-correcting for the spacing and is able to define a robust divergence angle, it easily generates temporal instabilities. As a kind of tradeoff, the mechanism of phyllotaxis is thus intrinsically robust in space, and less robust in time. Moreover, this model suggests that particular factors promote the occurrence of co-initiations. First, the bigger the meristem is compared to organ size (low Γ), the less robust is the system to co-initiations. Second, fast evolution of the size of the meristem or noise on the activation threshold for organ formation in the peripheral zone are plausible perturbations of the system that could trigger co-initiations in plants.

1.3. AHP6 controls specifically the rhythmicity of the plastochron by a mechanism involving cytokinin inhibitory fields.

We identified the *ahp6* mutation in *Arabidopsis* as a genetic background where co-initiations are specifically increased. In the frame of the current understanding of phyllotaxis, we could propose three different hypothesis for this phenotype, given the possible origins for co-initiations discussed

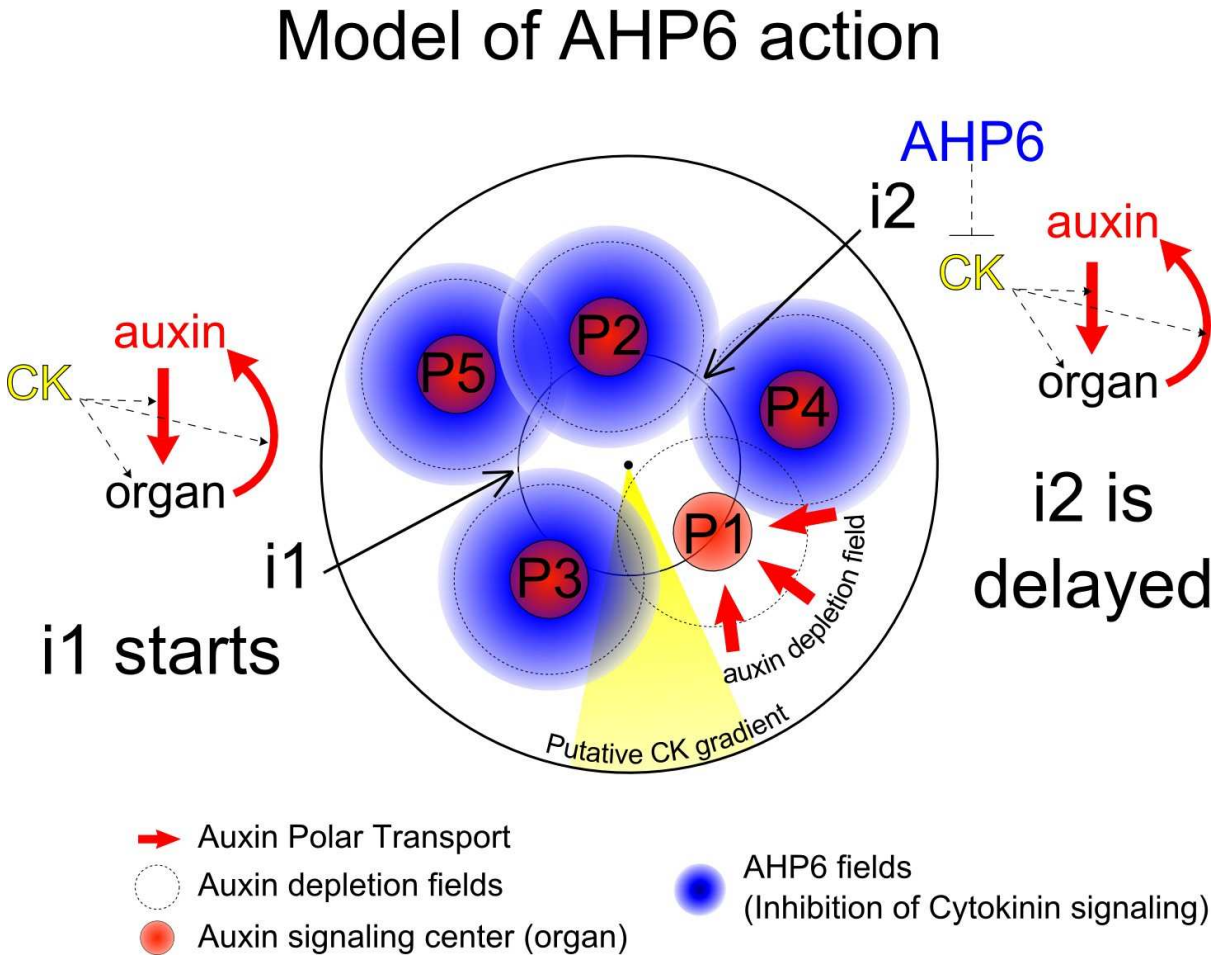

Figure 2:Proposed model for AHP6 action. See text for details.

above. First, *AHP6* loss could speed up the transition of Γ during development or increase the noise affecting the activation threshold. Second, *ahp6* mutants could have lower Γ or other modified parameters producing a context in which small perturbations are more likely converted into permutations. Third, *AHP6* could be part of a specific mechanism that increases the robustness to temporal instabilities. This hypothesis imply that the simple mechanism of Snow and Snow hypothesis, if it is true, would still function, but not alone: another mechanism would overcome the plastochron irregularities and avoid co-initiation. Whereas we found no evidences supporting the first two hypotheses, we accumulated data supporting this third one (see chapter 2).

First, we found that AHP6 protein creates cytokinin inhibitory fields emanating from primordia. We showed that these fields are functional, because they inhibit non cell-autonomously cytokinin in the peripheral zone. Our results further indicate that AHP6 also limit the number of organ co-initiation non cell-autonomously, through the action of those fields. To support this, we showed that:

(1) Consecutive initia (noted i1 and i2) are exposed to differential concentration of AHP6 because of the pattern of the fields. This creates differential signaling of cytokinin between consecutive initia, with higher signaling in the older initium (i1), first bound to emerge.

(2) In wild type plants, cytokinin signaling co-exists with auxin signaling in organ initia: the two hormonal signaling increase together as initium gets older, in a developmental progression. Exogenous treatment of CK promote auxin signaling in the peripheral zone, suggesting that CK signaling boost auxin signaling in initia. Since auxin is upstream of AHP6 activation, this suggests a positive feedback loop between auxin and cytokinin during organogenesis.

(3) Abolishing the differential of AHP6 levels between consecutive initia (mutant or overexpressor) increases co-initiations and abrogates the developmental progression of CK/auxin signaling between initia.

Based on these data, we can propose the following mechanism to explain how *AHP6* controls the stability of the plastochron. According to the current vision, auxin fields position the site of initia, determined by the convergence of PIN1 pumps. This convergence leads to a local increase in auxin signaling. However, the development of the initium is not instantaneous: it follows a developmental progression, during which auxin signaling builds up. AHP6 fields would control this precise stage. Indeed, cytokinin signaling promotes the increase of auxin signaling in initia, likely by modifying the competence of cells to respond to auxin. It could alter their sensitiveness threshold, their kinetics of response, or absolute level of response, etc. As a consequence, the emergence of an

initium would be faster when it is exposed to higher cytokinin signaling (figure 2). The pattern of AHP6 fields in the meristem ensures that only one initium in the peripheral zone is free from AHP6 influence: the others are exposed to high AHP6 concentration, which would slow down their emergence by buffering cytokinin signaling. Thus, a temporal sequence naturally emerges from the geometry of AHP6 fields in the meristem and from its potential specific action on the timing of early initium development.

We further tested this hypothesis by using a computational model based on the S&S hypothesis with noise. We first showed that AHP6 fields can't be equivalent to auxin fields (i.e., acting on organ positioning during organ initiation, see chapter 3). Indeed, if two fields determine the formation of organs, the different positional information given by the competing fields generates either irregular unstable arrangements or unusual arrangements never observed in nature. In very special cases though, two fields could cooperate if they are in resonance: this was proposed in a mathematical study investigating the properties of fields generated by mechanical buckling and auxin (Newell et al. 2008). Alternatively, we found that a second field can correct co-initiations if it behaves like a filter on the age of primordia (acting after the site organ initiation has been specified). We also showed that this requires an inhibitory effect, i.e. if they make organ younger or delay their emergence (Chapter 3, figure 5). Interestingly, to be efficient, these filter fields must be super-imposed to the main inhibitory field, should be activated with a delay of around one plastochron after organ formation and be wider than the main field (Chapter 3, figure S4). Excepted for the last characteristics for which we do not have any data, this profile fits remarkably with the characteristics of AHP6 fields: observed AHP6 fields behave thus as a *bona fide* threshold noise filter, as defined by our theoretical study.

Reciprocally, the “S&S” model with noise and filter indicates us interesting mechanisms concerning the cytokinin-auxin crosstalk: the cytokinin inhibitory fields could act on auxin signaling (which is modeled by the activation threshold) to delay organ emergence. This suggests that the effect cytokinin inhibition in the peripheral zone could be to slow down the kinetics of auxin signaling activation in initium. We are currently testing this hypothesis.

Altogether, this mechanism for AHP6 role in phyllotaxis explains the subtle phenotype of the mutant. The loss of AHP6 will not create more co-initiations *per se* because co-initiations are first generated by the lack of temporal robustness of auxin fields. So *ahp6* mutants and wild-type plants can have the same number of co-initiations if they grow in an environment in which auxin inhibitory fields functions ideally, generating few possibilities of simultaneous organ initiations. To

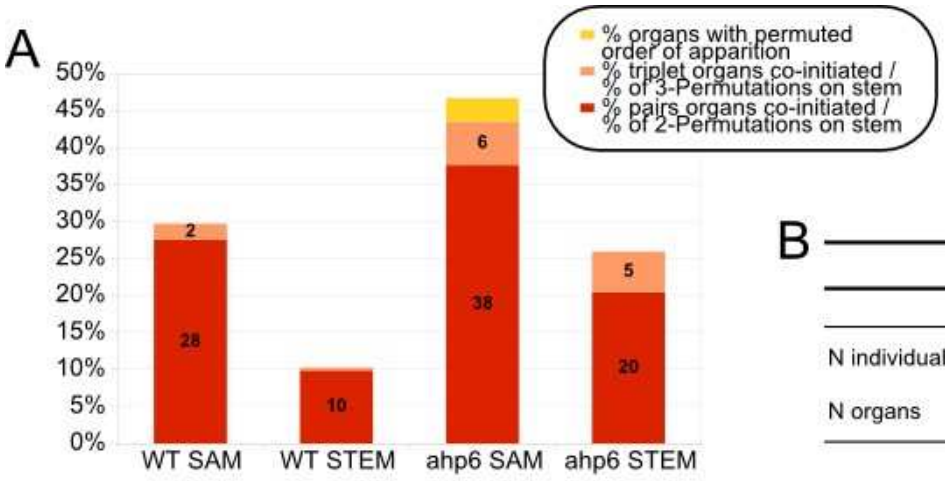

B

	WT samples		*ahp6-1*	
	SAM	Stem	SAM	Stem
N individuals	20	82	33	89
N organs	134	2487	254	2904

Figure 3:**Comparison of the number of co-initiations observed in meristem with the number of permuted organs on stem.** (**A**) Histograms showing percentages of the number of co-initiations scored from live-imaging observations (chapter 2) and percentages of organs involved in 2-Permutations and 3-Permutations calculated from the results of the analysis of post-meritematic divergence angle sequences (chapter 1). The comparison is made for wild-type and *ahp6-1* mutants (percentages are indicated in bars). This comparison suggests that two co-initiated primordia have equal chances to be positioned in the right order or to permuted later on the stem, notably in *ahp6* mutant were the filter mechanism is lost. (**B**) Characteristics of the two samples compared are given in the table.

this respect, the AHP6 filter effect can be seen as a "fail-safe" redundant mechanism, that specifically confer robustness to plastochron instabilities in phyllotactic system.

1.4. Importance of plastochron regularity in the control of the segmented architecture of shoots.

The regularity of the plastochron can have important consequences on the architecture of the shoot. *ahp6* mutants have an increased number of non-elongated internodes, which are much more frequent in permuted sub-sequences of phyllotaxis. Interestingly, we found that the half of non-elongated internode was associated with permutations (chapter 1) and we counted twice as much co-initiations in the meristems as the number of 2-permutations on the stem (chapter2, see also figure 3 in this part). This suggests that (i) half of the organs co-initiated in the SAM are later permuted on the stem (ii) a significant number of non-elongated internodes in baseline segments could come from the other half of co-initiated organs. We thus propose that the temporal separation between organ initiation is a important determinant for the development of the internode. The genetic regulation of internode specification and development only begins to be elucidated. It has been shown that it involves heterodimers between two classes of TALE (three-amino-acid-loop-extension) homeobox proteins (Hamant & Pautot 2010): the members of the knotted1-like homeobox (KNOX) family such as STM and KNAT1/BREVIPEDICULLUS and the members of the BELLRINGER1-like homeodomain family (BELL) like PENNYWISE or POUNDFOULISH (Smith & Sarah Hake 2003; Kanrar et al. 2006). On of the function of these heterodimers could be to exclude the expression of other transcription factors from the internode, like *KNAT2* and *KNAT6* (Ragni et al. 2008), or *CUC2* (Peaucelle et al. 2007). It will be interesting to investigate how this program is controlled by the events of early organ formation and by the interactions of co-initiated initia.

The segmentation of the stem in repetitive units (an internode and a subtending organ) called phytomers is thus at least partially controlled in the meristem by AHP6 fields: the temporal regularity is converted in a spatial regularity of phytomer along the stem. In animals, the segmentation of the antero-posterior axis relies on different mechanisms. In the growing notochords of vertebrates, the dynamic segmentation into somites is controlled by an internal molecular clock coupled to a spatial gradients of morphogens. In the growing apex of plants, the mechanism controlling phytomer production is not totally understood, but it seems to be radically different. In particular, no molecular clock sets the pace of the system: it emerges from the dynamics of organ

formation. In this respect, AHP6 fields can be seen as a mechanism ensuring the robustness of this particular “phyllotactic clock”.

I.2. Auxin inhibitory fields: new insights on the spacing mechanism controlling phyllotaxis.

Although our research oriented us to consider the temporal pattern of phyllotaxis, we also obtained interesting data concerning the spacing mechanism of phyllotaxis, notably about the dynamic interactions between organs.

2.1. New arguments supporting the existence of local inhibitory fields

First evidences of local repulsive interactions came from pioneering microsurgery experiments (see Introduction: (M. Snow & R. Snow 1932; M. Snow & R. Snow 1933; Wardlaw 1949; Didier Reinhardt et al. 2005). However, these experiments were very invasive and needed to be interpreted with caution, since artifacts due to other responses, like wounding for example, could be the cause of the results observed. However, they are to our knowledge, the only experimental evidence that the position of organ formation is controlled by the nearest contact neighbors. Then, series of experiments using exogenous chemical treatments, genetics and modern molecular biology led to the “auxin model”, where repulsive fields are created by auxin depletion fields around primordia. These experiments provided the first cellular and molecular basis for the mechanism governing phyllotaxis. Although not invasive, these techniques are based on the observation of extremely perturbed meristems, like the naked apices from *pin1* mutants (Okada et al. 1991) or NPA-treated plants (D Reinhardt et al. 2000)(NPA is a drug inhibiting polar auxin transport). Besides, in this plants, the phenotype is drastic, with a complete loss of organs: it is therefore not possible to study the dynamic relationships between organs and their neighbors. To date, there is no experimental way to investigate separately the crucial role of auxin for organ formation and its specific role for organ spacing.

In this context, we chose an original approach to study phyllotaxis without perturbing directly the organogenesis or meristem integrity (see chapter1). We let the pattern develop and we inferred from the sequences of divergence angles measured on elongated stems the events that occurred in the meristem. We then developed a pipeline of methods that allowed us identifying patterns revealing particular relationships between organs. Notably, we interpreted two important features in

our data as new experimental arguments supporting the existence of local repulsions between organs along the contact parastichies.

First, as discussed above, permutations in the order of appearance of organs along the stem are predicted by a dynamic model of local inhibitory fields, with either the "Hofmeister" hypothesis or the "Snow and Snow" hypothesis (as defined by Douady and Couder, (1996a)). Moreover, considering that biological system are submitted to noise and that changes in meristem size during development imposes transition to the system, such permutations should be expected in many plants and could even be frequent. Permutations were reported in real plants for the first time by Couder (1998), in one sunflower with a rare Lucas spiral phyllotaxis (compared to the most common Fibonacci spiral, see table 1 in Introduction). Our data show that these permutations are very common in *Arabidopsis,* even in wild-type plants with normal Fibonacci phyllotaxis. Thus, our characterization of permutations can be seen as a important argument supporting a conserved mechanism of local repulsive interactions in plant phyllotaxis.

Second, we observed that the most probable length of intervals of synchronized organs between two permutations events follow a particular law: most of the time, a new permutation occur 1 or 3 organ initiation after the end of a preceding permutation. We found that the disposition of the organ in this situation was particular: permuted organs align along the same contact parastichies (see Chapter 1, figure 6). This suggests that if an organ is involved in a permutation, it would transmit its defect to its nearest neighbors, promoting a new permutation if organogenesis has returned to a normal sequence meanwhile. Although below the statistical threshold of relevance, we might also detect the effect of contact parastichies in the oscillations of unperturbed sequences of divergence angles (chapter 1, figure 8). Nonetheless, it would be necessary to increase the precision of angle measure to prove it. Together, these data are the first evidence of the effect of contact parastichies in the positioning of new primordia in plants that grew without being experimentally perturbed.

2.2. New predictions concerning the auxin fields in the SAM.

The current biological mechanism explaining phyllotaxis is based only on auxin depletion fields. Altogether, our data indicate two predictions concerning these auxin fields: (1) they should generate co-initiations as those seen in *ahp6* mutants and (2) the size of the auxin depletion field should only reach the nearest neighbors.

In *ahp6* mutants, we observed very complex patterns of permutations, notably due to various chaining of permutations involving two to three organs. According to our model, the loss of AHP6

fields does not modify auxin fields, it only reveals the intrinsic capacity of auxin fields to generate co-initiation. Thus, *ahp6* mutants are a very interesting genetic background to investigate the characteristic of auxin fields, because the temporal defects they generate are no more hidden by the AHP6 fields. Moreover, the current models of phyllotaxis, either abstract (like "S&S" models) or more realistic (like cell-based models of polar auxin transport with a virtual growing SAM), should reproduce co-initiations patterns as seen in *ahp6* mutants. This could help constraining the parameter space used in these models or even indicate how to elaborate better models.

To date, the size of auxin fields is not precisely known. Since there is no tools available to precisely measure auxin concentrations in plant tissues, auxin depletion fields have never been observed directly. Instead, a indirect approach have been proposed: assuming that PIN1 carriers pump auxin out of cells, a map of the direction of auxin fluxes between cells was established from the observed polarization of PIN1 proteins in *Arabidopsis* meristems. Then, using computational models, a virtual map of auxin concentrations was calculated based on this PIN1 protein network, suggesting an accumulation in primordia (de Reuille et al. 2006). Conversely, it possible to determine the area of cells that contributed to form the peak of auxin in each organ. The authors called it the influence zone of a primordium and it might correspond to the inhibitory depletion field of auxin (Stoma et al. 2008). However, the meristematic zone studied was quite small, including only three primordia: it is therefore not possible to see the influence zone of the nearest neighbors (with 3 and 5 parastichies like *Arabidopsis*, it is necessary to have at least 6 primordia in the same picture, since the contact neighbors of the 1st organ are the 4th and the 6th). Alternatively, our laboratory recently developed an auxin signaling sensor, DII-VENUS, which allows doing observations and measurements of the region experiencing auxin signaling around a primordium (Vernoux et al. 2011). This promising tool will help us analyzing further the dynamics of auxin signaling using live imaging, focusing on the relationships between organs along contact parastichies. However, we will also need to determine what is the biological meaning of this zone compared to the supposed auxin depletion field. The results of such research will be quite important: if the size of auxin field is compatible with the parastichies, then a model based on auxin alone is plausible. However, if auxin fields do not fit the expected size, additional factors must be involved in the spacing mechanism of organs during phyllotaxis.

I.3. Other inhibitory fields ? Proposition of a model with multiple hierarchical fields.

Many questions concerning the control of phyllotaxis and its robustness are still unanswered. In particular, our data illustrate how robust is the spatial positioning: even in highly perturbed *ahp6* mutants, the divergence angle remains precisely around the golden angle or around multiples of the golden angle generated by permutations (see Chapter 1). While in theory, mechanisms based on local inhibitory fields explain this robustness, it is still unclear how a biological mechanism can reproduce this property. Indeed, to generate a stable pattern, it is required that the control parameters of the system (size of the inhibitory fields and size of the central zone, given by Γ) stay relatively constant. As shown by models, a very rapid evolution of Γ requires long transitions before the pattern stabilizes and to much noise can even disrupt the pattern. But in real plants, experimental data indicate that at least the size of the central zone may not be stable over time (Geier et al. 2008) and can adapt rapidly to changes in the dynamic CLV3/WUS regulatory loop (Reddy et al. 2004). Besides, PIN proteins have been shown to respond very rapidly to changes in auxin concentration, notably in roots, while in the SAM, exogenous auxin treatments never perturb the phyllotaxis. Again, it would be necessary to visualize auxin fields *in vivo* to determine whether they are stable over time.

The principles of the mechanism we propose for AHP6 could help us understanding how different mechanisms can cooperate during the formation of the pattern. Importantly, only one main field (excepted if several fields are in resonance) must bring the positional information for organ initiation to generate a stable pattern. To date, experimental data support that this main field is made by auxin depletion zone around primordia. Then, like AHP6 fields, we propose that several other fields could provide robustness to phyllotaxis. They could act as a filter on the auxin field, to regulate some of its property. Thus, they would not control organ positioning by themselves, but they could for example buffer variations of the size auxin fields or of the central zone over time. For example, it is possible that another field than AHP6 filters out specifically the distichous angles we observed with the threshold noise in the S&S model (chapter 3): it would thus explain why such angles are not observed in *ahp6* mutants. The recent feedback of mechanical stresses on PIN1 polarity could be seen as such an additional mechanical field (Heisler et al. 2010). With the development of various signaling sensors for different signaling pathways, we can hope that the existence of such fields will be investigated in the future.

I.4. A new role for cytokinin in organogenesis reveals the complexity of hormonal crosstalk controlling development.

Our results suggest that cytokinin promotes the first step of organ initiation and acts in a positive feedback loop with auxin (see chapter 2, see also figure 2). In the literature, the interplays between auxin and cytokinin are complex and sometimes contradictory. In the shoot meristem, an antagonism between auxin and cytokinin actions is often described. Some data indicate that cytokinin regulate cell cycle, they have been shown to be involved in stem cell maintenance in the central zone and they are thought to inhibit differentiation in organs. Auxin would rather trigger differentiation and cell expansion in the peripheral zone. However, this antagonism is questioned by several data. First, during *in vitro* plant regeneration, different ratios of auxin and cytokinin induce different fates: high auxin/cytokinin ratios promote roots whereas increasing cytokinin concentrations to auxin will induce shoots. These classical *in vitro* studies thus already suggested that whereas auxin and cytokinin would be rather antagonistic in roots, they could act in synergy in shoots. Second, recent molecular data, including ours, also sustain a synergy between auxin and cytokinin during organogenesis in shoots (see in Introduction).

This positive role for cytokinin in organogenesis suggests another possible effect of AHP6 fields during development: they could buffer variation of cytokinin levels. Indeed, many data indicate that the concentration of cytokinin in the SAM are not constant in time. Firstly, cytokinin levels increase during the vegetative to floral transition (Jacqmard et al. 2002; Corbesier et al. 2003). Secondly, it has been shown that cytokinin in shoot increases with the strenght of evapo-transpiration, because this enhances the root-to-shoot cytokinin transport (R. Aloni et al. 2005). Thirdly, a recent study in *Arabidopsis* showed that cytokinin signaling in the SAM was lowered in the dark (Yoshida et al. 2011).Thus, cytokinin concentration in the SAM depends on both developmental and environmental factors. Sudden increase in cytokinin signaling in the SAM could trigger more co-initiations and perturb phyllotaxis. AHP6 fields would then be important in these particular physiological conditions. To test this hypothesis, it would be pertinent to see whether the phenotype of *ahp6* mutant is enhanced when evapo-transpiration increases.

Moreover, recent data raise interesting questions about additional roles of AHP6 fields. In the brassicacea *Sinapsis alba* (closely related to *Arabidopsis*), new plasmodesmata were shown to be formed at the onset of flowering and concomitantly (S Ormenese et al. 2000), the central symplasmic field increases (Sandra Ormenese et al. 2002). The authors also showed that exogenous applications of cytokinin also induce the formation of plasmodesmata (Sandra Ormenese et al.

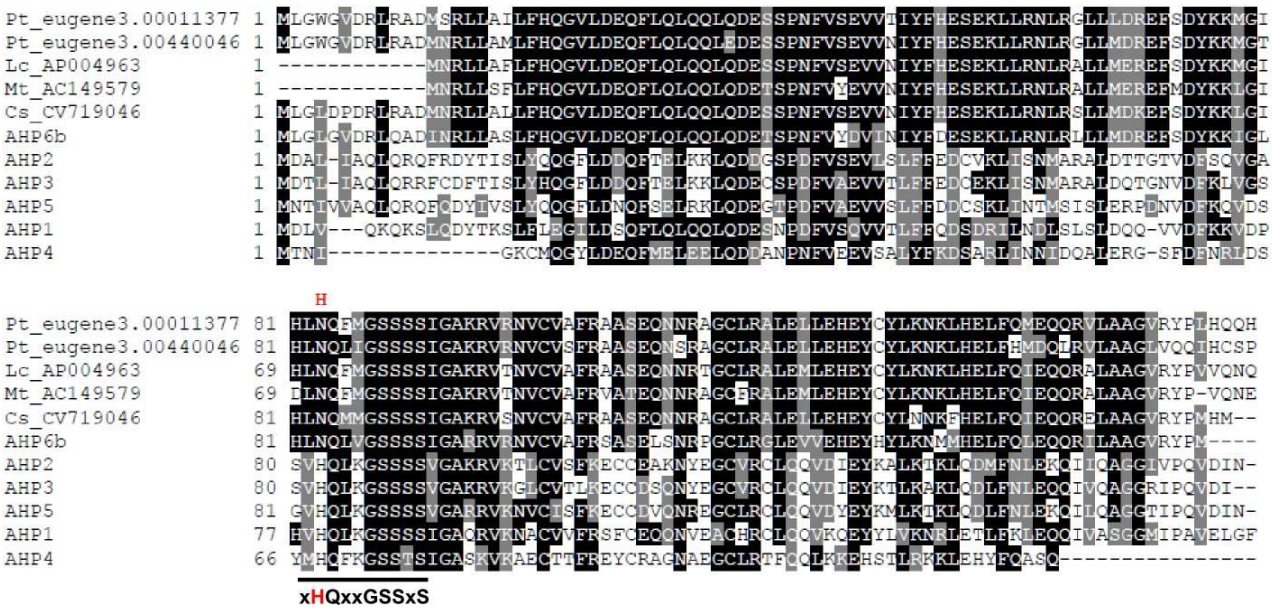

Figure 4: **Presence of genes encoding putative pseudo-HPt in various eudicots** (From Mähönen *et al*, 2006, figure S6). Alignment of pseudo HPt sequences from *Citrus sinensis* (CV719046 cDNA), *Lotus corniculatus* (AP004963 genomic DNA), *Medicago truncatula* (AC149579 genomic DNA) and *Populus trichocarpa* (eugene3.00011377 genomic DNA supported by BI138846 and CK101773 cDNAs; eugene3.00440046 genomic DNA) with *Arabidopsis thaliana* HPts (AHP1-6 genomic and cDNA). Phosphoaccepting histidine (marked by a red H above alignment) in the conserved xHQxxGSSxS motif is lacking from the pseudo HPts.

2006), suggesting that the natural increase of cytokinin level in SAM during floral transition is responsible for the increase in the central symplasmic fields and could alter the exchange of many signaling molecules in the SAM. As a consequence, it is possible that AHP6 fields also interfere with this effect of cytokinin and limit the exchange of some signaling molecules through plasmodesmata. Comparing the size of the symplasmic fields between wild type and *ahp6* mutant plants could provide a first answer to this topic. Interestingly, since AHP6 likely moves through plasmodesmata, cytokinin could even promote the establishment of AHP6 fields: those latter would then act in a negative feedback loop on cytokinin signaling.

In a wider perspective, auxin/cytokinin ratios could be a fundamental parameter of meristem architecture and phyllotaxis. In *Arabidopsis*, the loss of the feedback loop of AHP6 on auxin in *ahp6* mutants produces plastochron instabilities and leads to perturbations of phyllotaxis. In Maize, the loss of another cytokinin signaling inhibitor, type-A ARR *ABPHYL1*, triggers a more drastic phenotype, with a change from a distichous to a decussate phyllotaxis. More generally, auxin/cytokinin crosstalk impacts both the size of stem cell niche and organogenesis, which are the two main terms of the control parameter Γ from the model of Douady and Couder (see Introduction, figure 11). This indicates that understanding the combination of the signaling of these two hormones may be important to explain the robustness of phyllotaxis, and also its diversification between species during evolution.

I.5. Why has a mechanism evolved that limits co-initiations in phyllotaxis?

Our data support a model in which auxin inhibitory fields determine organ positioning and AHP6 fields tune the periodicity of organ emergence. However, since the global pattern of phyllotaxis is not disrupted by permutations, one might wonder about the evolutionary advantage conferred by a specific mechanism limiting their occurrence.

The conservation of a gene and its expression patterns in the course of evolution is often used to suggest the conservation of its role and hence, the potential importance of its function. Available phylogenetic data indicate that AHP6 is likely conserved throughout the eudicots (figure 4) (Mähönen et al. 2006) but is not present in rice and maize, two monocots (figure 5). Thus, AHP6 is not a conserved regulator of phyllotaxis in all angiosperms. However, it would be necessary to look for AHP6 orthologs in oher monocots, in basal angiosperms (e.g. *Amborella trichopoda*) and in

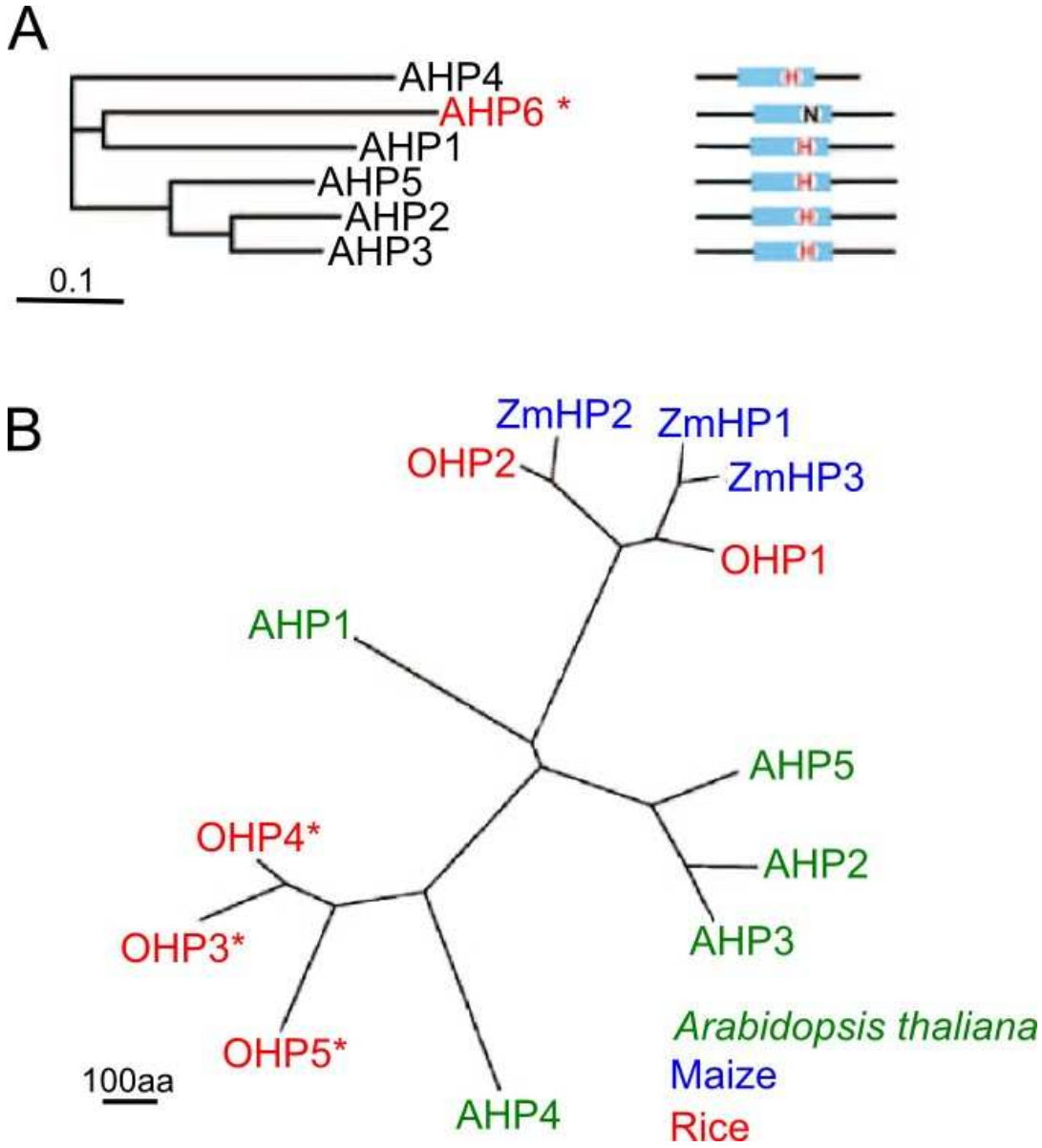

Figure 5: **Phylogeny of HPt and pseudo-HPt in Arabidopsis, Maize and Rice**. (**A**) Phylogenetic tree of the 5 HPt and of the pseudo-HPt AHP6 in *Arabidopsis thaliana.* For each protein the corresponding structure is indicated on the right. The conserved transmitter domain with the conserved Histidine (H) residue that gets phosphorylated is indicated as a blue box. Note it is substituted in AHP6. Adaptated from Müller B., 2011 (**B**) Phylogenetic tree of the HPt from Arabidopsis, Maize (*Zea mais*) and Rice (*Oriza sativa*). AHP6 was omitted in this study. Adapted from Ito Y. *et al.*, 2006. Both trees were calculated using full-length protein sequences. The scale bars represent 0,1 amino acids substitution per site in A, 100 amino acid residues in B.

gymnosperms to resolve AHP6 phylogeny and determine whether it first appeared in eudicots or alternatively was in monocots. The maize genome contains three Histidine phosphotransfer HPt (HPt) proteins and no pseudo HPt as has been reported so far. Interestingly, the rice genome contains two HPt proteins (OHP1 and OHP2) and three pseudo HPt proteins (OHP3 to 5), that are not direct orthologs of AHP6, but that exhibit the same natural substitution of the conserved histidine residue necessary for phosphotransfer activity (Figure 5)(Ito & Kurata 2006). This tree indicates that the gene family of HPt and pseudo-HPt have greatly evolved since the separation of eudicots and monocots and even since the separation of rice and maize. Moreover, the tree suggests the convergent evolution of HPt into intracellular inhibitors of cytokinin signaling in some monocots and dicots species. This observation raises the possibility that the function of these cytokinin signaling inhibitors has been conserved despite the divergent molecular evolution of the gene family. To confirm these hypotheses, analysis of rice mutants for these three pseudo-HPt and the determination of their expression patterns, notably in the shoot, would be very helpful.

An important fact could explain the divergence of pseudo-HPt between eudicots and rice and maize: these two plants, as most other poales, show a distichous phyllotaxis. According to "S&S" models (see above), this type of phyllotaxis with high Γ is not likely to produce co-initiations: it is thus possible that no mechanism controlling the robustness of plastochron has evolved in this phylogenetic group. However, the regulatory loop between auxin and *ABPHYL1* in maize (Lee, Johnston, et al. 2009), where no pseudo-HPt have been reported, and the strong phyllotactic phenotype of the *abphyl1* mutant (Jackson & S Hake 1999) still suggests that the expression of cytokinin signaling inhibitors during organogenesis is important for the control of phyllotaxis. It would be interesting to determine whether ABPHYL1 protein moves in fields outside organs and acts non-cell autonomously. We could imagine that in the last common ancestor of monocots and eudicots, a mechanism of auxin-induced, cytokinin signaling inhibitory fields already existed and that it then evolved differently: it would control the regularity of the plastochron in plants with a spiral phyllotaxis, as in most eudicots, while in plants with distichous phyllotaxis, as polaes, it would regulate the size of the central zone, as suggested for the role of ABPHYL1. Note however that a role for ABPHYL1 on the plastochron has recently been proposed. Observing that the plastochron length increases in *abphyl1* mutants, Lee *et al* (2009; 2009) proposed that ABPHYL1 could regulate the plastochron in the organ by controlling the strength of the auxin flux. In this model, cells in the peripheral zone would take more time to differentiate and the increase in SAM size would be primarily due to an accumulation of cells in the peripheral zone rather than more

proliferation of stem cells in the center. To test this hypothesis, it would be necessary to measure the size of the stem cell pool in *abphyl1* mutants, using CLV3 expression as reporter for example.

Based on these data, we could propose as a working hypothesis for evo/devo studies that the regulation of plastochron by cytokinin inhibitors expressed early in organ formation has a common evolutionary origin in angiosperms, although divergent molecular networks could have evolved in the different clades in correlation with the evolution of the type of phyllotaxis. To test this hypothesis, it would be necessary to develop an evo/devo approach on phyllotaxis, with a systematic comparison of the type of phyllotaxis, the presence of post-meristematic permutations, the presence of co-initiations in the meristem and the expression of cytokinin inhibitors generating fields of protein expression.

Despite the lack of data supporting a conservation of the AHP6 mechanism in angiosperms, we can propose possible reasons to explain that this mechanism has been selected during evolution, at least in eudicots. This hypothesis implies that co-initiations should lower the fitness of plants. However, demonstrating this would not be trivial, since it is still unknown whether having regular patterns of phyllotaxis confers increased fitness. Some authors think that the regular organ arrangement around axes does not improve the fitness *per se.* In this scenario, auxin would have been selected as the mechanism regulating organogenesis for some other unknown reason and its capacity to generate regular phyllotaxis would have evolved by chance. On the other hand, the evolutionary advantage of phyllotaxis is defended by two different hypotheses (Kuhlemeier 2007): phyllotaxis could optimize light capture (F Valladares & R. Pearcy 1998; King et al. 2004; R. W. Pearcy et al. 2005) or packing of organs in the meristem (Airy 1873). Related to this last hypothesis, we observed that inflorescences of *ahp6* mutants are more opened and that their meristem is less protected. This phenotype should be precisely quantified and it should be determined whether permutations are responsible for it. More opened meristem could be caused by the perturbations of internode development which is increased by co-initiations. We could determine experimentally if *ahp6* meristems are less protected than wild-type ones from damages caused by of insects or other environmental factors. In this case, the mechanism of AHP6 could provide an optimization of mechanical protection provided by compact phyllotaxis.

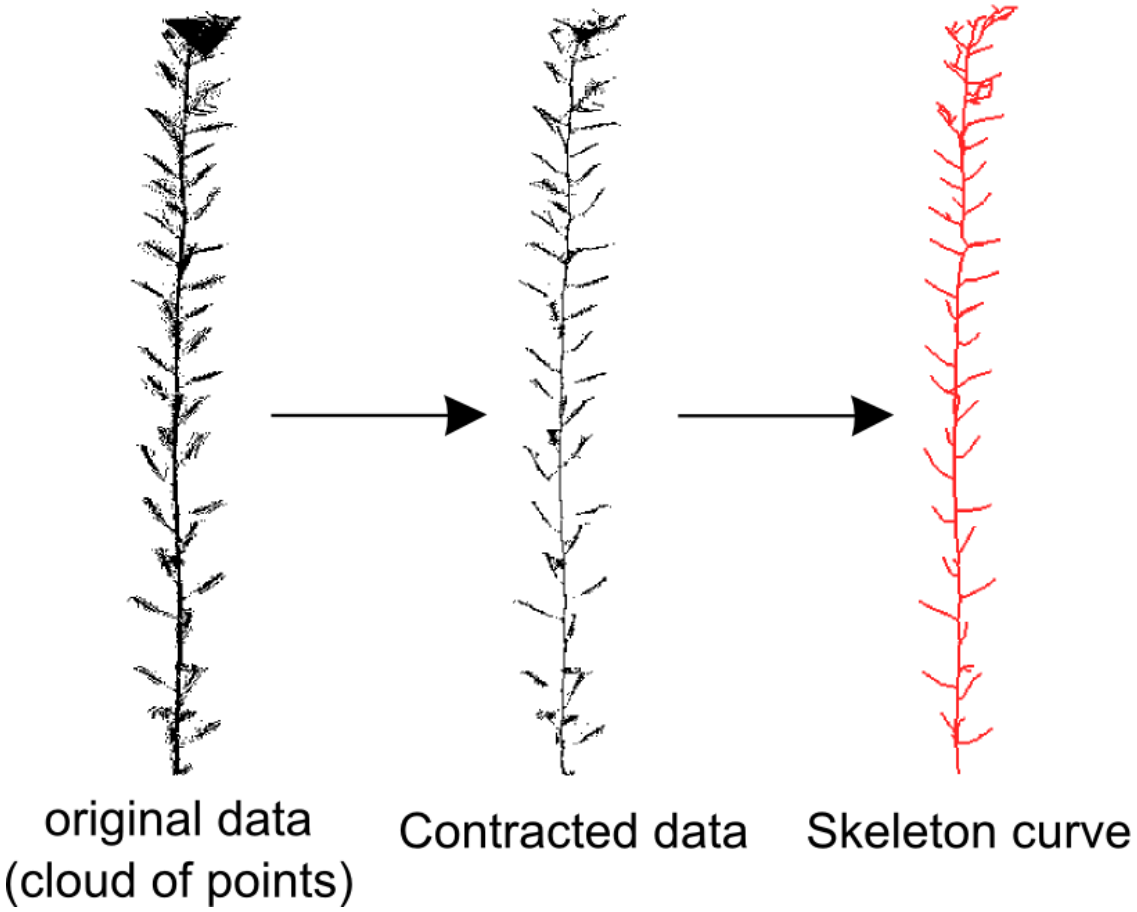

Figure 6:**Reconstruction of *Arabidopsis* phyllotaxis from laser-scanner data**. A stem of mature *Arabidopsis thaliana* was acquired with a laser scanner in 3D (in coll. With S. Carre, G. Louarn and D. Combes, INRA,URP3F, Lusignan) and the architecture was reconstructed by computer (in coll. with F. Boudon and C. Preuksakarn, INRIA Virtual Plant, Montpellier) The next step will be to extract the sequences of divergence angles and internode lengths.

II. PERSPECTIVES

In this last part, I suggest possible directions of research I would find relevant to follow in a next future.

II.1. Phenotyping phyllotaxis in different plants

Our work proved the relevance of measuring full sequence of divergence angles on large populations. It illustrates how powerful statistics can be to characterize perturbations, and how it can give significant insights on the developmental mechanisms of phyllotaxis.

Beyond the example of Sunflower and *Arabidopsis*, we propose that permutations should be widely present in phyllotaxis of vascular plants, especially in high order spiral phyllotaxis. Moreover, in many studies focusing on model plants like *Arabidopsis*, authors mentioned the existence of phyllotactic phenotypes in mutants, without precisely characterizing the perturbations. We provide now a pipe-line of method to identify permutations in perturbed phyllotaxis of different plant species or mutants. However, the time-consuming acquisition of measures of divergence angles or internode lengths may be an hindrance to the development of this approach. We are now considering new techniques to acquire phyllotactic parameters in a fast and reliable manner. We already tested a technique based on automatic laser 3D-scanning of plant stems followed by computational extraction of divergence angle and internode length (figure 6). The development of such techniques should promote phenotyping of phyllotaxis in many plants, and could boost the research on phyllotaxis. For example, high-throughput acquisition techniques could allow systematic evo-devo approaches, or genetic screens for new regulators of phyllotaxis in genetic model plants.

Our work also demonstrated the importance of conducting post-meristematic and meristematic analysis in parallel. After careful meristem observation, we explained permutations by a perturbation of the rhythmicity of the plastochron. However, permutations could be also caused by other mechanisms (see chapter 1, in discussion). For example, in the epidermis of the meristem, peaks of auxin could form with a regular plastochron and permutation would appear later, because of perturbations in the timing of the vascular connection of the flower bud to the stem or because of perturbations in the timing of internode development. Alternatively, rhythmicity of the plastochron could be the same, while the order of emergence would be permuted. Considering these hypotheses,

permutations in stems indicate a general perturbation in the timing of early organ development in the SAM. However, identifying the precise step which is affected requires a comparison between meristematic and post-meristematic analysis.

In the future, a more systematic phenotyping of phyllotaxis at microscopic and macroscopic levels by similar methods as we used should help answering these questions: (1) At which frequency permutations can be found in the phyllotaxis of different species? (2) Are permutations always caused by co-initiations? (3) what are the factors promoting this phenotype and the correlation with the type of phyllotaxis? (4) do other class of phyllotactic perturbations exist?

II.2. Exploring the molecular network behind the effect of AHP6 fields and the auxin-cytokinin crosstalk

We propose that downstream of auxin-induced organogenesis, AHP6 fields regulate the timing of the formation of younger organs, notably through a feedback on auxin. However, the molecular players of this regulatory loop are still unknown and I would propose to dissect more precisely the following steps.

First, we are interested in identifying the transcription factors that activate AHP6. The auxin-activated ARF transcription factors are obvious targets, notably ARF5/MONOPTEROS (MP), which is expressed in the peripheral zone. In a collaboration, we are currently testing the binding of MP to *AHP6* promoter by *in vitro* assay (using an Electrophoretic Mobility Shift Assay). A larger screen could be carried out using different techniques, like a yeast one-hybrid screen. A crucial aspect of AHP6 transcription is that it starts with a delay compared to the auxin reporter DR5: this allows AHP6 to function non cell autonomously and creates differential expression between I1 and I2. It would be thus interesting to understand how this precise timing of activation of AHP6 is regulated.

Then, if AHP6 buffers the cytokinin signaling in the peripheral zone, the positive elements of the cytokinin transduction pathway that are present in the peripheral zone (PZ) are not clearly identified. Studies suggest that the type-B ARR1, ARR10 and ARR12 are the major transcription factors of this gene family to be active in the shoot (R. D. Argyros et al. 2008; Ishida et al. 2008): the expression of these candidates in I1 and I2 could be first investigated. Besides, the identification of the transcription factors mediating cytokinin signaling in the PZ will allow looking for their targets, notably to determine if they directly control elements of auxin synthesis, transport or

signaling, supporting the positive feedback we propose. In parallel, it should be determined which parameters of auxin signaling are modified by cytokinin: the kinetics of the response or the level of the reponse or both. Experiments to test this issue are underway. We could also imagine that auxin and cytokinin act in synergy because their respective transcription factors activate common targets: to this respect, a comparison of ARF and type-B ARR genes targets from data in the literature or by bio informatics could be instructive.

Moreover, the genetic interaction I showed between PINOID and AHP6 indicate a direction for investigating the link between auxin transport and cytokinin signaling. First, it is necessary to analyze precisely the phyllotaxis of *ahp6* -/- x *pid* +/- plants to determine if their enhanced phenotype is due only to permutations or if additional defects are present. Then the observations of several reporters of auxin and cytokinin signaling could indicate why phyllotaxis strongly loose its robustness in this genetic background.

Finally, the link between auxin and cytokinin could be also explored in a different context. In the flower, *AHP6* is expressed in incipient floral organ and *ahp6* mutants have additional sepals, petals and stamens. The explanation of this phenotype is not clear. Different regulators between flower and the SAM could be responsible for the differences. Interestingly, floral phyllotaxis is whorled: an exciting hypothesis would be that the same crosstalk are conserved between the two tissue, but that the different dynamics of the pattern formation in the two context lead to different developmental outputs.

II.3. Exploring the auxin fields by new experimental and modeling approaches.

How dynamic polar auxin transport generates robust self-organization remains an important question in phyllotaxis.

As discussed above, the visualization of the dynamics of auxin depletion field is a major challenge. Combining analysis of PIN1 polarization, DII-VENUS expression patterns (indicating the input in the auxin signaling pathway and in many cases, revealing local auxin concentrations) and DR5 expression patterns (resulting from auxin signaling outputs) in living plants is now indispensable to understand how the pattern emerge from auxin transport, perception and transduction, respectively. Moreover, comparison of genetic wild type and *ahp6* mutant

backgrounds would give interesting information on how the auxin system behaves without an important feedback.

Research on auxin and phyllotaxis during the last decade has proved how models were valuable to understand how this complex system works. The abstract models based on dynamic systems have allowed considerable progress in the understanding of the process. Moreover, since most of the real biological parameters concerning auxin are unknow (e.g. auxin concentrations production and decay, pumping rates of PIN proteins, affinity with receptors, etc.), they remain extremely powerful to test hypothesis on the mechanisms of phyllotaxis. However, we found that the model we used were more robust to plastochron instabilities than the auxin fields likely are, because we did not reproduce realistic perturbations compared to our experimental data. A sensitivity analysis could indicate better parameters to generate realistic perturbations. Other sources of noise we have not tested could also give better results. Alternatively, this could suggest that other models could better describe the phenomenon. Their major simplification is to transform organ formation in a discrete event (Douady & Couder 1996c; Green 1996): organs appear instantaneously and at a point on the generative ring. In reality, organogenesis is rather gradual and occur continuously over space in the area corresponding to the peripheral zone. Since co-initiations and AHP6 fields seems to involve precisely this developmental window of early organ emergence, it is possible that models including a progressive formation of an initium would generate interesting temporal instabilities and produce relevant biological predictions.

References – Conclusions & Perspectives

Airy, H., 1873. On leaf-arrangement. *Proceedings of the Royal Society*, 21, p.176.

Aloni, R. et al., 2005. Root-synthesized cytokinin in Arabidopsis is distributed in the shoot by the transpiration stream. *Journal of Experimental Botany*, 56(416), p.1535-1544.

Argyros, R.D. et al., 2008. Type B response regulators of Arabidopsis play key roles in cytokinin signaling and plant development. *The Plant Cell*, 20(8), p.2102-2116.

Corbesier, L. et al., 2003. Cytokinin levels in leaves, leaf exudate and shoot apical meristem of Arabidopsis thaliana during floral transition. *Journal of Experimental Botany*, 54(392), p.2511-2517.

Couder, Y., 1998. Initial transitions, order and disorder in phyllotactic patterns: The ontogeny of Helianthus annuus. A case study. *ACTA SOCIETATIS BOTANICORUM POLONIAE*, 67(2), p.129-150.

Douady, S. & Couder, Y., 1996a. Phyllotaxis as a dynamical self organizing process .1. The spiral modes resulting from time-periodic iterations. *JOURNAL OF THEORETICAL BIOLOGY*, 178(3), p.255-274.

Douady, S. & Couder, Y., 1996b. Phyllotaxis as a dynamical self organizing process .2. The spontaneous formation of a periodicity and the coexistence of spiral and whorled patterns. *JOURNAL OF THEORETICAL BIOLOGY*, 178(3), p.275-294.

Douady, S. & Couder, Y., 1996c. Phyllotaxis as a dynamical self organizing process .3. The simulation of the transient regimes of ontogeny. *JOURNAL OF THEORETICAL BIOLOGY*, 178(3), p.295-&.

Geier, F. et al., 2008. A quantitative and dynamic model for plant stem cell regulation. *PloS One*, 3(10), p.e3553.

Green, P.B., 1996. Transductions to generate plant form and pattern: an essay on cause and effect. *Annals of Botany*, 78(3), p.269-281.

Hamant, O. & Pautot, V., 2010. Plant development: A TALE story. *Comptes Rendus Biologies*, 333(4), p.371-381.

Heisler, M.G. et al., 2010. Alignment between PIN1 polarity and microtubule orientation in the shoot apical meristem reveals a tight coupling between morphogenesis and auxin transport. *PLoS Biology*, 8(10), p.e1000516.

Ishida, K. et al., 2008. Three type-B response regulators, ARR1, ARR10 and ARR12, play essential but redundant roles in cytokinin signal transduction throughout the life cycle of Arabidopsis thaliana. *Plant & Cell Physiology*, 49(1), p.47-57.

Ito, Y. & Kurata, N., 2006. Identification and characterization of cytokinin-signalling gene families in rice. *Gene*, 382, p.57-65.

Jackson, D. & Hake, S, 1999. Control of phyllotaxy in maize by the abphyl1 gene. *Development (Cambridge, England)*, 126(2), p.315-323.

Jacqmard, A. et al., 2002. In situ localisation of cytokinins in the shoot apical meristem of Sinapis alba at floral transition. *Planta*, 214(6), p.970-973.

Kanrar, S., Onguka, O. & Smith, H.M.S., 2006. Arabidopsis inflorescence architecture requires the activities of KNOX-BELL homeodomain heterodimers. *Planta*, 224(5), p.1163-1173.

King, S., Beck, F. & Luttge, U., 2004. On the mystery of the golden angle in phyllotaxis. *PLANT CELL AND ENVIRONMENT*, 27(6), p.685-695.

Kuhlemeier, C., 2007. Phyllotaxis. *Trends in Plant Science*, 12(4), p.143-150.

Kwiatkowska, D, 1995. Ontogenetic changes of phyllotaxis in Anagallis arvensis L. *ACTA SOCIETATIS BOTANICORUM POLONIAE*, 64(4), p.319-325.

Kwiatkowska, Dorota, 2008. Flowering and apical meristem growth dynamics. *Journal of Experimental Botany*, 59(2), p.187-201.

Lee, B., Johnston, R., et al., 2009. Studies of aberrant phyllotaxy1 Mutants of Maize Indicate Complex Interactions between Auxin and Cytokinin Signaling in the Shoot Apical Meristem. *PLANT PHYSIOLOGY*, 150(1), p.205-216.

Lee, B., Yu, S. & Jackson, D., 2009. Control of Plant Architecture: The Role of Phyllotaxy and Plastochron. *JOURNAL OF PLANT BIOLOGY*, 52(4), p.277-282.

Meicenheimer, R.D., 1982. CHANGE IN EPILOBIUM PHYLLOTAXY DURING REPRODUCTIVE TRANSITION. *AMERICAN JOURNAL OF BOTANY*, 69(7), p.1108-1118.

Meicenheimer, R.D., 1998. Decussate to spiral transitions in phyllotaxis. Dans *Symmetry in Plants*.

Mähönen, A.P. et al., 2006. Cytokinin signaling and its inhibitor AHP6 regulate cell fate during vascular development. *Science (New York, N.Y.)*, 311(5757), p.94-98.

Müller, B., 2011. Generic signal-specific responses: cytokinin and context-dependent cellular responses. *Journal of Experimental Botany*, 62(10), p.3273-3288.

Newell, A., Shipman, P. & Sun, Z., 2008. Phyllotaxis: Cooperation and competition between mechanical and biochemical processes. *JOURNAL OF THEORETICAL BIOLOGY*, 251(3), p.421-439.

Okada, K. et al., 1991. Requirement of the Auxin Polar Transport System in Early Stages of Arabidopsis Floral Bud Formation. *The Plant Cell*, 3(7), p.677-684.

Ormenese, S et al., 2000. The frequency of plasmodesmata increases early in the whole shoot apical meristem of Sinapis alba L. during floral transition. *Planta*, 211(3), p.370-375.

Ormenese, Sandra, Bernier, Georges & Périlleux, C., 2006. Cytokinin application to the shoot apical meristem of Sinapis alba enhances secondary plasmodesmata formation. *Planta*, 224(6), p.1481-1484.

Ormenese, Sandra et al., 2002. The shoot apical meristem of Sinapis alba L. expands its central symplasmic field during the floral transition. *Planta*, 215(1), p.67-78.

Pearcy, R.W., Muraoka, H. & Valladares, Fernando, 2005. Crown architecture in sun and shade environments: assessing function and trade-offs with a three-dimensional simulation model. *The New Phytologist*, 166(3), p.791-800.

Peaucelle, A. et al., 2007. Plants expressing a miR164-resistant CUC2 gene reveal the importance of post-meristematic maintenance of phyllotaxy in Arabidopsis. *Development (Cambridge, England)*, 134(6), p.1045-1050.

Preuksakarn, C. et al., 2010. Reconstructing plant architecture from 3D laser scanner data. Dans 6th International Workshop on Functional-Structural Plant Models. p. 16-18.

Ragni, L. et al., 2008. Interaction of KNAT6 and KNAT2 with BREVIPEDICELLUS and PENNYWISE in Arabidopsis inflorescences. *The Plant Cell*, 20(4), p.888-900.

Reddy, G.V. et al., 2004. Real-time lineage analysis reveals oriented cell divisions associated with morphogenesis at the shoot apex of Arabidopsis thaliana. *Development (Cambridge, England)*, 131(17), p.4225-4237.

Reinhardt, D, Mandel, T & Kuhlemeier, C, 2000. Auxin regulates the initiation and radial position of plant lateral organs. *The Plant Cell*, 12(4), p.507-518.

Reinhardt, Didier et al., 2005. Microsurgical and laser ablation analysis of leaf positioning and dorsoventral patterning in tomato. *Development (Cambridge, England)*, 132(1), p.15-26.

de Reuille, P.B. et al., 2006. Computer simulations reveal properties of the cell-cell signaling network at the shoot apex in Arabidopsis. *Proceedings of the National Academy of Sciences of the United States of America*, 103(5), p.1627-1632.

Smith, H.M.S. & Hake, Sarah, 2003. The interaction of two homeobox genes, BREVIPEDICELLUS and PENNYWISE, regulates internode patterning in the Arabidopsis inflorescence. *The Plant Cell*, 15(8), p.1717-1727.

Snow, M. & Snow, R., 1932. Experiments on phyllotaxis I - The effect of isolating a pininordium. *PHILOSOPHICAL TRANSACTIONS OF THE ROYAL SOCIETY OF LONDON SERIES*, 221, p.1-43.

Snow, M. & Snow, R., 1933. Experiments on phyllotaxis II - The effect of displacing. *PHILOSOPHICAL TRANSACTIONS OF THE ROYAL SOCIETY OF LONDON SERIES*, 222, p.353-400.

Stoma, S. et al., 2008. Flux-based transport enhancement as a plausible unifying mechanism for auxin transport in meristem development. *PLoS Computational Biology*, 4(10), p.e1000207.

Valladares, F & Pearcy, R., 1998. The functional ecology of shoot architecture in sun and shade plants of Heteromeles arbutifolia M. Roem., a Californian chaparral shrub. *OECOLOGIA*, 114(1), p.1-10.

Vernoux, T. et al., 2011. The auxin signalling network translates dynamic input into robust patterning at the shoot apex. *Molecular Systems Biology*, 7, p.508.

Wardlaw, C., 1949. EXPERIMENTAL AND ANALYTICAL STUDIES OF PTERIDOPHYTES . 14. LEAF FORMATION AND PHYLLOTAXIS IN DRYOPTERIS-ARISTATA DRUCE. *ANNALS OF BOTANY*, 13(50), p.163-&.

Yoshida, S., Mandel, Therese & Kuhlemeier, Cris, 2011. Stem cell activation by light guides plant organogenesis. *Genes & Development*, 25(13), p.1439-1450.

General list of figures

Chapter	Figure number	Title	Page
Introduction	Figure 1	Phyllotaxis is the geometrical pattern made by plant organs around axes.	16
	Figure 2	Phyllotaxis is a feature shared by a vast majority of land plants	18
	Figure 3	Shoot Apical Meristems (SAM) produce all the aerial part of seed plants .	20
	Figure 4	Major types of phyllotaxis.	20
	Figure 5	Definition of some parameters used in the description and quantification of phyllotaxis.	22
	Figure 6	Expressing the divergence angle as fraction of a turn.	24
	Figure 7	Functional zonation of the shoot apical meristem.	24
	Figure 8	Experimenting phyllotaxis by microsurgery on meristems.	26
	Figure 9	Switch from a decussate to a spiral phyllotaxis.induced by microsurgery	28
	Figure 10	Modeling phyllotaxis as a physical dynamical system	32
	Figure 11	Modeling organ interactions in meristems	32
	Figure 12	Phase diagram of phyllotaxis explained by the control parameter Γ	34
	Figure 13	Geometrical scheme explaining transitions of phyllotaxis in the Fibonacci branch upon decrease of parameter Γ.	36
	Figure 14	Structural and functional organization of the SAM in *Arabidopsis thaliana*.	42
	Figure 15	Reaction-diffusion models explaining the formation of biological patterns.	56
	Figure 16	Polar auxin transport controls organogenesis and phyllotaxis in the SAM.	60
	Figure 17	Signaling network controlling organogenesis in the SAM of *Arabidopsis thaliana*	78
Chapter 1	Figure 1	Examples of measured divergence angle sequences in wild-type *Arabidopsis* and *ahp6-1* mutant plants	136
	Figure 2	Fit of the divergence angle frequency distribution by the mixture of observation distributions.	140
	Figure 3	Hidden Markov chains restricted to the modeling of 2-permutations	142
	Figure 4	Examples of final consensus optimal labeling of measured sequences	144
	Figure 5	Proportions of non-canonical angles per sequence in wild-type and mutants show overlapping phenotypes	148
	Figure 6	Frequency distributions for the number of successive synchronized organs between two permutations.	154
	Figure 7	Propagations of permutations over intervals of synchronized organs correlate with contact parastichies.	154
	Figure 8	Sample auto-correlation function of divergence angles within baseline segments	160
	Figure 9	Schematic summary of permutation patterns found in *Arabidopsis* Phyllotaxis	162
	Figure 10	Model of phyllotaxis affected by permutations and putative roles of AHP6	164
	Figure S1	Device used to measure successive divergence angles between siliques	182
	Figure S2	Explanation of the M-shaped perturbation motif by a permutation in the apico-basal order of organ along the stem.	183
	Figure S3	Stationarity of sequences	183
	Figure S4	Ranked posterior probabilities of the optimal labelings of the divergence angle sequences computed using the estimated hidden Markov chains	184
	Figure S5	Von Mises observation distributions with common concentration parameter centered on the multiples of the divergence angle	184
	Figure S6	Pipe-line of methods used to analyze the phyllotactic sequences.	185
	Figure S7	Comparison of the Frequency distributions for the number of successive synchronized organs between two permutations and after a 2-permutation in wild-type and *ahp6-1* mutants.	185
	Figure S8	Structure of the stem between permuted organs	186
Chapter 2	Figure 1	AHP6 is a pseudo Histidine-Phosphotransfer protein (pseudo HPt) that inhibits cytokinin signaling.	188
	Figure 2	*AHP6* regulates phyllotaxis	194
	Figure 3	*AHP6* regulates the periodicity of organ initiation at the shoot apical meristem.	196
	Figure 4	*AHP6* is activated downstream of auxin during organ initiation.	198
	Figure 5	AHP6 acts non-cell autonomously by generating cytokinin-inhibitory fields in the shoot apical meristem	200
	Figure 6	Strong phyllotaxis defects of *ahp6 x pid-9* +/- plants suggest a synergy between AHP6 fields and the dynamics of auxin transport in the control of phyllotaxis	234
	Figure 7	Synergistic interaction of PINOID and AHP6 in floral and carpel development	236
	Figure S1	Expression of the regulators of cytokinin signalling and biosynthesis in the different domains of the shoot apical meristem	221
	Figure S2	*AHP6* is a regulator of cytokinin signalling that is specifically enriched in lateral organs.	222
	Figure S3	*AHP6* regulates floral phyllotaxis	223

	Figure S4	Explanation of the deviations from the canonical phyllotactic sequences by the permutation hypothesis.	224
	Figure S5	The size of the stem cell niche is not affected by the *ahp6* mutation	225
	Figure S6	*AHP6* regulates the temporal sequence of *DR5::VENUS* activation at the shoot apical meristem	226
	Figure S7	*AHP6* does not affect the mean rate of organ initiation but rather the stability of the plastochron	227
	Figure S8	*AHP6* expression is regulated independently of cytokinins in the shoot apical meristem.	228
	Figure S9	The *pAHP6::AHP6-GFP* construct complements *ahp6* phyllotaxis phenotype	229
	Figure S10	*AHP6* imposes a progressive activation of Cytokinin signalling activation in initia	230
	Figure S11	Exogenous Cytokinin treatment increases auxin signaling in organogenetic zones of the meristem.	231
	Figure S12	Model of the control of the organ initiation temporal sequence by AHP6 inhibitory fields at the shoot apical meristem	232
Chapter 3	Figure 1	Phyllotaxis, from observations to an abstract model	256
	Figure 2	The model with noise on the threshold for organ initiation.	258
	Figure 3	The model with noise on the size of the competent circle	260
	Figure 4	Alterations as a function of noise strength,	262
	Figure 5	Noise correction by a secondary field	266
	Figure S1	Alterations of divergence angle and plastochron as a function of noise strength	274
	Figure S2	Alterations as a function of Γ	276
	Figure S3	Alterations of divergence angle and plastochron as a function of Γ	278
	Figure S4	Correction effect of the secondary field depends both on its size (d) and its delay of activation.T2	280
	Figure S5	Fast decrease of Γ creates M-shaped motif and null plastochrons.	280
Conclusions and Perspectives	Figure 1	The number of possible co-initiations is likely constrained by the ratio of organ size to meristem size	292
	Figure 2	Proposed model for AHP6 action	296
	Figure 3	Comparison of the number of co-initiations observed in meristem with the number of permuted organs on stem	300
	Figure 4	Presence of genes encoding putative pseudo-HPt in various eudicots	312
	Figure 5	Phylogeny of HPt and pseudo-HPt in Arabidopsis, Maize and Rice	314
	Figure 6	Reconstruction of *Arabidopsis* phyllotaxis from laser-scanner data	318

General list of Tables

Chapter	Table number	Page
Introduction	Table 1	10
	Table 2	36
Chapter 1	Table 1	140
	Table 2	146
	Table 3	146
	Table 4	150
	Table 5	150
	Table 6	152
	Table 7	152
	Table S1	186
Chapter 2	TABLE 1	234
	Table S1	212

Origin of pictures and photographs re-used in the different figures of this manuscript

Chapter	Figure	Photograph/Picture	Reference
Introduction	1A	Daisy (Leucanthemum sp.)	http://www.math.smith.edu
	1B	Pine cone	http://www.math.smith.edu
	1C	Brassica oleracea var. Botrytis	http://www.lps.ens.fr/~douady/PhyllotaxisIndex.html
	2A	Araucaria sp	Web reference no more available
	2B	Nymphaea adorata	© 2005 zen Sutherland (http://tolweb.org,)
	2C	Ephedra antisyphilitica	© Steffi M. Ickert-Bond (http://tolweb.org,)
	2D	Psilotum nudum	© Australian National Botanic Gardens (http://tolweb.org,)
	2E	Equisetum pratense	© 2008 Miika Silfverberg (http://tolweb.org)
	2F	Cyatheales sp .	http://eu.fotolia.com
	2G	Selaginella delicatula	© 2009 Shipher (士緯) Wu (吳), (http://tolweb.org)
	2H	*Polytrichastrum formosum*	http://www.cebe.be/mousses/
	2I	chara	© 2002+ by Cara Lea Council-Garcia and The University of New Mexico.
	2J	Coleochaete	http://www.botany.wisc.edu ;Copyright © 2008 The Board of Regents of the University of Wisconsin System
	3	Entire figure	Vernoux T. *et al.*, CSHP 2010 (Fig1 A,B,C)
	7	Entire figure	Vernoux T. *et al.*, CSHP 2010 (Fig1 D)
	8A	Lupinus albus	http://www.prota4u.org
	8C	Dryopteris dilatata	Photo © Franck Le Driant / FloreAlpes.com
	8E,F	Tomato / laser ablation	Reinhardt D. *et al.*, Development 2003
	9	Entire figure	Snow and Snow, 1935
	10A,B	Experiment of Douady and Couder	Douady S. and Couder Y., J. theor. Biol 1996
	14	Entire figure	Besnard F. *et al.*, CMLS 2011
	15	Turing Patterns	Kondo S. *et al.*, Science 2010
	16	Entire figure	Besnard F. *et al.*, CMLS 2011
	17	Entire figure	Besnard F. *et al.*, CMLS 2011
Discussion and Perspectives	4	Alignment of amino-acids	Mähönen, AP. et al, 2006
	5A	Phylogenetic tree of AHP	Müller B., J. Exp. Bot. 2011
	5B	Phylogenetic tree of Hpt proteins in *Arabidopsis*, rice and Maize	Ito Y. *et al*, Gene 2006